PB82-108358

Fuel Decomposition and Flame Reactions in Conversion of Fuel Nitrogen to NOx

Rockwell International
Canoga Park, CA

Prepared for

Industrial Environmental Research Lab.
Research Triangle Park, NC

1978

U.S. Department of Commerce
National Technical Information Service
NTIS

USE SPECIAL DROPOUT BLUE PENCIL
ONLY TO INDICATE CORRECTIONS
CLASSIFICATION
PAGE
STARTING LINE

PB82-108358

EPA-600/7-81-158

EPA-1

FUEL DECOMPOSITION AND FLAME REACTIONS IN CONVERSION OF FUEL NITROGEN TO NO_x

by

A. E. Axworthy, D. R. Kahn, V. H. Dayan,
and D. O. Woolery, II

Rocketdyne Division
Rockwell International
6633 Canoga Avenue
Canoga Park, California 91304

CENTERLINE

Contract No. 68-02-1886
ROAPs No. 21ADG-08/21BCC-12
Program Element No. 1AB014

EPA Project Officer: G. Blair Martin

Industrial Environmental Research Laboratory
Office of Energy, Minerals, and Industry
Research Triangle Park, NC 27711

Prepared for

U. S. ENVIRONMENTAL PROTECTION AGENCY
Office of Research and Development
Washington, DC 20460

REPRODUCED BY
NATIONAL TECHNICAL
INFORMATION SERVICE
U.S. DEPARTMENT OF COMMERCE
SPRINGFIELD, VA 22161

WARNING LINE
STOP
DOCUMENT NUMBER
PAGE NUMBER
CLASSIFICATION

NOTICE

THIS DOCUMENT HAS BEEN REPRODUCED FROM THE BEST COPY FURNISHED US BY THE SPONSORING AGENCY. ALTHOUGH IT IS RECOGNIZED THAT CERTAIN PORTIONS ARE ILLEGIBLE, IT IS BEING RELEASED IN THE INTEREST OF MAKING AVAILABLE AS MUCH INFORMATION AS POSSIBLE.

IERL-RTP-1253

TECHNICAL REPORT DATA
(Please read Instructions on the reverse before completing)

1. REPORT NO.

2.

3. RECIPIENT'S ACCESSION NO. PB82 108358

4. TITLE AND SUBTITLE
Fuel Decomposition and Flame Reactions in Conversion of Fuel Nitrogen to NO_x

5. REPORT DATE

6. PERFORMING ORGANIZATION CODE

7. AUTHOR(S)
A.E. Axworthy, D.R. Kahn, V.H. Dayan, and D.O. Woolery, II

8. PERFORMING ORGANIZATION REPORT NO.

9. PERFORMING ORGANIZATION NAME AND ADDRESS
Rockwell International/Rocketdyne Division
6633 Canoga Avenue
Canoga Park, California 91304

10. PROGRAM ELEMENT NO.

11. CONTRACT/GRANT NO.
68-02-1886

12. SPONSORING AGENCY NAME AND ADDRESS
EPA, Office of Research and Development
Industrial Environmental Research Laboratory
Research Triangle Park, NC 27711

13. TYPE OF REPORT AND PERIOD COVERED
Final; 6/75-4/78

14. SPONSORING AGENCY CODE
EPA/600/13

15. SUPPLEMENTARY NOTES IERL-RTP project officer is G. Blair Martin, Mail Drop 62, 919/541-7504.

16. ABSTRACT The report describes an experimental and analytical research program conducted to provide information on the chemical phenomena involved in the conversion of air and fuel nitrogen to NOx. Under Task 1, Fuel Decomposition, early (pre-flame) reactions of fuel nitrogen species were investigated using one- and two-stage reactors. Inert pyrolysis experiments, carried out with several fuel oils, showed that the primary nitrogen-containing product was a tarry material that decomposed to HCN at high temperature (1100 C). Oxidative pyrolysis experiments, involving model compounds (pyridine, benzonitrile, NH3, and HCN), fuel oils, and coals, showed that the primary products were NH3 and HCN at lower temperature, and N2 and N2O at higher temperature. Task 2, Combustion Kinetics, was carried out in a low-pressure flat flame burner. The formation of thermal, prompt, and fuel NO was investigated in CH4-O2-N2 flames doped with NH3 or HCN. In addition, the formation of fuel NO was investigated in a H2-CO-O2-Ar-NH3 flame. This simulated the combustion of a future low-Btu fuel containing NH3 as an impurity. HCN was shown to be a significant intermediate for all flames where the fuel contained hydrocarbon. Calculations were made during Task 3, Data Analysis, on the H2-CO-O2-Ar-NH3 flame using a detailed kinetic-diffusion model.

17. KEY WORDS AND DOCUMENT ANALYSIS

a. DESCRIPTORS		b. IDENTIFIERS/OPEN ENDED TERMS	c. COSATI Field/Group	
Pollution	Pyrolysis	Pollution Control	13B	07D
Flames	Decomposition Reactions	Stationary Sources	21B	
Combustion		Fuel Decomposition		07B,07C
Kinetics	Nitrogen Oxides	Fuel Nitrogen	20K	
Fuel Oil	Ammonia		21D	
Coal				

18. DISTRIBUTION STATEMENT
Release to Public

19. SECURITY CLASS *(This Report)*
Unclassified

20. SECURITY CLASS *(This page)*
Unclassified

21.

22. PRICE

EPA Form 2220-1 (9-73)

DISCLAIMER

This report has been reviewed by the Industrial Environmental Research Laboratory (RTP), U.S. Environmental Protection Agency, and approved for publication. Approval does not signify that the contents necessarily reflect the views and policies of the Agency, nor does mention of trade names or commercial products constitute endorsement or recommendation for use.

ABSTRACT

An experimental and analytical research program was conducted to provide information on the chemical phenomena involved in the conversion of air and fuel nitrogen to NO_x. The program was divided into three tasks. Under Task 1, Fuel Decomposition, the early (preflame) reactions of fuel nitrogen species were investigated using both single- and two-stage reactors. Additional inert pyrolysis experiments were carried out with several fuel oils. The oxidative pyrolysis experiments involved model compounds (pyridine, benzonitrile, NH_3 and HCN), fuel oils, and coals. The Task 2, Combustion Kinetics, study was carried out in a low-pressure flat flame burner. The formation of "thermal," "prompt," and "fuel" NO was investigated in CH_4-O_2-N_2 flames doped with small amounts of NH_3 or HCN. In addition, the formation of fuel NO was investigated in a H_2-CO-O_2-Ar-NH_3 flame. This simulated the combustion of a future low Btu fuel containing some ammonia as an impurity. Calculations were made under Task 3, Data Analysis, on the H_2-CO-O_2-Ar-NH_3 flame using a detailed kinetic-diffusion model.

CONTENTS

Page

Summary 1

Task 1 - Fuel Decomposition 1

Task 2 - Combustion Kinetics. 3

Task 3 - Data Analysis. 4

Introduction. 5

Task 1: Fuel Decomposition 11

Background 11

Inert Pyrolysis of Pyridine - Confirmation of Previous Results. 14

Inert Pyrolysis of Fuels. 14

Oxidative Pyrolysis of Model Compounds. 34

Secondary Reactions in Model Compound Oxidative Pyrolysis 50

Oxidative Pyrolysis of Fuels. 63

Task 2: Combustion Kinetics. 87

Experimental 88

Input-Output Experiments. 93

Test Plan-Detailed Probing Experiments. 111

Addition of 2500 ppm Ammonia to Fuel-Rich CH_4-O_2-Ar Flame 111

Fuel-Rich CH_4-O_2-N_2 Flame 124

Fuel-Lean CH_4-O_2-N_2 Flame 162

Simulated Low Btu Fuel Combustion (H_2-CO-O_2-Ar) 176

Task 3: Data Analysis 229

Conclusions from Kinetic-Diffusion Calculations 237

Appendix A

Description of Fuel Samples 239

Appendix B

Chemical Analysis Techniques. 245

Appendix C

Temperature Measurement in Flames 255

Appendix D

Measurement of Nitrogen Species in Products of Low-Pressure Hydrocarbon Flames 269

ILLUSTRATIONS

Page

1-1. Quartz Fuel Pyrolysis Apparatus 16

1-2. HCN Yield vs Temperature in Single-Temperature Inert Pyrolysis of a No. 6 Fuel Oil 23

1-3. Hydrogen Cyanide Yield From the Two-Stage Inert Pyrolysis of a No. 6 Fuel Oil 25

1-4. Hydrogen Cyanide Yields From the Inert Pyrolysis of Coals With Second Stage at 1100 C 30

1-5. Model Compound Oxidative Pyrolysis. 37

1-6. Extent of Reaction as a Function of Temperature and Model Compound Concentration 39

1-7. Products From Oxidative Pyrolysis of Pyridine 41

1-8. NO and NO_2 Yields From Pyridine 45

1-9. Products From Oxidative Pyrolysis of Benzonitrile 46

1-10. NO and NO_2 Yields From Benzonitrile 49

1-11. Oxidation of HCN and NH_3 Under Pyrolysis Conditions 51

1-12. Comparison of Rates of Oxidation of HCN and NH_3 With Yield Profiles From Model Compounds. 53

1-13. Effect of NH_3 on Oxidation Rate of HCN 57

1-14. Products From Two-Stage Oxidative Pyrolysis of Pyridine With First Stage at 716 C 61

1-15. Nitrous Oxide Yield as a Function of Second-Stage Temperature . . . 69

1-16. Nitrous Oxide From No. 6 Fuel Oil H 71

1-17. HCN From No. 6 Fuel Oil H (first stage at 850 C). 72

1-18. HCN From No. 6 Fuel Oil H (first stage at 750 C). 75

1-19. Carbon Dioxide Yield as a Function of Second-Stage Temperature (first stage at 850 C). 79

1-20. CO_2 and Ethane Yields From Oxidative Pyrolysis of No. 6 Fuel Oil H (first stage at 850 C) 81

2-1. Design of the Flat-Flame Burner 89

2-2. Schematic of the Flat-Flame Burner System 90

2-3. Experimental Scheme for Determination of NO, NO_2, NH_3 and HCN 92

2-4. Input-Output Experiment III(c) - Temperature Profile 100

2-5. Input-Output Experiment III(c) - Thermal NO Profile 101

ILLUSTRATIONS (Continued)

Page

2-6. Input-Output Experiment IV - NO Output vs ϕ 104

2-7. Input-Output Experiment IV - Temperature at 80 mm vs ϕ 105

2-8. Input-Output Experiment V(a) - NH_3 Conversion vs NH_3 Concentration. 108

2-9. Catalytic Removal of NO on Stainless Steel at 840 C 110

2-10. Detailed Experiment 1 - Temperature Profile 115

2-11. Detailed Experiment 1 - Temperature Profile 116

2-12. Detailed Experiment 1 - NO and NO_2 Mole Fraction Profiles 117

2-13. Detailed Experiment 1 - NH_3, HCN and NO Mole Fraction Profiles. . . 118

2-13A. Calculated Gas Residence Times as a Function of Distance Above Burner 120

2-14. Detailed Experiment 1 - NH_3 and HCN Mole Fraction Profiles. 121

2-15. Detailed Experiment 1 - Species Flux Profiles 123

2-16. Experiment 2 - Temperature Profile. 128

2-17. Experiment 2 - Temperature Profile. 129

2-18. Experiment 2 - NO Mole Fraction Profile 130

2-19. Experiment 2 - NO, NO_2 and HCN Mole Fraction Profiles 132

2-20. Experiment 2 - Species Flux Profiles. 133

2-21. Experiment 2 - Species Flux Profiles. 134

2-22. Comparison of Flame Temperature Profiles from Experiments 2 and 3 137

2-23. Experiment 3 - NH_3, HCN and NO Mole Fraction Profiles 138

2-24. Experiment 3 - NH_3, HCN and NO Mole Fraction Profiles 139

2-25. Experiment 3 - Species Flux Profiles. 140

2-26. Experiment 3 - Species Flux Profiles. 141

2-27. Comparison of NO Molar Flux Profiles from Experiments 2 and 3 142

2-28. Comparison of Molar Flux Profiles for HCN and NO From Experiments 2 and 3 143

2-29. Mole Fraction Profiles of Major Species from Experiment 3 (ϕ= 1.5) 146

2-30. Molar Flux Profiles of Major Species from Experiment 3 (ϕ= 1.5) 148

ILLUSTRATIONS (Continued)

Page

2-31. Flowmeter Calibration Curve for 4.0% HCN in N_2 Gas Mixture 150

2-32. Comparison of Flame Temperature Profiles from Experiments 2 and 4 152

2-33. Experiment 4 - Temperature Profile. 153

2-34. Experiment 4 - Species Mole Fraction Profile. 154

2-35. Experiment 4 - Species Mole Fraction Profiles 155

2-36. Experiment 4 - Species Flux Profiles. 157

2-37. Experiment 4 - Species Flux Profiles. 158

2-38. Comparison of NO Flux Profiles from Experiments 2, 3 and 4. 159

2-39. Comparison of HCN and NO Flux Profiles from Experiments 2, 3 and 4. 160

2-40. Experiment 5 - Temperature Profile. 163

2-41. Experiment 5 - Temperature Profile. 164

2-42. Experiment 5 - NO Mole Fraction Profile 166

2-43. Experiment 5 - NO and NO_2 Mole Fraction Profiles. 167

2-44. Experiment 5 - NO Flux Profile. 168

2-45. Experiment 5 - NO and NO_2 Flux Profiles 169

2-46. Experiment 6 - Temperature Profile. 172

2-47. Experiment 6 - Temperature Profile. 173

2-48. Comparison of NO Mole Fraction Profiles from Experiments 5 and 6 174

2-49. Experiment 6 - Species Mole Fraction Profiles 175

2-50. Comparison of NO Flux Profiles from Experiments 5 and 6 176

2-51. Comparison of Species Flux Profiles from Experiments 5 and 6 177

2-52. Mole Fraction Profiles of Major Species from Experiment 6 ($\phi = 0.8$) 179

2-53. Molar Flux Plots of Major Species from Experiment 6 180

2-54. Adiabatic Flame Temperatures vs ϕ 183

2-55. Experiment 8 - Temperature Profile. 189

2-56. Experiment 8 - Temperature Profile. 190

2-57. Experiment 8 - Species Mole Fraction Profiles 192

ILLUSTRATIONS (Continued)

Page

2-58. Experiment 8 - Species Mole Fraction Profiles. 193
2-59. Experiment 8 - Species Flux Profiles 195
2-60. Experiment 8 - Species Flux Profiles 196
2-61. Mole Fraction Profiles of Major Species from Experiment 8 198
2-62. Molar Flux Profiles of Major Species from Experiment 8 199
2-63. Experiment 9 - NO Mole Fraction Profile. 201
2-64. Experiment 9 - NO Mole Fraction Profile. 202
2-65. Experiment 9 - NO Flux Profile 203
2-66. Experiment 9 - NO Flux Profile 204
2-67. Comparison of Species Molar Flux Profiles from Experiments 8 and 9. 205
2-68. Comparison of Species Flux Profiles from Experiments 8 and 9. 206
2-69. Comparison of H_2 and O_2 Mole Fraction Profiles from Experiments #8 and #10 209
2-70. Comparison of CO and CO_2 Mole Fraction Profiles from Experiments #8 and #10 210
2-71. Comparison of H_2O Mole Fraction Profiles from Experiments #8 and #10 211
2-72. Experiment 10 - Species Mole Fraction Profiles 214
2-73. Experiment 10 - Species Mole Fraction Profiles 215
2-74. Experiment 10 - Species Flux Profiles. 216
2-75. Experiment 10 - Species Flux Profiles. 217
2-76. Effect of Additive Type on NO Yields in Fuel-Rich H_2-CO-O_2-Ar Low Pressure Flame 219
2-77. Effect of Additive Type on NO Yields in a Fuel-Rich H_2-CO-O_2-Ar Low Pressure Flame 220
2-78. Experiment 11 - Species Mole Fraction Profiles 221
2-79. Experiment 11 - Species Mole Fraction Profiles 222
2-80. Experiment 11 - Species Flux Profiles. 223
2-81. Experiment 11 - Species Flux Profiles. 224
2-82. Effect of NH_3 Additive Concentration on NO Yields in Fuel Rich H_2-CO-O_2-Ar Low Pressure Flame. 225
2-83. Effect of NH_3 Additive Concentration on NO Yields in a Fuel-Rich H_2-CO-O_2-Ar Low Pressure Flame 226

ILLUSTRATIONS (Concluded)

Page

3-1. Comparison of Measured and Calculated Mole Fraction Profiles for Major Species 234

3-2. Free Radical Concentrations Predicted by Model 235

3-3. Comparison of the Measured and Calculated Mole Fraction Profiles of the Nitrogen Species 236

USE SPECIAL DROPOUT BLUE PENCIL
ONLY TO INDICATE CORRECTIONS CLASSIFICATION PAGE
STARTING LINE

TABLES

Page

1-1. Hydrogen Cyanide Yields From Fuels Under Inert Pyrolysis Conditions at 1100 C. 19
1-2. HCN Yields From the Two-Stage Pyrolysis of a No. 6 Fuel Oil. 22
1-3. Hydrogen Cyanide Yields From Two-Stage Inert Pyrolysis of a Pittsburgh No. 8 Seam Coal. 28
1-4. Inert Pyrolysis of Doped Oils at 1100 C 33
1-5. Stoichiometry and Mole Change in Pyridine Oxidation 35
1-6. Extent of Reaction of NH_3 and HCN as a Function of Temperature. . 52
1-7. Products From the Oxidative Pyrolysis of HCN. 55
1-8. Products From Reaction of a Mixture of HCN (0.7%) + NH_3 (0.7%) + He (23.6%) + O_2 (75%). 59
1-9. Fuel Oil Single-Stage Oxidative Pyrolysis 65
1-10. Nitrogen Products From the Oxidative Pyrolysis of No. 6 Fuel Oil H (First Stage = 850 C). 77
1-11. Summary of Data on HCN Formation From Pittsburgh No. 8 Coal in Two-Stage Reactor 84
2-1. Task 2 Input-Output Test Plan 94
2-2. Results of Input-Output Experiment IB 96
2-3. Results of Input-Output Experiment III(a) 98
2-4. NO Formation vs NH_3 Additive Concentration in Input-Output Experimental Series V(a) 107
2-5. Results of Detailed Probing at Top of Flame Front in Input-Output Experiment V(b) 112
2-6. Test Plan for Detailed Probing Experiments 113
2-7. Comparison of Experimentally Measured NO Formation Rates With Those Predicted by Equilibrium Zeldovich Kinetics. 170
2-8 Preliminary Observations of H_2-CO-O_2-Ar Flame 185
2-9. Results of Temperature Measurements in Experiment No. 7 With H_2-CO-O_2-Ar Flame 188
3-1. Reactions Included in Kinetic Diffusion Model 230
A-1. Analysis of Synthoil. 240
A-2. Analysis of Synthoil Feed Coal. 240
A-3 Samples of Synthetic Fuels for Use in Rocketdyne Project for EPA on Combustion NO_x 241

DOCUMENT NUMBER
PAGE
CLASSIFICATION
TYPIST

TABLES (Concluded)

Page

A-4. Comparison of Analyses on Aerotherm Pulverized Coal Samples 242
B-1. Effect of Temperature on HCN Recovery. 248
C-1. Thermocouple Heat Transfer Coefficients Calculated at Conditions of Experiment #8 265
D-1. Candidate Solid Absorbents Tested for Selective Removal of HCN 275
D-2. Summary of Solid Absorbent Performance in Removing HCN, NH_3, NO and NO_2, Respectively, from Gas Mixtures 276
D-3. Sample Case Data Summary 279

SUMMARY

An experimental and analytical research program was conducted to provide additional information on the chemical phenomena involved in the conversion of air and fuel nitrogen to NO_x in the combustion of fossil fuels. The experimental techniques developed under the previous program (EPA Contract 68-02-0635) were improved to permit the chemistry to be studied in more detail.

The program was divided into three tasks. The pyrolysis and oxidative pyrolysis of fuels and model fuel nitrogen compounds was investigated in quartz microreactors in Task 1. Low-pressure flat-flame burner studies were conducted under Task 2, and in Task 3 an attempt was made to fit some of the burner results to a preliminary kinetic-diffusion model. The flat-flame burner study was extended to investigate the formation of thermal (prompt) NO as well as fuel NO from a methane flame and the formation of fuel NO in a simulated low Btu fuel (CO and H_2) flame.

TASK 1 - FUEL DECOMPOSITION

Additional inert pyrolysis experiments were conducted under this task but the major effort involved oxidative pyrolysis studies.

Inert Pyrolysis

HCN yields were measured from coals, fuel oils and alternative fuels under inert conditions. Most of the inert pyrolysis experiments were carried out in a two-temperature-zone reactor and it was established that most of the HCN is not produced directly in the primary varporization-pyrolysis process but forms later in the secondary reactions of volatile nitrogen species. The alternative liquid fuels derived from coal and oil shale produced strikingly larger percentage yields of HCN. When the model fuel nitrogen compounds benzonitrile and quinoline were added to oils, the fraction of the model compound converted to HCN was about the same as was obtained with the model compound alone.

Oxidative Pyrolysis and Oxidation

In the oxidative pyrolysis experiments, the products were measured as a function of temperature for two model compounds (pyridine and benzonitrile), three oils and one coal. Two-stage reactors were employed in some of the oxidative studies to investigate again the role of secondary reactions.

The model compounds were decomposed at a high oxygen concentration (75%) over a range of temperatures. The product distributions were quite similar in general with large amounts of HCN, NH_3 and CO forming around 700 C from both pyridine and benzonitrile. At temperatures above 750 C, the major oxidation products are CO_2, N_2, N_2O and, in the case of benzonitrile, NO. The formation of large yields of N_2O (up to 45%) was quite unexpected.

Two-stage oxidative pyrolysis experiments established that the N_2 and N_2O observed at the higher temperatures formed in the secondary reactions of the NH_3, HCN and volatile tars formed in the primary reaction process. The oxidation of NH_3 and HCN alone was also investigated and N_2O was found to form in large yields from HCN (up to 50%) and as a minor product from NH_3 (about 10%). The addition of NH_3 to HCN was found to stabilize the HCN with respect to oxidative decomposition.

In the two-stage oxidation of fuel oils, only small amounts of N_2O (on the order of 5%) formed but the oxygen concentrations were lower than in the model compound experiments. Minor amounts of N_2O ($\sim$2%) even formed in the oxidative pyrolysis of coal. In general, the presence of oxygen only increased slightly the HCN yields from fuel oil over those obtained under inert conditions. It was found that about 10% of the volatile nitrogen from a No. 6 fuel oil is in an extremely reactive form that, in the presence of some oxygen, can be converted to HCN at temperatures as low as 460 C. Only moderate amounts of NO formed in the oxidative pyrolysis of fuel oil.

TASK 2 - COMBUSTION KINETICS

Low pressure, flat-flame burner studies were conducted to investigate further the mechanisms and kinetics involved in the conversion of fuel-nitrogen intermediates (such as NH_3 and HCN) to NO_x in methane flames. In addition, the rates and mechanisms for the formation of thermal and fuel NO in the flame front were compared directly, and the formation of fuel NO from NH_3 (which could be present as an impurity) was investigated in a simulated low Btu fuel ($CO + H_2$).

An experimental technique was developed in which NH_3 and HCN could be measured accurately at low concentrations in these 0.1 atm. flames by oxidizing the NH_3 and HCN to NO and measuring the NO in a chemiluminescent analyzer. By employing a quartz probe and various combinations of selective catalytic converters and a chemical trap for HCN, each nitrogen species could be measured at various distances above the burner. Coated Pt/Pt-Rh thermocouples were used to obtain temperature profiles in the methane flames but were found to be unsatisfactory in the CO-H_2-O_2-Ar flames.

The rates and mechanisms of formation of thermal (prompt) and fuel NO were compared by studying CH_4-O_2-N_2 and CH_4-O_2-Ar-NH_3 flames under identical conditions. Under fuel rich conditions, both flames generated relatively high concentrations of HCN and both the prompt and fuel NO appeared to form through an HCN intermediate. The HCN profiles were very similar. Only about one-fourth as much prompt NO formed under fuel-lean conditions indicating that prompt NO forms via the reaction of fuel fragments with N_2 resulting in the formation of the HCN intermediate (the Fenimore mechanism).

The CO-H_2-O_2-Ar-NH_3 flame, which was studied in detail only under fuel-rich conditions, gave some very unexpected results. The ammonia was converted to NO in high yield and then, just above the flame front, much of the NO was consumed and a small amount of the consumed NO reformed slowly far above the flame front. These results indicate that some very unusual nitrogen species form from NH_3

in this flame. It was shown that most of the NO consumption at the top of the luminous zone is promoted by nitrogen species. Very long-lived nitrogen species are also formed as evidenced by the slow formation of NO more than 40 mm above the burner and the observation that the added NH_3 changes the color of the flame even farther above the burner. When NO and NH_3 were added to the feed gas simultaneously, the rapid consumption of both the NO and NH_3 occurred below the luminous zone. Apparently a direct reaction occurs that is similar to that involved in the Denox process.

TASK 3 - DATA ANALYSIS

An attempt was made to fit the results obtained with the $CO-H_2-O_2-Ar-NH_3$ flame to a 59 reaction mechanism using a kinetic-diffusion model. The predicted concentration profiles for both the major species and the nitrogen species were quite different from those measured experimentally. This probably resulted both from the uncertainty in certain physical parameters, such as the temperature profile between the burner and the luminous zone, and from difficiencies in the reaction rate set. Interestingly, the kinetic model predicts that moderate concentrations of O_2 are present above the flame front of this fuel-rich flame and this was observed experimentally.

INTRODUCTION

An experimental and analytical research program was conducted to provide information on fuel decomposition and flame reactions required for the development of a complete understanding of the chemical phenomena involved in the conversion of fuel nitrogen to NO_x. This effort was an extension of a previous study conducted under EPA Contract 68-02-0635 and much of the background for the present study is contained in the previous report (Ref. 1).

This program was divided into three tasks. Task 1: Fuel Decomposition, consisted of experimental studies of the types of chemical reactions fuel nitrogen species can undergo as the fuel reacts in the early (preflame) stages of combustion. Task 2: Combustion Kinetics, extended the experimental study of fuel and thermal NO_x formation in flames to other conditions, fuels and additives. Under Task 3: Data Analysis, an attempt was made to analyze some of the combustion results in terms of a quantitative chemical scheme.

One class of pollutants that is of concern, both in its own right and as an intermediate in the production of photochemical smog, is nitrogen oxides (NO_x). About 99% of the NO_x generated by man's activities is produced during the combustion of fossil fuels and nearly all is produced as nitric oxide. Of that, mobile and stationary sources each contribute approximately 50%; however, some projections indicate an increasing role of stationary sources in coming years. Mobile sources use light liquid fossil fuels with low levels of chemically bound nitrogen (i.e., <0.05 wt %) and produce predominantly thermal NO_x by high-temperature fixation of atmospheric nitrogen. By contrast, stationary sources also burn large amounts of heavy fuels (coal and residual oil) that contain significant amounts (0.2 to 1.8 wt %) of chemically bound nitrogen and produce fuel NO_x as well as thermal NO_x. Small-scale experimental studies have indicated that fuel NO_x may account for as much as 90% of the total NO_x from pulverized-coal combustion (Ref. 2) and 75% of that from heavy-oil combustion (Ref. 2

---

1. Axworthy, A.E., G.R. Schneider, M.D. Schuman, and V.H. Dayan, "Chemistry of Fuel Nitrogen Conversion to Nitrogen Oxides in Combustion," EPA-600/2-76-039 (NTIS No. PB 250373/AS), February 1976.

through (4). It has been estimated that, in the United States, 25% of the combustion-generated NO_x may be attributable to fuel-nitrogen conversion (Ref. 5).

With experimental combustion systems it has been shown that the fraction of fuel nitrogen converted to NO_x under fuel-lean conditions decreases as the nitrogen content increases, but the absolute amount of NO_x formed increases (Ref. 3 through 6). This has recently been verified by correlation of some available coal- and oil-fired combustion data (Ref. 7). It has been found that up to 90% reduction of NO_x can be achieved for residual oil and doped distillate oil with staged combustion (Ref. 3 through 8). It was also shown that up to 80% control of total NO_x from coal can be achieved by proper burner design (Ref. 9). The results of these small-scale experiments have guided the EPA Industrial Environmental Research Laboratory (IERL-RTP) program in two directions: (1) development and application of NO_x control technology for stationary sources buring coal and

---

2. Pershing, D.W., G.B. Martin, and E.E. Berkau, "Influence of Design Variables on the Production of Thermal and Fuel NO from Residual Oil and Coal Combustion," AIChE Symposium Series No. 148, 1975, 71, 19 (presented at the 66th Annual AIChE Meeting, 1973).

3. Turner, D.W., R.L. Andrews, and C.W. Siegmund, "Influence of Combustion Modification and Fuel Nitrogen Contents on Nitrogen Oxides Emissions from Fuel Oil Combustion" (presented at 64th Annual AIChe meeting, 1971) AIChE Symposium Series No. 126, 1972, 68, 55.

4. Muzio, L.J., R.P. Wilson, Jr., and C. McComis, "Package Boiler Flame Modifications for Reducing Nitric Oxide Emissions - Phase II of III, EPA-R2-73-292b (NTIS No. PB 236752/AS), June 1975.

5. Flagan, R.C., "The Formation of NO from Organic Nitrogen Contained in Fossil Fuels," Ph.D. Thesis, Massachusetts Institute of Technology, 1973.

6. Martin, G.B. and E.E. Berkau, "An Investigation of the Conversion of Various Fuel Nitrogen Compounds to Nitrogen Oxides in Oil Combustion" (Presented at 64th Annual AIChE Meeting, 1971) AIChE Symposium Series No. 126, 1972, 68, 45.

USE SPECIAL DROPOUT BLUE PENCIL
ONLY TO INDICATE CORRECTIONS
CLASSIFICATION
PAGE
STARTING LINE

heavy oil; and (2) fundamental studies of the chemistry and mechanisms of evolution of nitrogen compounds from real fuels and of subsequent reaction of the nitrogen-containing intermediates. This second type of study should provide valuable guidance for optimization of practical control technology by pointing to methods of enhancing the conversion of the fuel nitrogen to molecular nitrogen.

A part of the EPA program, a study of the chemical reactions involved in the formation of fuel NO_x was conducted at Rocketdyne. A portion of this study, reported previously (Ref. 1 and 10), involved the determination of the fate, under conditions of inert pyrolysis, of synthetic (model) fuel-nitrogen compounds and natural fuel nitrogen contained in fuel oils and coals. The rates of pyrolysis of the model nitrogen compounds were also investigated.

Once the fuel is introduced into the combustion zone of a combustor it may experience a wide range of reaction histories including: (1) mixing with air and subsequent reaction at equivalence ratios ranging from rich to lean;

---

7. Dykema, O.W. and R.E. Hall, "Analysis of Gas-, Oil-, and Coal-Fired Utility Boiler Test Data," pp IV-115 to -162, Proc. Stationary Source Combustion Symposium, Vol. III. Field Testing and Surveys, EPA-600/2-76-152c (NTIS No. PB 257146/AS), June 1976.
8. Martin, G.B. and E.E. Berkau, "Evaluation of Various Combustion Modification Techniques for Control of Thermal and Fuel-Related Nitrogen Oxide Emissions" (presented at 14th Symposium (Int.) on Combustion), 1972
9. Heap, M.P., T.M. Lowes, R. Walmsley, and H. Bartelds, "Burner Design Principles for Minimum NO_x Emissions," pp 141-171, Proc. Coal Combustion Seminar, 19-20 June 1973, EPA-650/2-73-021 (NTIS No. PB 224210/AS), September 1973.
10. Axworthy, A.E., V.H. Dayan, and G.B. Martin, "Reactions of Fuel Nitrogen Compounds under Conditions of Inert Pyrolysis," FUEL, 57, 29 (1978).

DOCUMENT NUMBER
PAGE NUMBER

CLASSIFICATION
TYPIST 7
PROOFED
CORRECTED
FORM 608-B-31 REV 7-70

(2) devolatilization and pyrolysis under inert, fuel-rich conditions either in a fuel cloud or in the mantle around individual droplets or particles; (3) devolatilization and/or pyrolysis under slightly oxidative conditions as above; and (4) mixing of the devolatilization and pyrolysis products with air and subsequent reaction over a range of stoichiometries. While all of these processes have some elements in common, the actual reaction path of the nitrogen intermediates and the ratio of nitric oxide to molecular nitrogen in the product may be substantially different.

The inert pyrolysis experiments (Ref. 1 and 10) were carried out to investigate the types of reactions that may occur in the fuel-rich preflame zone and to determine if the pyrolysis rates are such that reaction is likely to occur in this zone. The results indicate that fuel-nitrogen compounds form high yields of hydrogen cyanide when pyrolyzed in the absence of oxygen. Since these yields increase with temperature, relatively large amounts of hydrogen cyanide may form in the early stages of a diffusion flame (surrounding a fuel particle or droplet) where the heating rates are quite high. In fact, these results suggest that hydrogen cyanide may be the principal intermediate in the formation of fuel NO_x.

Modeling of the diffusion flame will be required to determine at what point the fuel-nitrogen compounds will decompose thermally. They may be so thermally stable that they can survive far enough into the flame front to react with oxygen species diffusing through the flame before undergoing thermal decomposition. Therefore, oxidative pyrolysis may be an important step in the conversion of fuel nitrogen to NO_x in combustion.

Under Task 1 of the program reported herein, the oxidative pyrolysis of fuels and model fuel-nitrogen compounds was investigated, and the study of the inert pyrolysis of fuels was extended with emphasis on the mode of HCN formation.

In the previous study (Ref. 1), the combustion kinetics of the nitrogen species that could form in the preflame reactions (HCN and NH_3) were investigated in a premixed CH_4-O_2-Ar flame. It was found that HCN is a key intermediate in the formation of NO under fuel-rich conditions whether the nitrogen is added to the feed gas as NH_3, NO or HCN. The HCN, added or formed in the flame front, is converted slowly to NO well above the luminous zone.

These flat-flame burner experiments were extended under Task 2 of the present study to investigate any interaction between the reactions leading to the formation of "fuel" and "thermal" NO_x. In addition, the mechanism of fuel NO_x formation from a simulated low Btu fuel (CO-H_2-NH_3) was investigated experimentally.

Under Task 3, in a joint effort with the Energy and Environmental Research Corporation, an attempt was made to analyze some of the flat-flame burner data from Task 2 using a detailed, quantitative kinetic-diffusion computer model.

TASK 1: FUEL DECOMPOSITION

In the pyrolysis studies that were conducted during the previous program (Ref. 1, 10, and 11), fossil fuels and model nitrogen compounds were pyrolyzed in an inert atmosphere (helium) in small quartz flow reactors. HCN was the major volatile nitrogen compound formed in all cases, indicating that HCN probably forms from nitrogen-containing fuels during the initial, preflame stages of combustion and may be the principal intermediate in the formation of fuel nitric oxide. These previous results are summarized in the next section.

Additional inert pyrolysis experiments were conducted under this task but the major effort involved oxidative pyrolysis studies. HCN yields were measured from coals, fuel oils, and alternative fuels under inert conditions. Most of the inert pyrolysis experiments involved the use of a unique two-temperature-zone reactor to determine whether the HCN is produced directly in the primary vaporization-pyrolysis process or forms later in the secondary reactions of volatile nitrogen species.

In the oxidative pyrolysis experiments, the products were measured as a function of temperature for two model compounds (pyridine and benzonitrile), three oils, and one coal. Two-stage reactors were employed in some of the oxidative studies to investigate again the role of secondary reactions.

BACKGROUND

A brief summary follows of the results of the pyrolysis study conducted under contract 68-02-0635 (Ref. 1 and 10).

---

11. Axworthy, A.E., G.R. Schneider, and V.H. Dayan, "Chemical Reactions in the Conversion of Fuel Nitrogen to NO_x," Proceedings of the (First) Stationary Source Combustion Symposium, September 1975, Vol. I, Fundamental Research, EPA-600/2-76-152a, Rockwell International, Rocketdyne Division, Canoga Park, CA, June 1976.

Preceding page blank

Model Compound Pyrolysis (Inert)

Model compound vapors, diluted to a concentration of 3% in helium, were passed through a quartz capillary reactor at temperatures between 900 and 1100 C with a nominal residence time in the heated zone of 1 second. Samples of the model compound liquid 0.2 µl in size were vaporized into the preheated carrier gas stream before it entered the reactor.

Under these inert pyrolysis conditions, HCN and a carbonaceous residue are the major nitrogen-containing products derived from pyridine and benzonitrile--the two model compounds that were studied in detail. The fraction of the organic nitrogen that is converted to HCN rather than being contained in the residue increases with temperature. The HCN yields from benzonitrile and pyridine at 960 C are 49 and 40%, respectively. At 1100 C, however, the HCN yield from benzonitrile is 82%, and all of the pyridine-N is converted to HCN. No molecular nitrogen and only minor amounts of ammonia form from the inert pyrolysis of the model fuel nitrogen compounds. At the lower temperature, pyridine forms a few percent of benzonitrile, quinoline, and acrylonitrile.

Based on the kinetic parameters obtained from the pyrolysis of the model fuel nitrogen compounds, it was established that even in the absence of oxygen the organic nitrogen compounds present in fossil fuels should decompose in much less than a millisecond at a temperature around 1700 K (Ref. 1). It was postulated, therefore, that when a diffusion flame surrounds a coal particle or oil droplet the volatile fuel-nitrogen compounds will be mostly converted to HCN before reaching the flame front.

Fossil Fuel Pyrolysis (Inert)

Two bituminous coals and six No. 6 fuel oils were rapidly heated in a quartz reactor to either 950 or 1100 C. The volatile pyrolysis products formed were carried through the reactor in a helium stream and the nitrogen-containing species were measured. The fuel samples, 1 to 2 milligrams in size, were placed in a miniature quartz boat that was moved very quickly into the preheated reactor. The residence time of the volatile products in the heated zone was about 1 second.

The fraction of organic fuel nitrogen that was converted to HCN under these conditions ranged from 15 to 25% at 950 C and from 23 to 42% at 1100 C (Ref. 1 and 10). In each case, the amount of HCN formed at 950 C was about six-tenths of that formed at 1100 C. Wilmington crude oil yielded 30% HCN at 950 C and 50% at 1100 C.

The NH_3 and N_2 formed in these fossil fuel experiments were measured together (after converting any NH_3 to N_2). The total amount of NH_3 plus N_2 formed from the fuel oils (measured as N_2) was nearly independent of the nitrogen content of the oil and of the temperature, and ranged from 0.5 to 0.8 micrograms of N_2 per milligram of oil (5 to 29%). Because these values are only slightly greater than the solubility of N_2 in oils, it appears that the amounts of NH_3 and N_2 formed under these inert pyrolysis conditions are quite small (i.e., most of the measured N_2 was dissolved N_2). One of the coals yielded slightly more N_2 plus NH_3 (1.1 micrograms per milligram), but this was equivalent to only 9% of the fuel-N. It was established, therefore, that NH_3 and N_2 are only minor products of the rapid, high-temperature inert pyrolysis of fossil fuels. This would be predicted from the model compound results.

It was assumed that the remainder of the fuel nitrogen was contained in the char and in the carbonaceous residue that formed on the reactor wall from the volatiles. Since it has been demonstrated (Ref. 12) that much of the fuel nitrogen in coals is nonvolatile at these temperatures and would remain in the char, the amounts of HCN formed may represent nearly all of the organic nitrogen contained in these fuels which is volatile at 1100 C. It was not possible to distinguish in these experiments between HCN formed in the primary pyrolysis process and that formed from the secondary reactions of the volatile organic nitrogen species.

---

12. Pohl, J.H., and A.F. Sarofim, "Kinetics of Devolatilization and Oxidation of Coal Nitrogen," 16th Symposium (International) on Combustion, 491, 1976.

INERT PYROLYSIS OF PYRIDINE - CONFIRMATION OF PREVIOUS RESULTS

At the start of this contract, pyridine vapor was pyrolyzed at 1107 and 955 C to ensure that the large HCN yields obtained previously (Table 12 of Ref. 1 and Table 2 of Ref. 10) can be reproduced. Four HCN measurements were made previously at the higher temperature giving a yield of 102 ±4% and three at the lower temperature giving 39.4 ±4.2%. In the present experimental series, two measurements were made at 1107 C, giving yields of 91 and 101% in fair agreement with the previous results. In a single experiment at 955 C, 62% of the pyridine decomposed and 44% of the nitrogen in the decomposed pyridine was converted to HCN, again in agreement with the earlier results.

INERT PYROLYSIS OF FUELS

A few additional inert pyrolysis experiments were carried out in the single-stage fuel reactor developed under the previous contract (Ref. 1). However, most of the inert pyrolysis experiments in this study were done in a two-stage reactor that is very similar in design to the single-stage reactor, but is significantly different in one respect. This two-stage reactor was also used in the study of the oxidative pyrolysis of fuels that is reported in a later section of this report.

In the single-stage reactor developed previously, the fuel pyrolyzes and the volatiles react at about the same point in the reactor. In the two-stage reactor, the stop position of the quartz boat and the 2 cc bubble in which the volatiles react are separated by 15 cm of 2 mm ID tubing. This permits the reaction of the volatiles to be carried out at conditions (temperature and carrier gas composition) different than those under which the fuel undergoes vaporization and the resulting char pyrolyzes. Therefore, the first stage simulates the conditions at or near the surface of a burning fuel droplet or particle, and the second stage the zone between the droplet and the flame front where the temperature and oxygen concentration are increasing.

The available analyses of the fuel samples used in this study are presented in Appendix A.

Experimental

Shown schematically in Fig. 1-1 are the single-stage fuel reactor used in the previous study (Ref. 1) and the two-stage reactor developed and used in the present investigation. In both reactors, the volatiles formed from the pyrolysis of the fuel sample in the quartz boat (that can be moved rapidly into the preheated reactor) flow through a downstream 2 cc volume microreactor in which secondary reactions can occur. In the single-stage reactor, the quartz boat and the microreactor are at the same temperature and the carrier gas is of the same composition at each of these points. With the two-stage reactor, however, the temperatures at the stop position of the boat and at the microreactor can be controlled at temperatures differing by as much as 500 C, and oxygen can be introduced into the microreactor only. Thus, the fuel can be pyrolyzed in helium at a given temperature and the volatiles formed can be reacted downstream at a different temperature in either an inert or oxidizing atmosphere. Only the two-temperature-zone feature of this reactor was employed in the inert pyrolysis experiments. It has been demonstrated in the inert pyrolysis experiments that operation of the two-stage reactor with both stages at the same temperatures gives, as expected, results nearly equivalent to those obtained in the single-stage reactor.

Two-Stage Reactor. The two-stage reactor consists of 2 mm ID quartz capillary tubing that has a 2 cm^3 bulb at a point about 24 cm into the 32 cm heated zone. In the inert pyrolysis experiments, 40 cm^3 (STP)/min helium flows through the reactor at atmospheric pressure. A thin-walled quartz boat, containing a 1.5 to 2.0 mg fuel sample, is quickly moved into the preheated reactor to its stop position about 8 cm into the heated zone. The volatile pyrolysis products are carried through the downstream bulb, where the average residence time is about 0.7 second (at 1100 C), and out of the heated zone. The hydrogen cyanide is scrubbed from the carrier gas stream and measured using the sensitive barbituric acid colorimetric method described in Appendix C of Ref. 1.

USE SPECIAL DROPOUT BLUE PENCIL
ONLY TO IN CORRECTIONS

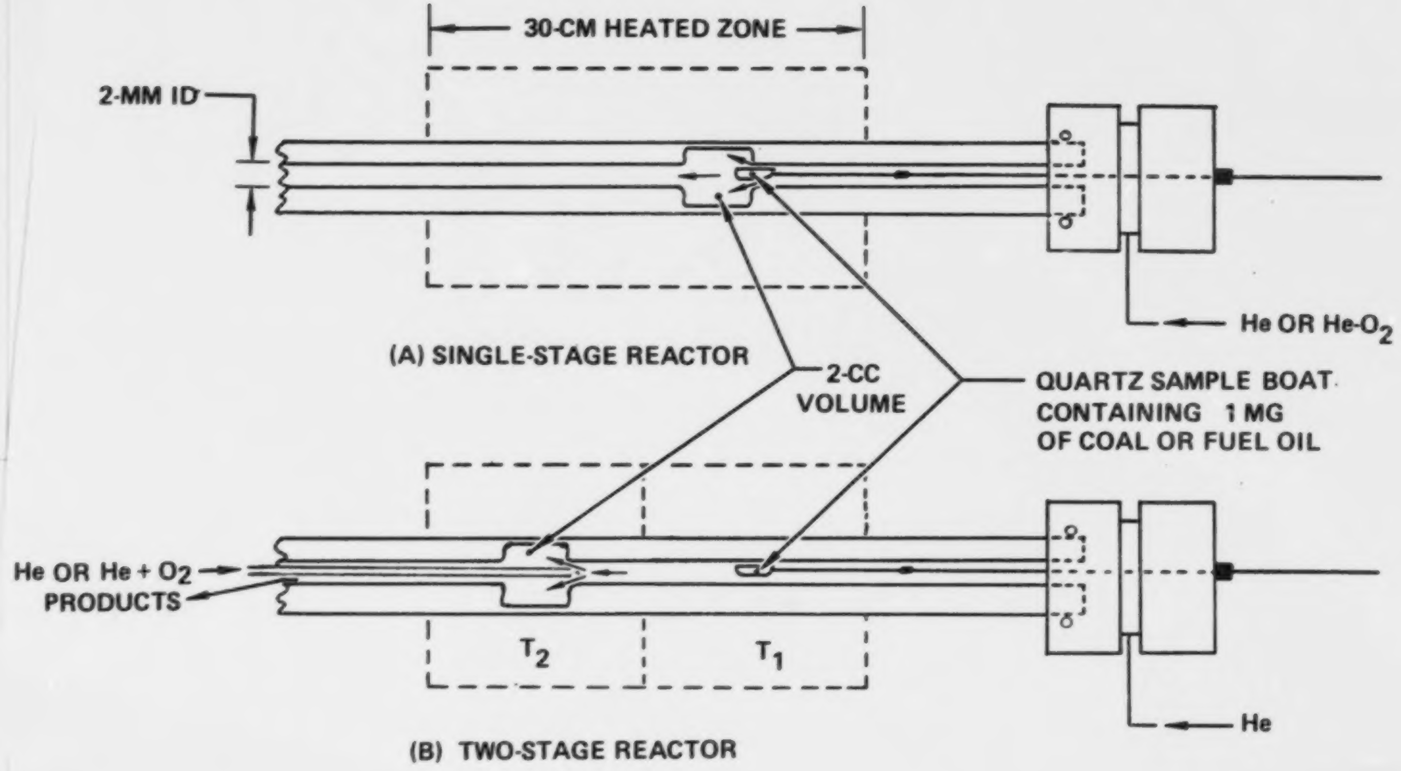
30-CM HEATED ZONE
2-MM ID
He OR He-O_2
(A) SINGLE-STAGE REACTOR
2-CC VOLUME
QUARTZ SAMPLE BOAT CONTAINING 1 MG OF COAL OR FUEL OIL
He OR He + O_2
PRODUCTS
T_2
T_1
He
(B) TWO-STAGE REACTOR

Figure 1-1. Quartz Fuel Pyrolysis Apparatus (Vertical Scale is Greatly Expanded for Clarity)

TYPIST 16

The unique feature of this reactor is that the volatile pyrolysis products can react further at a temperature different from that at which the fuel pyrolyzes (the volume of the first stage of the reactor is only 0.25 cm^3). The center tap of the multitap Marshall furnace is grounded and separate power supplies are connected to each half of the heating element.

The ceramic liner of the Marshall furnace used for the two-stage experiments emitted a volatile material that is corrosive toward quartz. The exterior surface of the first two-stage reactor deteriorated with time and the reactor finally broke. An identical reactor was installed and a quartz sleeve was placed around this reactor to protect it. The quartz sleeve was replaced periodically.

As before, the carbonaceous residue that forms in the reactor was burned out with oxygen after each experiment. A small quantity of HCN was passed through the reactor after every few experiments to determine if the reactor had become catalytic and was promoting decomposition of some of the HCN formed from the fuel nitrogen (Ref. 1). The reactor became catalytic once during the fuel oil experiments and, as expected, several times during the coal experiments. Each time this occurred, the reactor was etched lightly with 30% hydrofluoric acid to return it to a passive condition (Ref. 1) and the experiments run after the previous HCN calibration were repeated.

Single-Stage Reactor. The quartz fuel pyrolysis reactor that was used throughout the 68-02-0635 program was calibrated with HCN in preparation for this program. Repeatable experiments at 1100 C established that 25% of the injected HCN decomposed when the quartz sample boat was in the reactor at its stop position. Moving the boat out of the heated zone resulted in 15% HCN decomposition in duplicate experiments. This reactor and boat were etched with HF after the last coal sample had been run under the previous program and re-etching of the boat at the start of this program did not reduce its activity toward HCN.

A review of these and our previous HCN calibration results has led to the following conclusions: (1) a new quartz surface does not decompose a significant amount of HCN even at 1100 C; (2) when coal is pyrolyzed, a residue that cannot be burned off remains on the quartz surface causing HCN decomposition at 1100 C;

(3) this coal residue can be removed by etching; and (4) after long periods of heating at 1100 C (probably greater than 100 hours) and exposure to carbonaceous residues, the quartz surface becomes porous and catalytic toward HCN decomposition. This last condition, which cannot be changed by etching, was encountered with the model compound reactor during the previous program requiring a new reactor to be installed. In a recent examination of that discarded reactor, it was found that the interior surface is "frosted" in appearance. The fuel reactor boat also developed a porous appearing surface. This slow change in the quartz surface at high temperature could result from devitrification of the quartz or reaction with the carbonaceous residues that are deposited. The latter is more likely since only the interior wall of the reactor becomes frosted.

A new single-stage fuel oil reactor and sample boat were constructed for use during portions of the present program. A calibration gas containing 4% HCN in N_2 was prepared and measured quantities of this gas were used to determine the amount of HCN decomposition in the new fuel reactor. These experiments, with a more appropriate amount of HCN, demonstrated reproducibly that only 4% of the HCN is decomposed at 1102 C, which is in approximate agreement with previous observations with large HCN samples. This extent of HCN loss is taken into account in the HCN formation experiments that are reported.

HCN from Fuels at 1100 C

Before presenting the results obtained under the two-temperature-zone condition, the additional single-temperature results will be reported. Using the single-stage fuel reactor and experimental techniques described previously (Ref. 1 and 10), HCN yields were measured from the inert pyrolysis of two additional oils. These are denoted as samples H and I in Table 1-1. The experiments were conducted at 1100 C to give the maximum yields attainable in this apparatus. The helium carrier gas flowrate was increased from the 20 cm^3 (STP)/min used previously (Ref. 1) to 40 cm^3/min to give the smallest practical residence time (about 0.7 second). The effect of carrier gas flowrate was not investigated but the level of the HCN yields obtained and some chemical kinetic considerations

TABLE 1-1. HYDROGEN CYANIDE YIELDS FROM FUELS UNDER INERT PYROLYSIS CONDITIONS AT 1100 C[(a)]

	Fuel Sample[(h)]	% N	μgm Hydrogen Cyanide Per mg of Fuel	Nitrogen to Hydrogen Cyanide[(g)], %
H.	No. 6 Fuel Oil[(b)]	0.71	6.1	44.5 ±0.3
I.	Liquefied Coal (SYNTHOIL)	1.3	12.8	51.0 ±0.3
J.	Treated Shale Oil[(c)] (Full Boiling Range)	0.27	3.1	60.0 ±1.3
K.	Treated Shale Oil[(c)] (Middle Distillate)	0.18	2.4	69.5 ±2.5
III.	Pittsburgh No. 8 Seam Coal	1.2	5.5	23.6 ±1.5
IV.	Montana Coal[(d)]	0.93	4.8	26.8 ±0.3
V.	Montana Coal[(e)] (Lignite-A, hvA-b)	0.61	2.8	23.8 ±1.6
VI.	COED Char[(f)]	0.99	0.3	1.7 ±0.1

[(a)] 40 cm^3/min Helium Carrier Gas and Atmospheric Pressure

[(b)] Supplied by Ultrasystems Corporation

[(c)] Supplied by Gulf Research and Development Company

[(d)] Supplied by Aerotherm/Acurex Corporation

[(e)] Supplied by Massachusetts Institute of Technology

[(f)] Supplied by University of Arizona

[(g)] Average of Duplicate Experiments

[(h)] Additional Information on These Fuel Samples is Presented in Appendix A discussed later suggest that the HCN yield is relatively insensitive to flowrate at 1100 C.

In addition, two shale oils, three coals, and a char were pyrolyzed under inert conditions in the two-stage reactor with both stages at 1100 C. This should be nearly equivalent to operating the single-stage reactor at 1100 C. The samples pyrolyzed in this manner are denoted in Table 1-1 as J, K, and III through VI.

The No. 6 fuel oil and the three coals listed in Table 1-1 gave HCN yields in the same range (22 to 50%) as did the fuels tested previously (Ref. 1). The liquefied coal (SYNTHOIL) gave a 51% yield and the treated shale oils produced HCN in yields of 60 and 70%, respectively.

The No. 6 fuel oil, sample H in Table 1-1, gave an HCN yield of 44%. This is the largest percentage yield that has been obtained from a petroleum-based No. 6 fuel oil but is less than the 50% HCN yield obtained from Wilmington Crude Oil. The HCN yield from this No. 6 fuel oil amounts to 6.1 μgm HCN per mg of oil (or 6.1 gm of HCN per kilogram), which is about the same as was formed from a No. 6 fuel oil (obtained mainly from California crudes) that contained twice as much fuel nitrogen and from Wilmington Crude Oil (Ref. 1 and 10).

The sample of liquefied coal prepared by the SYNTHOIL process (fuel I in Table 1-1), which contains 1.3% nitrogen, produced twice as much as HCN as any oil that has been tested. The amount of HCN produced was 12.8 μgm/mg, which represents an HCN yield of 51.0%.

The two hydrotreated shale oils gave large HCN percentage yields of 60 and 70%, respectively, under these conditions but the amounts of HCN produced were only 3.1 and 2.4 μgm/mg because of the low nitrogen contents of these treated oils. The first of these oils (J in Table 1-1) was a treated, full-boiling-range shale oil that contained 0.27% N and 0.04 S. The raw oil before treatment contained 2.05% N and 0.57% S. The second oil (K) was a treated middle distillate that contained 0.18% N and 0.04% S after treatment and 1.60% N and 0.57% S before. These shale oils were apparently severely treated because they contain only about

1/8 of the nitrogen present in the untreated oils and about 7% of the sulfur. The full-range shale oil (J) is thixotropic. It will not pour from an open bottle after standing overnight, but becomes very fluid when stirred. Shale oil K, the middle fraction of J, is very fluid. The shale oil samples were introduced into the quartz pyrolysis boat with a 1 microliter syringe giving sample weights of 0.88 and 0.82 milligrams with oils J and K, respectively.

Two additional experiments were carried out with shale oil K in which the sample size was increased to 2 microliters. Under these conditions, the HCN yields increased slightly to 76.9 and 70.2% the average yield being 74% compared with 69% for the smaller sample size. This small increase in HCN yield with sample size could result from the higher average hydrogen concentration in the carrier gas as it passes through the second stage.

These limited results with a liquefied coal and two treated shale oils suggest that the fuel nitrogen compounds in these oils form HCN more readily during rapid inert pyrolysis than do those in No. 6 petroleum-based fuel oils. It would be premature, however, to generalize that alternative fuels of these types are more prone to form fuel NO_x because they may form more HCN in combustion than do petroleum-based oils.

The HCN yields obtained from the inert pyrolysis of three coals at 1100 C are listed in Table 1-1. Two coals were studied previously at 1100 C (Ref. 1). All five of the coals gave HCN yields in the range of 24 to 30%. The amount of HCN produced was from 3 to 8.5 μgm/mg.

A sample of the char from the COED coal liquefaction process (sample VI in Table 1-1) gave only a 2% yield of HCN at 1100 C. This was somewhat expected because the COED process involves a high-temperature pyrolysis that should drive much of the volatile nitrogen out of the char.

HCN from Two-Stage Pyrolysis of Baseline No. 6 Fuel Oil

The inert pyrolysis studies were extended to a two-stage (i.e., a two-temperature-zone) reactor to investigate the role of secondary reactions. It was suggested (Ref. 1) that most of the HCN is formed in secondary reactions of the volatiles rather than in the initial fuel vaporization/pyrolysis process. If this is the case, the HCN yield should increase with the temperature at which the volatiles react and be fairly independent of the vaporization temperature--particularly for oils where the amount of nitrogen left in the residue is expected to be nearly independent of temperature. Listed in Table 1-2 are the HCN yields obtained from a No. 6 fuel oil (sample H in Table 1-1) in the two-stage reactor with various temperature combinations.

TABLE 1-2. HCN YIELDS FROM THE TWO-STAGE PYROLYSIS OF A NO. 6 FUEL OIL[a]

(Atmospheric Pressure, Helium at 40 cc/min)

First-Stage Temperature, C	Second-Stage Temperature, C		
	1100	950	750
	HCN Yield, %		
1100	46.2 ±1.9	41.9 ±1.3	34.8 ±0.8
950	40.8 ±1.2	23.5 ±0.7	13.6 ±1.7
750	38.5 ±2.0	23.7 ±0.4	4.4 ±0.7

[a] Oil H in Table 1-1

The results obtained with both stages at the same temperature, which should be equivalent to the single-stage reactor condition, are plotted on linear scales in Fig. 1-2A and in the Arrhenius form in Fig. 1-2B. Under this single-temperature condition, the HCN yield drops from 46% at 1100 C to 4% at 750 C. The decrease in the HCN yield of a factor of 2 between 1100 and 950 C is in the range observed for other fuels in the single-stage experiments (Ref. 1).

USE SPECIAL DROPOUT BLUE PENCIL
ONLY TO INDICATE CORRECTIONS
CLASSIFICATION
PAGE
STARTING LINE

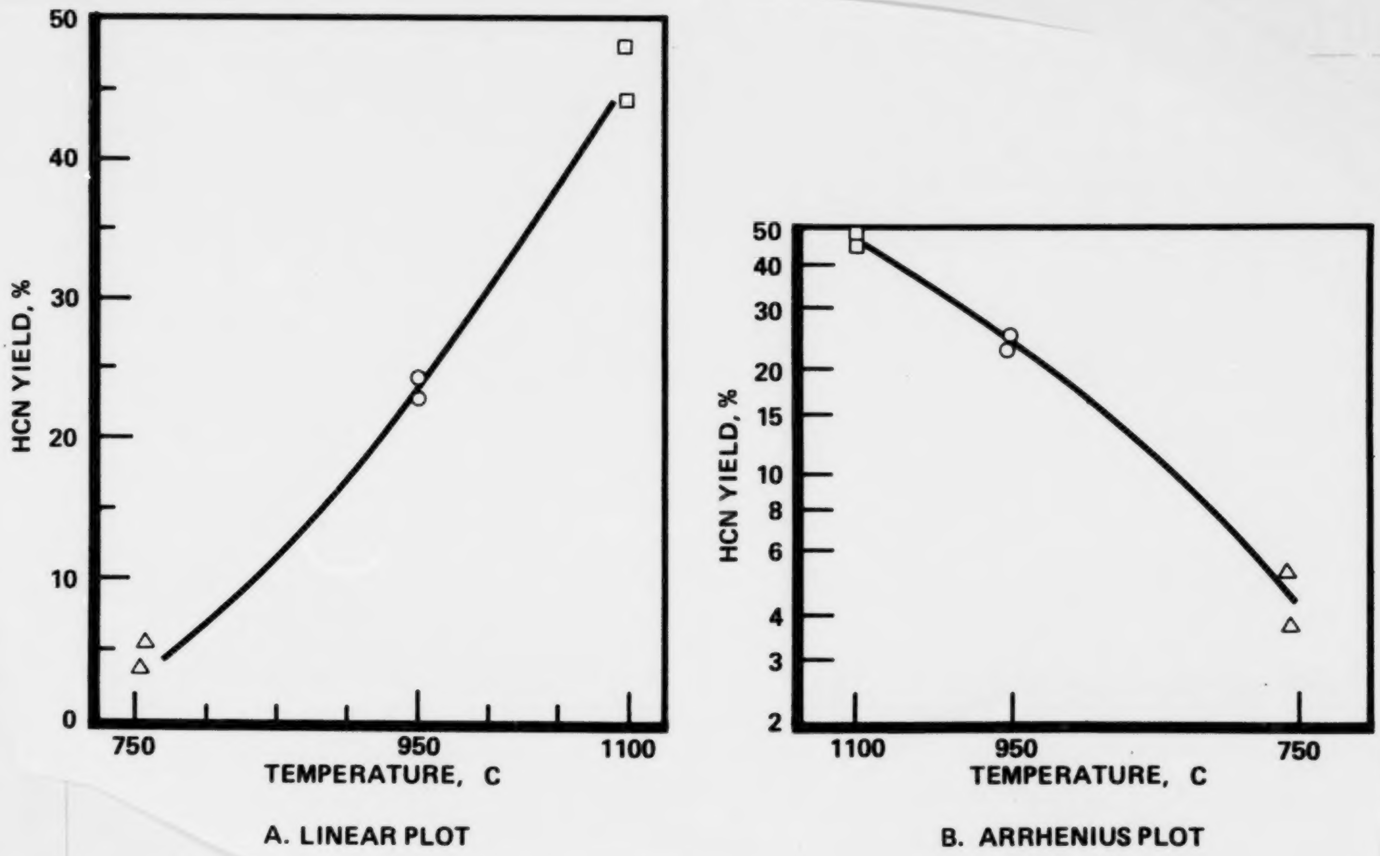

A. LINEAR PLOT

B. ARRHENIUS PLOT

Figure 1-2. HCN Yield vs Temperature in Single-Temperature Inert Pyrolysis of a No. 6 Fuel Oil

The Arrhenius plot in Fig. 1-2B shows a slight curvature, but the average apparent activation energy for HCN formation is 19 kcal/mole over this temperature range. This apparent activation energy may result from a combination of the temperature dependencies of the following factors: (1) the fraction of fuel-N that remains in the fuel residue, (2) the fraction of the volatile fuel nitrogen species that decomposes before exiting the reactor, (3) the formation of HCN from the fuel-N species that do react, and (4) the inclusion of nitrogen in the carbonaceous residue that forms from the volatiles. It will be shown in the next section that the results of two-temperature experiments with this fuel oil indicate that the amount of nonvolatile nitrogen that remains in the residue, effect item (1) above, does not change appreciably over this temperature range.

Since the apparent activation energy in Fig. 1-2B may result from the differences between the activation energies of three individual processes, the activation energy for the chemical reaction that forms HCN may be much larger.

The HCN yields listed in Table 1-2 for various temperature combinations are plotted in Fig. 1-3 as a function of second-stage temperature. With the first stage (boat stop position) at 750 C, increasing the second-stage (2 cm^3 bulb) temperature from 750 to 1100 C increases the hydrogen cyanide yield from 4 to 38% (lower curve). This establishes that under these conditions, at least 34% of the nitrogen in this oil is converted to hydrogen cyanide in the second stage, which is far removed from the zone in which the initial vaporization/pyrolysis process occurs.

The HCN yields obtained with the first stage at 950 C are similar to those obtained with the first stage at 750 C except for a higher yield when the second stage is at 750 C. These results indicate that little additional fuel nitrogen is volatilized when the pyrolysis temperature is increased to 950 C but considerable HCN is now formed in the first stage (an amount that represents at least 10% of the total fuel nitrogen). Even this HCN produced in the first stage is formed in secondary reactions because when the first-stage temperature is lowered to 750 C, this additional amount of HCN forms instead in the second stage at 950 C

USE SPECIAL DROPOUT BLUE PENCIL
ONLY TO INDICATE CORRECTIONS

CLASSIFICATION

PAGE

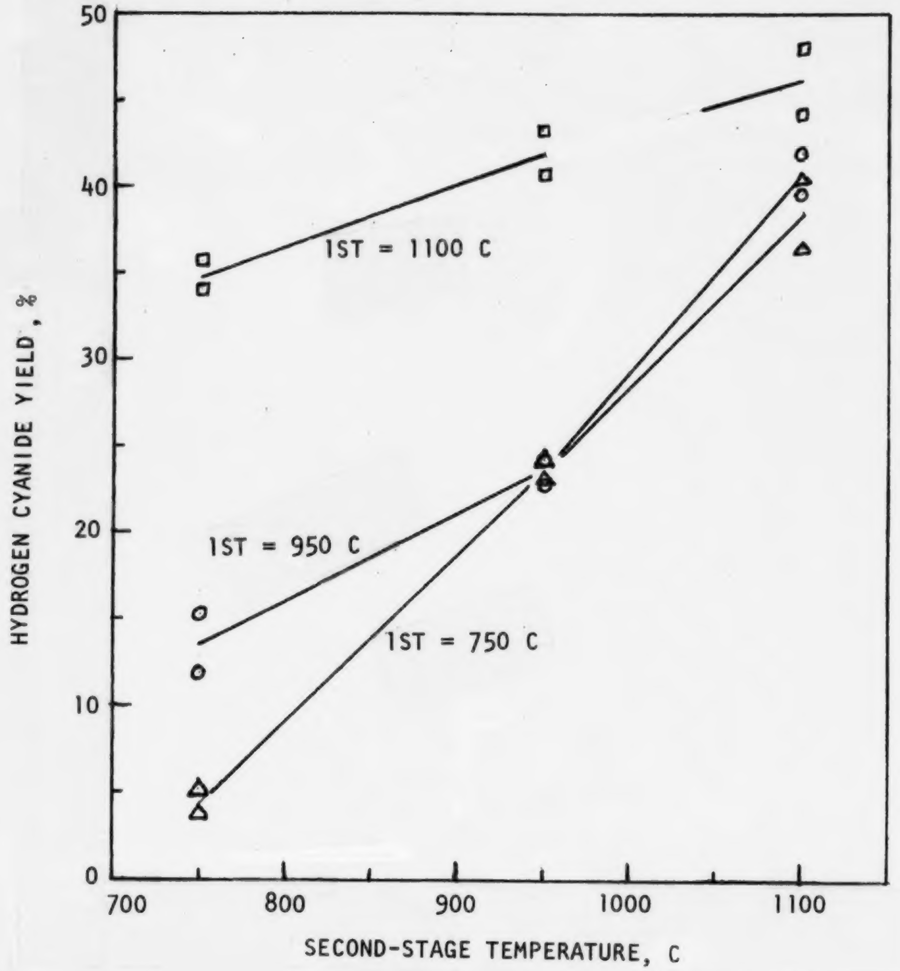

Figure 1-3. Hydrogen Cyanide Yield From The Two-Stage Inert Pyrolysis of a No. 6 Fuel Oil

WARNING LINE

STOP

DOCUMENT NUMBER

CLASSIFICATION

TYPIST

25

(as demonstrated by the yields at a second-stage temperature of 950 C being the same whether the first stage is at 750 or 950 C).

The first stage of the two-stage reactor was constructed of 2 mm ID quartz capillary tubing and had a volume of only 0.25 cc. The second stage contained the 2 cc microreactor in which the volatiles had sufficient residence time to react. The oil samples were nominally 1.8 mg in size; this amount of oil should form about 0.8 cc of hydrogen during pyrolysis (calculated at 950 C). Therefore, the residence time of the volatiles in the first stage will be even less than 10% of the second-stage residence time and the microreactor volume is required to prevent the hydrogen formed from expelling the volatiles from the heated zone before they can react.

When the temperature of the first stage is increased to 1100 C, the maximum yield of HCN (with the second stage at 1100 C) increases to 46% indicating a small increase in the total amount of reactive volatile fuel nitrogen species produced in the first stage. However, the HCN yields with the second stage at 750 or 950 C are much larger when the first stage is at 1100 C. Apparently the rates of secondary pyrolysis of most of the volatile fuel nitrogen species become so high at 1100 C that these species react in the first stage to form HCN despite the short residence time in this temperature zone.

It appears that the HCN yield curves in Fig. 1-3 result from the competition between several complex chemical processes. Based on the results obtained with the model compounds (Ref. 1), we can speculate as to the role of temperature in determining the HCN yields obtained from this fuel oil. Most of the nitrogen in the reacted model compound appeared to either form HCN or be contained in a carbonaceous residue formed on the reactor wall, depending on the temperature. The temperature affected both the fraction of the model compound that reacted and the ratio of HCN formed to the amount of nitrogen contained in the residue formed from the model compound vapors.

The nitrogen compounds in the fuel oil no doubt consist of a mixture of chemical types with a range of "volatilities" and thermal stabilities. When the second stage is at 1100 C, the model compound results suggest that all volatile fuel nitrogen species reaching the second stage will react in the second stage forming HCN in nearly a 100% yield. If this is the case, the yields shown at the right side of Fig. 1-3 represent the amount of volatile fuel nitrogen species formed in the first stage at each temperature. Nearly 40% of the fuel nitrogen is vaporized at 750 C, and, as might be expected for a fuel oil, only a little more is driven off at a pyrolysis temperature of 1100 C. The remainder of the fuel nitrogen presumably remains in the first-stage residue, but we have not attempted to measure the nitrogen contents of the fuel residues.

The model compound results (Ref. 1 and 10) indicate that, when the second stage is at 950 C, part of the volatile fuel nitrogen species will pass through the reactor with the nitrogen structure intact (the 50% decomposition temperatures for the model compounds ranged from 905 to 954 C), part will form HCN and part will be contained in the residue that forms in the second stage. The results at the lower center of Fig. 1-3 indicate that about one-half of the volatile fuel nitrogen that reaches the second stage forms HCN in the second stage at 950 C. Presumably part of the remainder exits the reactor and part is condensed into the second-stage residue.

With the first stage at 1100 C (upper curve in Fig. 1-3), however, most of the HCN forms in the first stage and varying the second-stage temperature has only a small effect on the yield. Although the HCN *yield* has a rather small temperature coefficient (the apparent activation energy of the lower curve in Fig. 1-3 is 17 kcal/mol), the *rate* of pyrolysis of the volatile species should have an activation energy on the order of 70 kcal/mole (Table 1 of Ref. 10). The rate of a reaction with an activation energy this large will increase by a factor of 280 between 750 and 950 C and by another factor of 23 between 950 and 1100 C. It is not surprising, therefore, that the formation of much of the HCN from the volatile nitrogen species should occur in the first stage of the reactor when it is at 1100 C.

When the second stage is at 750 C, the volatile fuel-nitrogen species should pass through the second stage without undergoing any significant amount of reaction. Thus, the HCN yields at the left side of Fig. 1-3 represent the HCN formed in the first stage. With both stages at 750 C, the yield was 4%. Decreasing the second-stage temperature further to 550 C with the first stage at 750 C (not shown in the figure) only decreased the yield to 3%. Therefore, a small amount of HCN either forms in the primary pyrolysis process or forms rapidly at 750 C from thermally unstable non-heterocyclic intermediates (probably amines).

These results establish that most or possibly all of the HCN formed in the inert pyrolysis of this fuel oil forms from the secondary pyrolysis of volatile nitrogen species produced or released in the initial vaporization/pyrolysis process.

HCN From Coals in Two-Stage Reactor

The Pittsburgh No. 8 Seam coal (sample III in Table 1-1) was pyrolyzed at four temperature combinations giving the results listed in Table 1-3. The nominal size of the coal samples was 2 milligrams. The largest yield of HCN was obtained with both stages at a nominal temperature of 1100 C. However, decreasing the first-stage temperature to 750 C did not decrease the yield within experimental error. This result demonstrates that 23% of the fuel nitrogen is contained in volatile reactive nitrogen species produced at 750 C and no additional fuel nitrogen is volatilized at 1100 C (at least not in a reactive form).

TABLE 1-3. HYDROGEN CYANIDE YIELDS FROM TWO-STAGE INERT PYROLYSIS OF A PITTSBURGH NO. 8 SEAM COAL[(a)]

Temperature, C		Nitrogen to Hydrogen Cyanide,[(b)] %
First Stage	Second Stage	
1108	1100	23.6 ±1.5
745	1100	22.6 ±0.3
750	750	7.2 ±0.7
600	1100	17.6 ±1.3

(a) Fuel III in Table 1-1
(b) Average of duplicate experiments

On the other hand, reducing the second-stage temperature from 1100 to 750 C decreases the HCN yield by a factor of three. This establishes that at least two-thirds (and probably much more) of the HCN that forms from this coal with the second stage at 1100 C forms in the second stage from volatile fuel nitrogen species. Therefore, coals and oils behave similarly in that under these inert pyrolysis conditions most of the HCN forms in the secondary pyrolysis of the volatiles produced in the fuel pyrolysis process.

Comparing the second and fourth lines in Table 1-3, it can be seen that the fraction of the bound-nitrogen in this coal that is volatilized is only decreased by one-third when the pyrolysis temperature is decreased from 750 to 600 C. The data from Table 1-3 obtained with the second stage at 1100 C are plotted as solid circles in Fig. 1-4 as a function of the first-stage temperature. The flatness of this curve (sample III) demonstrates the limited effect the pyrolysis temperature has on the amount of volatile nitrogen species produced from this coal over this temperature range.

Coal samples I and II from the previous study (Table 5 of Ref. 10 and Appendix A) were also pyrolyzed with the first stage at 600 C and the second at 1100 C; the HCN yields obtained are also plotted in Fig. 1-4. These data points are connected by broken lines with the yields obtained in the single-stage reactor at 1100 C (Ref. 10). The shapes of the broken curves are uncertain, because no measurements were made at intermediate first-stage temperatures, but they do indicate that the effect of the first-stage temperature is much larger for these two coals.

Finally, the HCN yield from the COED char (sample VI in Table 1-1) was found to be independent of the first-stage temperature (Fig. 1-4).

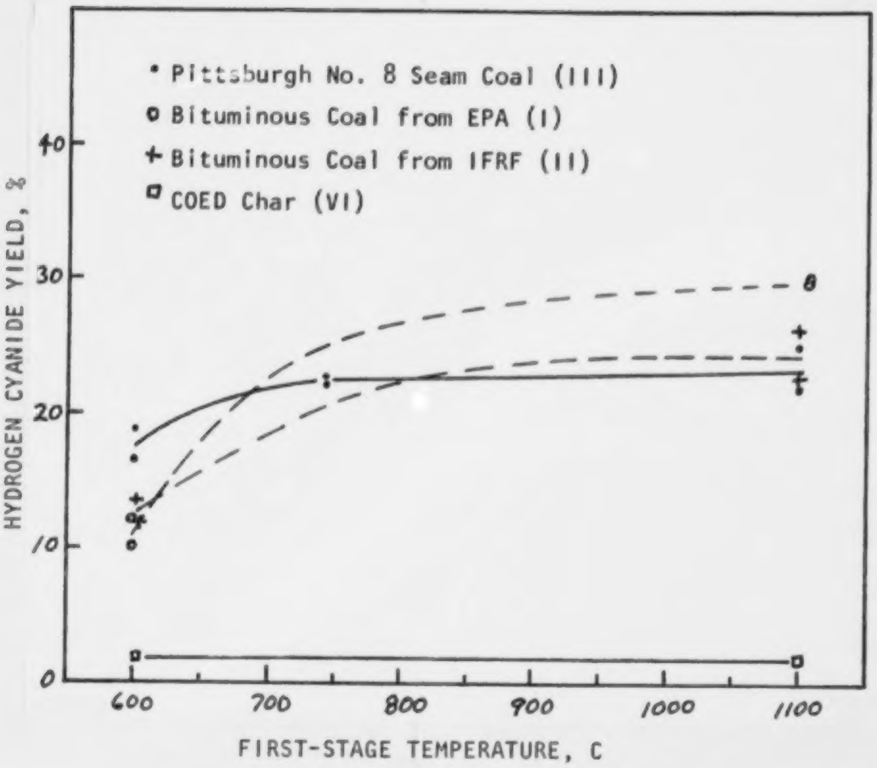

Figure 1-4. Hydrogen Cyanide Yields From The Inert Pyrolysis of Coals With Second Stage at 1100 C

Discussion of a Related Study

Recently Sugiyama et al. reported (Ref. 13) the results of their study of the inert (and oxidative) pyrolysis of the model compound pyridine from 680 to 775 C in a stainless-steel reactor. They obtained much less hydrogen cyanide than we did (Ref. 1 and 10) and state that in our inert pyrolysis study "the formation of molecular nitrogen was not sufficiently examined." This is an interesting claim since they report nitrogen yields of only a few percent from the inert pyrolysis of pyridine in their system. The fact is that by using a quartz reactor we demonstrated that N_2 is not a product of the homogeneous inert pyrolysis of pyridine (Ref. 1). In a stainless-steel reactor, however, we obtained N_2 yields from pyridine of up to 90% (page 33 of Ref. 10), indicating that molecular nitrogen forms via heterogeneous reactions only.

It is our conclusion that the inert pyrolysis data of Sugiyama et al. do not give any information regarding the products of the homogeneous decomposition of pyridine because the temperature was not high enough to decompose pyridine (Ref. 10). In their system in the absence of oxygen, about 30% of the pyridine reacted (catalytically?) before reaching the reactor and virtually none reacted within the reactor (their Fig. 5). The prematurely reacted pyridine formed ammonia in high yield and the ammonia decomposed only slightly while passing through the reactor. If Sugiyama et al. had gone to higher reactor temperatures, our experience indicates that any HCN formed would have decomposed on the wall of their stainless-steel reactor.

Inert Pyrolysis of Oils Doped with Model Compounds

Single-stage inert pyrolysis experiments were conducted at 1100 C with two low-nitrogen-content oils that had been "doped" with benzonitrile or quinoline to bring their nitrogen contents to about 2%. The purpose was to determine if any of the species formed in the pyrolysis of those oils interact with the nitrogen species in some manner that affects the amount of HCN that is formed from the

---

13. Sugiyama, S. et al., "Reducing Fuel NO_x Emission: N_2 Formation from Fuel N," Env. Sci & Tech, 12, 175 (1978).

model compounds. Pyridine was too volatile for such experiments so less-volatile model compounds were used.

A simple volatility test was conducted in which individual 1 microliter samples of (1) model compound, (2) diesel oil, or (3) model compound diluted with the diesel oil were placed on a tared piece of aluminum foil and the weight loss measured as a function of time for several minutes. This simulates the conditions that exist when the fuel samples are being loaded into the boat before it is placed in the cooled side tube of the reactor. Neat pyridine evaporated at an initial rate of about 25% per minute and was lost rapidly under these conditions even when diluted 10:1 in the oil. The diesel oil lost about 1.5% of its weight per minute, but this is not a problem unless a significant portion of the nitrogen additive is lost also. Neat benzonitrile only evaporated about 1.5% per minute indicating that, when diluted in oil, its loss from the sample during loading should be insignificant. Quinoline was not tested in this manner but it should have a satisfactory volatility also.

The results of these doped fuel pyrolysis experiments are listed in Table 1-4. Each result is based on the average of two or three experiments and the reproducibility was quite good. The undoped EPA in-house No. 6 fuel oil gave an HCN yield of 40.7%, which is slightly greater than the yield of 37.0% that was obtained in the previous study (oil E in Table 3 of Ref. 10). In calculating the results of the experiments, it was assumed that the conversion of the base fuel-N to HCN was 40.7%.

TABLE 1-4. INERT PYROLYSIS OF DOPED OILS AT 1100 C

(Single Stage, 20 cc/min Helium)

Oil	Additive, (% by weight)	% Fuel-N	% Additive-N	% Additive-N to HCN
No. 6 Fuel Oil-H(c)	None	0.22	--	40.7 ±0.2(a)
No. 2 Diesel	Benzonitrile (12.74%)	0.03	1.73	80.6 ±1.1(b)
No. 6 Fuel Oil-H	Benzonitrile (15.34%)	0.22	2.08	68.7 ±1.2(b)
No. 2 Diesel	Quinoline (19.29%)	0.03	2.09	63.0 ±0.6(b)
No. 6 Fuel Oil-H	Quinoline (19.03%)	0.22	2.06	63.2 ±0.4(b)

(a) Yield of HCN from Fuel-N (no additive in this oil sample)
(b) Assuming Fuel-N gives 40.7% yield of HCN
(c) See Table 1-1

When benzonitrile was added to a No. 2 diesel fuel (also sold as No. 2 heating oil), an HCN yield of 80.6% was obtained. This is about the same as the 82% yield obtained previously from benzonitrile alone at 1100 C in the model compound apparatus (Ref. 1). When benzonitrile was added to the No. 6 fuel oil, the HCN yield decreased by 15% indicating a small interaction with the fuel decomposition products.

Quinoline gave the same yield of HCN, 63%, when added to either oil. The HCN yield from quinoline alone was not measured in the model compound apparatus but quinoline would be expected to give a somewhat lower yield than benzonitrile because it forms larger amounts of carbonaceous residue (Ref. 1).

The results obtained with the doped oils under these conditions do not indicate any major interaction between the nitrogen compounds and the oil substrate. Because of differences between the molecular weights, however, some of the model compound may pyrolyze before the oil does, thereby masking a part of any interaction that does occur.

Conclusions - Inert Pyrolysis

Our results demonstrate conclusively that nearly all of the HCN that is produced in the inert pyrolysis of fuel oils and coals forms in the secondary pyrolysis of volatile nitrogen species evolved in the initial (primary) pyrolysis of the fuel.

The inert pyrolysis at 1100 C of oils doped with the model compounds benzonitrile and quinoline gave about the same HCN yields as did the neat model compounds. This indicates that there is no major interaction between the nitrogen compounds and the oil substrate under these conditions.

OXIDATIVE PYROLYSIS OF MODEL COMPOUNDS

A detailed study was conducted of the oxidative pyrolysis and oxidation of pyridine and benzonitrile. The major goal was to identify and measure the nitrogen-containing products of oxidative pyrolysis to determine what nitrogen intermediates may be important in the conversion of fuel nitrogen to NO_x in combustion. The model compound vapor was flowed continously through the reactor and an excess of O_2 was employed so that its concentration would remain essentially constant even at complete reaction.

Some preliminary experiments on the oxidative pyrolysis of pyridine and benzonitrile were conducted under the previous program (page 125 of Ref. 1). In those experiments, 0.2 μl samples of the model compound were vaporized into a helium carrier gas stream containing 3 to 10% oxygen. The results at the higher temperatures suggested that the extent of reaction was limited by depletion of the available oxygen. This was probably the case since, as can be seen from Table 1-5, from 3 to 6 moles of O_2 are required to oxidize one mole of pyridine and the peak pyridine concentration in the sample slug was estimated to be about 3% (page 125 of Ref. 1).

TABLE 1-5. STOICHIOMETRY AND MOLE CHANGE IN PYRIDINE OXIDATION

	REACTION	MOLE CHANGE PER MOLE PYRIDINE REACTED
(1)	$C_5H_5N + 3.00\ O_2 = 4\ CO + 2.0\ H_2O + 1.0\ HCN$	+3.00
(2)	$C_5H_5N + 3.00\ O_2 = 5\ CO + 1.0\ H_2O + 1.0\ NH_3$	+3.00
(3)	$C_5H_5N + 1.25\ O_2 = 2.5\ H_2O + (C_5N)_s$	+0.25
(4)	$C_5H_5N + 3.75\ O_2 = 5\ CO + 2.5\ H_2O + 0.5\ N_2$	+3.25
(5)	$C_5H_5N + 4.00\ O_2 = 5\ CO + 2.5\ H_2O + 0.5\ N_2O$	+3.00
(6)	$C_5H_5N + 5.00\ O_2 = 4\ CO_2 + 2.0\ H_2O + 1.0\ HCN$	+1.00
(7)	$C_5H_5N + 5.50\ O_2 = 5\ CO_2 + 1.0\ H_2O + 1.0\ NH_3$	+0.50
(8)	$C_5H_5N + 6.25\ O_2 = 5\ CO_2 + 2.5\ H_2O + 0.5\ N_2$	+0.75
(9)	$C_5H_5N + 6.50\ O_2 = 5\ CO_2 + 2.5\ H_2O + 0.5\ N_2O$	+0.50
(10)	$C_5H_5N + 2.00\ O_2 = 4\ CO + 2.0\ H_2 + 1.0\ HCN$	+4.00
(11)	$C_5H_5N + 5.00\ O_2 = 5\ CO_2 + 2.5\ H_2 + 0.5\ N_2$	+2.00

To get around the problem of oxygen depletion, the procedure was modified under this program so that the concentration of model compound vapor was not more than 1.4% and the carrier gas contained 75% oxygen. In this way only up to about 10% of the oxygen could be consumed even if the model compound were completely oxidized.

Experimental

The experimental procedures employed in this phase of the pyrolysis study were similar to those developed previously (Ref. 1). The model compound experiments were again carried out in a reactor that was simply a heated section of 2 mm ID quartz capillary, but the model compound vapor was continuously passed through the reactor rather than introduced on a batch basis. This permitted the model compound concentration to be held constant and controlled accurately; in addition, the effluent stream could be sampled periodically without timing the sampling procedure.

The experimental conditions and a schematic of the apparatus are presented in Fig. 1-5. In each experiment a 3:1 O_2/He mixture was passed continuously through a quartz capillary reactor (2 mm ID) at atmospheric pressure and a flowrate of 40 cm^3/min (measured at room temperature). The heated portion of the reactor was 30 cm in length. The gas entering the reactor contained 10 torr of model compound vapor in most experiments and 1 torr in others. The reactor effluent passed through a heated line (∿ 200 C) to a 5 cm^3 loop in a heated Carle gas sampling valve from which samples were diverted periodically to gas chromatographs, or through an aqueous bubbler system to collect the HCN or NH_3 for colorimetric analysis (Ref. 1).

The concentration of the model compound in the carrier gas entering the reactor was controlled by the temperature of the liquid sample in the saturator (Fig. 1-5). Because the saturated helium is diluted 3:1 with O_2 before entering the reactor, the water bath around the saturator was held at the temperature where the model compound vapor pressure was either 40 or 4 torr. For pyridine these temperatures are 38.0 and 0 C, respectively. For benzonitrile they are 100 and 37 C.

Conditions for the gas chromatographic analyses of the product gas stream were as follows:

Gas Constituent	Column	Temperature	Detector
Unreacted model compound and organic products	Chromosorb 103	Temperature programmed (60 to 240 C)	Flame ionization
N_2 and CO	Molecular sieve 5A	Ambient temperature	Thermal conductivity
N_2O and CO_2	Molecular sieve 5A	Isothermal 160 C	Thermal conductivity
$(CN)_2$	Poropak Q	120 C	Thermal conductivity

A. CONDITIONS

- 2-MM ID QUARTZ REACTOR
- 40 CC/MIN OF 75% O_2 - 25% He CARRIER GAS
- ATMOSPHERIC PRESSURE
- CONTINUOUS FLOW OF SAMPLE VAPOR

  1.4 MOLE PERCENT IN MOST EXPERIMENTS

  0.14 MOLE PERCENT IN SOME
- MEASURED UNREACTED COMPOUND, ORGANIC PRODUCTS, HCN, NH_3, NO, NO_2, N_2O, CO, CO_2, AND $(CN)_2$

B. APPARATUS

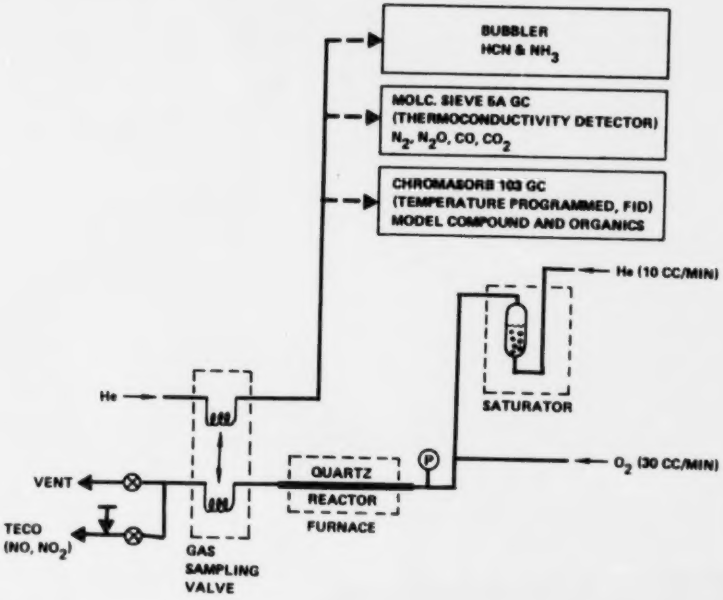
BUBBLER
HCN & NH_3
MOLC. SIEVE 5A GC
(THERMOCONDUCTIVITY DETECTOR)
N_2, N_2O, CO, CO_2
CHROMASORB 103 GC
(TEMPERATURE PROGRAMMED, FID)
MODEL COMPOUND AND ORGANICS
He (10 CC/MIN)
SATURATOR
He
O_2 (30 CC/MIN)
P
QUARTZ
REACTOR
FURNACE
VENT
TECO
(NO, NO_2)
GAS
SAMPLING
VALVE

Figure 1-5. Model Compound Oxidative Pyrolysis

In addition to the use of gas chromatographic analysis and the aqueous bubbler system, the amount of NO_x formed was evaluated by flowing the reactor effluent directly into a TECO chemiluminescence NO_x analyzer (with sample-flow-control capillary removed). A needle valve was placed between the reactor and the CA so that atmospheric pressure could be maintained in the model compound reactor. NO_2 was measured also by employing Saltzman's reagent in the bubbler. However, calibration with an NO_2 standard indicated that the amount of NO_2 measured (by either method) was much less than that actually entering the system. Apparently, the NO_2 reacts with moisture on the walls of the system downstream of the reactor. Also, it was found that much of any NO formed may not be recovered in these oxidative pyrolysis experiments (see Appendix B).

The modifications to the chemical analysis procedures required by the use of a carrier gas consisting mainly of oxygen are discussed in Appendix B. No major modifications were required for the model compound experiments because the sampling loop contained only 3 cm^3 (STP) of carrier gas when heated. In the oxidative pyrolysis of fuel (reported in a later section), however, over 100 cm^3 of carrier gas passed through the sampling system and most of the fuels contained sulfur. Considerable modifications were required to the trapping and analysis procedures (Appendix B) for those conditions. The small change in volume of <4% from the increase in the number of moles in the model compound experiments (Table 1-5) was ignored in calculating the product yields.

Effect of Temperature and Concentration on Oxidative Pyrolysis Rates

Shown in Fig. 1-6 as a function of temperature are the amounts of pyridine and benzonitrile remaining unreacted. Benzonitrile is much more stable than pyridine under the conditions of oxidative pyrolysis investigated. Reducing the reactant concentrations by a factor of 10 had only a small effect on the fraction reacted at a given temperature. This is in contrast to the inert pyrolysis results (Fig. 29 of Ref. 1), where a decrease in the pyridine concentration by an order of magnitude increased the 50% decomposition temperature by 60C. Measurements were not made with the higher concentration of benzonitrile below 720 C because a low volatility product forms at the lower temperatures which results in the eventual plugging of the system downstream of the reactor. A similar product formed from pyridine but not to as great an extent.

USE SPECIAL DROPOUT BLUE PENCIL
ONLY TO INDICATE CORRECTIONS
CLASSIFICATION
PAGE
START LINE

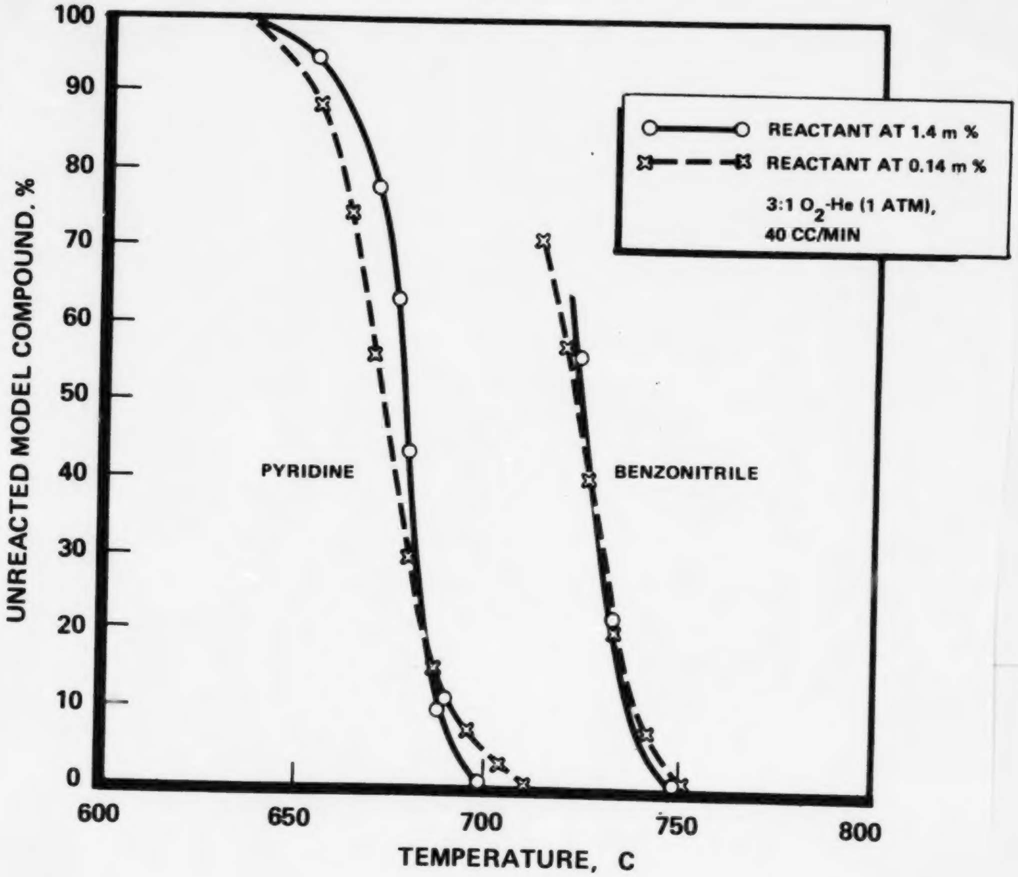

Figure 1-6. Extent of Reaction as a Function of Temperature and Model Compound Concentration

CENT
WARNING LINE
STOP
DOCUMENT NUMBER
PAGE NUMBER

CLASSIFICATION
TYPIST

Comparison of Fig. 1-6 with Fig. 29 and 33 of Ref. 1 demonstrates the accelerating effect of oxygen on the reaction rates of the model compounds. For pyridine the 50% decomposition temperature decreases from 954 to about 670 C and for benzonitrile from 922 to 730 C. Fig. 1-6

Products from Pyridine at Higher Concentration

The yields of nitrogen-containing products from the oxidative pyrolysis of pyridine are plotted in Fig. 1-7A as a function of temperature, and the carbon product yields are shown in Fig. 1-7B. The unreacted pyridine curve from Fig. 1-6 is reproduced on each of these plots for reference. The upper curves in Fig. 1-7A and 1-7B demonstrate that, within experimental error, all the nitrogen and carbon present in the pyridine is recovered in the volatile products above about 750 C. At lower temperatures, the recoveries decrease with both the nitrogen and carbon recoveries being about 80% at 720 C. This indicates that the C/N molar ratio in the nonvolatile products is about 5 as it is in pyridine. At temperatures below 750 C, a carbonaceous residue slowly builds up downstream of the reactor. Fig. 1-7A Fig. 1-7B

Only a few very small organic product GC peaks were obtained even at temperatures where only part of the pyridine reacted. This indicates that the organic products and intermediates formed are more reactive than the pyridine under similar conditions. The largest organic product peak has the same retention time as does acetonitrile on the Chromosorb 103 column (51% that of pyridine) but accounted for less than 10% of the nitrogen in the reacted pyridine.

At temperatures below 720 C, HCN is the major volatile nitrogen-containing product from pyridine (Fig. 1-7A), but NH_3 is also formed in appreciable quantities. This is in contrast to the results obtained in the previous inert pyrolysis study wherein NH_3 was formed in only very minor amounts. N_2O was found to be an appreciable oxidation product of pyridine, starting at 710 C, with the yield increasing to 45% at about 770 C. Molecular nitrogen, which was not formed in the inert pyrolysis of pyridine, does not form at 710 C, but its yield increases rapidly at slightly higher temperatures (in the same region where the yields of HCN and NH_3 decrease rapidly). The yields of NO and NO_2 from pyridine, shown

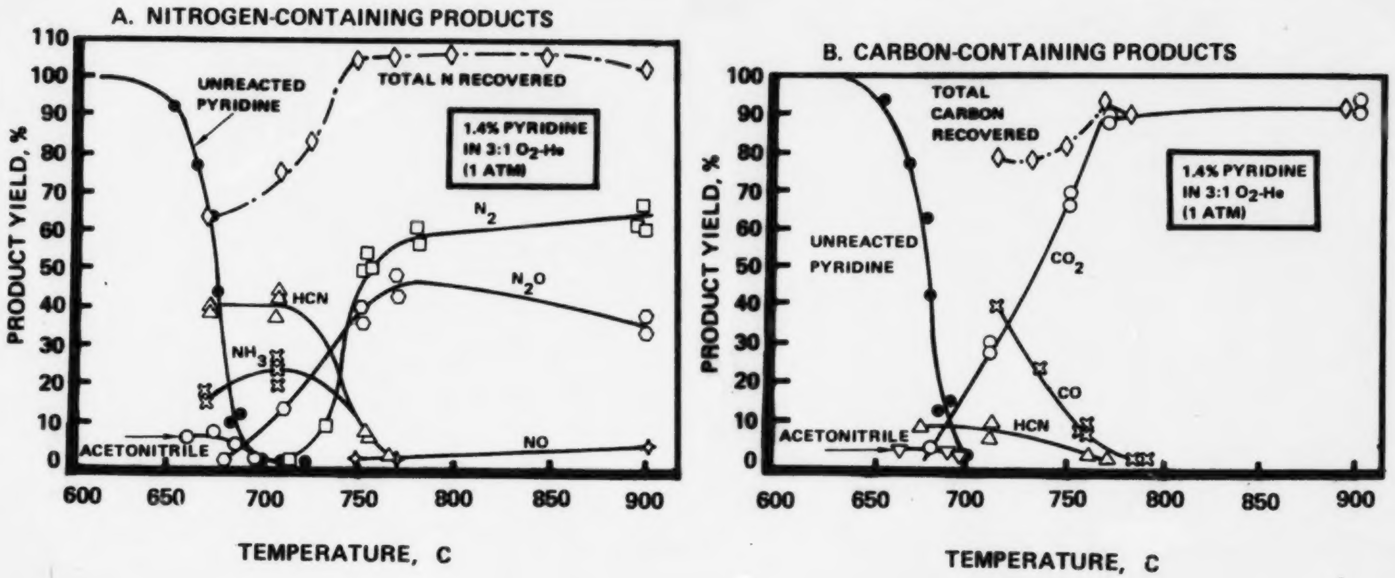

Figure 1-7. Products From Oxidative Pyrolysis of Pyridine
(yields based on reacted pyridine)

below, were quite small under these conditions (i.e., at the higher pyridine concentration), reaching maximum values at 900 C (but, note from Appendix B that these are only lower limits):

Temperature, C	Yield, %	
	NO	NO_2
710	0.7	0.05
749	0.5	0.1
900	3	0.7

Because cyanogen could form from the oxidative pyrolysis of pyridine and can interfere with the barbituric acid method for HCN, $(CN)_2$ was measured on a Poropak Q column. Its yield from pyridine at 710 C was only 0.7% Quantities of $(CN)_2$ equivalent to a yield of only a few percent were passed through the system and over 90% recoveries were obtained. This demonstrates that all $(CN)_2$ present in the products was measured and establishes the yield from pyridine at less than 1% at this condition.

At 720 C, equal amounts of CO and CO_2 are formed from pyridine (Fig. 1-7B). As the reactor temperature is increased, the CO yield decreases rapidly between 720 and 750 C while the CO_2 increases even more rapidly. The rate at which CO_2 should form via the homogeneous oxidation of CO (i.e., through the reaction $CO + OH = CO_2 + H$) can be estimated as follows. Extrapolating the high-temperature rate expression derived from the post-flame gas results of Sobolev (Ref. 14) to our conditions gives the predicted half-lives shown in the following tabulation (assuming that the mole fraction of H_2O is 0.03). Sobolev's data were obtained in the temperature range of 1600 to 2100 C so extrapolation to pyrolysis temperatures involves a rather large uncertainty. It can be seen from the tabulation,

---

14. Sobolev, G.F., "High Temperature Oxidation and Burning of Carbon Monoxide," Seventh Symposium (International) on Combustion, p. 386, 1958.

Temperature, C	550	600	650	700	750
CO Half-Life, sec					
Sobolev	0.9	0.4	0.2	0.07	0.04
Dryer	1.9	0.5	0.15	0.05	0.02

however, that the CO oxidation rate expression obtained by Dryer and Glassman (Ref. 15) in which the parentheses denote concentrations in moles/cm^3:

$$d\ln(CO)/dt = 10^{14.6}\exp(-40{,}000/RT)(H_2O)^{1/2}(O_2)^{1/4},\ \text{sec}^{-1} \qquad (1)$$

gives similar CO oxidation rates. This rate expression is based on data obtained over the temperature range 760 to 960 C, which overlaps the temperature range of the pyridine experiments.

The residence time of the carrier gas in the heated zone of the reactor under these conditions (1 atm, 40 cm^3/min, and 700 C) can be calculated from the upper curve in Fig. 28 of Ref. 1 for which the residence time was 0.6 second. Correcting the residence time for the differences in temperature, pressure, and flowrate gives 0.4 second for the present conditions. It can be seen from the above tabulation that one-half of the CO should react at 600 C under these conditions. Thus, little CO would be produced in the reaction products at 700 C even if much were to form initially. There is no apparent explanation for this discrepancy. A lower H_2O concentration would reduce the oxidation rate of CO but 98% of the expected H_2O (Table 1-5) would have to form H_2 instead to account for the observed CO since the oxidation rate is proportional to $(O_2)^{1/2}$.

---

15. Dryer, F., D. Naegeli, and I. Glassman, "Temperature Dependence of the reaction $CO + OH = CO_2 + H$," Combustion and Flame, 17, 270 (1971).

Products from Pyridine at Lower Concentration

The NO and NO_2 percentage yields (Fig. 1-8) were considerably higher when the pyridine concentration in the reactor feed was lowered by an order of magnitude. No other product measurements were carried out under these conditions because the sample sizes were quite small.

Products from Benzonitrile at Higher Concentrations

The products from the oxidative pyrolysis of benzonitrile are plotted in Fig 1-9. As with pyridine, nearly all the carbon is recovered in the volatile products above 750 C. Nitrogen recovery is approximately quantitative at 750 C, but drops off to about 80% at higher temperatures. At 722 C, where only 42% of the benzonitrile reacts, the recoveries of carbon and nitrogen (based on the reacted benzonitrile only) are 43 and 49%, respectively. This indicates that the C/N ratio in the nonvolatile products, which apparently form in a 45% yield at this temperature, is the same as in benzonitrile (i.e., a molar ratio of 7), suggesting that some type of "oxidative polymerization" takes place at the lower reaction temperatures.

Comparing Fig. 1-7A and 1-9A, it can be seen that the nitrogen products from benzonitrile and pyridine are quite similar. The major differences are that with benzonitrile the N_2O yield drops off to only 15% at the higher temperatures, and NO forms in 20% yield while NO was only a minor product from pyridine (at the higher concentration being discussed in this section). By coincidence, each of the four products (HCN, NH_3, N_2O, and N_2) are produced in about 25% yield from benzonitrile at 740 C (based on nitrogen in the reacted benzonitrile). The maximum NH_3 yield is about the same ($\sim$25%) from each of the two model compounds. However, the maximum HCN yield was only 25% from benzonitrile, compared with 40% from pyridine.

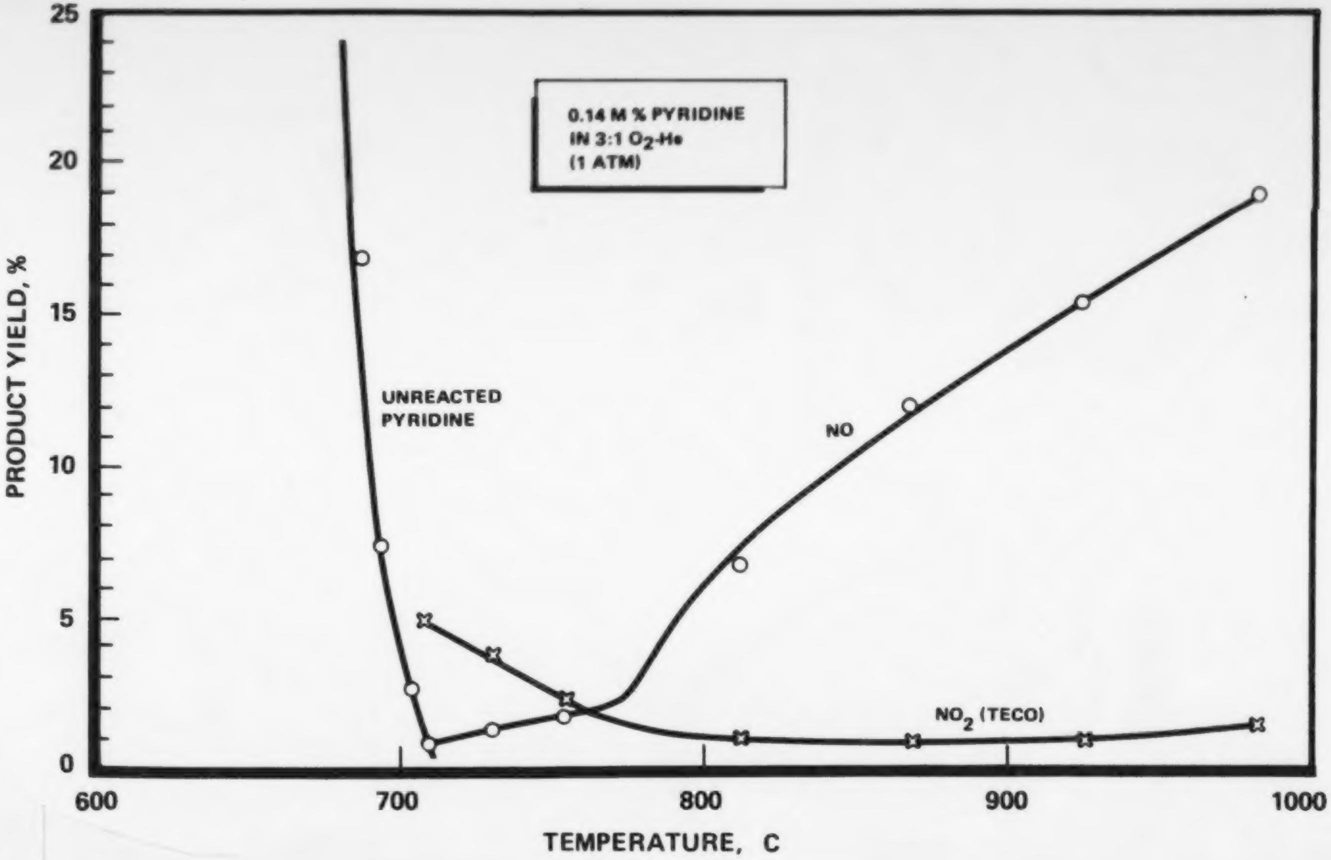

Figure 1-8. NO and NO_2 Yields From Pyridine (lower concentration experiments)

USE SPECIAL DROPOUT BLUE PENCIL
ONLY TO INDICATE CORRECTIONS
CLASSIFICATION
PAGE

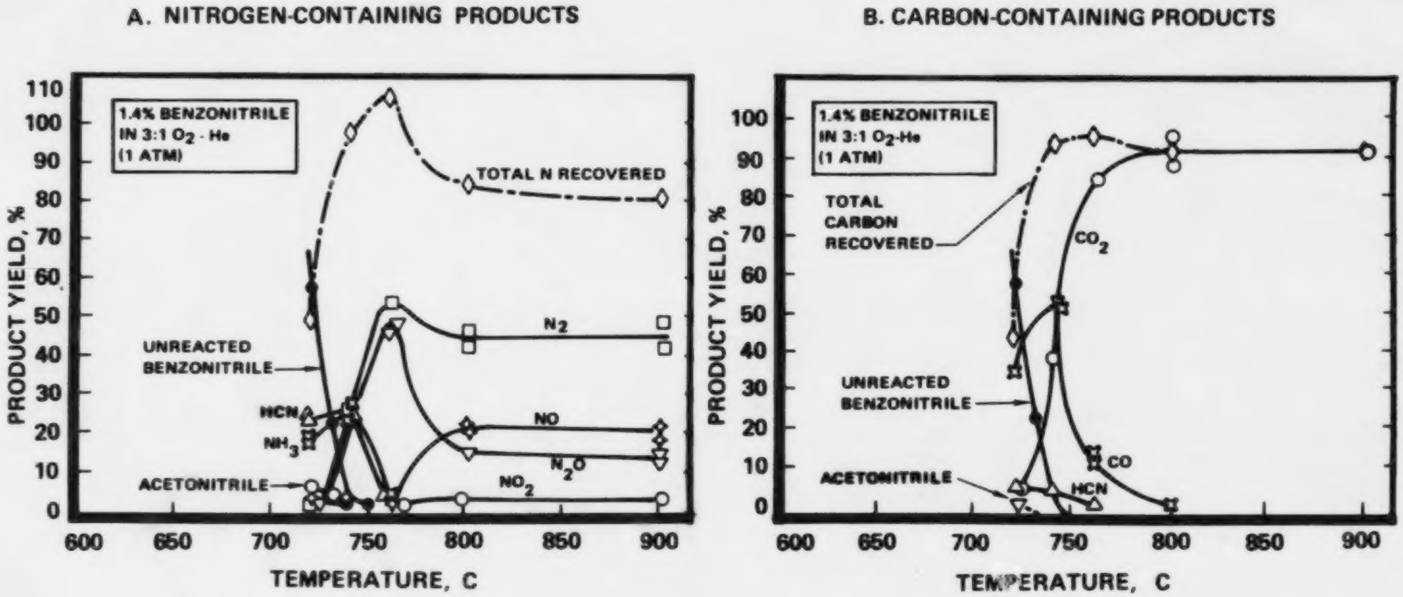

Figure 1-9. Products From Oxidative Pyrolysis of Benzonitrile
(yields based on reacted benzonitrile)

In both Fig. 1-7A and 1-9A, the N_2 yield increases abruptly from nearly zero at 720 C to about 53% at 750 C. The N_2 yield from pyridine continues to increase at higher temperatures; for benzonitrile, however, the N_2 yield decreases to 45%. Although the N_2O yield from both pyridine and benzonitrile reaches the same maximum (about 47%), the N_2O curves are quite different in shape. Benzonitrile forms no N_2O at 720 C, whereas pyridine forms about 15%. The N_2O yield from pyridine only decreases slightly from its maximum value as the temperature is increased, but the N_2O yield from benzonitrile drops to about 15% at temperatures above 800 C. For reasons that are not apparent, the total nitrogen species balance from benzonitrile also falls off at the higher temperatures, i.e., the increase in NO yield is not large enough to account for the decreased yields of N_2O and N_2.

The NO_2 yield from benzonitrile was low, reaching about 2% above 800 C. One possible explanation for the low nitrogen recovery from benzonitrile between 800 and 900 C would be that 20% or more NO_2 was actually formed in this region, but most of it was lost before reaching the TECO CA. Some of the NO_2 calibration experiments indicate that one mode of NO_2 loss, probably reaction with moisture on the wall, results in the formation of one-half mole of NO per mole NO_2 reacted. Thus, if 40% NO_2 formed from benzonitrile at the higher temperatures and reacted in this manner, this would account for the 20% yield of NO and the 20% of the nitrogen that is missing (see also the analysis problems in Appendix B).

Comparing Fig. 1-7B and 1-9B, the CO_2 and CO yield curves are quite similar. The CO_2 first approaches its maximum at about 760 C in both cases and the CO "burns out" at only a slightly higher temperature in the pyridine experiments than in the benzonitrile experiments.

Products from Benzonitrile at Lower Concentration

The NO and NO_2 yields from the oxidative pyrolysis of benzonitrile at the lower concentration are plotted in Fig. 1-10. These results are similar to those obtained in the lower concentration pyridine experiments. It is noteworthy that of the four conditions studied (two model compounds at two concentrations), only pyridine at the higher concentration (Fig 1-7A) did not produce about 20% NO at 900 C. An explanation for this is not apparent.

F. 1-10

Discussion of Model Compound Oxidative Pyrolysis Results

It can be seen from Fig. 1-7A and 1-9A that HCN, which is a major product of inert pyrolysis, is also formed in appreciable yields in oxidative pyrolysis. Ammonia, on the other hand, is a major product of oxidative pyrolysis although it was not important under inert pyrolysis conditions. It is not possible to establish from these data if the change in product composition as the reactor temperature is increased results from a change in the primary products of oxidative pyrolysis or from secondary reactions of the primary products before they exit the reactor. Other experiments, described in the next section, demonstrate that secondary reactions are important.

If secondary reactions are controlling the product distributions at the higher temperatures, the differences between the products from pyridine and benzonitrile must result mainly from the secondary reactions of the low-volatility products that are formed from the model compounds in the initial pyrolysis process. At temperatures below about 750 C, much of this material exits the reactor, leading to incomplete carbon and nitrogen balances and to the formation of deposits at the reactor exit and in the sampling valve. At higher temperatures, all of this low-volatility material reacts before exiting the reactor (at least in the case of pyridine) and may, therefore, affect the product distribution.

The results of this portion of the program have demonstrated that NH_3 and, somewhat surprisingly, N_2O must be considered in addition to HCN as possible intermediates in the formation of fuel NO_x in combustion.

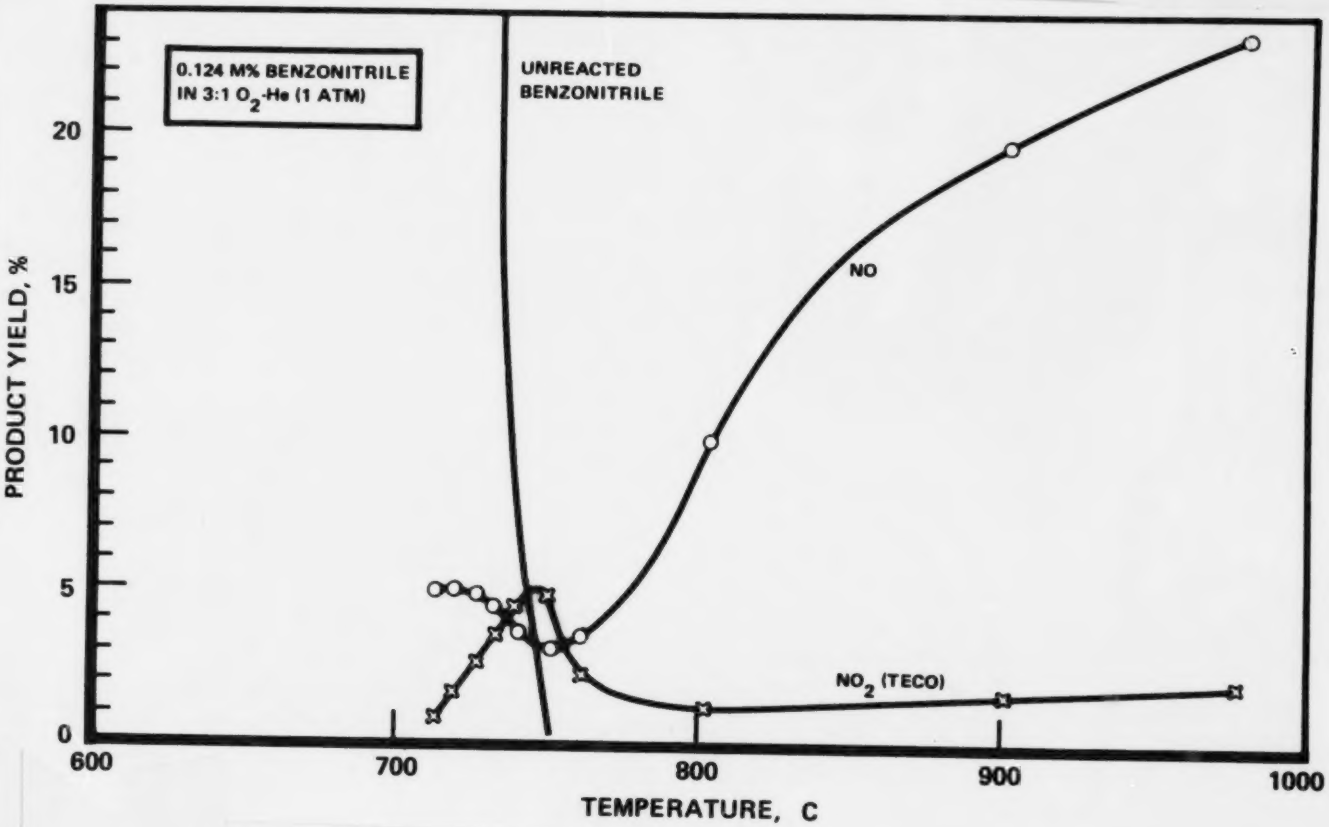

Figure 1-10. NO and NO_2 Yields From Benzonitrile (lower concentration experiments)

SECONDARY REACTIONS IN MODEL COMPOUND OXIDATIVE PYROLYSIS

It appears that an understanding of the marked changes in product distribution that occur over a rather narrow temperature range, Fig. 1-7A and 1-9A, will be important in the development of a detailed mechanism for fuel NO_x formation in combustion. For that reason, additional experiments were conducted to investigate directly the oxidation of HCN and NH_3 and indirectly all secondary reactions that might be occurring. The indirect study of the secondary reactions involved pyrolyzing pyridine in a two-temperature-zone reactor.

F 1-9A

Oxidation of HCN and NH_3

HCN and NH_3 were major products from both pyridine and benzonitrile but their yields fell off rapidly between 710 and 760 C, and the yields of N_2O and N_2 continued to increase rapidly in this temperature regime (Fig. 1-7A and 1-9A). This behavior could result from (1) a decrease in the primary yields of HCN and NH_3 with temperature, or (2) the oxidation in this temperature region of the HCN and NH_3 that still form in similar quantities in the primary process, or (3) reaction of HCN and NH_3 with other species that are present. Some preliminary experiments were carried out to determine the rate of consumption of HCN and NH_3 via reaction with O_2 alone under these conditions.

The results of this initial series of experiments to determine the oxidative stability of HCN and NH_3 are shown in Fig. 1-11. HCN and NH_3 were mixed separately with the 3:1 O_2/He carrier gas and passed through the model compound reactor under the usual conditions. The NH_3 results were unusual in that a larger extent of reaction occurred at 764 C than at 821 C. There is no apparent explanation for this since each data point in Fig. 1-11 represents two experiments that gave good reproducibility.

In Fig. 1-7A and 1-9A, the NH_3 and HCN yields from pyridine and benzonitrile become very small at about 770 C. It can be seen from Fig. 1-11 that the low

USE SPECIAL DROPOUT BLUE PENCIL
ONLY TO INDICATE CORRECTIONS
CLASSIFICATION
PAGE

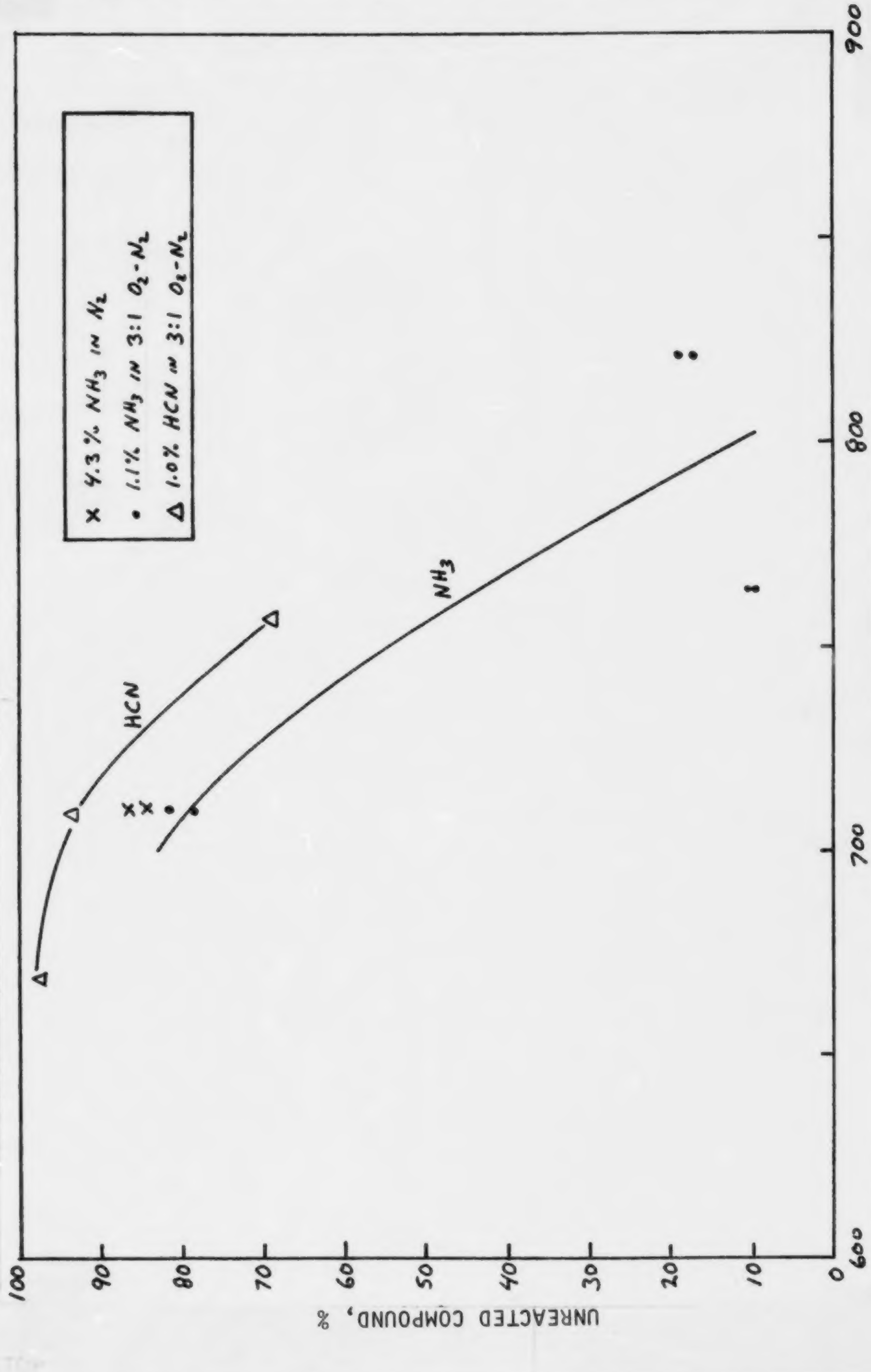

Figure 1-11. Oxidation of HCN and NH_3 Under Pyrolysis Conditions

DOCUMENT NUMBER
PAGE NUMBER
CLASSIFICATION

NH_3 yield from the model compounds at 770 C could result from the subsequent oxidation of most of the NH_3 that formed from the model compound but HCN is sufficiently stable at this temperature that its low yield must result from another cause.

Similar experiments with HCN and NH_3 were carried out a year later. The results are listed in Table 1-6 and plotted in Fig. 1-12. Also plotted in Fig. 1-12 for comparison are the HCN and NH_3 yields obtained previously from pyridine and benzonitrile. In the experiments in Table 1-6, a mixture containing 1% additive (HCN or NH_3), 24% N_2 and 75% O_2 flowed through the single-stage model compound reactor, as before, at a flowrate of 40 cm^3/min and atmospheric pressure. The unreacted HCN or NH_3 was determined by use of the Carle gas sampling valve and the bubbler.

T1-6
F1-12

TABLE 1-6. EXTENT OF REACTION OF NH_3 AND HCN AS A FUNCTION OF TEMPERATURE (1% added to 3:1 O_2/N_2, experiments listed in chronological order)

NH_3		HCN	
Temperature, C	% Unreacted	Temperature, C	% Unreacted
308	101 ±1.5	308	97.9 ±0.4
602	96.3 ±0.2	604	102.2 ±0.4
700	103 ±5	700	86.9 ±1.1
760	46.3 ±0	760	63.4 ±0.1
820	2.8 ±0.3	820	3.9 ±0.3
790	4.1 ±0.1	790	30.5 ±0.3
760	46.9 ±0.9	778	42.5 ±0.3
775	19.1 ±0.4	734	83.0 ±0.4
745	65.0 ±1.6		
701	93.5 ±1.7		

Some reproducibility problems were encountered initially in the NH_3 experiments and these were traced to hang-up of some of the NH_3 in the stainless-steel line

USE SPECIAL DROPOUT BLUE PENCIL
ONLY TO INDICATE CORRECTIONS
CLASSIFICATION
PAGE
STARTING LINE

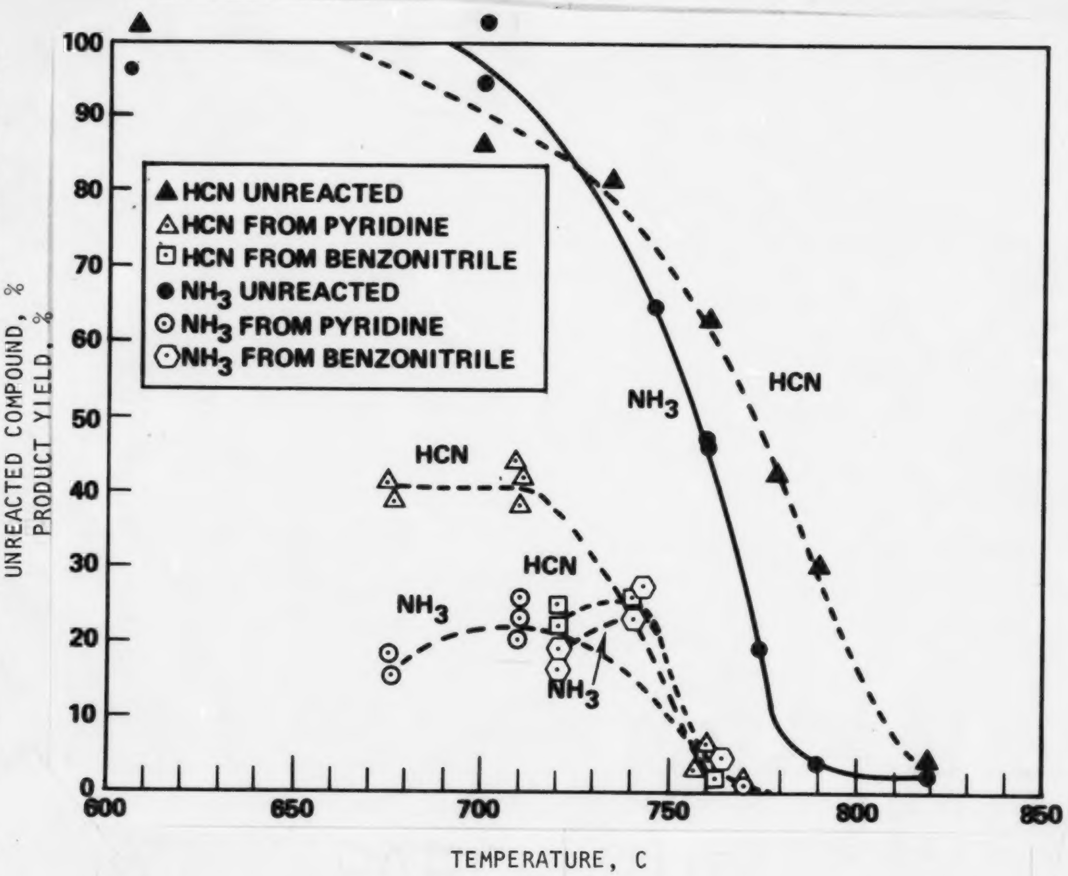

Figure 1-12. Comparison of Rates of Oxidation of HCN and NH_3 With Yield Profiles From Model Compounds (in 75% O_2 at 1 Atmosphere)

WARNING LINE
STOP
DOCUMENT NUMBER
PAGE NUMBER

CLASSIFICATION
TYPIST

53

to the bubbler and the later evolution of this NH_3. This may have been responsible for the unusual results that were obtained in the NH_3 experiments in Fig. 1-11. It can be seen from Fig. 1-12, that as in Fig. 1-11, the fraction of the NH_3 that reacts increases rapidly between 730 and 790 C. This overlaps the region in which the NH_3 yields from the model compounds decrease rapidly indicating that part of this decrease may result from NH_3 reaction with O_2. It does not appear, however, that this is the only factor involved since nearly one-half of the added NH_3 remains unreacted at 760 C and the NH_3 yields from the model compounds have decreased by about 85% at this temperature.

The HCN results in Fig. 1-12 were more readily reproducible and the previous data point of 69% unreacted at 756 C (Fig. 1-11) is in agreement with the HCN results in Fig. 1-12. Although the HCN may begin to react with O_2 at a lower temperature than does NH_3, HCN is less reactive at the higher temperatures. Since the temperature at which HCN begins to react rapidly (about 750 C) is above the temperature zone where the HCN yields (especially that from pyridine) have dropped off dramatically, the direct reaction of HCN with O_2 is not the cause for the decrease in the HCN yields from the model compounds.

Products of Oxidation of NH_3 and HCN. The products measured from the oxidative pyrolysis of HCN are listed in Table 1-7. Somewhat surprisingly, the simple oxidation of HCN yields nearly 50% N_2O under these conditions (75% O_2). The remainder of the HCN-N forms molecular nitrogen. The N_2O and CO_2 yields were measured in a single-stage reactor. The N_2 and CO yields were measured later in a two-temperature zone reactor that was in use at that time (discussed in a following section). This is not expected to affect the product distribution because the first zone of the two-zone reactor was held at 600 C where no reaction will occur (Fig. 1-12). This discovery that N_2O somehow forms in the oxidation of HCN gave a strong clue to the mode of N_2O formation from the model compounds.

T 1-7

TABLE 1-7. PRODUCTS FROM THE OXIDATIVE PYROLYSIS OF HCN

First-Stage Temperature, C	Second-Stage Temperature, C	% N_2O	% CO_2	% N_2	% CO
728	728	4	(a)		
773	773	28	(a)		
793	793	44	63		
815	815	48	78		
858	858	48	77		
900	900	46	82		
600	794			40	3
600	850			58	0
600	900			48	0

(a) not measured

Some N_2O also forms from NH_3 oxidation under these conditions but the yields are much smaller. Under single-stage conditions, the following N_2O yields were obtained from ammonia:

Temperature, C	734	753	776	797	819	883
% N_2O	8	10	11	11	10	8

With the first stage at 716 C and the second at 778 C, the N_2O yield from NH_3 was again 10%.

As far as we know, N_2O has not been reported previously as a product of the low-temperature oxidation of HCN and NH_3. However, MacLean and Wagner (Ref. 16) observed the formation and decay of N_2O early in a NH_3-O_2 flame. Sternling and

---

16. MacLean, D. I. and H. G. Wagner, "The Structure of the Reaction Zones of Ammonia-Oxygen and Hydrazine Decomposition Flames," Eleventh Symposium (International) on Combustion, 871, 1966.

Wendt (Ref. 17) point out that the mechanism of N_2O formation in the combustion of NH_3 is not understood. N_2O has the potential to form NO in combustion because the reactions

$$O + N_2O = NO + NO$$

and

$$O + N_2O = N_2 + O_2$$

are fast and are believed to have about equal rates.

Effect of NH_3 on HCN Oxidation Rate. A considerable number of preliminary experiments were carried out on the oxidative pyrolysis of mixtures of HCN and NH_3 (about 0.7% of each in the 3:1 O_2/He carrier gas). Some reproducibility problems were encountered so the conclusions from this experimental series were tentative. It appeared, however, that the presence of NH_3 strongly inhibits the oxidation of HCN. In the temperature range of 780 to 800 C, replacing the NH_3 flow with helium decreased substantially the amount of unreacted HCN and greatly increased the amounts of N_2O and CO_2 formed.

The above experiments were repeated over the temperature range of 775 to 835 C. The amount of unreacted HCN obtained is plotted in Fig. 1-13 as a function of reactor temperature. These results definitely establish that the oxidative stability of the HCN is greatly increased in the presence of NH_3 and its decomposition products. This suggests that the HCN oxidizes via a chain mechanism and the NH_x species somehow promote the rate of chain termination.

This observation that NH_3 increases the stability of HCN makes it even less likely that the HCN curve obtained from pyridine is determined by simple

---

17. Sternling, C. V. and J. O. Wendt, "Kinetic Mechanisms Governing the Fate of Chemically Bound Sulfur and Nitrogen in Combustion," EPA-650/2-74-017 (NTIS-PB 230 895/AS), 1974.

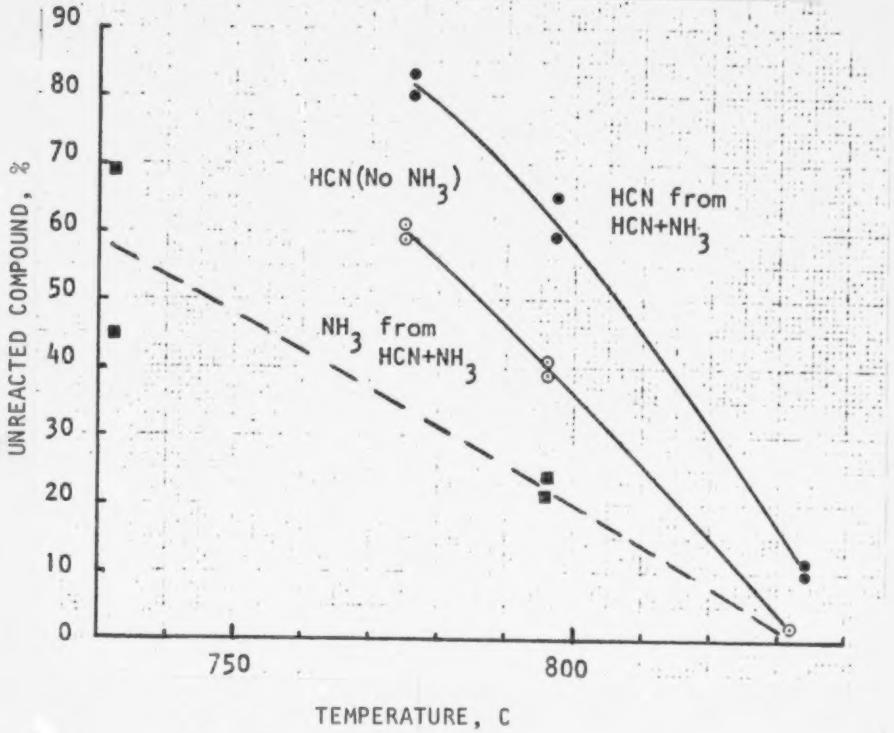

Figure 1-13. Effect of NH$_3$ on Oxidation Rate of HCN (75% O$_2$, 1 atm)

oxidation of the HCN. A more likely explanation is that species formed in the oxidation of the heavy volatiles initiate the reaction of the HCN (and possibly of the NH_3 as well).

The sensitivity of the technique used to measure unreacted NH_3 is much lower than that used for HCN. For this and possibly some other unknown reasons, the NH_3 measurements were not very reproducible in these experiments. The amount of unreacted NH_3 (from the HCN-NH_3 mixtures) was 23 ±2% at 796 C and 58 ±12% at 730 C (Fig. 1-13). In the previous experimental series, only 10% NH_3 remained unreacted at 796 C. In any event, sufficient NH_3 remains unreacted at about 800 C under these conditions to account for its inhibiting effect.

Effect of NH3 on HCN Decomposition Products. The product yields obtained from the oxidation of the HCN-NH_3 mixture are listed at the top of Table 1-8 (as the percentage of the carbon or nitrogen in the total reactants including that which did not react, if any). Duplicate measurements were made of each product and the reproducibility was good. Listed at the top of Table 1-8 are the amounts of HCN and NH_3 that do not react at each temperature (from Fig. 1-13). It can be seen from the footnote to the table that, when oxidized individually at these temperatures, HCN forms about 75% CO_2, little CO, 45% N_2O and 50% N_2, and NH_3 forms about 10% N_2O and 90% N_2.

In the second section of Table 1-8, the product yields from the HCN-NH_3 mixture are calculated on the basis of the amounts of HCN and NH_3 reacted, and are compared with yields predicted if each reactant yielded the products obtained when it is oxidized alone (footnote). The measured and predicted mass balances are also listed. It is of considerable interest that the total nitrogen balances are quite good but at 797 C much less N_2O and much more N_2 are formed from the mixture. Since the experiments were quite reproducible, these results establish that when NH_3 inhibits the oxidation of HCN, it also inhibits the formation of N_2O from HCN (the yields from the decomposed HCN being about 70% N_2 and only 27% N_2O).

TABLE 1-8. PRODUCTS FROM REACTION OF A MIXTURE OF HCN (0.7%) + NH_3 (0.7%) + He (23.6%) + O_2 (75%)

	789 C	797 C	834 C	898 C
Yields Based on Reactants				
Unreacted HCN (%)	80	57	10	0
Unreacted NH_3 (%)	32	19	~2	~0
CO_2 (% of HCN-C)	NM	7,6	74,76	89,86
CO (% of HCN-C)	3,3	5,5	3,3	NM
N_2O (% of HCN-N + NH_3-N)	NM	10,11	32,32	28,30
N_2 (% of HCN-N + NH_3-N)	44,44	50,54	67,67	NM
Yields Based on Reacted HCN & NH_3, %				
CO_2				
Measured	NM	15	83	88
Predicted$^{(a)}$	NM	65	77	82
CO				
Measured	15	11	3	NM
Predicted$^{(a)}$	NM	3	0	0
N_2O				
Measured	NM	17	34	29
Predicted$^{(a)}$	23	28	29	27
N_2				
Measured	100	84	72	NM
Predicted$^{(a)}$	62	67	71	70
Carbon Balance				
Measured	NM	27	87	≥ 88
Predicted$^{(a)}$	NM	68	77	82
Nitrogen Balance				
Measured	≥ 100	101	106	NM
Predicted$^{(a)}$	85	95	100	97

(a) Based on the following expected percentage yields:

	780 C	797 C	834 C	898 C
CO_2 from HCN	NM	65	77	82
CO from HCN	NM	3	0	0
N_2O from HCN	35	45	48	46
N_2O from NH_3	11	11	10	8
N_2 from HCN	35	45	52	48
N_2 from NH_3	89	89	90	92

The presence of NH_3 also appears to greatly decrease the CO_2 yield from HCN and increase slightly the CO yield. The net effect, however, is to greatly decrease the amount of reacted carbon that is recovered in the measured products. The only apparent explanation is that part of the HCN forms a carbonaceous residue (containing little or no nitrogen) that deposits downstream from the reactor and the amount of this unmeasured residue increases when NH_3 is present.

Two-Stage Oxidative Pyrolysis of Pyridine

The model compound reactor (2 mm ID quartz capillary tubing) was converted to a two-temperature-zone reactor by use of a multi-tap Marshall furnace. As before, the carrier gas flowing into the reactor was a 3:1 O_2/He mixture containing 1.4% pyridine vapor, the total flowrate was 40 cm^3/min, and the reactor was at atmospheric pressure.

In this series of experiments, the temperature of the first half of the reactor was held constant at 716 C and the second half temperature was varied from 346 C (second-stage heater off) to 875 C. About 98% of the pyridine reacts in the first stage under these conditions. Therefore, any changes in product concentration with second-stage temperature must result from secondary reactions of species formed from pyridine.

The results obtained in the two-stage oxidative pyrolysis of pyridine are plotted in Fig. 1-14. The product yields plotted at the left side of the figure (second stage at 350 C) are essentially the amounts formed in the first stage because little reaction will occur in the second stage at this low temperature. The two dashed mass balance curves at the top of the figure indicate that about one-half of the carbon and one-fourth of the nitrogen from the decomposed pyridine is in the form of semivolatile pyrolysis products that pass through the second stage at 350 C. This is in agreement with the nitrogen balance in Fig. 1-7A but is less than the carbon balance in Fig. 1-7B. This is because less CO and, particularly CO_2, were formed in the first stage of the two-stage reactor than were formed in the single-stage reactor. Plugging of the lines to the Carle gas

USE SPECIAL DROPOUT BLUE PENCIL
ONLY TO INDICATE CORRECTIONS
CLASSIFICATION
PAGE

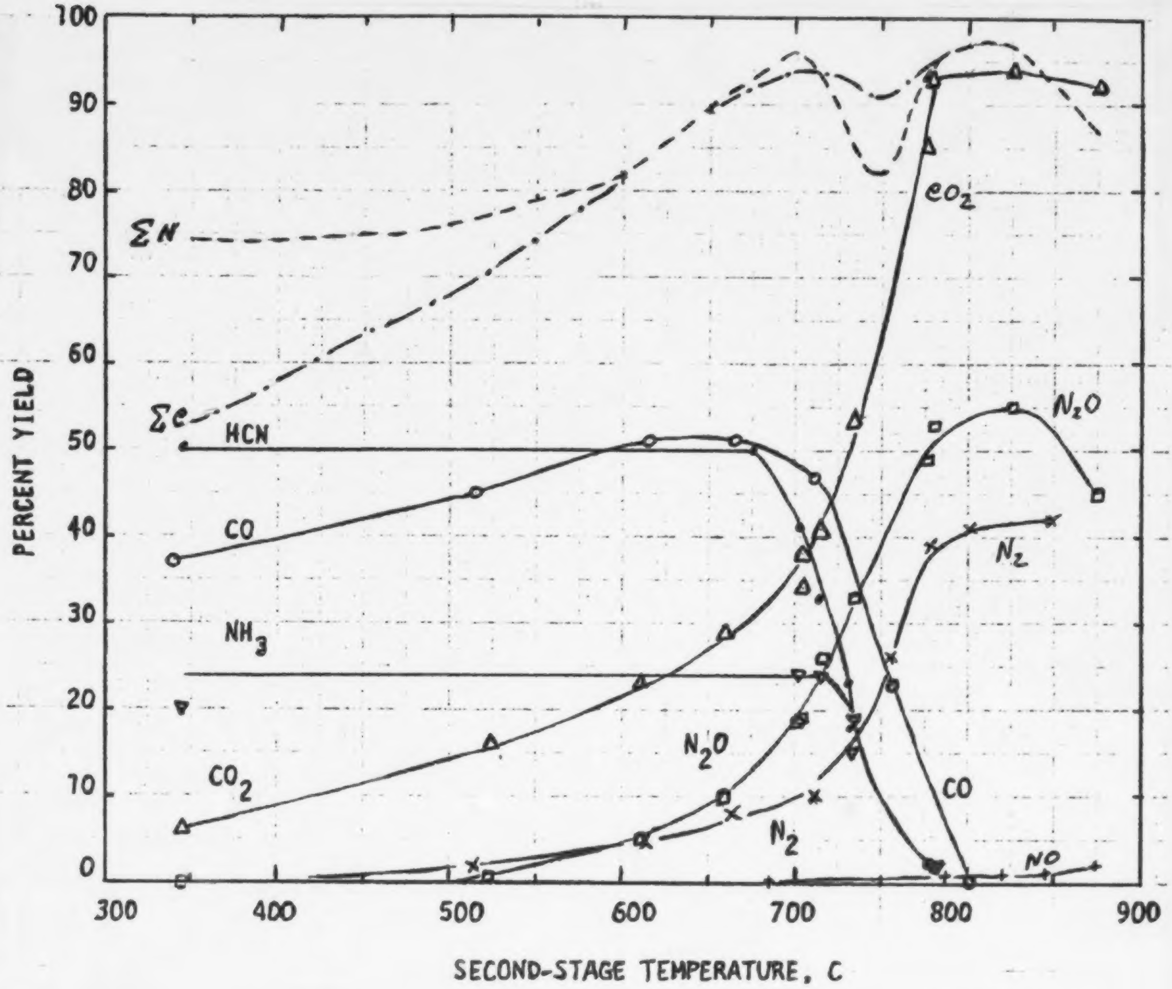

Figure 1-14. Products From Two-Stage Oxidative Pyrolysis of Pyridine With First Stage at 716 C (1.4% pyridine, 75% O_2, 1 atm)

WARNING LINE
LIMIT
DOCUMENT NUMBER
PAGE NUMBER
CLASSIFICATION

sampling valve also occurred in the present study when the second stage was below about 750 C. This also suggests that some low-volatility, nitrogen-containing species form in the oxidative pyrolysis process. The yields of HCN and NH_3 from the first stage are similar to those from the previous single-stage experiments at this temperature (Fig. 1-7A).

As the second-stage temperature is increased, the HCN and NH_3 formed in the first stage do not react in the second stage until a temperature of near 700 C is reached. Below 500 C, however, part of the higher molecular weight material is oxidized to CO and CO_2. Just above 500 C, N_2 and N_2O begin to form in the second stage from these heavy volatiles. Above 700 C, the HCN, NH_3, and CO are converted in the second state to CO_2, N_2, and N_2O.

The similarity between the high-temperature products from the single-stage (Fig. 1-7) and dual-stage (Fig. 1-14) reactors establishes that nearly all of the high-temperature products, including N_2O, form in secondary reactions rather than in the initial oxidative pyrolysis of pyridine. Since the products formed below about 700 C (Fig. 1-14) form mainly from the high molecular weight volatiles, the fractions of the total yields of N_2, N_2O, and CO_2 (above 800 C) that form in the second stage from these volatiles are about 24, 35, and 40%, respectively*. The remainder of the total N_2, N_2O, and CO_2 form from the HCN and NH_3 that was produced in the first stage.

The results in Fig. 1-14 are in agreement with a model in which the primary oxidative pyrolysis of pyridine forms mainly HCN, NH_3, CO, and high molecular weight C-N-H species. At high enough temperatures, the high molecular weight material then forms N_2O and N_2 in about a 2:1 ratio, about one-half of the HCN and NH_3 forms N_2O and one-half forms N_2. This is more N_2O from NH_3 than would be expected from simple oxidation because the experiments presented above indicate that under these conditions HCN forms about 50% N_2O but NH_3 only forms about 10%.

---

*$N_2(700)/N_2(825) = 10/42 = 0.24$; for N_2O and CO_2 the ratios are 19/55 and 37/94.

Conclusions - Model Compound Pyrolysis

The oxidative pyrolysis of the model fuel nitrogen compounds pyridine and benzonitrile yields HCN as the major initial product and NH_3, which did not form to any appreciable extent under inert pyrolysis conditions, is also a significant product. Quite surprisingly, N_2O forms in about a 50% yield from each of these model compounds at about 760 C. The oxidative pyrolysis results indicate that NH_3 and N_2O, in addition to HCN, may be important intermediates in the formation of fuel NO_x in combustion.

Based on the more detailed study of the secondary reactions in the oxidative pyrolysis of pyridine, the initial oxidative products at 716 C are HCN, NH_3, CO, and higher molecular weight volatiles. The latter species contain about one-half of the carbon and one-fourth of the nitrogen from the pyridine. When these products are heated for a longer time or above 750 C, the volatiles react first forming CO_2, CO, N_2O, and N_2. Then at higher temperatures or at longer times, the HCN and NH_3 undergo secondary reactions to form N_2O and N_2. Only minor amounts of NO and NO_2 are observed in these oxidative pyrolysis experiments. NO could have formed as an intermediate and then reacted with NH_3, for example, to form N_2 or N_2O.

OXIDATIVE PYROLYSIS OF FUELS

The single- and two-stage reactors shown in Fig. 1-1 were used to study the oxidative pyrolysis or fuel oils and coal. Only a limited investigation was carried out in the single-stage reactor because the measured products included those formed in the slow oxidation of the char.

Single-Stage Oxidative Pyrolysis of Fuel Oils

The conditions were those used previously in the single-stage inert fuel pyrolysis studies except that lower temperatures were employed and oxygen was present in the carrier gas system. It should be noted that under these single-stage conditions all the sample eventually reacts and, unlike inert pyrolysis, no residue is left in the quartz boat. The products measured include both those formed from the oxidation of the volatile portion of the oil and those formed in the heterogeneous oxidation of the char. In some of the experiments, the boat was removed from the reactor after approximately one-half of the sample had reacted to determine how much of the HCN formed in the later stages of reaction. Listed in Table 1-9 are the nominal reaction times and yields of HCN and NH_3 obtained in the experiments in which the sample was allowed to react to completion.

Experiments in addition to those in which the products were measured were carried out to determine the time for the entire sample to react. This was done by removing the boat periodically from the heated zone for inspection. At 700 C with only O_2 flowing, the sample flared up and the light reflected in such a way that the flame was visible outside of the furnace. With 20% O_2 in helium, the time for complete reaction of a 1.3 mg sample of Oil-A increased from 8 seconds at 700 C to about 8 minutes at 500 C (Table 1-9). Oil-G reacted substantially slower under the same conditions. The oil samples would initially be present as a drop at one point in the boat. Shortly after the samples were heated, they flowed to cover the interior surface of the boat and then formed a char that gradually reacted.

The oxygen flowrate was such that about 9 seconds would be required to oxidize 1.5 mg of fuel oil if the products were CO and H_2 and about 25 seconds if CO_2 and H_2O formed. At 700 C, about 8 seconds is required for the fuel to react and, therefore, the rate may be oxygen limited. It is not likely that NO would form to an appreciable extent under these oxygen-lean conditions. At 500 C, however, 7 or 8 minutes are required and there should be a rather large excess of oxygen.

Under these conditions, the HCN yields increased with decreasing temperature (Table 1-9). The maximum yield of HCN was obtained at 500 C where the reaction rate is quite slow and the reaction is almost certainly heterogeneous. It is possible that at the higher furnance temperatures, self-heating of the sample surface increases the temperature to the point where part of the HCN formed undergoes oxidative pyrolysis. Calibration samples of HCN passed through this

TABLE 1-9. FUEL OIL SINGLE-STAGE OXIDATIVE PYROLYSIS

(1 atm, 40 cc/min)

	No. 6 Fuel Oil-H[(a)] (0.71% N)			No. 6 Fuel Oil-F[(b)] (0.38% N)		Pyridine (17.7% N)
		Yield[(d)], %				
Condition	Reaction Time,[(c)] seconds	HCN	NH_3	Reaction Time[(c)], sec	HCN Yield, %	NH_3 Yield, %
700 C, 100% O_2	1	6.0 10.6 7.2				2.3
700 C, 20% O_2	8	6.2 3.9		12		12.1
650 C, 20% O_2	16	10.0	11.2 12.1			0.45
600 C, 20% O_2	40	12.1 12.4		75	7.1 7.4	
500 C, 20% O_2	420 to 480	23.4 22.7 23.9	13.2 14.2	720	16.7 15.9	0.14

(a) See Table 1-1.

(b) See Table 3 of Ref. 10

(c) For 1.3 mg sample.

(d) The yields of NO and NO_2 were less than 1 and 5%, respectively, at these conditions.

fuel reactor underwent only 15% reaction in 100% O_2 at 700 C. Therefore, the surface temperature of the sample would have to have been well in excess of 700 C for any HCN to have been lost once it was formed. The maximum yield of HCN from Oil-A under these oxidative conditions was 23%, while Oil-H produced only about two-thirds of this HCN yield.

Under conditions where the maximum HCN yield was obtained and the rate was the slowest, 500 C, it was found that about one-half of the HCN formed from Oil-A during the first 3-1/2 minutes of reaction and about one-half during the final 3-1/2 minutes. In a similar experiment at 600 C, 72% of the HCN formed during the first 20 seconds of reaction and 28% formed during the remaining 20 seconds of reaction.

Ammonia measurements were made only with Oil-A at 650 and 500 C (Table 1-9). The ammonia yields were 11.5 and 13.5%, respectively. One microliter samples of pyridine also were passed through the fuel reactor under these conditions and the amount of NH_3 formed was measured (Table 1-9). Practically no NH_3 formed below 700 C, indicating that pyridine-type fuel nitrogen compounds will not react homogeneously under these conditions. At 700 C, a 12% yield of NH_3 was obtained from pyridine, but this decreased to 2.3% when the oxygen concentration was increased. The decrease in NH_3 may result from oxidation of the NH_3 that formed before it exited the reactor.

Only minor amounts of NO and NO_2 were formed under these conditions (Table 1-9). An experiment showed that bubbling the carrier gas/calibration gas containing NO_2 through the Saltzman solution gave quantitative recovery of NO_2. In these single-stage oxidative pyrolysis experiments, the NO_2 yields were somewhat less than 1% at both 500 and 700 C. Passing the NO_2-N_2 calibration gas sample through the heated reactor gave NO_2 recoveries of only about 20% at each temperature. Even so, the yields of NO_2 from the oil must have been less than 5% at both temperatures.

The single-stage oxidation results indicate that 60% or more of the fuel nitrogen does not form HCN, NH_3, NO, or NO_2. Nitrogen and possibly N_2O apparently account for the remainder of the fuel nitrogen.

Two-Stage Oxidative Pyrolysis of Fuel Oils

The two-stage reactor shown in Fig. 1-1B was used to study the oxidative pyrolysis of oils and a coal. The fuel is pyrolyzed in an inert atmosphere in the first stage and the volatile products formed react in a 2:1 O_2/He mixture in the second stage. The reactor is operated at atmospheric pressure. Helium flows through the first stage at 20 cc/min (STP) and O_2 flows into the second stage at 40 cc/min, giving a 2:1 O_2/He mixture in the second stage in the absence of any sample. This experiment simulates in some respects the conditions that fuel nitrogen species may encounter in the preflame region when a fuel droplet or particle is surrounded by a diffusion flame. The fuel pyrolyzes in a fuel-rich zone and then encounters increasingly higher temperatures and oxygen concentrations as it travels into the flame front. The oil results will be presented first.

In the model compound experiments, the oxygen concentration was maintained at a nearly constant value by keeping the pyridine concentration low (1.4% or only about 13 micrograms/cm^3 of carrier gas). The effective second-stage oxygen concentration in the fuel experiments will depend in part on how rapidly the fuel pyrolyzes in the first stage (estimated at 1 to 2 seconds). For example, a 1.5 milligram sample of oil contains between 35 and 80 micromoles of hydrogen. If all were converted to H_2 (which is unlikely), this would form from 0.7 to 1.5 cm^3 of H_2 at 25 C or up to 5 cm^3 at 700 C, which would displace or consume most of the O_2 in the second stage. Also, it will be seen that about 40% of the carbon in the fuel is converted to CO_2 in the second stage consuming in the process about 3 cm^3 of O_2 (measured at 700 C). Since the second stage is only about 2 cm^3 in volume, some of the fuel vapor may react under fuel-rich conditions a second or so after the fuel sample is introduced. However, the remaining fuel vapor will mix with more O_2 before it exits the reactor (which is essentially a stirred flow reactor with an O_2/He carrier gas flowrate of 1.5 volumes/sec at 700 C) and may, therefore, react in the presence of excess O_2.

The experimental procedures used to trap and measure the various reaction products under these oxidative pyrolysis conditions are described in Appendix B. A method of trapping N_2 and CO from an oxygen-rich carrier gas was not developed and, therefore, these species were not measured in this experimental series.

N_2O Yields. The relatively low sensitivity of the N_2O measurement technique (Appendix B) limited these studies to coals and fuel oils containing nearly 1% nitrogen. The first series of experiments was conducted with SYNTHOIL (1.3% N, fuel I of Table 1-1) and a No. 6 fuel oil (1.41% N) derived from a California crude (fuel C of Ref. 10 and third fuel in Table 6 of Ref. 1).

Plotted in Fig. 1-15 as a function of second-stage temperature are the N_2O yields obtained with the first stage at 850 C. The scatter in the data probably resulted from working near the limit of the analytical procedure but could have resulted from a variability in the amount of fuel-N that reacted in the second stage. Detailed analysis of the data indicated that part of the scatter was related to the size of the fuel samples which ranged from 1.3 to 1.9 milligrams. The larger samples generally gave smaller yields of CO_2 and, particularly, N_2O because of the increased competition for oxygen in the second stage. In a few of the SYNTHOIL experiments a flash was observed just after the sample was introduced indicating ignition had occurred in the second stage.

The N_2O yield from SYNTHOIL appears to reach its maximum value near 770 C which is the same region where the N_2O yield from benzonitrile peaked (Fig. 1-9A). In the two experiments with the No. 6 fuel oil (Fig. 1-15), the average N_2O yield is somewhat less than the average of the SYNTHOIL data at this temperature.

Based on our previous model compound and inert pyrolysis results, the maximum amount of N_2O that might have formed from the SYNTHOIL would be expected to be about 25%. One-half of the fuel-N would be expected to enter the second stage

USE SPECIAL DROPOUT BLUE PENCIL
ONLY TO INDICATE CORRECTIONS
CLASSIFICATION
PAGE
STARTING LINE

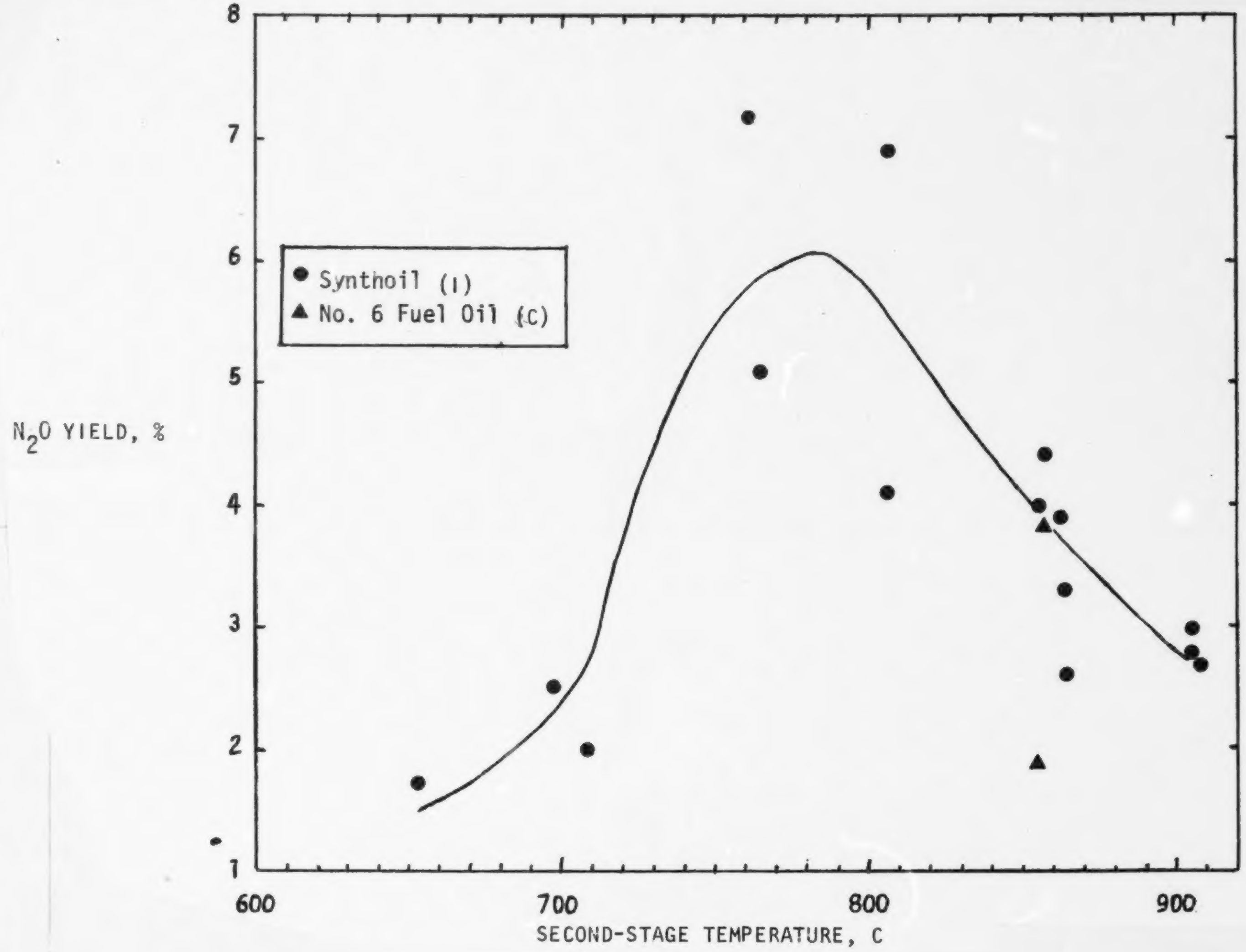

Figure 1-15. Nitrous Oxide Yield as a Function of Second-Stage Temperature (first stage at 850 C)

DOCUMENT NUMBER

(based on the HCN formed in inert pyrolysis experiments - Table 1-1) and one-half of this could form N_2O (model compound results). The fact that only about one-fourth of the predicted maximum N_2O yield of 25% actually forms is in agreement with the limitation on the amount of available oxygen as discussed above.

The yields of N_2O were also measured from No. 6 fuel oil H (Table 1-1). As before the oil was pyrolyzed in the first stage under inert conditions at 850 C. The volatiles formed were oxidized in the second stage at various temperatures. The method used to measure N_2O does not have sufficient sensitivity to give accurate results for fuels containing less than about 1% nitrogen. This fuel oil (0.71% N) was included in these two-stage oxidative pyrolysis experiments, however, because it is of considerable interest and was studied the most extensively in the two-stage inert pyrolysis experiments (Fig. 1-3).

The N_2O yields measured from this oil (Fig. 1-16) again showed considerable scatter and some dependence on sample size. The first experimental series gave slightly higher percentage N_2O yields than did the two oils ran previously. The yields obtained in the second series (at 850 C second-stage temperature) were about the same as those obtained previously with SYNTHOIL. Within experimental error, each of these three oils gave similar yields of N_2O.

HCN Yields. The amount of HCN formed from oil H under these same conditions (first stage at 850 C) was determined over the second-stage temperature range of 460 to 900 C; the results are plotted in Fig. 1-17. A few experiments were also conducted in which the second-stage oxygen flow as turned off (i.e., under two-stage inert pyrolysis conditions). Under oxidative pyrolysis conditions, the bubbler solution (Appendix B) was held at 0 C to reduce sulfite interference. Tests not shown in the figure demonstrated that the HCN yields were lower both when $CdCO_3$ was used in the oxidative experiments and when it was not used in the inert experiments.

With the first stage at 850 C, the average HCN yield under oxidative conditions, denoted by the solid curve in Fig. 1-17, reached a minimum of about 7% at a

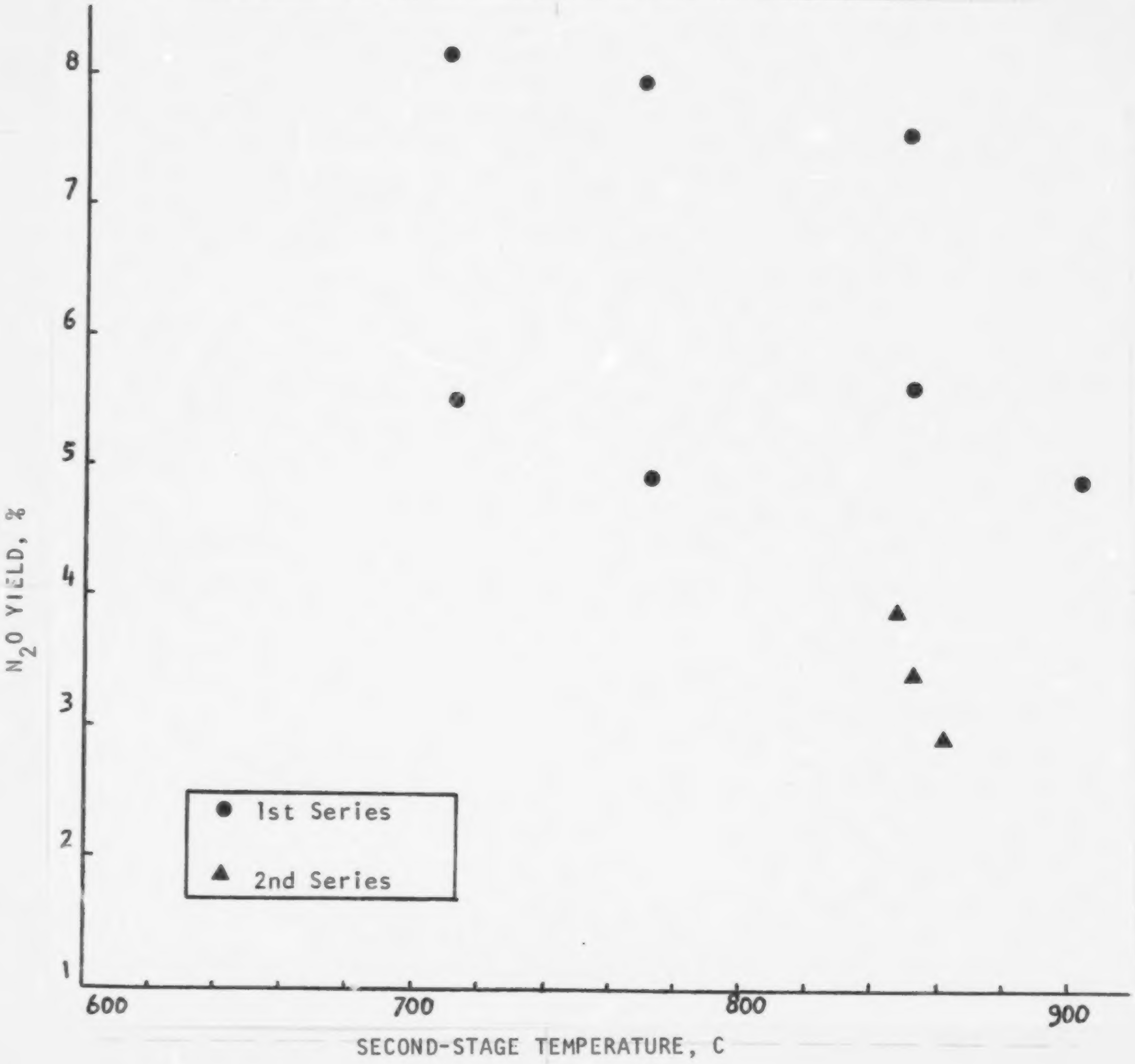

Figure 1-16. Nitrous Oxide from No. 6 Fuel Oil H (First Stage at 850 C)

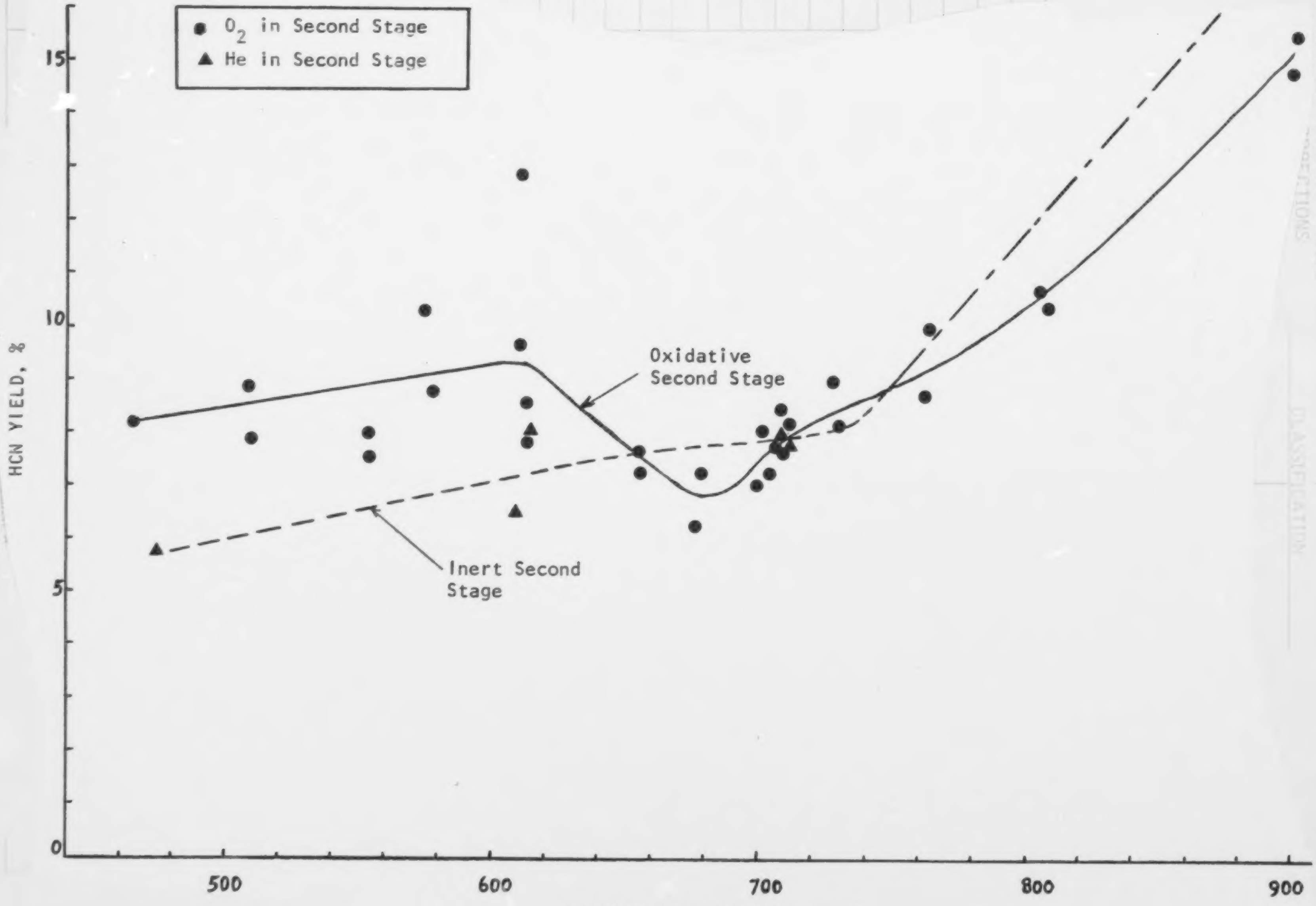

Figure 1-17. HCN From No. 6 Fuel Oil H (first stage at 850 C)

second-stage temperature of 690 C. As this temperature is decreased further, the HCN yield increases to about 10% at 600 C and then only decreases slightly at second-stage temperatures as low as 460 C. The dotted curve drawn in Fig. 1-17 from 460 to 750 C represents the average results obtained in those experiments in which the O_2 flow was off. The broken curve above 750 C denotes the HCN yields expected if the O_2 had been turned off at these temperatures. This curve was estimated by taking the average between the lower two curves in Fig. 1-3 in which the first stage was at 750 and 950 C, respectively. This curve reaches 40% at 1100 C (Fig. 1-3), demonstrating that at least 40% of the nitrogen contained in this oil reaches the second stage in all of these experiments.

It can be seen from Fig. 1-17 that, with the first stage at 850 C, the additional amount of HCN formed from the oxidative pyrolysis of this oil is small. Above a second-stage temperature of 800 C, the HCN yield is slightly less with O_2 flowing to the second stage than under inert conditions, suggesting that some of the HCN formed is oxidized. Between 650 and 800 C (second stage), the HCN yield is essentially the same whether the O_2 flow is on or off. The HCN formed with the O_2 on may well form via oxidative pyrolysis but it would have formed thermally in the absence of any oxygen. Below 650 C, the presence of the oxygen increases the HCN yield somewhat (about 2%) demonstrating that some volatile nitrogen species reach the second stage that readily form HCN under oxidative conditions at low temperatures. This indicates the presence of some extremely reactive forms of nitrogen that undergo oxidative pyrolysis at much lower temperatures than does pyridine. These are probably amines or other non-heterocyclic forms of nitrogen.

It will be seen later that the CO_2 yield falls off in the same temperature region below which the HCN yield begins to increase above that obtained in the absence of oxygen. At the higher temperatures (above 650 C), all of the available oxygen may be consumed in forming CO_2 and H_2O so that the nitrogen species encounter an essentially inert atmosphere. At the lower temperatures, however, the oxygen reacts to a lesser extent apparently resulting in an oxygen concentration sufficient to catalyze the formation of some HCN.

The competition for oxygen in the second stage of this reactor could be considered as a weakness in the experimental procedure. It should be noted, however, that a similar competition for oxygen will be important in an actual combustion system. The effective mixture ratio at a given point in a combustor will not only depend on the equivalence ratio in that zone but on the amount of CO, CO_2, and H_2O that has formed.

A few two-stage experiments were conducted in which this oil was pyrolyzed in the first stage at 750 C rather than at 850 C as had been the case in all of the experiments reported above. The purpose was to lower significantly the amount of HCN that would form with the O_2 flow off. These results are plotted in Fig. 1-18, where the broken line above 750 C indicates the amount of HCN that would have formed if the O_2 flow were off and is reproduced from Fig. 1-2A. Interestingly, the HCN yields obtained in the oxidative experiments were the same (within experimental error) whether the first stage was at 750 or 850 C (Fig. 1-17 and 1-18).

The HCN yield with the second stage at 550 C (Fig. 1-18) increases from 3% under inert conditions to 9% under oxidative conditions. It should be noted that the residence time in the second stage increases by a factor of 3 in these experiments when the O_2 flow to the second stage is shut off. Thus, at least 6% of the nitrogen in this fuel (and possibly 8 or 9%) is in a form that is relatively volatile and is readily converted to HCN under mild conditions of oxidative pyrolysis. Although this is not a major fraction of the fuel nitrogen, it could affect the ultimate limit to the reduction of NO_x by combustion modification techniques. Even with the second stage at 465 C (Fig. 1-18), the HCN yield is 6%.

The results plotted in the lower two curves in Fig. 1-3 and in Fig. 1-17 and 1-18 indicate that when this oil is pyrolyzed at 750 C, about 10% of the fuel nitrogen is evolved in a form that can be readily converted to HCN (1) via thermal reactions below 950 C (Fig. 1-3) or (2) via oxidative pyrolysis at temperatures as

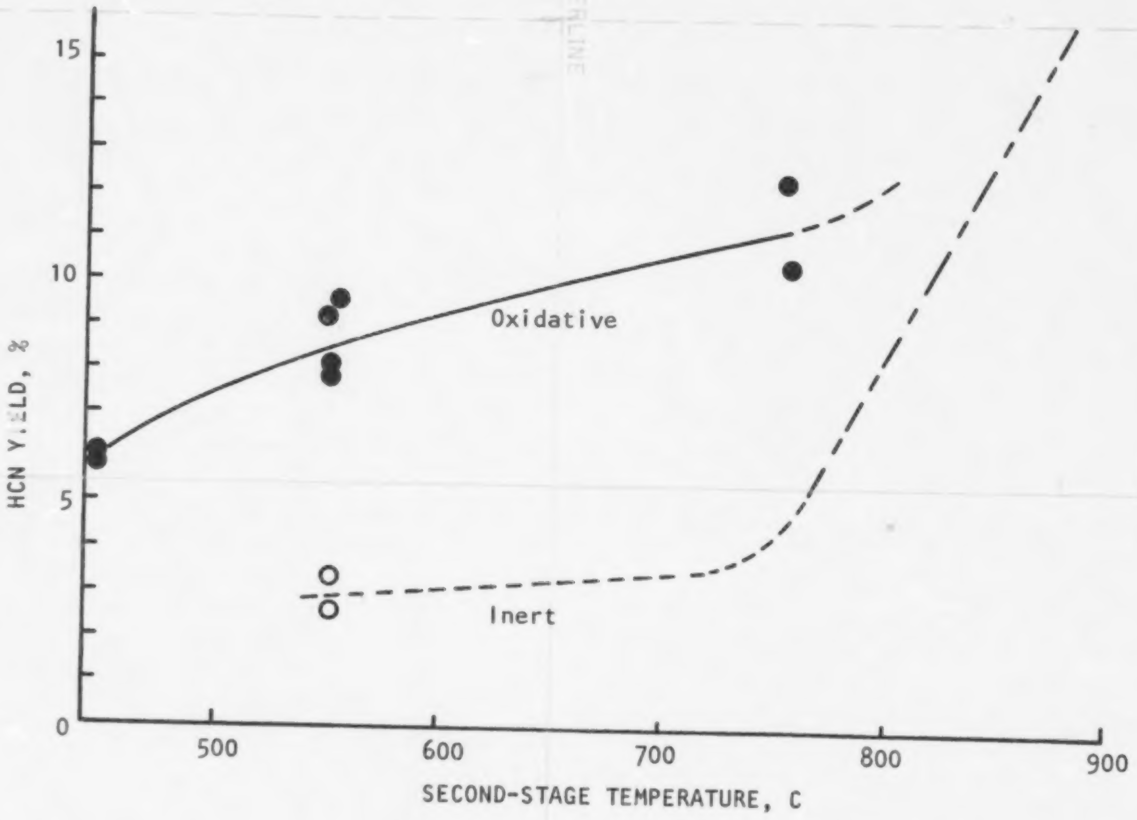

Figure 1-18. HCN From No. 6 Fuel Oil H (first stage at 750 C)

low as 460 C (Fig. 1-17 and 1-18). This particular fuel nitrogen fraction in this oil appears to be particularly prone to form NO_x but it may also be the most amenable to control by combustion modification because this nitrogen will be evolved early under fuel-rich conditions where it might be possible to convert HCN or its precursors mainly to N_2.

The HCN yields were also measured from two other oils with the first stage at 750 C and the second at 550 C. The following results were obtained:

	HCN Yield, %	
	Oxidative	Inert
No. 6 Fuel Oil (0.71% N) (Fuel H in Table 1-1)	9	3
No. 6 Fuel Oil (1.41% N) (Fuel C in Table 3 of Ref. 10 and Third Fuel in Table 6 of Ref. 1)	5	1.7
SYNTHOIL (1.3% N) (Fuel I in Table 1-1)	10	1.5

It can be seen that these two oils, particularly the SYNTHOIL, also contain some volatile fuel nitrogen that readily undergoes oxidative pyrolysis to HCN.

The final comment that should be made regarding these HCN results is that the highest yield obtained in two-stage oxidative pyrolysis was less than half of the 23% HCN yield that was obtained from this oil in a single-stage oxidative pyrolysis at 500 C (Table 1-9). In the single-stage experiments, of course, all of the fuel nitrogen came into contact with O_2 (rather than perhaps only 40%) and the reaction, presumably heterogeneous, was very slow.

Nitric Oxide Yields. The modified trapping procedure for NO (Appendix B) was used to measure the amounts of NO formed in the two-stage oxidative pyrolysis of Fuel Oil H. With the first (inert) stage at 850 C and the second (oxidative) stage at 900 C, the observed NO yield was 14% which becomes 20% when corrected for the losses in the measurement technique. With both stages at 1100 C, the NO yield (corrected) was 16%. The NO yield from this fuel oil was later remeasured (in duplicate) with the first stage at 850 C and the second stage at 900 C. These repeat experiments gave uncorrected NO yields of 12 and 10% which are in fair agreement with the previous value of 14%.

NH_3 Yields. The NH_3 yields were measured from the oxidative pyrolysis of Fuel Oil H under these two-stage conditions but the amounts of NH_3 produced were not large enough to measure accurately. However, the reagent blanks were rather high and the NH_3 yields could have been on the order of 10%. The ultimate sensitivity of the phenate method should permit measurement of the amount of NH_3 produced under these conditions, but the preparation of very high purity reagent solutions would have been required.

Nitrogen Product Yields. The yields of N_2O, HCN, NO, and NH_3 obtained from Fuel Oil H with the first stage at 850 C are summarized in Table 1-10. Since NO was only measured at 900 C, this is the only temperature at which the nitrogen balance can be calculated.

TABLE 1-10. NITROGEN PRODUCTS FROM THE OXIDATIVE PYROLYSIS OF NO. 6 FUEL OIL H
(First Stage = 850 C)

Product	Second-Stage Temperature, C				
	500	600	700	800	900
N_2O			~6%	~5%	~5%
HCN					
Total	8%	10%	8%	11%	16%
ΔO_2	3%	2%	-	-1%	-2%
NO					17 ±3%
NH_3			<10%		
Total					36%

It can be interpolated from the inert pyrolysis results (Fig. 1-3) that with the first stage at 850 C about 38% of the fuel-N reaches the second stage in a reactive form. It can be seen from Table 1-10 that when the second stage is at 900 C under oxidative conditions, 37% of this reactive volatile nitrogen forms HCN, 45% forms NO and 13% forms N_2O.

Carbon Dioxide and Ethane Yields. As discussed in Appendix B in the fuel oxidative pyrolysis experiments, the CO_2 and N_2O are trapped on molecular sieve 13X at room temperature. After the trap is purged with helium, the trap is warmed to 150 C to release the CO_2 and N_2O and these are separated and measured by gas chromatography. In the first CO_2 results presented below, and all of the N_2O measurements presented earlier, a molecular sieve 5A column (at 210 C) was used on the GC. It was found, however, that some ethane forms and it is not separated from the CO_2 peak on this column. Therefore, the column was changed to Poropak Q (at 40 C) because it separates ethane from CO_2. It does not completely separate N_2O from CO_2 but, because of the composition of the fuels, the N_2O interference in the CO_2 peak is negligible (but not the other way around).

SYNTHOIL. Most of the CO_2 measurements with SYNTHOIL were made with the 5A GC column giving the results in Fig. 1-19. (The SYNTHOIL contained 95% carbon and the No. 6 fuel oil, also plotted in this figure, 87%). The average CO_2 yield from the SYNTHOIL is apparently 40% at all temperatures. The CO was not measured but the constant CO_2 yield suggests that all of the CO was converted to CO_2 even at 660 C. Little CO_2 formed at this temperature in the pyridine experiments but its formation is H_2O catalyzed and the water vapor concentration may be much higher in the fuel experiments.

This lack of effect of temperature on the CO_2 yield was unexpected and might result partly from the limitation on the amount of available oxygen. Much of the fuel carbon would be expected to reach the second stage in an oil experiment. Indeed, relatively large amounts of carbonaceous residue are deposited downstream of the second stage in these experiments and, as in the model compound experiments, finally plugged the tube and had to be removed. It was pointed out

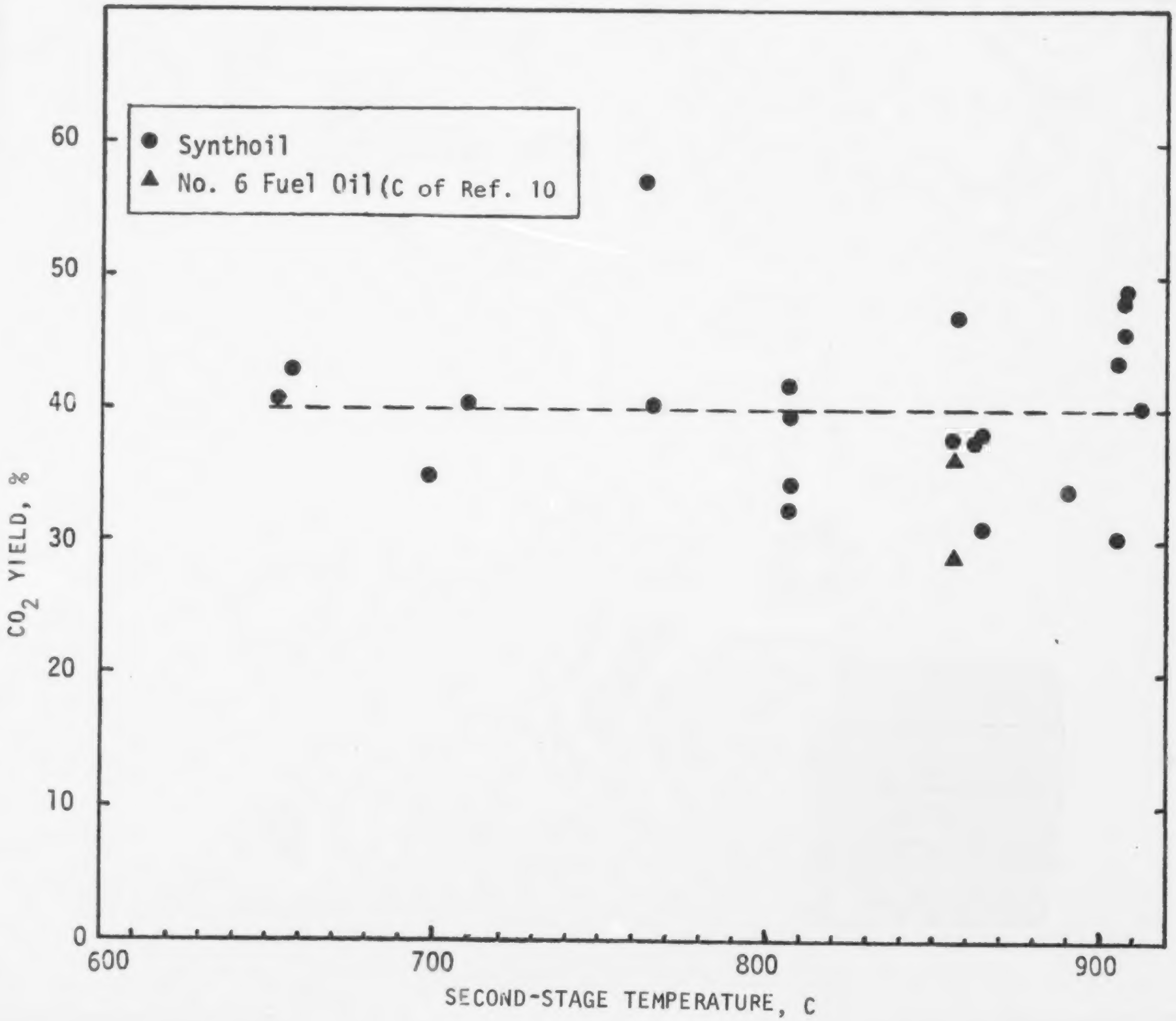

Figure 1-19. Carbon Dioxide Yield as a Function of Second-Stage Temperature (first stage at 850 C)

earlier in this report that the formation of the amount of CO_2 shown in Fig. 1-19 requires more oxygen than is initially present in the second stage.

Later experiments with SYNTHOIL using the Poropak GC column established that the CO_2:ethane ratio from SYNTHOIL at a second-stage temperature of 850 C is 70:1. Therefore, the CO_2 yields shown in Fig. 1-19 for SYNTHOIL probably are accurate at all temperatures.

High-Nitrogen Fuel Oil. The initial CO_2 measurements with the high nitrogen fuel oil (fuel C of Ref. 10) are plotted in Fig. 1-19. The test data points at a second-stage temperature of 850 C averaged about 33%. This condition was remeasured later using the Poropak GC column and it was found that the CO_2 yield was actually 23% and the ethane yield was 7%.

Baseline No. 6 Fuel Oil. Shown in Fig. 1-20, as a function of second-stage temperature, are the CO_2 and ethane yields from the baseline oil H used throughout the program. The ethane yield decreases gradually as the second-stage temperature is increased and the CO_2 yield increases.

The largest ethane yields were obtained in two experiments with the second stage at 450 C and with no O_2 flowing into the reactor. This establishes that the ethane forms in the initial first-stage inert pyrolysis of the oil. In the oxidative pyrolysis experiments, about one-half of the ethane reacts in the second stage when it is at 900 C.

Oxidative Pyrolysis of a Coal

A few oxidative pyrolysis experiments were conducted with a Pittsburgh No. 8 Seam Coal (III in Table 1-1). The results of this portion of the study turned out not to be very informative but are reported here for completeness.

N_2O and CO_2 Yields. The N_2O and CO_2 measurements with this coal, which contains 1.2% nitrogen, was carried out with both stages at 850 C. A quartz-wool plug was installed between the first and second stages of the reactor to prevent ash or

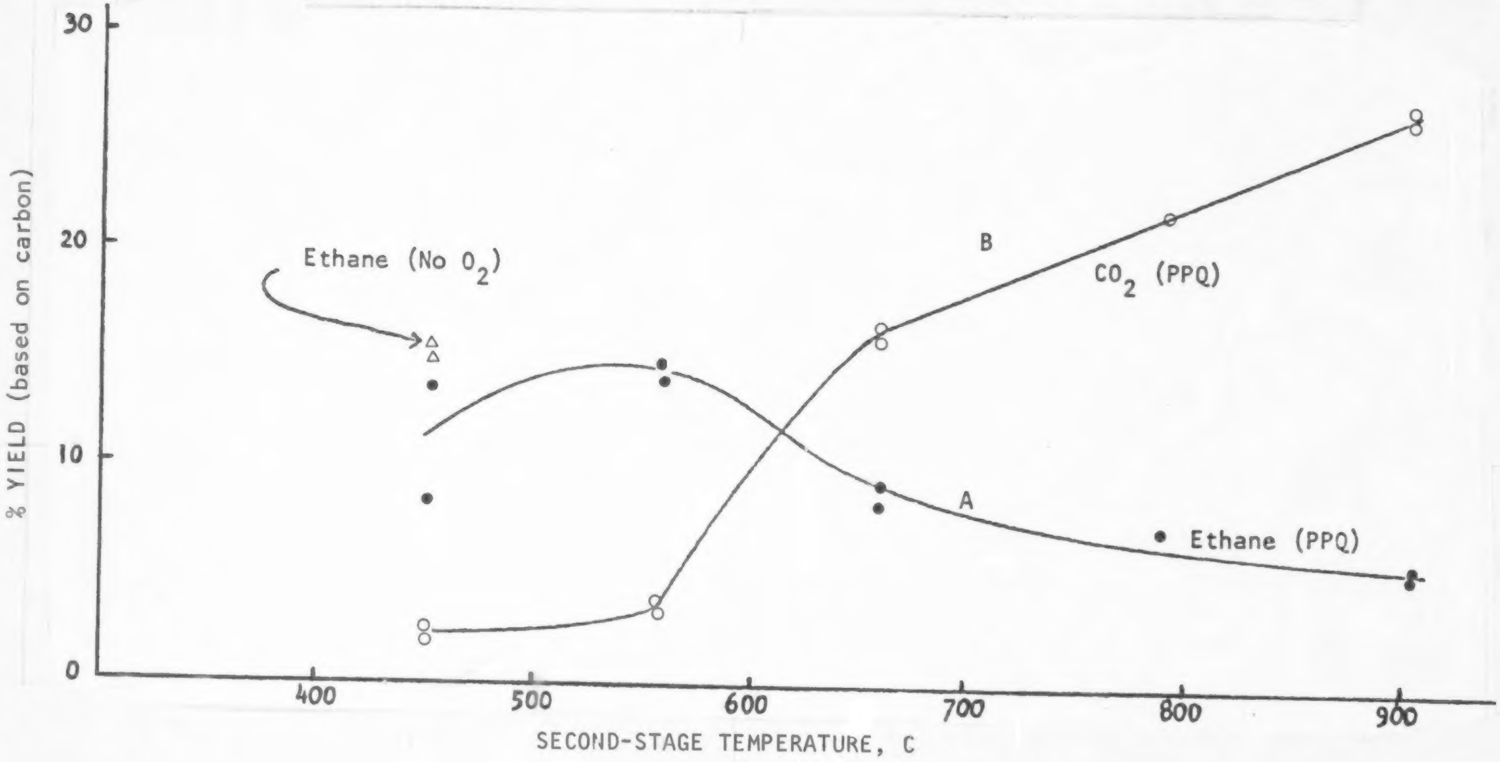

Figure 1-20. CO_2 and Ethane Yields from Oxidative Pyrolysis of No. 6 Fuel Oil H (First Stage at 850 C)

any other particulates from being carried into the second stage. This coal apparently forms several species that have GC and trap retention times similar to those of N_2O and CO_2. By keeping the trap freshly repacked it was possible, however, to measure the N_2O yield from this coal. The value obtained was 1.7 ±0.4%. The measured CO_2 yield was 31 ±2%.

As far as we know, this is the first time that N_2O has been observed from the oxidative pyrolysis of a coal. Of course, the small yield reduces the importance of this observation but the potential for some N_2O formation in coal combustion is established. This N_2O yield is about one-half that obtained from the oil H at this temperature (the oil gave a 4% N_2O yield at 850 C and 6% at 850 C/770 C). This might have been expected since the percentage of "volatile" fuel nitrogen in the oil is about twice that of the coal. This conclusion is based on the previous observation that the maximum HCN yield from the oil (under inert pyrolysis conditions at 1100 C/1100 C) is 45%, while that from the coal is only 24%.

HCN Yields. It was demonstrated earlier that the amount of HCN formed from a No. 6 fuel oil in the two-stage reactor under oxidative second-stage conditions is the same or somewhat greater than that formed under inert conditions depending upon the temperature (Fig. 1-17 and 1-18). Similar experiments were attempted with the Pittsburgh No. 8 Seam Coal.

It was shown in Table 1-3 that this coal yields 24% HCN under inert conditions with both stages at 1100 C and that this HCN yield does not decrease when the first-stage temperature is decreased to 745 C. Those results established that at least 24% of the nitrogen in this coal is volatile at 750 C and reaches the second stage in two-stage experiments.

Reducing the second-stage temperature to 750 C under inert conditions reduces the HCN yield to 7% demonstrating that most of the HCN formed at 1100 C forms in secondary reactions in the second stage of the reactor.

The results of the present experimental series, carried out under both inert and oxidative conditions, are listed in Table 1-11 in the order in which the experiments were performed. Each experiment number represents a pair of duplicate experiments and the reproducibility at each condition is quite good as shown in the last column of the table. In these coal experiments, both stages were held at a nominal temperature of 750 C.

In experiments 2 and 4, the coal was pyrolyzed under inert conditions giving HCN yields between 4.8 and 6.8%. The average yield of 5.4 ±0.7% is somewhat lower than the yield of 7.2 ±0.7 obtained previously (Table 1-3) and this can probably be attributed to the effect of this coal on the catalytic activity of the quartz reactor as discussed below.

It was expected that under oxidative second-stage conditions the HCN yield would increase or remain about the same. It can be seen from the results of experiments 1 and 3 that flowing oxygen into the second stage decreases the HCN yield to 0.55 ±0.1%. There is no obvious explanation for this unexpected but reproducible result since the fuel oil results in Fig. 1-17 indicate that any HCN formed should survive the second stage even at temperatures up to 900 C.

During this series, a number of HCN calibration experiments were conducted to determine the stability of HCN under these experimental conditions. Previously in this program, all HCN calibrations were made with 0.4 cc of pure HCN (about 440 μgm). Since the fuel samples contain only about 15 μgm of nitrogen, the calibration procedure has now been improved by using 0.2 cc of 5% HCN (about 11 μgm). Calibration experiment A was carried under inert conditions (750/750 C) after experiment 2. The result indicated that much of the HCN was destroyed but a leak was found that prevented the extent of the catalytic activity of the reactor to be established exactly.

A new two-stage reactor was then installed and three fuel oil samples were run to measure the NO yields. Those results were reported above. Before restarting the coal experiments, HCN calibration experiments B and C (Table 1-11) were

TABLE 1-11. SUMMARY OF DATA ON HCN FORMATION FROM PITTSBURGH NO. 8 COAL IN TWO-STAGE REACTOR

		Temperature, C			
Experiment	Type	First Stage	Second Stage	Second-Stage Condition	% HCN
1	Coal	757	755	Oxidative	0.4, 0.5
2	Coal	756	755	Inert	5.1, 5.0
A	HCN Calibration (experimental problem but reactor apparently catalytic)				
* Replaced reactor					
B	HCN Calibration	757	757	Inert	87, 89
C	HCN Calibration	755	758	Oxidative	69, 69
3	Coal	754	754	Oxidative	0.8, 0.5
D	HCN Calibration	751	551	Oxidative	92, 91
E	HCN Calibration	753	752	Oxidative	36, 33
F	HCN Calibration	757	754	Inert	73, 74
4	Coal	753	757	Inert	6.8, 4.8
G	HCN Calibration	755	757	Inert	41, 53

carried out in this nearly new reactor. The following tabulation compares the calibration results obtained in this reactor with both stages at about 750 C:

Experiment	Number of Coal Samples Pyrolyzed	% HCN Recovered	
		Inert	Oxidative
B	0	87, 89	
C	0		69, 69
F	2	73, 74	
E	2		36, 33
G	4	41, 53	

The 88% recovery obtained in experiment B indicated that the wall of the reactor had become slightly catalytic toward HCN decomposition during the three fuel oil experiments. The lower recovery when the oxygen was flowing (experiment C) established that catalytic oxidation of HCN (in the second stage) occurs to an even greater extent. After the first two coal samples were run in this new reactor, the amount of HCN consumed in the calibration experiments more than doubled under both inert and oxidative conditions. This effect of coal on the activity of the second stage was not expected because a quartz wool plug is positioned between the stages to prevent the carryover of ash particles. Following two more coal experiments, the reactor was quite catalytic even under inert conditions and no more HCN measurements were made.

Nitric Oxide Yields. Two additional oxidative pyrolyses experiments with the Pittsburgh No. 8 seam coal (850 C/900 C) gave uncorrected NO yields of 5.9 and 5.7%. Calibration experiments conducted after each of these coal experiments gave NO recoveries of only 32 and 20%, respectively. It appeared, therefore, that the actual amount of NO formed in the second stage is considerably larger than the 6% measured in these first two coal experiments.

The reactor was then etched to remove any residues that interfere with NO formation. Two additional coal experiments were carried out and these gave uncorrected NO yields of 10.0 and 5.4%, respectively. An NO calibration conducted after the latter experiment gave an NO recovery of 52% indicating that the condition of the reactor was inhibiting the formation of NO somewhat in the final coal experiment. These results are consistent, therefore, with the conclusion that in a freshly etched reactor the NO yield from the coal is about 14% under these conditions (with about 30% of this NO passing through) the trapping system. After one coal experiment, however, the residue in the reactor reduces the NO yield appreciably.

The corrected NO yields obtained from two-stage oxidative pyrolysis (with the stages at 850 and 900 C, respectively) are 20% from the oil and 14% from the coal (based on the total nitrogen in the fuels). Since about 40% of the oil nitrogen is volatile under the first stage conditions (Table III of Ref. 3) and 24% of the coal nitrogen is volatile (as discussed above) about one-half of the fuel nitrogen reaching the second stage is converted to NO in the oil experiments and about 60% is converted to NO in the coal experiments.

TASK 2: COMBUSTION KINETICS

The effort under this task extended the flame studies previously carried out under Contract 68-02-0625 (Ref. 1). Low-pressure, flat-flame burner studies were conducted to investigate further the mechanisms and kinetics involved in the conversion of fuel-nitrogen intermediates (such as NH_3 and HCN) to NO_x in combustion. In addition, the rates and mechanisms for the formation of thermal and fuel NO in the flame front were compared directly, and the formation of fuel NO was investigated in a simulated low Btu fuel ($CO + H_2$).

The firm conclusions that could be drawn from our previous flat-flame burner study of CH_4-O_2-Ar flames were limited by the fact that the measurement techniques employed could not distinguish between HCN and NH_3 (however, the sum of the concentrations of these two species could be measured approximately). The HCN and NH_3 were oxidized to NO and measured as NO in a TECO chemiluminescent analyzer (CA). Even with this limitation, most of the tentative conclusions from that study have been confirmed in this and other investigations. These conclusions included: (1) NH_3 reacts rapidly in or below the luminous zone whereas HCN reacts more slowly with much of the HCN surviving the luminous zone in both rich and lean flames; (2) in a rich flame, much of the NH_3 is converted to HCN which then reacts very slowly above the luminous zone to form NO; (3) in a lean flame, HCN reacts rapidly just above the luminous zone; (4) nearly all of the NO that exits the reactor forms above the top of the luminous zone (just above and in high yield in lean flames and far above and in low yields in rich flames); and (5) NO added to a rich flame is rapidly consumed in the luminous zone (forming some HCN) and then partially reforms.

In the flame studies reported here, high fuel-N concentrations (2500 ppm NH_3-total basis) were employed in some of the experiments to obtain more detailed data under the conditions of the previous study. In many of the experiments, however, the additive concentrations (NH_3 or HCN) were only 50 ppm (total basis) so that the thermal NO and the thermal-N intermediates would not be insignificant compared to the fuel NO and fuel-N intermediates. This permitted the formation of thermal NO to be compared with the formation of fuel NO. Three types of flames were studied in this investigation: (1) CH_4-O_2-Ar as used in the previous study to investigate fuel NO only, (2) CH_4-O_2-N_2 to study simultaneously thermal and fuel NO formation, and (3) H_2-CO-O_2-Ar-NH_3 to follow fuel NO formation in a simulated low Btu fuel.

EXPERIMENTAL

The low-pressure flat-flame burner apparatus built for the previous program was used in this study with only minor modifications. Major changes were made, however, in gas analysis train.

The design of the burner head, the thermocouple support, and the quartz microprobe is discussed in Ref. 1 and shown in Fig. 2-1. Shown in Fig. 2-2 is a schematic of the flat-flame burner system. The burner head is enclosed in a glass envelope to maintain the nominal operating pressure of 0.1 atm. The purge gas is introduced below the burner head and flows around it. During an experiment, either the thermocouple or the microprobe was placed over the centerline of the burner and the burner was moved up and down to vary the distance between the probe and the burner top.

A stainless screen attached to the top of the burner head serves as a flame holder (Fig. 2-1). This screen is 1.1 mm thick and the bottom of the screen (top of the burner head) is arbitrarily defined as zero on the distance scales plotted later in some of the figures. Not shown was another screen above the probe and thermocouple. This was required for stable operation of the burner under some conditions.

In the methane flames, coated Pt/Pt-Rh thermocouples were used to measure the temperature as in the previous program. However, these thermocouples were found to be unsatisfactory for prolonged use in the CO-H_2 flames and a coated Ir/Ir-Rh thermocouple had to be used. The temperature measurement techniques and the associated problems are described in Appendix C and in the later discussions of the experimental results.

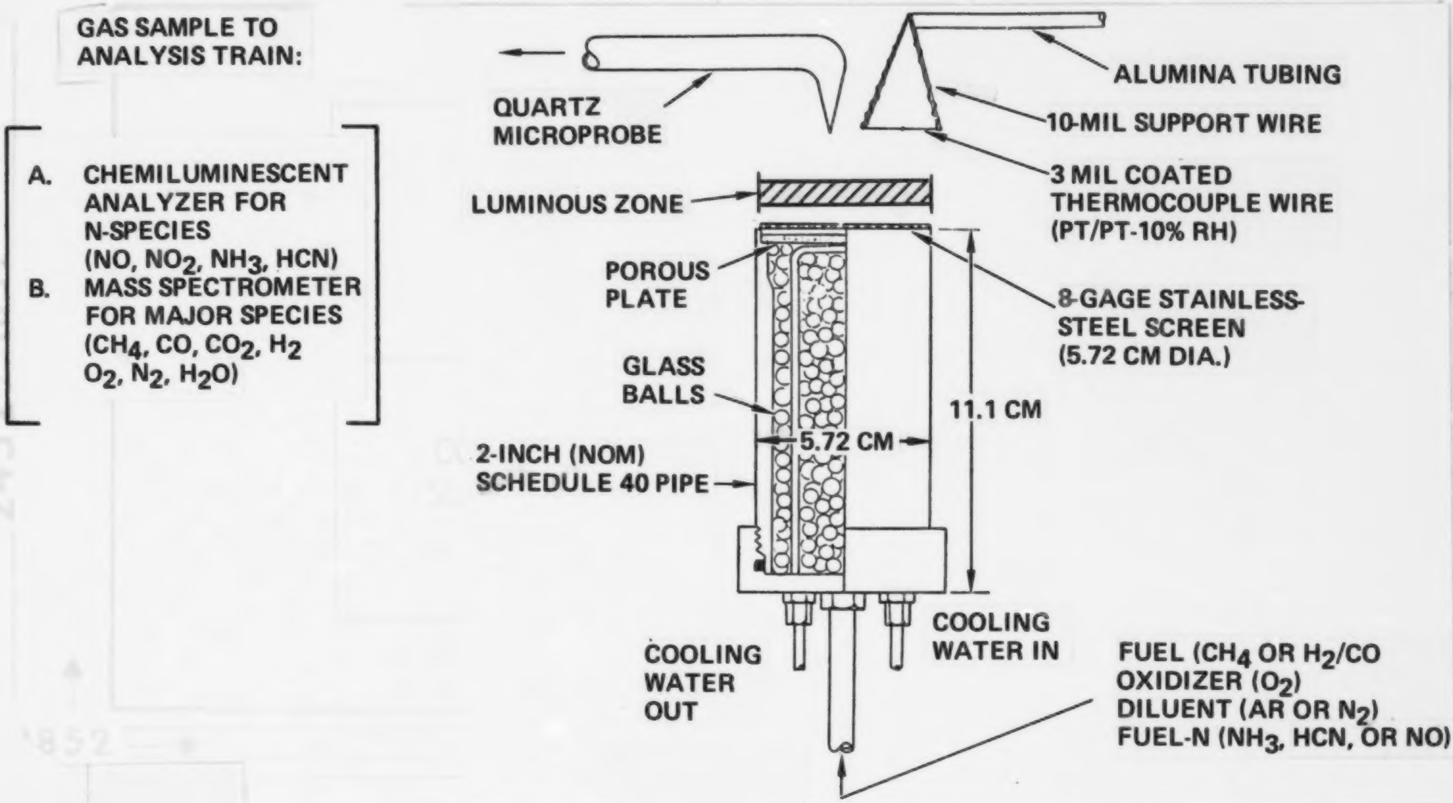
GAS SAMPLE TO ANALYSIS TRAIN:
A. CHEMILUMINESCENT ANALYZER FOR N-SPECIES (NO, NO_2, NH_3, HCN)
B. MASS SPECTROMETER FOR MAJOR SPECIES (CH_4, CO, CO_2, H_2 O_2, N_2, H_2O)
QUARTZ MICROPROBE
ALUMINA TUBING
10-MIL SUPPORT WIRE
3 MIL COATED THERMOCOUPLE WIRE (PT/PT-10% RH)
LUMINOUS ZONE
POROUS PLATE
8-GAGE STAINLESS-STEEL SCREEN (5.72 CM DIA.)
GLASS BALLS
11.1 CM
5.72 CM
2-INCH (NOM) SCHEDULE 40 PIPE
COOLING WATER IN
COOLING WATER OUT
FUEL (CH_4 OR H_2/CO
OXIDIZER (O_2)
DILUENT (AR OR N_2)
FUEL-N (NH_3, HCN, OR NO)

Figure 2-1. Design of the Flat-Flame Burner (Cut-Away View)

USE SPECIAL DROPOUT BLUE PENCIL
ONLY TO INDICATE CORRECTIONS
CLASSIFICATION
PAGE

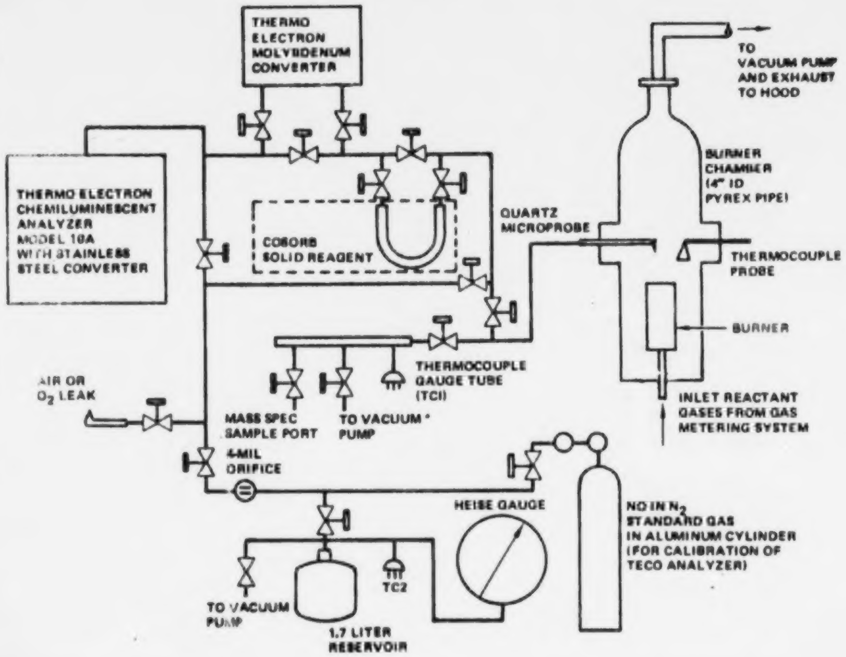
THERMO ELECTRON MOLYBDENUM CONVERTER
TO VACUUM PUMP AND EXHAUST TO HOOD
THERMO ELECTRON CHEMILUMINESCENT ANALYZER MODEL 10A WITH STAINLESS STEEL CONVERTER
BURNER CHAMBER (4" ID PYREX PIPE)
QUARTZ MICROPROBE
COSORB SOLID REAGENT
THERMOCOUPLE PROBE
BURNER
THERMOCOUPLE GAUGE TUBE (TC1)
AIR OR O_2 LEAK
MASS SPEC SAMPLE PORT
TO VACUUM PUMP
INLET REACTANT GASES FROM GAS METERING SYSTEM
4-MIL ORIFICE
HEISE GAUGE
NO IN N_2 STANDARD GAS IN ALUMINUM CYLINDER (FOR CALIBRATION OF TECO ANALYZER)
TO VACUUM PUMP
TC2
1.7 LITER RESERVOIR

Figure 2-2. Schematic of the Flat-Flame Burner System

TYPIST 90

As before, the sonic orifice at the tip of the quartz microprobe was used to meter the gas sample into the CA. The pressure dropped across this orifice from 76 torr to about 1 torr the nominal operating pressure of the CA reaction chamber. The NO concentration as measured by the CA under these conditions was proportional to the flowrate of the sample through the sonic orifice and the NO concentration in the sample. The CA was calibrated by flowing a standard gas mixture through a 4-mil orifice. The opening on the quartz probe was calibrated by flowing this same calibration gas through the probe in a calibration chamber (Fig. 45 of Ref. 1). The flow through the probe during a combustion experiment was calculated using the sonic orifice equation (Ref. 1), taking into account the temperature of the probe at the time of the measurement and the molecular weight and γ of the gas sample (assuming chemical equilibrium). The measured NO concentration is corrected by the ratio of the sample flowrate to the flowrate during the calibration of the probe. Evacuated glass flasks could also be filled through the quartz probe for mass spectrometric measurement of the concentration of the stable species. A number of changes were made in the gas analysis train at the start of this study so that the concentrations above the burner of NO, NO_2, HCN, and NH_3 could be measured independently. In the previous study, the moly converter in the CA was operated at 1073 K and air was introduced into the sample to give partial oxidation of NH_3 and HCN to NO (Fig. 46 of Ref. 1) so these could be measured (as NO) with the CA. In the present study, the moly converter was operated at 623 K so that the only reaction that took place in it was reduction of NO_2 to NO. A stainless-steel converter was added which, when heated to 1070 K and with sufficient oxygen added to the sample, oxidized all of the NH_3 to NO and at least 80% of the HCN. This stainless-steel converter also reduced NO_2 to NO. Another important modification of the analysis system was a trap containing the solid reagent COSORB. This trap removes HCN and NO_2 if the product stream is passed through it before going to the converters and the CA.

As shown in Fig. 2-3 and described in more detail in Appendix D, the concentrations of the various nitrogen compounds in the gas sample collected by the probe can be determined by passing the gas through various paths, that may or may not include the trap and one of the converters, before reaching the CA. Depending upon the path chosen (Fig. 2-3), the measured NO will include the NO present in the combustion gas sample and the NO formed in one of the converters from the

USE SPECIAL DROPOUT BLUE PENCIL ONLY TO INDICATE CORRECTIONS CLASSIFICATION PAGE STARTING LINE

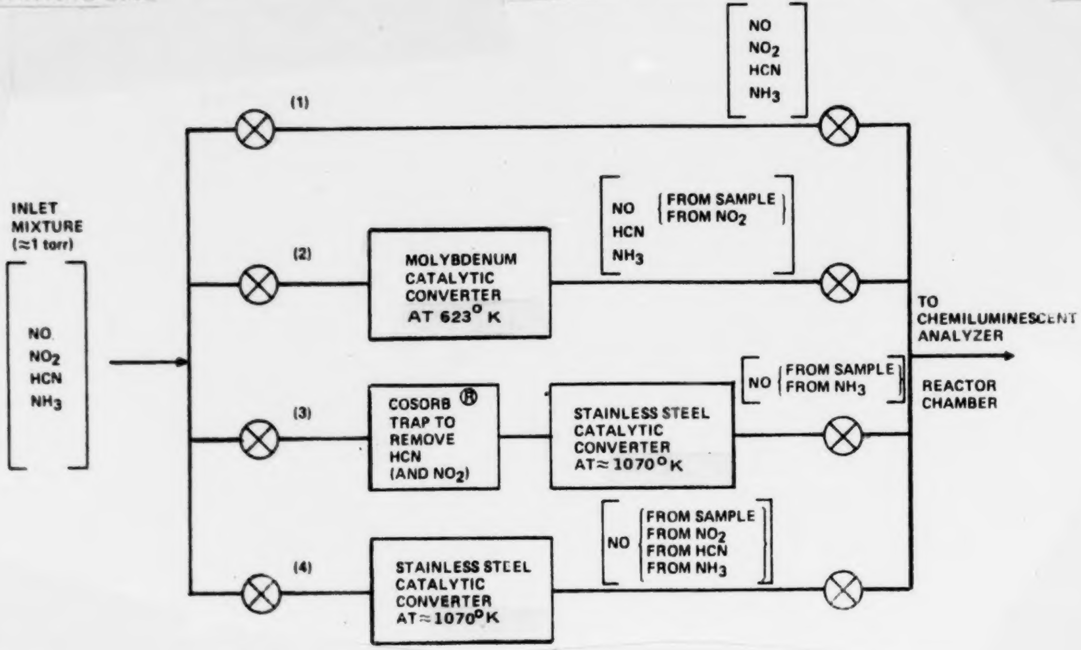
INLET MIXTURE (≈1 torr)
NO
NO2
HCN
NH3
(1)
(2)
(3)
(4)
NO
NO2
HCN
NH3
MOLYBDENUM CATALYTIC CONVERTER AT 623° K
NO { FROM SAMPLE FROM NO2
HCN
NH3
COSORB ® TRAP TO REMOVE HCN (AND NO2)
STAINLESS STEEL CATALYTIC CONVERTER AT ≈ 1070° K
NO { FROM SAMPLE FROM NH3
STAINLESS STEEL CATALYTIC CONVERTER AT ≈ 1070° K
NO { FROM SAMPLE FROM NO2 FROM HCN FROM NH3
TO CHEMILUMINESCENT ANALYZER
REACTOR CHAMBER

Figure 2-3. Experimental Scheme for Determination of NO, NO_2, NH_3 and HCN

CENTERLINE

other nitrogen species. By measuring the NO formed under each of the four conditions shown in Fig. 2-3, the concentrations of the four species (NO, NO_2, HCN, and NH_3) can be calculated by solving four simultaneous equations that also include the calibration factor for the conversion of HCN to NO in the stainless-steel converter (Appendix D).

The measurement technique described above (and in Fig. 2-2 and 2-3) is rather complicated and time consuming. It appears, however, to be the only way to measure these nitrogen species which may be present at concentrations as small as 5 ppm in a gas sample at a pressure that must be much less than 0.05 atm to give rapid quenching in the sonic orifice. Conversion of these species to NO takes advantage of the extreme sensitivity of the chemiluminescent analyzer in which NO is oxidized to NO_2^* with O_3 and the fluorescence of the NO_2^* is measured by a sensitive optical technique.

WARNING LINE STOP DOCUMENT NUMBER

Measurement of the major species in these flames (CH_4, O_2, CO, CO_2, and H_2) is also difficult at the low sample pressures but can be accomplished by the use of mass spectrometric analysis (Ref. 1). Evacuated flasks are opened to the probe during a run until the pressure in the flask reaches one torr. The inlet line to the flask is then fused shut to preclude any leakage and the sample is analyzed in a mass spectrometer a few days later.

INPUT-OUTPUT EXPERIMENTS

Before initiating detailed probing experiments with the methane flame, a number of "input-output" experiments were conducted to establish the general features of the flame and the modified apparatus as well as the optimum conditions for detailed probing. In most of these experiments, only the composition of the gas at the "output" of the burner was measured (80 mm above the burner). In others, the gas composition was measured at a few selected points.

The input-output test plan is shown in Table 2-1 and the objective of each test is described. The first three input-output test series (IA, IB and II) were with argon as the diluent to extend the previous burner study. In the remaining input-output experiments, nitrogen was used as the diluent to establish the conditions required to compare the formation of thermal NO with the formation of fuel NO. In experimental series III, the diluent ratio, DR*, was decreased from the value of 1.0 for air to obtain a temperature and N_2 concentration where a measurable amount of thermal NO would form.

---

*The diluent ratio (molar) is defined as

$$DR = \frac{\text{Diluent}/O_2}{(N_2/O_2)_{\text{air}}} = \frac{(N_2 \text{ or Ar})/O_2}{3.76}$$

TABLE 2-1. TASK 2 INPUT-OUTPUT TEST PLAN

(Species and temperature measured at 0.1 atm and d=80 mm, except where noted)

Series	Diluent	DR	ϕ***	Additive	ppm Additive		Feed Rate, cc/min	Description
					Total Basis	CH_4 Basis		
IA*	Ar	1	0.8	NH_3	2500	31,900	7520	(a) Check NO yield vs previous study (b) Vary H_2O flow and check effect on temperature and NO yield (c) "Measure" NO_2, HCN and NH_3 to ensure that zero blanks are obtained (d) Check importance of purge gas flowrate on NO (mixing effects downstream)
IB**	Ar	1	1.5	NH_3	2500	18,300	6247	Measure NO, NO_2, NH_3, and HCN just above the flame front and also at d=80 mm
II	Ar	1	0.8	N_2	1250	15,900	7520	Demonstrate that N2 once formed is not converted to NO
III	N_2	1.0 to 0.5	0.8	None	0	0	7520 Only up to temperature limit of apparatus	(a) Determine thermal NO as a function of N_2/O_2 ratio (none is expected at DR=1) (b) At DR where measurable thermal NO forms, vary cooling water rate and observe effect (c) At DR where thermal NO forms, measure NO and temperature at d=5, 10, 20, 30, 60, and 80 mm (d) At ϕ=1.5 and DR where thermal NO forms at ϕ=0.8, measure HCN, NH_3, NO_2, and NO just above the flame front
IV	N_2	0.7	0.5 to 1.5	NH_3	(vary)	31,900	7520	Determine NO yield from NH_3 in CH_4-air flame holding the N-content of the fuel constant at 2.83 wt %
V	N_2	0.7	0.8, 1.5	NH_3	wt % N in CH_4 2.5,0.5 and 0.1		7520	(a) Determine effect of additive concentration on NO yield (b) At ϕ=1.5, measure HCN, NH_3, NO_2, and NO @ d=80 mm and also just above the flame front at two N-additive concentrations

*Conditions same as Flame 1 in previous program (Ref. 1)

**Conditions same as Flame 4 in previous program (Ref. 1)

***The equivalence ratio, ϕ, is defined as:

$$\left[\frac{\text{Fuel}}{\text{Air}}\right] \div \left[\frac{\text{Fuel}}{\text{Air}}\right]_{\text{stoichiometric}}$$

USE SPECIAL DROPOUT BLUE PENCIL
ONLY TO INDICATE CORRECTIONS
CLASSIFICATION
PAGE

Input-Output Experiment IA (CH_4-Ar-O_2-NH_3, ϕ=0.8)

Experiment IA was a repeat of the conditions employed in Flame 1 of the previous program: 2500 ppm NH_3 (total basis) was added to a fuel-lean CH_4-O_2-Ar flame (0.1 atm) at an equivalence ratio of 0.8 and a diluent ratio of 1.0. The total feed rate was 7520 cm^3/min at 298 K and 1 atm. Nitrogen species and temperature were measured at 80.0 mm downstream of the burner. A 96.5% conversion of the NH_3 additive to NO and a downstream temperature of 1648 K was obtained. There was no detectable NO_2, NH_3 or HCN at this location. The input-output experiments of the previous program gave 81.9% conversion and 1731 K under these conditions.

Decreasing the cooling water flowrate through the burner from 960 to 234 cm^3/min produced no change in the measured NO concentration or downstream temperature. The cooling water passes through a tube immediately below and in contact with the sintered porous plate of the burner. It appears that varying the temperature of the sintered metal plate is not a feasible method of controlling the flame temperature.

Varying the argon purge gas flowrate does have a small influence on the measured NO concentration. Decreasing the purge gas flow by a factor of 3 resulted in an increase of several percent in the NO yield. This is probably due in part to a reduction in the convective heat transfer from the inner combustion gas stream to the outer purge gas annulus, and to less physical mixing of the two streams. The purge gas flowrate was maintained at a constant value in all remaining experiments.

Input-Output Experiment IB (CH_4-Ar-O_2-NH_3, ϕ=1.5)

Experiment IB was a repeat of the conditions employed in the fuel-rich Flame 4 of the previous program: 2500 ppm NH_3 (total basis) was added to a CH_4-O_2-Ar flame (0.1 atm) at an equivalence ratio of 1.5 and a diluent ratio of 1.0. The total feed rate was 6247 cm^3/min at 296 K and 1 atm. Nitrogen species and temperature were measured both at 80.0 and 5.50 mm downstream of the burner; the latter distance corresponding to the top of the luminous zone approximately 2.5 mm below the point of the maximum axial temperature. The results of experiment IB are summarized in Table 2-2. At the position 5.50 mm above the burner, the gas temperature was found to be 1987 K compared with 1920 K in the previous study (Fig. 68 of Ref. 1) and 78% of the initial NH_3 additive was recovered as HCN. This confirms that NH_3 reacts in the fuel-rich flame to form high yields of HCN most of which survives the flame front. This conclusion was only obtained indirectly from the Flame 4 results of Ref. 1 because HCN and NH_3 could not be separated. The HCN mole fraction measured at this point in the previous study (1.25 msec in Fig. 69 of Ref. 1) was about 40% of the initial NH_3. It is now established that NH_3 reacts in the fuel-rich flame forming high yields of HCN most of which survives the flame front.

TABLE 2-2. RESULTS OF INPUT-OUTPUT EXPERIMENT IB
(NH_3 Addition to Fuel-Rich CH_4-O_2-Ar Flame)

Axial Distance From Top of Burner, mm	Axial Temperature, K	Combustion Product Composition		
		Species	Concentration (ppm)	Percent of Initial NH_3 Additive
80.00	1565	NO	794	31.8
		NO_2	--	--
		HCN	107	4.3
		NH_3	--	--
5.50	1987	NO	418	16.5
		NO_2	6	0.2
		HCN	1964	77.7
		NH_3	100	4.0

At 80.0 mm downstream, the gas temperature was determined to be 1565 K and the NO yield was 31.8% (Table 2-2). An input-output experiment was not conducted during the previous program under these exact conditions but comparison with similar experiments A-8 and I-1 (Table 21 of Ref. 1) indicates good agreement.

Input-Output Experiment II (CH_4-Ar-O_2-N_2, ϕ=0.8)

The purpose of experiment II was to confirm that N_2 once formed is not reconverted to NO. 1250 ppm N_2 (total basis) was added to a CH_4-O_2-Ar flame under the same conditions that were employed in experiment IA. Adding N_2 rather than NH_3 simulates the situation that would exist in experiment IA if all of the NH_3 were converted to N_2 in the flame front. At the measurement location of 80.0 mm downstream of the burner, less than 0.3 ppm NO was detected. This result confirms one of the indirect conclusions obtained during the previous program, namely that none of the NO that appeared to form from NH_3 and HCN formed from N_2 as an intermediate.

Input-Output Test Series III (CH_4-N_2-O_2, ϕ=0.5, "Thermal NO" - Nitrogen Diluent)

Input-output experiments III through V provided the first opportunity to investigate in this burner CH_4-O_2 flames with N_2 as the diluent rather than argon. Thermal NO formation was studied in Series III (no additive), while the objective of experiment IV was to determine the effect of equivalence ratio on NO yield from NH_3 holding the N-content of the fuel constant at 2.78% w. The purpose of input-output experiment V was to analyze the effect of additive concentration (0.1 to 2.5% w N in CH_4) on NO yield. Input-output test series III was conducted first mainly to observe CH_4-O_2-N_2 flame structure and stability over a range of diluent ratios and to establish the most appropriate diluent ratio for use in experiments IV and V.

Input-output experiment III(a) involved the investigation of a CH_4-O_2-N_2 flame (0.1 atm) at an equivalence ratio of 0.8 and diluent ratios ranging between 1.0 and 0.5. The total feed rate was 7520 cm^3/min. Thermal NO and temperature were measured at 80.0 mm downstream of the burner and the results are given in Table 2-3. An Arrhenius plot of the data in Table 2-3 gave an apparent activation energy of 50.3 kcal/mole. A similar Arrhenius plot using the adiabatic flame temperature gave an apparent activation energy of 17.3 kcal/mole. Since the Zeldovich mechanism predicts an activation energy of 135 kcal/mole (assuming that O atoms are in equilibrium with O_2), the thermal NO did not increase nearly as rapidly with decreasing diluent ratio as was expected.

TABLE 2-3. RESULTS OF INPUT-OUTPUT EXPERIMENT III(a)

Diluent Ratio $N_2/(3.76\ O_2)$	Gas Temperature at d = 80.0 mm, K	NO Concentration at d = 80.0 mm, ppm
1.0	1576	6.2
0.9	1579	6.8
0.8	1594	7.6
0.7	1611	8.5
0.6	1626	10.2

This suggests that the actual maximum flame temperature increases much less rapidly than the adiabatic temperature, because the flame moves closer to the burner as the diluent ratio is decreased. Another explanation, proven later in this study, is that the Zeldovich mechanism does not dominate under these conditions.

As the diluent ratio was reduced, the luminous zone moved closer to the top of the burner, until at DR = 0.5 the bottom of the luminous zone nearly impinged upon the top of the burner screen. Since this latter condition caused severe overheating of the burner screen and would not be suitable for detailed probing studies, no temperature and composition data were obtained at DR = 0.5.

In experiment III(b) conducted at DR = 0.6, decreasing the cooling water flowrate through the burner from 1000 to 200 cm^3/min produced no change in downstream temperature or NO concentration. This result agrees with the data obtained in experiment IA and confirms that varying the temperature of the sintered metal plate does not provide a feasible method of controlling the flame temperature.

Experiment III(c) was performed under the same conditions reported above in III (a), except that a constant diluent ratio of 0.7 was employed. The latter value was chosen by approximately matching the adiabatic flame temperature at this condition to that of a CH_4-O_2-Ar flame at ϕ = 0.8 and DR = 1.0*. The measured temperature and NO concentration profiles as a function of distance downstream of the burner are shown in Fig. 2-4 and 2-5. The temperature decreased from 1988 K 5.5 mm above the burner to 1635 K at 80 mm, and the thermal NO profile increased gradually from 5.1 ppm at 5.0 mm reaching a maximum of 10.2 ppm at 50 mm. The NO concentration decreased slightly from its maximum value to 9.5 ppm at 80 mm and this was probably caused by gradual mixing of the central combustion gases with the outer annular N_2 purge gas stream.

Flux calculations were not made for the input-output experiments but it appears that the maximum rate of thermal NO formation occurs from 10 to 20 mm above the burner under these conditions. The temperature in this region is 10 to 50 degrees below the maximum flame temperature but the maximum oxygen atom concentration probably occurs there.

The objective of input-output experiment III(d) was to probe a fuel-rich CH_2-O_2-N_2 flame (Ø = 1.5) just above the flame front to measure NO, NO_2, HCN and NH_3 under conditions where measurable thermal NO forms when Ø = 0.8. Based upon the results of III(c) a diluent ratio of 0.7 was employed, while the total flowrate was maintained constant at 7520 cc/min. Measurements were made at 6.05 mm downstream of the burner, or approximately 0.7 mm above the top of the luminous zone, and at 80.0 mm. At 6.05 mm, the measured temperature and thermal NO concentration were 1984 K and 8.9 ppm, respectively, while at 80 mm these values were found to be 1617 K and 38.9 ppm. Note that the thermal NO formed at Ø = 1.5 and d = 80 mm is nearly a factor of 4 higher than that formed at Ø = 0.8 and d = 80 mm at approximately the same downstream temperature (Fig. 2-4 and 2-5).

Upon passing the sampled combustion gas through the stainless-steel converter at 840 C to determine if "thermal" NH_3 and HCN were present at the top of the

---

*This temperature is about 2300 K as shown later in Fig. 2-54.

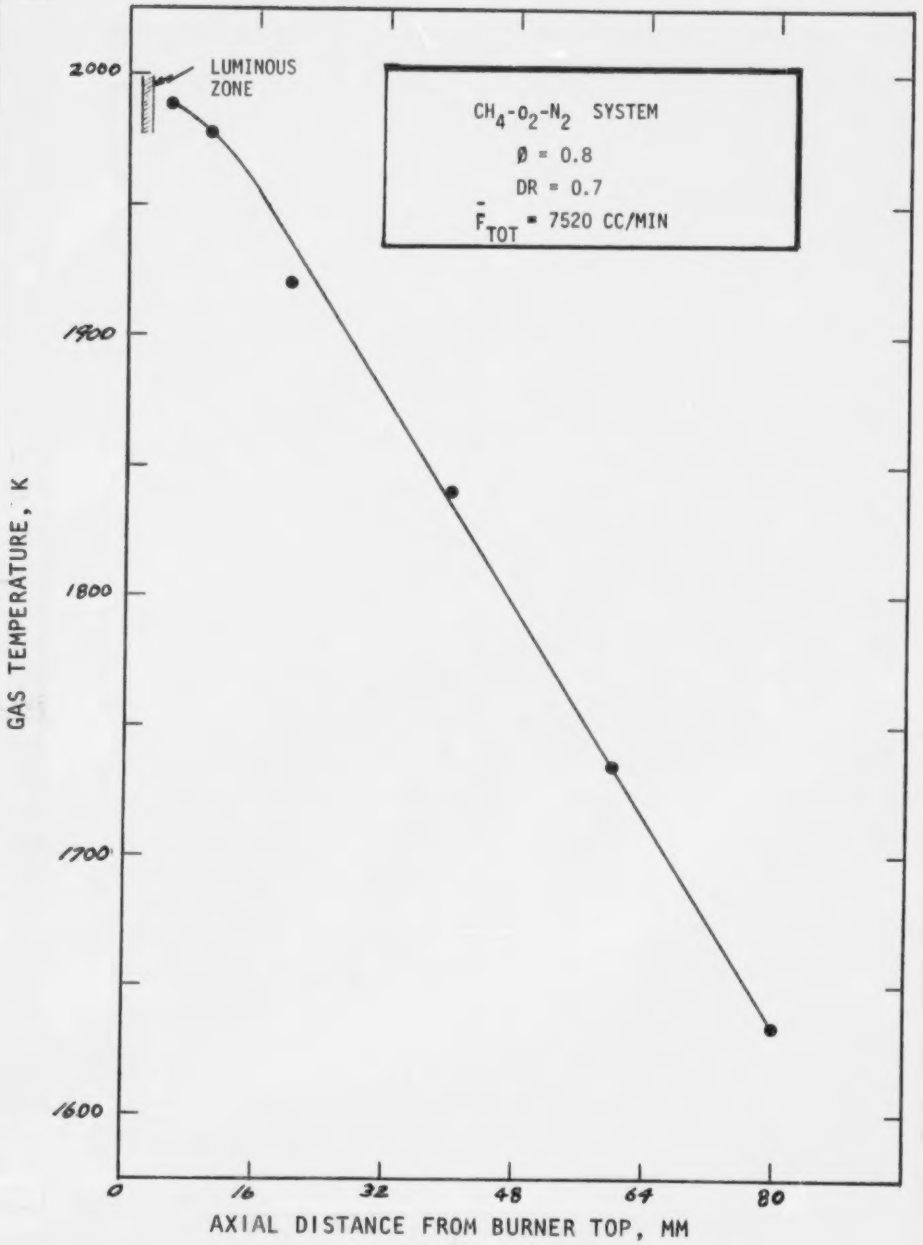

Figure 2-4. Input-Output Experiment III(c) - Temperature Profile

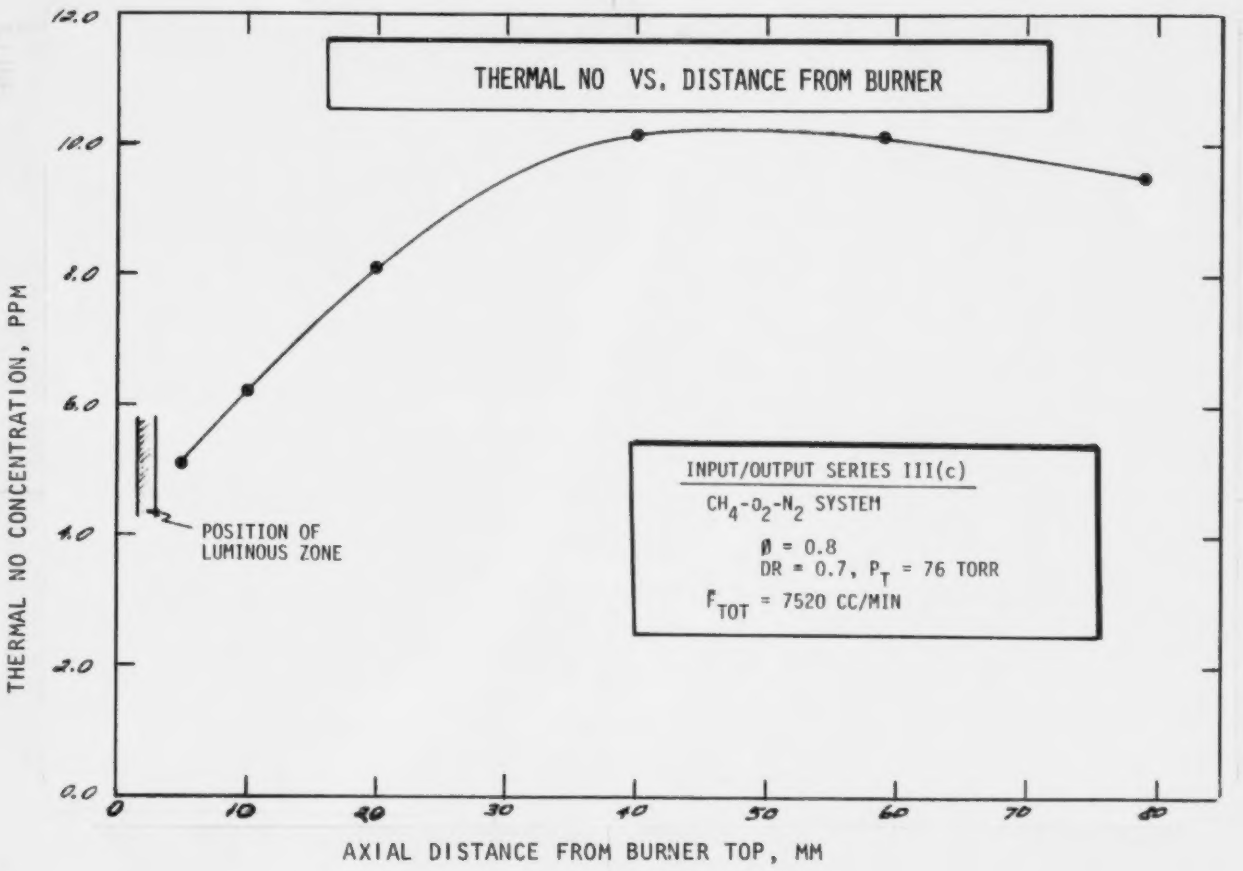

Figure 2-5. Input-Output Experiment III(c) - Thermal NO Profile

USE SPECIAL DROPOUT BLUE PENCIL
ONLY TO INDICATE CORRECTIONS
CLASSIFICATION
PAGE
STARTING LINE

luminous zone, the NO_x reading of the chemiluminescent analyzer increased only slightly above the value obtained in the NO mode (i.e., with the converter bypassed). However, after about 13 minutes at this new condition, the NO_x reading decreased suddenly by an order of magnitude and held constant at this lower value thereafter. Parks el al. (Ref. 18), in a study of the formation and emission of NO in a fluidized bed combustor, have also made NO analyses with a Thermo-Electron Model 10A Chemiluminescent NO-NO_x Gas Analyzer containing a stainless steel converter. They found that with very rich mixtures (fuel-air equivalence ratio of 1.2 or more) the TECO analyzer did not measure properly in its NO_x operating mode. They ascribed the discrepancy to the catalytic destruction of NO in the stainless-steel converter. Our analysis system contains a controlled air leak between the probe and the stainless-steel converter but the amount of oxygen introduced in this manner was apparently insufficient. It was decided that the problem of the catalytic removal of NO in the stainless-steel converter in fuel-rich mixtures should be investigated further in input-output experiment V(b) in which, at $\phi = 1.5$, HCN and NH_3 were to be measured just above the flame front at two NH_3 additive concentrations. The results of these studies, including the effect of adding more oxygen, are reported in a later section (Fig. 2-9).

Input-Output Experiment IV (CH_4-O_2-N_2-NH_3, $\phi = 0.5$-1.5)

The purpose of input-output experiment IV was to determine the effect of equivalence ratio on NO yield from NH_3 holding the N-content of the fuel constant at 2.78 wt%. The experiment involved the investigation of a CH_4-O_2-N_2 flame (0.1 atm) at a diluent ratio of 0.7 (changed from the planned value of 1.0 for the reasons discussed above) and equivalence ratios ranging from 0.5 to 1.5. On a total concentration basis, the NH_3 additive ranged from 2077 ppm at $\phi = 0.5$ to 5513 ppm at $\phi = 1.5$. At $\phi = 0.6$, the NH_3 concentration was 2461 ppm of the total flow which is similar to the additive concentrations used in the argon diluent flames of the previous program. The total feed rate was 7520 cc/min. Measurements of the NO concentration and temperature were made at 80 mm downstream of the burner. The results of experimental series IV are summarized in Fig. 2-6 and 2-7.

---

18. Parks, D. J., and E. A. Fletcher, "Formation and Emission of Nitric Oxide in Fluidized Bed Combustion", Environ. Sci. Technol. 9 (8), 749-756 (1975).

Figure 2-6 is a plot of the NO yield on a percentage basis as a function of equivalence ratio. As expected, the conversion of NH_3 to NO remains high at very lean conditions (>90% at ϕ = 0.5 to 0.7), but begins to drop off at ϕ = 0.8 to 0.9. Thereafter, the percent yield of NO decreases almost lineraly with equivalence ratio. The same effect of equivalence ratio on NO yield was obtained in the screening experiments conducted under the previous program using HCN and NH_3 additives in CH_4-O_2-Ar flames (Fig. 53 of Ref. 1). In the previous experiments, the total additive concentration was maintained constant at approximately 2500 ppm. The yield of NO from NH_3 at $\phi \leq 0.8$ has been consistently higher in the present program (~90 to 95%) compared to that reported in the previous work (~83 to 84%) and this higher yield has been tentatively attributed to more extensive calibration of the additive metering system. The slightly lower NO yield in the present study at ϕ = 1.5 would be expected from the higher additive concentration now employed at this equivalence ratio (5513 vs 2500 ppm).

Figure 2-7 shows the variation in the measured downstream temperature (corrected for radiation) as a function of equivalence ratio. Again the general trends were somewhat similar to those in the screening experiments of the previous program (Table 24 of Ref. 1). The measured temperature reached a maximum at an equivalence ratio of 1.1 and the luminous zone was closest to the burner screen (flame holder) at this condition causing the screen to glow with a faint reddish hue. As the flame was made increasingly fuel lean (maintaining the diluent ratio at 0.7), the luminous zone decreased in intensity and at ϕ = 0.7 began to move away from the top of the burner. At ϕ = 0.5, the luminous zone became very diffuse and partially lifted off the burner but was stable. When the equivalence ratio was increased above 1.1, the luminous zone was still intense at ϕ = 1.3 but was widening and moving away from the burner. Increasing ϕ to 1.5 served only to move the luminous zone further downstream. Thus, the increase in the measured combustion gas temperature between ϕ = 1.3 and 1.5 was apparently a result of the increase in the distance of the luminous zone from the burner (at a nearly constant flame intensity) with a concomittant decrease in heat loss to the top of the burner.

USE SPECIAL DROPOUT BLUE PENCIL ONLY TO INDICATE CORRECTIONS
CLASSIFICATION
PAGE

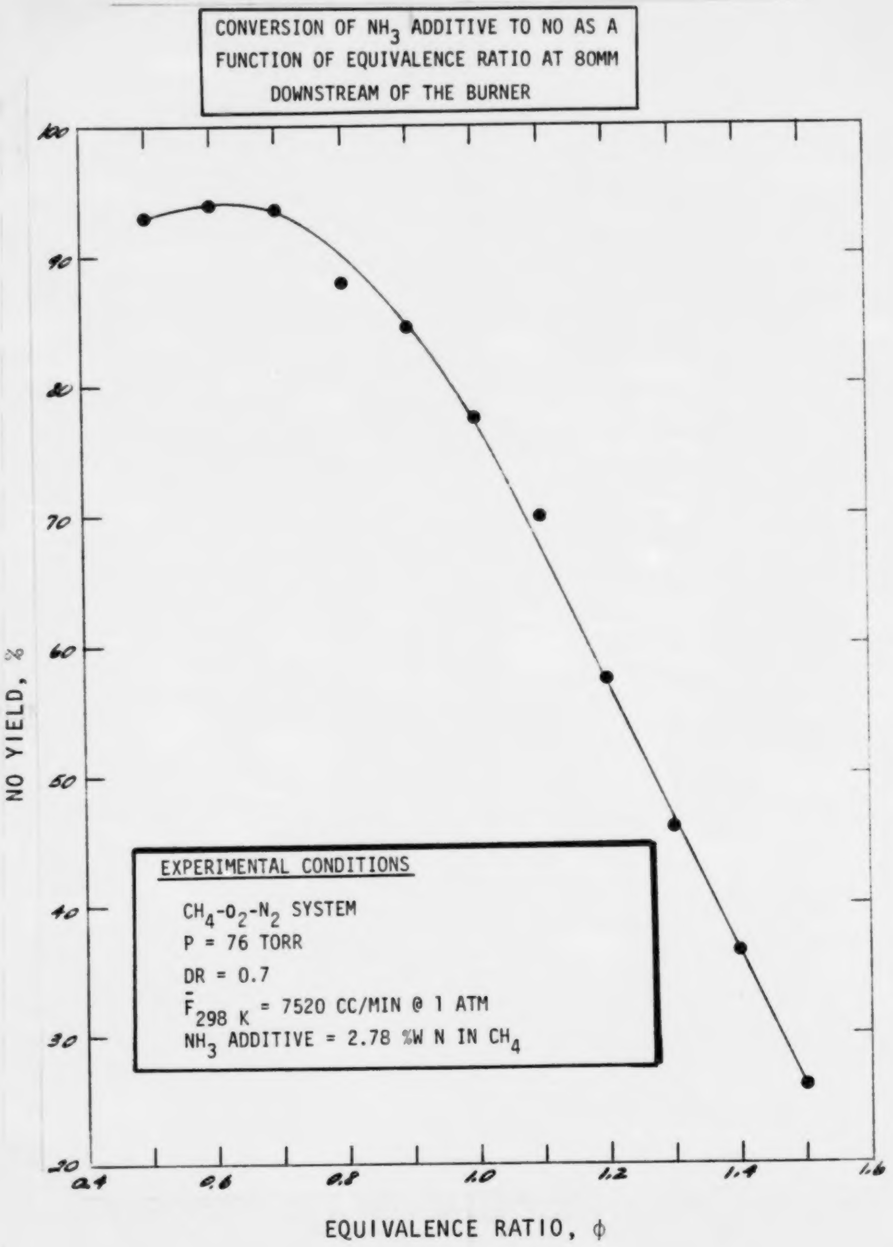

Figure 2-6. Input-Output Experiment IV - NO Output vs ϕ

TYPIST 104

USE SPECIAL DROPOUT BLUE PENCIL
ONLY TO INDICATE CORRECTIONS
CLASSIFICATION
PAGE
STARTING LINE

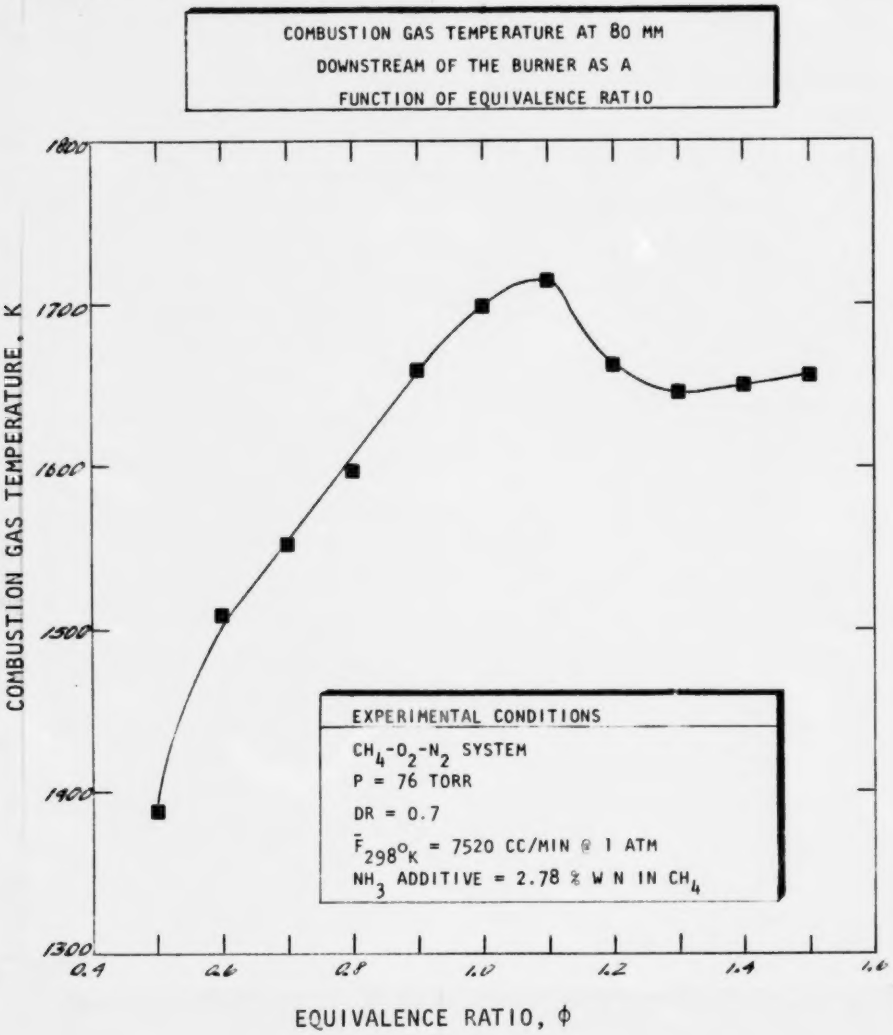

Figure 2-7. Input-Output Experiment IV - Temperature at 80 mm vs ϕ

WARNING LINE
STOP
DOCUMENT NUMBER
PAGE NUMBER
CLASSIFICATION

Input-Output Test Series V (CH_4-N_2-O_2-NH_3, Ø = 0.8, 1.5)

The primary objective of the series V input-output experiments was to determine the effect of additive concentration (0.1 to 2.5 wt% N in CH_4) on NO yield. Ammonia was added to a CH_4-O_2-N_2 flame (0.1 atm) at a diluent ratio of 0.7 and equivalence ratios of 0.8 and 1.5. The total feed rate was maintained constant at 7520 cc/min. In series V(a), the NO concentration and combustion gas temperature were measured at 80 mm downstream for both equivalence ratios and also at 6.05 mm (top of the luminous zone) for Ø = 1.5. The results obtained are presented in Table 2-4 and Fig. 2-8.

T2-4
F2-8

The amounts of fuel NO formed were calculated by subtracting from the measured NO the amount of thermal NO that would have been present in the absence of NH_3 additive. This is not strictly rigorous because (1) possible interactions of the reactions forming thermal and fuel NO are ignored and (2) the mole fractions were corrected rather than fluxes and, therefore, diffusion is not taken into account. However, the correction for thermal NO was relatively small except in the one measurement at 0.1 wt% N at 80 mm and Ø = 1.5.

As expected, the conversion of NH_3 to NO increased as the additive concentration decreased at a given equivalence ratio and position. The second NO yield listed in Table 2-4 is obviously spurious and should be lower by about 10%. The fuel NO yields were considerably higher at Ø = 0.8 than at Ø = 1.5 in agreement with the series IV results (Fig. 2-6).

F2-6

In experiment V(b) at Ø = 1.5, HCN, NH_3, NO and NO_2 were to be measured at d = 80 mm and just above the flame front at two NH_3 additive concentrations. Determination of HCN and NH_3 requires passage of the gas sample through the stainless-steel converter (at 840 C) of the chemiluminescent analyzer. A controlled air leak is employed in the present analytical system upstream of the stainless-steel converter to provide sufficient O_2 to react with HCN and NH_3 to form NO under fuel-rich conditions. The leak consists of a small hole in a piece of quartz tubing (similar to the probe) which admits air at 1 atm to the gas sampling stream which is maintained at approximately 1 torr. Using this same analytical

106

TABLE 2-4. NO FORMATION VS NH_3 ADDITIVE CONCENTRATION IN INPUT-OUTPUT EXPERIMENTAL SERIES V(a)

Ø	wt % N in CH_4	Axial Distance From Top Of Burner, mm	Gas Temperature, K	Average Thermal NO (From III(c) and III(d)), ppm	Total Measured NO, ppm	Fuel NO Only, ppm	NH_3 Additive Concentration ppm	% NH_3 Converted to NO
0.8	2.5	80.00	1623	9	2610	2601	2873	90
	0.5	80.00	1620	9	599	590	569	104
	0.1	80.00	1609	9	118	109	114	96
1.5	2.5	80.00	1627	39	1455	1416	4953	29
	0.5	80.00	1623	39	581	542	982	55
	0.1	80.00	1627	39	157	118	196	60
1.5	2.5	6.05	1974	9	736	727	4953	15
	0.5	6.05	1996	9	229	220	982	22
	0.1	6.05	1983	9	52.4	43.5	196	22

USE SPECIAL DROPOUT BLUE PENCIL
ONLY TO INDICATE CORRECTIONS
CLASSIFICATION
PAGE
STARTING LINE

CONVERSION OF NH_3 TO NO VS. ADDITIVE CONCENTRATION

CH_4-O_2-N_2 FLAME
P_T = 76 TORR
DILUENT RATIO = 0.7
FEEDRATE = 7520 CC/MIN @ 298°C & 1 ATM

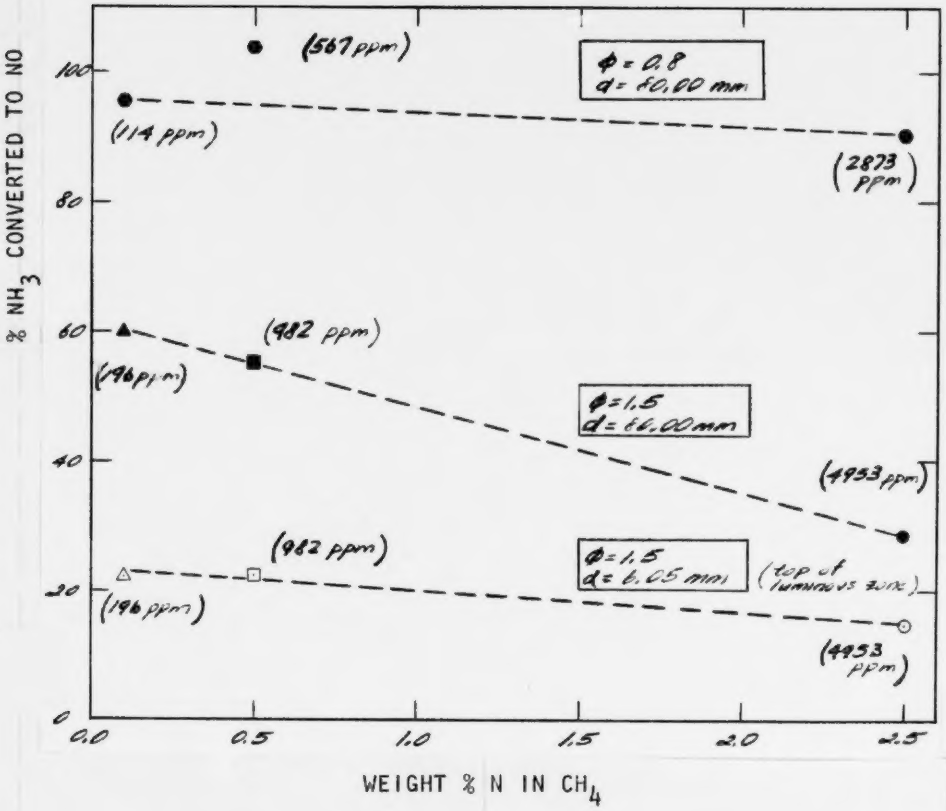

Figure 2-8. Input-Output Experiment V(a) - NH_3 Conversion vs NH_3 Concentration

WARNING LINE
STOP
DOCUMENT NUMBER
PAGE NUMBER

USE SPECIAL DROPOUT BLUE PENCIL ONLY TO INDICATE CORRECTIONS

scheme, a flame probing was conducted with 2.5 wt % N in the CH_4 (4953 ppm total basis) at d = 6.05 mm above the burner. As experienced earlier, following a brief induction period, the NO concentration dropped rapidly from about 3100 ppm to 70 ppm, as shown in Fig. 2-9, and the loss of NO in the converter was verified by passing a standard $NO\text{-}N_2$ mixture through the analysis system.

The activity of stainless steel toward the reactions of NO has been reported by Petersen and co-workers (Ref. 19). They found that a newly constructed 304 stainless-steel recycle batch reactor was significantly reactive to NO above 523 K. The extent of reactivity depended upon the pretreatment schedules used (oxidizing or reducing atmospheres), and whether the reactor surfaces were in an oxidized or a reduced state. Also, in a study of the $NO_2 \rightarrow NO$ reaction in a stainless-steel reactor, De Soete (Ref. 20) found that the NO concentration measured from a gas sample obtained near the flame front of a fuel-rich $C_2H_4\text{-}O_2\text{-}N_2$ gas mixture dropped to almost zero above 600 C. He concluded that this phenomenon will occur on a stainless-steel catalyst surface at high temperatures whenever the gas sample to be analyzed is overall reducing in composition (we do not agree with his conclusion that this results from direct reaction between NO and the reducing agent).

Based on these reported data, it was decided that a possible solution to the catalytic removal of NO on stainless steel would be to admit more O_2 via the air leak. This would probably change the composition of the gas sample from overall reducing to one of overall oxidizing. Thus, following the deactivation depicted in Fig. 2-9, a pure O_2 stream was flowed into the inlet to the "air" leak. This increased the O_2 admitted by the leak by a factor of 5. The result was dramatic and immediate. The NO concentration measured by the CA as the gas sample was passed through the stainless-steel converter at 840 C increased to slightly above its original value to 3300 ppm and was constant thereafter. Thus, it appears that the stainless-steel converter can be used to measure NO in fuel-rich mixtures, provided there is sufficient O_2 to make the gas sample overall oxidizing in composition.

---

19. Petersen, E.E., J. Landau, and E. Saucedo, "Micro and Macro Changes in a Stainless-Steel Catalyst During Reduction of NO," *The Catalytic Chemistry of Nitrogen Oxides*, Plenum Press, New York, 1965, pp. 119-131
20. De Soete, G. G., "La Formation des Oxydes D'Azote dans la Zone D'Oxydation des Flammes D'Hydroearbures (in French)", Institut Franeais der Petrole, Report 23309, June 1975, (Compte-Rendu Final des Travaux, Contrat No. 73-56, Avdc le Ministere de la Prutation de la Nature et de L'Envirinnement, 1. 4. 1973 Aer 31. 3. 1975).

USE SPECIAL DROPOUT BLUE PENCIL
ONLY TO INDICATE CORRECTIONS
CLASSIFICATION
PAGE
STARTING LINE

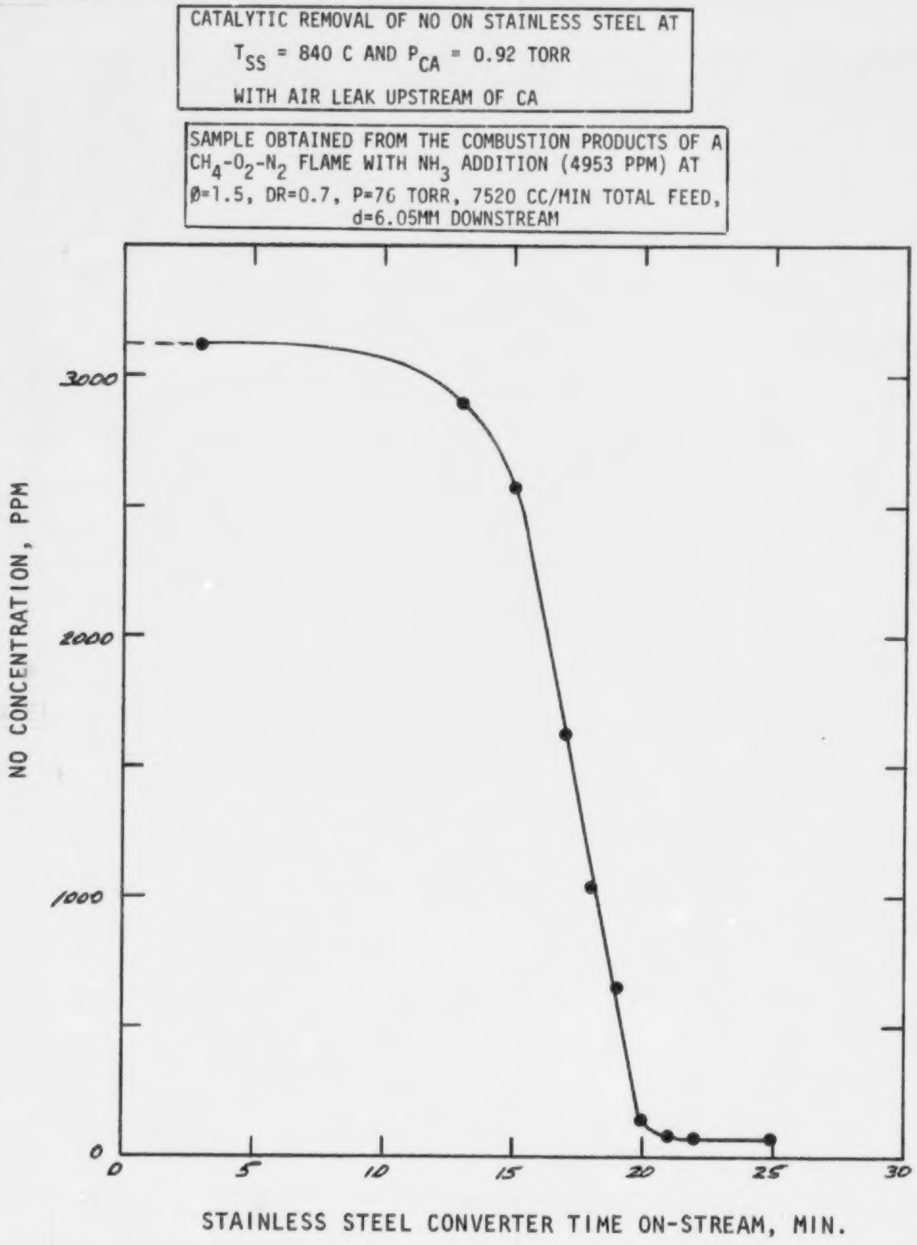

Figure 2-9. Catalytic Removal of NO on Stainless Steel at 840 C

WARNING LINE
STOP
DOCUMENT NUMBER
PAGE NUMBER
CLASSIFICATION

Using the O_2 leak, probing experiments were completed at d = 6.05 mm and $\phi = 1.5$ for the 2.5 and 0.5 wt % N in CH_4 N-additive concentrations. These data are summarized in Table 2-5. The results are similar to those obtained in input-output experiment IB for a fuel-rich CH_4-O_2-Ar flame with an NH_3 additive. The calculations reveal that a large fraction of the initial NH_3 additive is recovered as HCN, confirming again that NH_3 reacts in a fuel-rich flame to form high yields of HCN most of which survives the flame front. In each of the two N-additive levels, the HCN/NH_3 concentration ratio was found to be 25:1.

The measurements of HCN, NH_3 and NO_2 made at 70 mm at $\phi = 1.5$ and d = 80 mm were inconclusive due to an apparent outgassing of NO by the Cosorb solid reagent in these experiments. However, these data did indicate that very little, if any, HCN or NH_3 survive at this point downstream.

TEST PLAN-DETAILED PROBING EXPERIMENTS

The test plan for the 11 detailed flame probing experiments is presented in Table 2-6. Experiment No. 1 was carried out under the same conditions as flame 4 of the previous study (Ref. 1) in which a relatively high concentration of NH_3 was added to a rich CH_4-O_2-Ar flame. A CH_4-O_2-N_2 flame was investigated in experiments No. 2 through 6 so that the formation of thermal NO and fuel NO could be compared. The remaining five experiments (No. 7 through 11) involved the investigation of a H_2-CO-O_2-Ar flame to simulate a future low Btu alternative fuel that contains mainly CO and H_2. Ammonia was added to this flame to study fuel NO formation. Ammonia is a potential impurity in low Btu fuels depending on the manufacturing process employed. The results obtained with the methane flames will be presented first.

ADDITION OF 2500 PPM AMMONIA TO FUEL-RICH CH_4-O_2-Ar FLAME

In experiment No. 1, NH_3 was added to a rich CH_4-O_2-Ar flame in which the equivalence ratio, ϕ, was 1.5 and the diluent ratio, DR, was 1.0 (Table 2-6). The total pressure, as before, was 76 torr. These are the same conditions that were employed in flame No. 4 of Ref. 1 and in input-output experiment IB (Table 2-2).

TABLE 2-5. RESULTS OF DETAILED PROBING AT TOP OF FLAME FRONT IN INPUT-OUTPUT EXPERIMENT V(b)

Experimental Condition	wt % N in CH_4	Axial Distance From Top of Burner, mm	Axial Temperature, K	Combustion Product Composition		
				Species	Concentration, ppm	% of Initial NH_3 Additive
● CH_4-O_2-N_2 Flame ● P=0.1 atm ● Ø = 1.5 ● DR = 0.7 ● 7520 cc/min Feed rate at 298 K and 1 atm	0.5 (982 ppm total basis)	6.05	1996.3	NO	229*	22
				NO_2	--	--
				HCN	743	76
				NH_3	29	3.0
				TOTAL	1001	101.1
	2.5 (4953 ppm total basis)	6.05	1974.4	NO	736*	15
				NO_2	--	
				HCN	3260	66
				NH_3	131	2.6
				TOTAL	4127	83.1

*Includes about 9 ppm thermal NO

TABLE 2-6. TEST PLAN FOR DETAILED PROBING EXPERIMENTS

Experiment	Flame System	Diluent Ratio	ϕ	Total Feed Rate, cc/min	Additive Type	Additive Concentration, ppm	Description
1	CH_4-O_2-Ar (0.1 atm)	1.0	1.5	6247	NH_3	2500 (total basis)	• Repeat of Flame No. 4 in previous program (Ref.1) • Rate and extent of NH_3→HCN in fuel-rich flame • Rate of HCN conversion to NO • Concentration of HCN in exhaust of fuel-rich flame
2	CH_4-O_2-N_2 (0.1 atm)	0.7	1.5	7520	None	--	• Complete temperature and concentration probing to determine rate and location of thermal NO formation in fuel-rich flame • Rate and location of thermal HCN formation, if any
3	CH_4-O_2-N_2 (0.1 atm)	0.7	1.5	7520	NH_3	50 (total basis)	• Complete temperature and concentration probing • Extent and position of NO formation • Comparison of thermal vs fuel NO formation • Conversion of NH_3→HCN in fuel-rich flame • Mass spectrometry analysis for major species
4	CH_4-O_2-N_2 (0.1 atm)	0.7	1.5	7520	HCN	50 ppm (total basis)	• Detailed temperature and N-concentration probing • Rate and extent of HCN→NO • Compare HCN profiles experiments in 2 and 3
5	CH_4-O_2-N_2 (0.1 atm)	0.7	0.8	7520	None	--	• Detailed temperature and NO_x concentration probing only • Rate and location of thermal NO formation in fuel-lean flame
6	CH_4-O_2-N_2 (0.1 atm)	0.7	0.8	7520	NH_3	55 (total basis)	• Detailed NO_x concentration probing only • Extent and position of NO formation • Comparison of thermal vs fuel NO formation • Probe for NH_3 and HCN at one or two points around flame front • Mass spectrometry analysis for major species
7	H_2-CO-O_2-Ar (50 torr) (H_2/CO = 1.43)	1.9	0.8→1.8	8750	NH_3	4000 ppm (fuel basis)	• Preliminary experiment • Maximum temperature probing • At one DR (1.9), vary ϕ to obtain optimum luminous zone position for detailed probings
8	H_2-CO-O_2-Ar (50 torr) (H_2/CO = 1.43)	1.9	1.4	8750	NH_3	4200 ppm (fuel basis) 2740 ppm (total basis)	• Detailed temperature and N-concentration probing • Rate and location of NO_x formation • Detailed mass spectrometry analyses
9	H_2-CO-O_2-Ar (50 torr) (H_2/CO = 1.43)	1.9	1.4	8750	NO	3420 ppm (fuel basis) 2230 ppm (total basis)	• Fate of added NO in fuel-rich flame
10	H_2-CO-O_2-Ar (0.1 atm) (H_2/CO = 1.43)	1.9	1.4	8750	a) NO b) NH_3	1370 ppm (total basis) 1370 ppm (total basis)	• Detailed temperature and N-concentration probing • Effect of NO addition on **rates of N-species production** and disappearance • Detailed mass spectrometry analyses
11	H_2-CO-O_2-Ar (0.1 atm) (H_2/CO = 1.43)	1.9	1.4	8750	NH_3	1370 ppm (total basis)	• Detailed temperature and N-concentration probing • Effect of NH_3 concentration on **rates of N-species production and disappearance**

The principal purpose of experiment No. 1 was to investigate the formation of HCN from NH_3 and to follow the conversion of the HCN to NO. The results of flame No. 4 of the previous study suggested that HCN is a principal intermediate under these conditions, but the HCN could not be measured directly in that study.

The results obtained in experiment No. 1 are plotted in Fig. 2-10 through 2-14. The flame temperature measurements, corrected for radiation, are plotted in Fig. 2-10 and 2-11. The maximum flame temperature of 2029 K compares favorably with the value of 2080 K measured for flame No. 4 of the previous study (Fig. 68 of Ref 1) but the temperature measured at the bottom of the luminous zone is much higher in experiment No. 1 (1685 K versus ~1400 K). The temperature decreases almost linearly with distance beyond ~15 mm above the burner (Fig. 2-11). The temperatures measured in input-output experiment IB (Table 2-2) are plotted as triangles in Fig. 2-10 and 2-11 and agree quite well with experiment No. 1.

The measured mole fractions of NO and NO_2 are plotted in Fig. 2-12 and 2-13. The NO mole fraction is 600 ppm at the first measurement point just above the burner screen and increases slowly below the luminous zone. The NO mole fraction increases rapidly in the luminous zone, reaching a maximum value of 1000 ppm 25 mm above the burner where the flame temperatures is ~140 degrees below the maximum value. The NO mole fraction decreases with distance beyond 30 mm, suggesting that some of the purge gas begins to reach the centerline of the burner at these distances. The NO_2 reached its maximum mole fraction of 20 ppm in the center of the luminous zone.

It should be noted that, because of diffusion, the mole fraction curves do not give an exact indication of the location at which species are forming and disappearing (Fig. 55 of Ref 1). This information is contained in the flux plots to be discussed. However, the mole fraction profiles clearly demonstrate the ability of the present analytical system to distinguish between NO, NO_2, HCN, and NH_3.

The input-output NO yields from Table 2-2 are shown to agree well with those of the detailed measurements. The NO mole fraction profile from flame No. 4 (Fig. 69

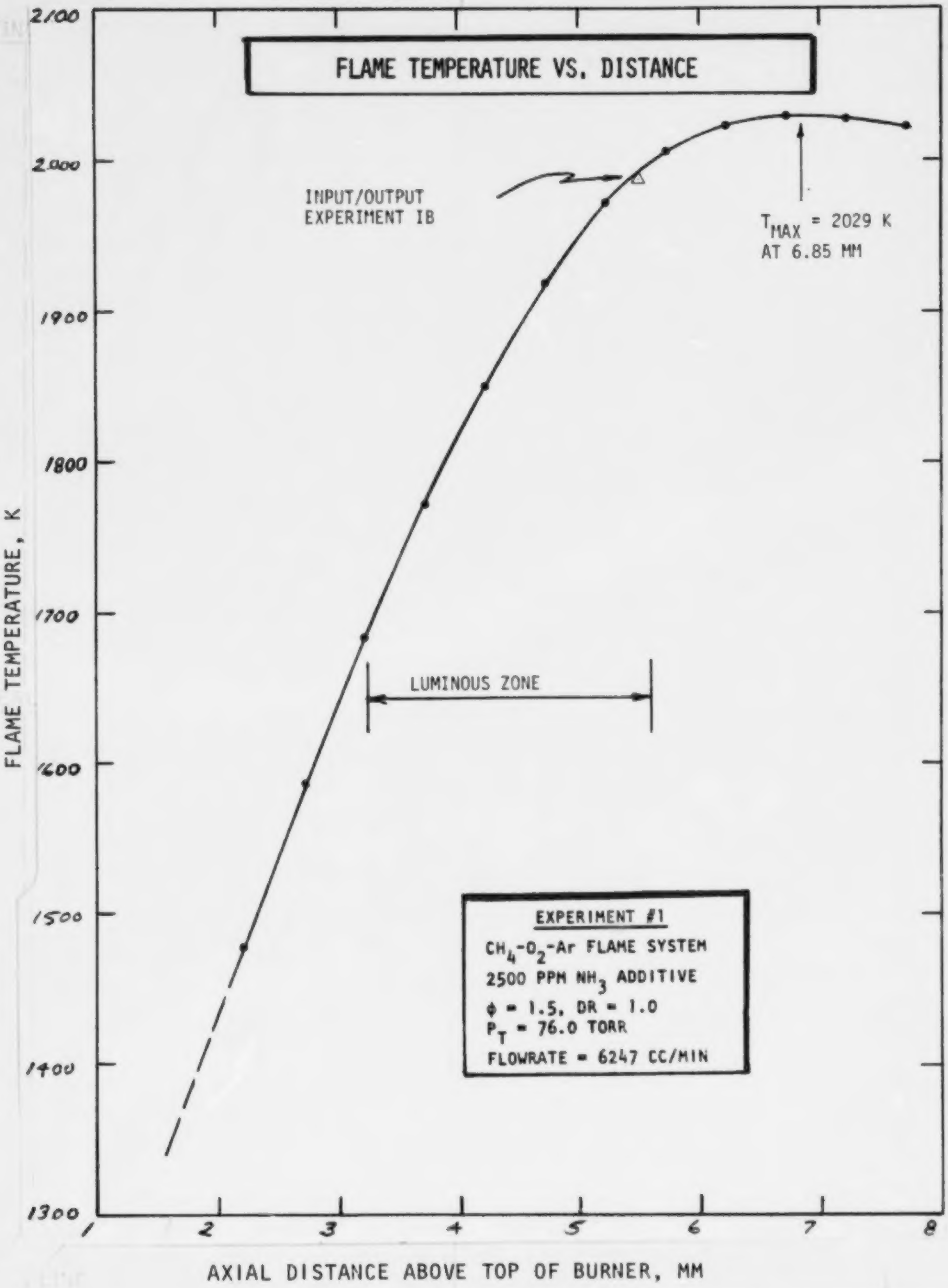

Figure 2-10. Detailed Experiment 1 - Temperature Profile

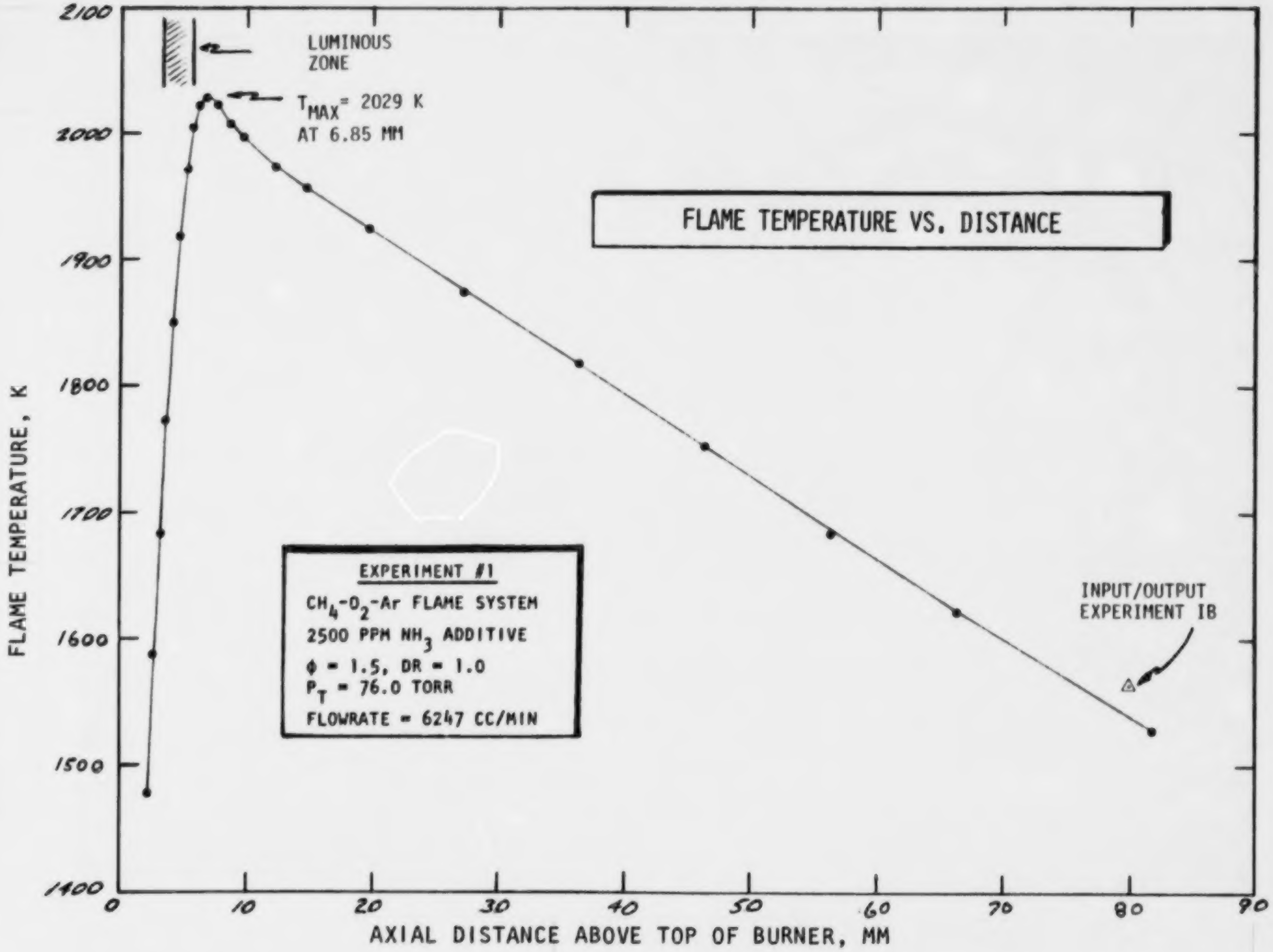

Figure 2-11. Detailed Experiment 1 - Temperature Profile

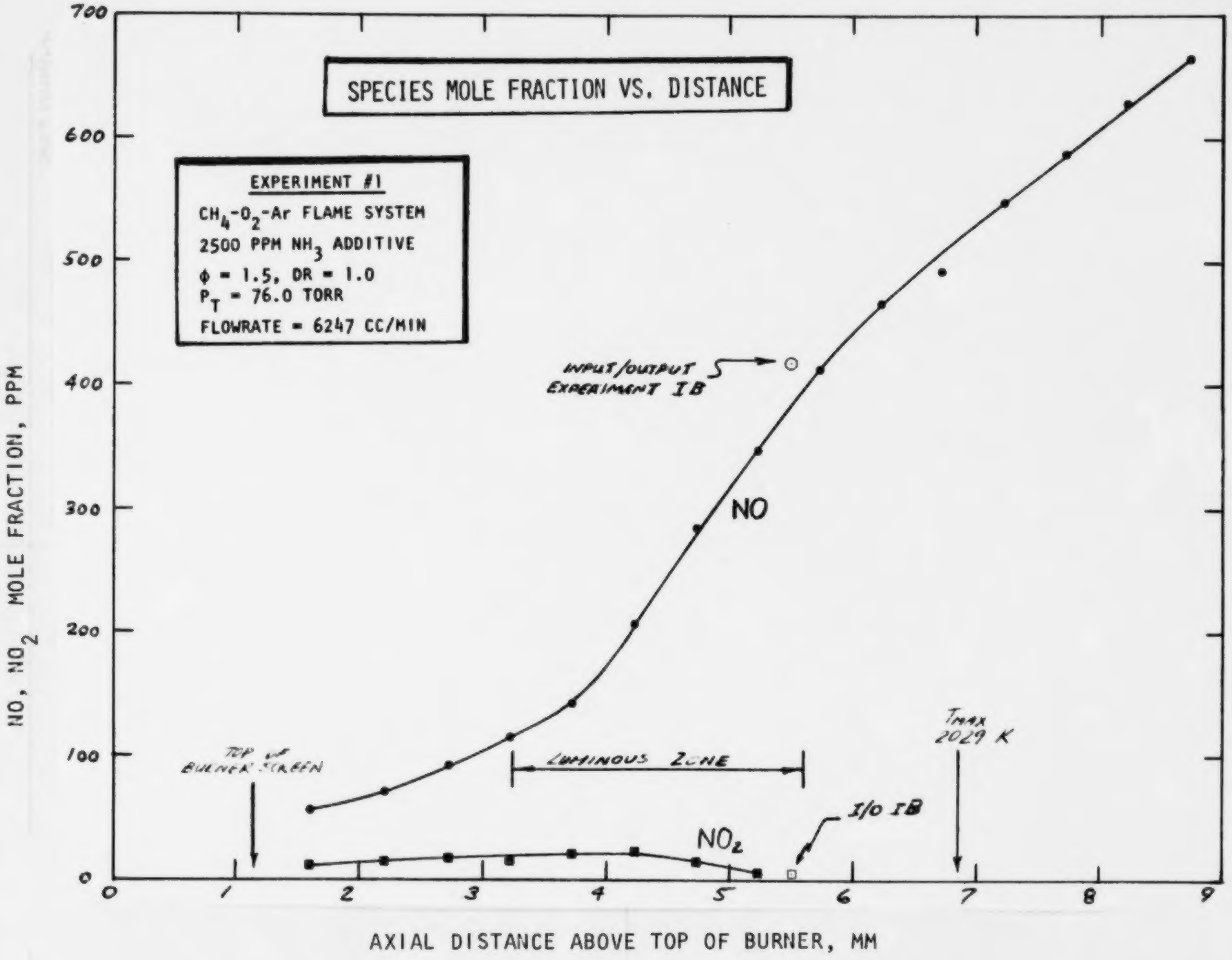

Figure 2-12. Detailed Experiment 1 - NO and NO_2 Mole Fraction Profiles

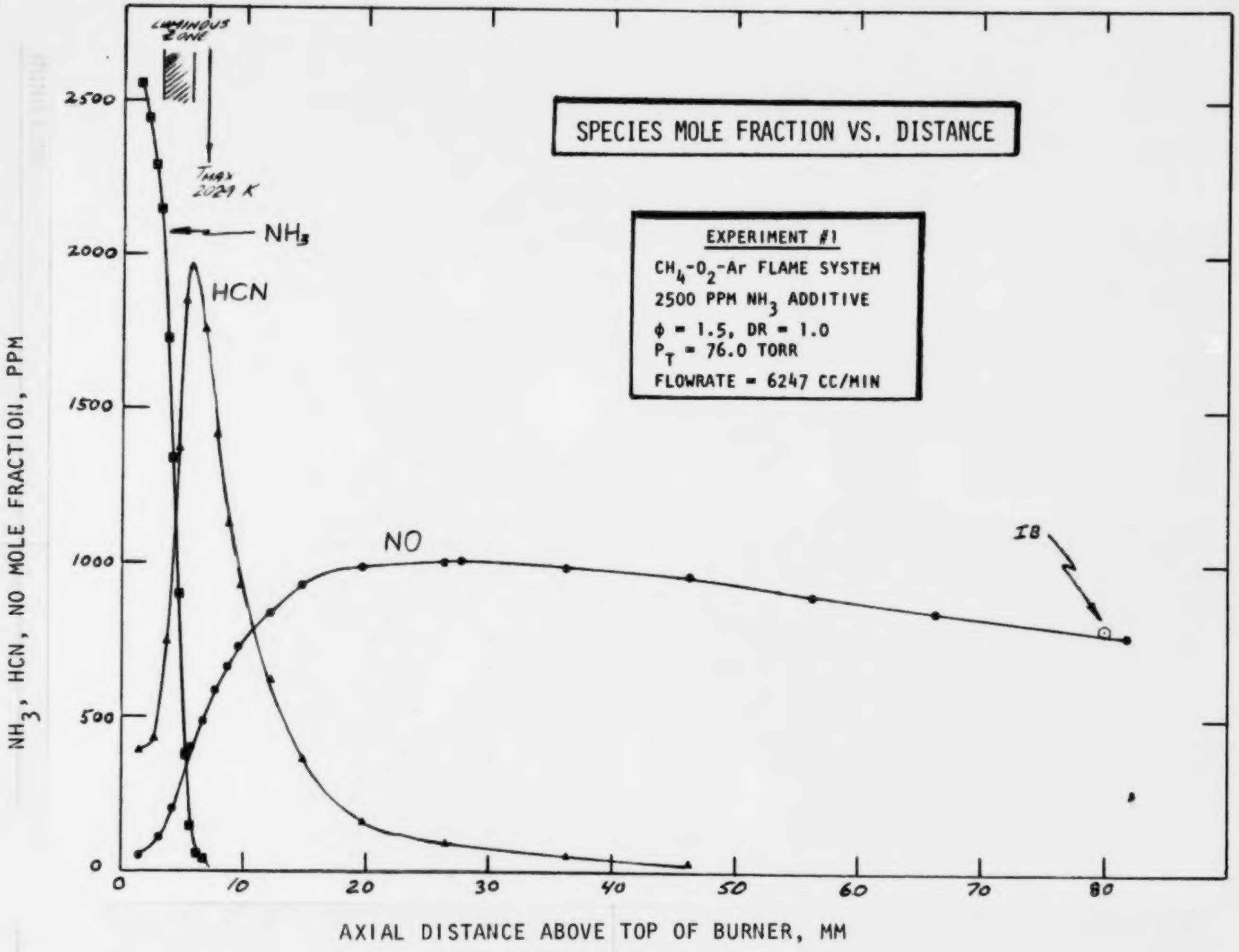

Figure 2-13. Detailed Experiment 1 - NH_3, HCN and NO Mole Fraction Profiles

of Ref. 1) was similar to that in Fig. 2-12, reaching a value of about 600 ppm at 11 mm, i.e., at 3.1 msec (the relationship between residence time above the burner and distance is shown in Fig. 2-13A; c.f. Fig. 56-58 of Ref. 1).

The measured mole fractions of NH_3 and HCN are plotted in Fig. 2-13 and 2-14. The NH_3 reacts rapidly in the luminous zone with most of the NH_3 being converted to HCN. The maximum mole fraction of HCN was 1910 ppm at the top of the luminous zone (5.7 mm). This is equal to 76% of the mole fraction of NH_3 in the feed gas. The HCN measured at 5.5 mm in input-output experiment IB (Table 2-2) was 1964 ppm, in agreement with the detailed experiment. The maximum mole fraction of HCN measured in flame No. 4 of the previous study (Fig. 69 of Ref. 1) was only about one-half of this value.

The HCN formed from the NH_3 then reacts slowly above the luminous zone forming NO in moderate yield. The input-output HCN measurement at 80 mm (107 ppm in Table 2-2) is considerably higher than that shown in Fig. 2-13.

A plot of the species flux provides more information since it takes into consideration the diffusion of each species and gives a more precise indication of the exact location at which species are forming and disappearing. As discussed in Ref. 1, the molar flux of species i (moles/cm^2·sec) in a one-dimensional flow is given by:

$$N_i = C_i \, (v + V_i),$$

where

C_i = concentration of species i (moles/cm^3)

v = gas velocity (cm/sec)

V_i = diffusion velocity of species i

= $\mathcal{D}_{ij} \left(\frac{1}{f_i}\right) \frac{df_i}{dx}$ (cm/sec)

f_i = mole fraction of species i

$\mathcal{D}_{ij}$ = diffusion coefficient for ith species diffusing through argon

USE SPECIAL DROPOUT BLUE PENCIL
ONLY TO INDICATE CORRECTIONS.
CLASSIFICATION
PAGE
STARTING LINE

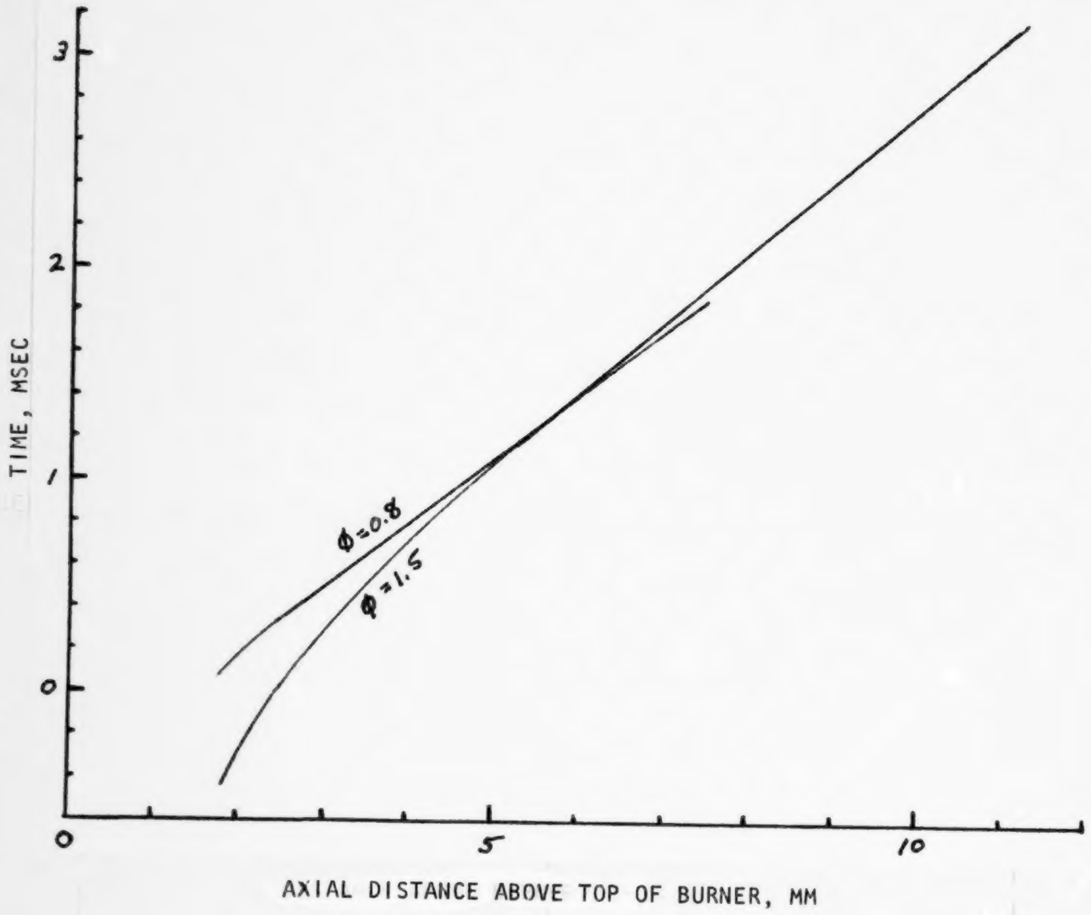

Figure 2-13A. Calculated Gas Residence Times as a Function of Distance Above Burner

WARNING LINE
STOP
DOCUMENT NUMBER
PAGE NUMBER

CLASSIFICATION
TYPIST

USE SPECI ROPOUT BLUE PENCIL
ONLY TO CORRECTIONS

CLASSIFICATION

PAGE

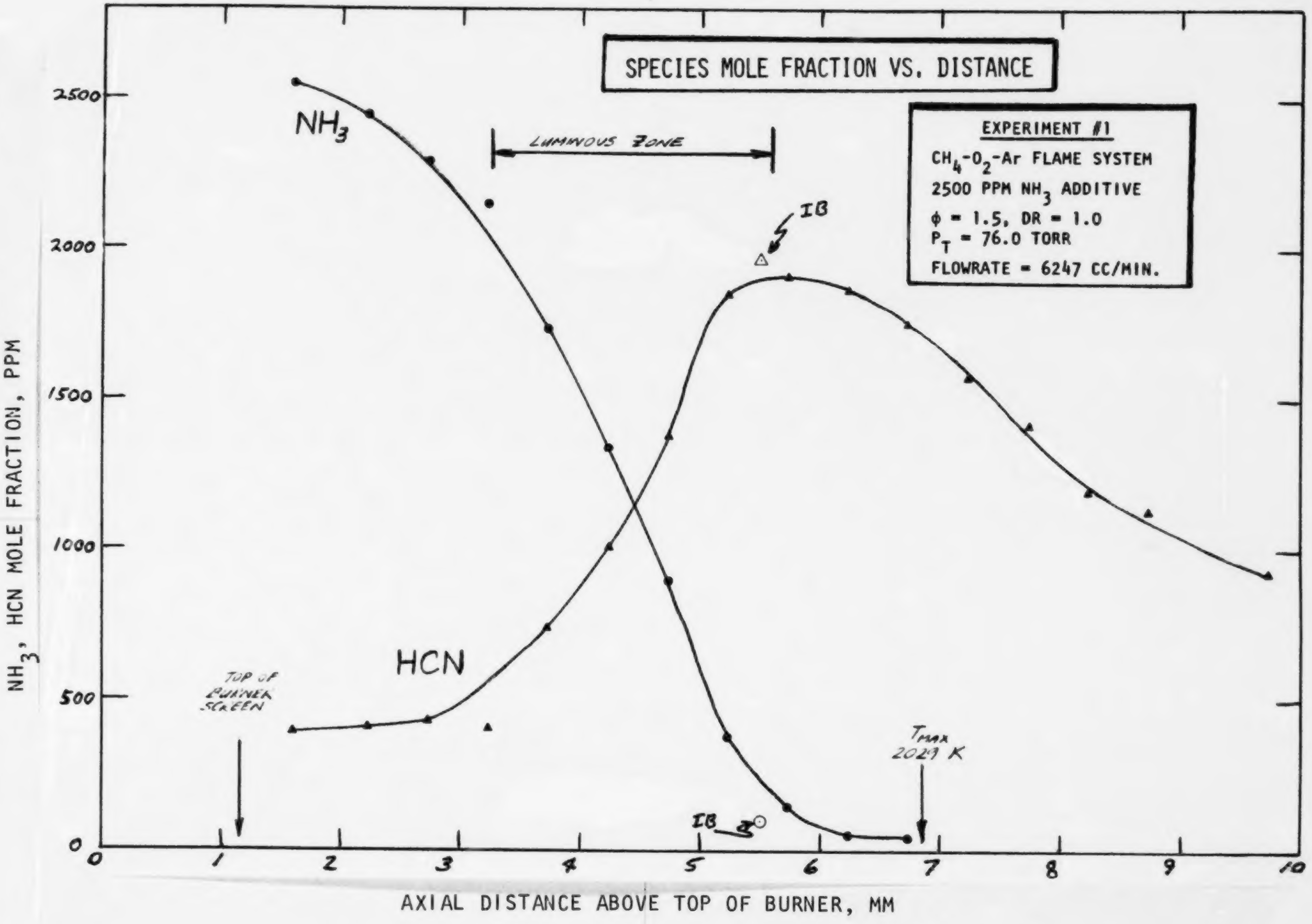

Figure 2-14. Detailed Experiment 1 - NH$_3$ and HCN Mole Fraction Profiles

DOCUMENT NUMBER

PAGE NUMBER

CLASSIFICATION

TYPIST

USE SPECIAL DROPOUT BLUE PENCIL
ONLY TO INDICATE CORRECTIONS
CLASSIFICATION
PAGE
STARTING LINE

Using the above equation and the temperature profile and mole fraction plots for NO, NO_2, HCN and NH_3 (including the slopes of these plots), the molar flux profile for each of the fuel nitrogen species was calculated for experiment No. 1. The reaction rate of species i at any point, Ri, is given by the slope of the flux plot on a distance scale because (Ref. 1):

$$R_i = \frac{d}{dz}\left[C_i(v+V_i)\right] = \frac{dN_i}{dx}$$

Figure 2-15 is a plot of the molar flux profiles for NH_3, HCN, and NO as a function of distance above the top of the burner. The NO_2 flux profile is not shown. However, values for the NO_2 flux increased from 0.23×10^{-9} moles/cm^2·sec at 1.6 mm above the burner to 7.8×10^{-9} at 5.2 mm. The NO_2 reacted completely to NO just below the top of the luminous zone (~ 6.0 mm).

NH_3 begins to react rapidly at about two-thirds of the way through the luminous zone and disappears above the top of the luminous zone at approximately the peak gas temperature. The rapid disappearance of the NH_3 coincides with the formation of HCN, with 65 to 80% of the NH_3 being converted to HCN. The molar flux of HCN is at a maximum at the peak gas temperature, thereafter decreasing gradually to 1% of the initial NH_3 flux at about 46 mm.

Although NO is detected below the luminous zone at the first measurement point (1.60 mm above the burner), the molar flux of NO does not begin to increase until the middle of the luminous zone. This establishes that little NO forms below the luminous zone and the NO present below the luminous zone has diffused out of that zone. The NO flux smoothly increases until a maximum is reached at approximately 28 mm above the burner. The maximum NO yield is 39%.

The NH_3 and HCN molar fluxes shown in Fig. 2-15 are somewhat erratic for the first seven data points (1.60 → 4.73 mm). One possible explanation for this behavior is that the Cosorb solid reagent used to trap out the HCN was not fully equilibrated. During the early part of the detailed concentration probing experiment, there was considerable drift in the NO_x reading of the chemiluminescent analyzer (CA) when used in conjunction with the Cosorb solid reagent.

USE SPECIAL DROPOUT BLUE PENCIL
ONLY TO INDICATE CORRECTIONS
CLASSIFICATION
PAGE
STARTING LINE

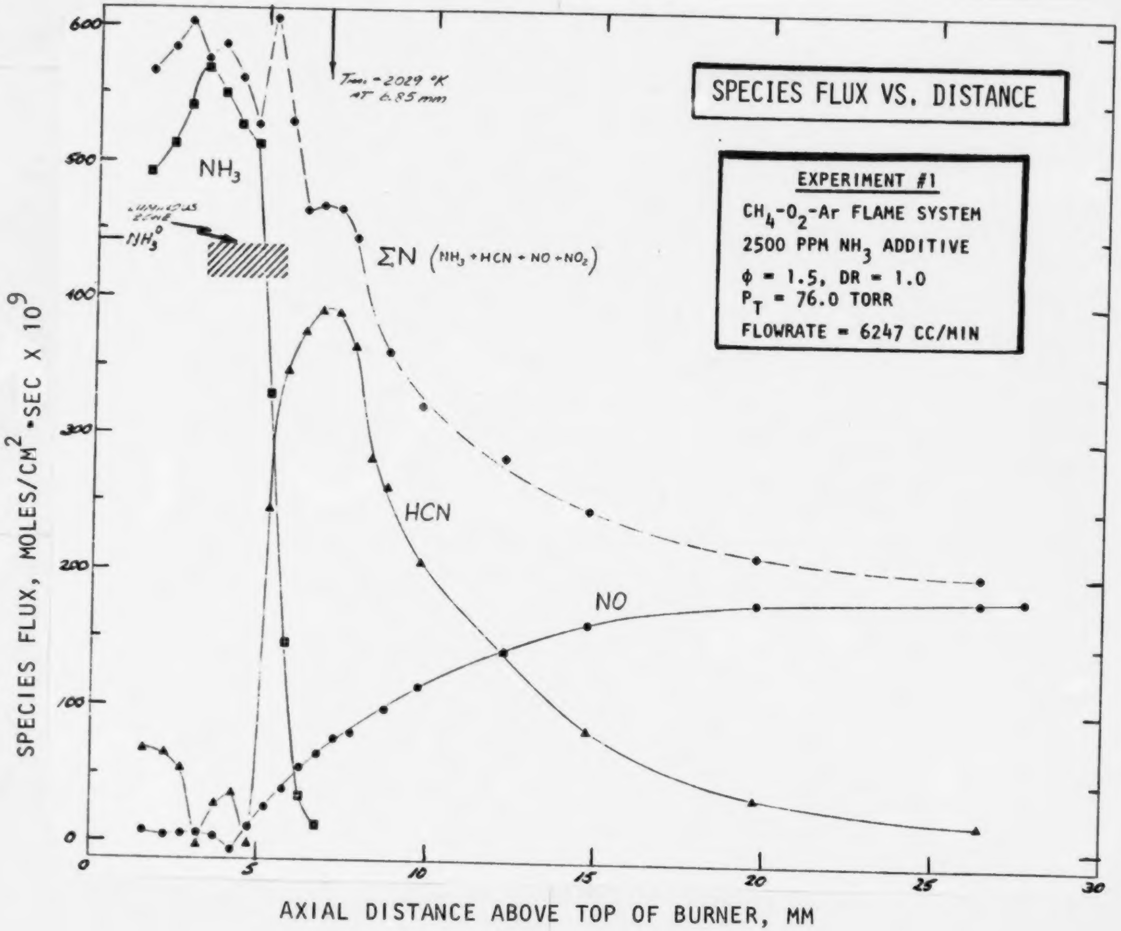

Figure 2-15. Detailed Experiment 1 - Species Flux Profiles

WARNING LINE
STOP
DOCUMENT NUMBER
PAGE NUMBER
CLASSIFICATION

It is evident from Fig. 2-15 that up to about 5 mm, the experimentally measured NH_3 flux exceeds the calculated flux of NH_3 input to the burner by as much as 30%. A number of post-calibration checks of the analytical system were therefore performed to determine possible causes for this discrepancy. The first check, which is a routine procedure following every experiment, was the calibration of the quartz microprobe. The total probe area enlargement was found to be less than 2%.

To check the initial NH_3 flux calculation, a cold-flow experiment was performed in which the flowrates of Ar, O_2, CH_4 and NH_3 were metered into the burner chamber at conditions identical to the actual hot-fire experiment (2500 ppm NH_3, 76.0 torr, 6247 cc/min, $\phi = 1.5$, DR = 1.0). Using the quartz microprobe, a sample of the gas was routed through the stainless-steel converter (1073 K) and into the CA reaction chamber. After applying the appropriate correction factors for flow through the probe, the NO mole fraction obtained was 2780 ppm (assuming 100% conversion efficiency of NH_3 on the converter) or 11% higher than the 2500 ppm NH_3 actually added. It was established by additional calibration (Appendix D) that about one-half of this 11% error was a real metering error and one-half resulted from the difference in molecular weight between the sample and the N_2-NO calibration gas ($NO_2^* + M \rightarrow NO_2$).

After making these corrections, the calculated NH_3 flux and total flux nitrogen species molar flux (broken curve in Fig. 2-15) very early in the flame are still considerably higher (about 25%) than the calculated inlet mole flux of NH_3. The cause of this difference was not fully explained. However, this should not significantly reduce the importance of the information obtained in this experiment. The rate, extent, and location of the conversion of NH_3 to HCN and HCN to NO has been established in a fuel-rich CH_4-O_2-Ar-NH_3 flame.

During the above cold-flow experiment, the radial position of the tip of the quartz microprobe was varied at a constant axial distance above the top of the burner (3.1 mm). There was virtually no effect of radial position on the CA reading even though the probe tip was moved ±5 mm from its normal position. It can be concluded, therefore, that the inlet gas emanating from the center region of the burner face is well mixed. During hot-fire conditions, the luminous zone is very uniform in color and intensity in the center region of the burner face which also supports this conclusion.

FUEL-RICH CH_4-O_2-N_2 FLAME

The purpose of this series of experiments, No. 2 through No. 4 in Table 2-6, with a rich CH_4-O_2-N_2 flame was to investigate the mechanism and rate of thermal NO_x formation under fuel-rich conditions and to compare directly thermal and fuel NO_x formation under identical conditions. These three detailed probing experiments were carried out at an equivalence ratio of 1.5, a diluent ratio of 0.7, a total pressure of 76 torr, and an inlet gas feed rate of 7520 cm^3/min (STP). These conditions were established in input-output experiment No. 4.

The reactants in experiment No. 2 contained no additive and, therefore, all of the NO formed from N_2 or from species formed from N_2. In experiments No. 3 and 6, 50 ppm NH_3 and 50 ppm HCN, respectively, were added to investigate the interactions, if any, between the reactions that form thermal NO and those that form fuel NO.

Before presenting the results of the series of experiments, some of the previous background will be discussed.

Fenimore (Ref. 21) observed that in fuel-rich hydrocarbon-air flames, a rapid transient formation of NO occurs in the "primary reaction zone" followed by the slower formation of additional NO in the post-flame gases. He termed the initial rapidly formed NO "prompt NO" and, since the slow rate observed in the post-flame gases agreed with that predicted by the well-known Zeldovich mechanism ($O + N_2 = NO + N$, etc.), concluded that prompt NO forms by some other mechanism. He proposed reactions such as:

$$CH + N_2 = HCN + N$$

$$C_2 + N_2 = CN + CN$$

---

21. Fenimore, C. P., "Formation of NO in Premixed Hydrocarbon Flames", Thirteenth Symposium (International) on Combustion, p. 373, 1970.

Bauer (in the discussion at the end of Ref. 21) cited data that indicate that attack on N_2 by C_1 and C_3 are more likely reaction paths.

Sarofim and Pohl (Ref. 22) studied NO formation in premixed methane-air flames at equivalence ratios, ϕ, from 0.89 to 1.15. They found that the peak rates of NO formation in the "flame zone" were 1 to 2 orders of magnitude greater than in the post-flame zone. They claim that even the peak rates they observed are in agreement with Zeldovich kinetics when the free radical concentrations are derived from the concentration of stable species by use of partial-equilibrium assumptions for the fast-flame reactions. Unfortunately, they did not carry their study to more fuel-rich conditions. In the discussion at the end of Ref. 22, Eberius pointed out that the prompt NO effect is greater at $\phi = 1.32$ and that he observed HCN at the ppm level under these conditions.

Sarofim and Pohl measured thermal NO concentrations of about 10 ppm at $\phi = 0.89$ ($T_{max} \cong 2000$ K) and 30 ppm at $\phi = 1.15$ ($T_{max} \cong 2050$ K). These trends are similar to those of the thermal NO yields observed in our input-output experiments. In experiment No. III(c) ($\phi = 0.8$, DR = 0.7, and $T_{max} \cong 1980$ K), we obtained a maximum NO concentration about 10 ppm (Fig. 2-4 and 2-5). The fuel-rich experiment No. III(d) ($\phi = 1.5$, DR = 0.7) gave NO yields of 9 ppm 0.7 mm above the luminous zone (T = 1984 K) and 39 ppm measured 80 mm above the burner (T = 1617 K). The detailed probing experiment No. 2 to be described was carried out under the same fuel-rich conditions as input-output experiment No. III(d).

It is stated on page 743 of Ref. 22 that the rate of NO formation is significantly higher "in the flame" than in the post-flame zone. Sarofim and Pohl do not designate the position of their luminous zone but it can be estimated from their Fig. 3 and 7 that, at $\phi = 1.15$, the top of the luminous zone is probably below 5 msec on their time scale, the maximum temperature is reached at 5 msec, and the maximum rate of NO formation occurs at about 6.7 msec. This is well above the luminous zone and in the same region where the maximum rate of CO oxidation occurs. It is apparent that Sarofim and Pohl include in their definition of the flame

---

22. Sarofim, A. F. and J. H. Pohl, "Kinetics of NO Formation in Premixed Laminer Flames", Fourteenth Symposium (International) on Combustion, P. 739, 1972.

125

zone the regions just above the luminous zone where the temperature continues to increase because of CO oxidation and recombination of radicals as well as somewhat beyond the point of maximum temperature. In the cited example, they must define the start of the post-flame region as about 8 or 9 msec (the point in their Fig. 7 where prompt NO formation ceases)--some 3 or 4 msec above the top of the luminous zone. This may well be a proper definition of the flame zone but it must be carefully defined in future discussions of where prompt NO forms.

Iverach et al. (Ref. 23) showed that in ethylene-air flames, for example, the Zeldovich mechanism could not reasonably account for the rapid early rate of NO formation above an equivalence ratio of about 1.15 (see Fig. 8 of Ref. 23). Their results at $\phi = 1.4$ would require the oxygen atom concentration to be about 3000 times its equilibrium value. The thermal NO data obtained in our experiment No. 2 (discussed below) permits us to determine accurately the maximum rate of NO formation in the fuel-rich flame and to compare this with the rate predicted by the Zeldovich mechanism at various levels of oxygen atom overshoot.

Perhaps the strongest evidence that much of the NO forms via a non-Zeldovich mechanism in fuel-rich premixed flames are the recent observations that considerable HCN forms as a measurable intermediate under these conditions. One of the major goals of experiment No. 2 was to measure the rate and extent of HCN formation from N_2 and to compare this with the formation of NO. Bachmaier et al. (Ref. 24) found that in their propane-air flame at $\phi = 1.1$, HCN reached a concentration of 12 ppm about 5 mm above the burner and then reacted completely. The yield of prompt (and total) NO was 60 ppm. At $\phi = 1.5$, however, the measured HCN reached 23 ppm at 15 mm and remained unchanged to the last measurement point at 45 mm while the amount of NO formed was less than 10 ppm under this condition. Haynes et al. (Ref. 25) measured up to 250 ppm HCN in acetylene-air flames at $\phi = 1.95$ but obtained less than 3 ppm HCN from their methane flames. However,

---

23. Iverach, D., K. S. Basden, and N. Y. Kirov, "Formation of NO in Fuel-Lean and Fuel-Rich Flames", Fourteenth Symposium (International) on Combustion, p. 767, 1972.
24. Bachmaier, F, K. H. Eberius and T. Just, "HCN in Premixed Hydrocarbon-Air Flames at One Atmosphere," Comb. Sci. and Tech, 7, 77 (1973).
25. Haynes, B.S., D. Iverach, and N.Y. Kirov, "The Behavior of Nitrogen Species in Fuel-Rich Hydrocarbon Flames", Fifteenth Symposium (International) on Combustion, p. 1103, 1974.

their burner would not stabilize CH_4 flames at $\phi > 1.20$. Yamagishi et al. (Ref. 26) observed that both HCN and NH_3 form in the partially mixed fuel-rich first stage of a two-stage combustor operating on CH_4-air. The amount of NO present in the exhaust gas of the fuel-lean second stage is about 80% of the sum of the HCN + NH_3 + NO in the exhaust of the first stage. The amount of NH_3 formed in the first stage decreased as the degree of premixing increased, suggesting that little NH_3 should form in a completely premixed flame.

R26

Detailed Flame Experiment No. 2 (Thermal NO)

The results obtained with the additive-free fuel-rich CH_4-O_2-N_2 flame (experiment No. 2 in Table 2-6) are plotted in Fig. 2-16 through 2-19. Any observed nitrogen species must have formed from molecular nitrogen. The measured temperature profiles (corrected for radiation) are plotted in Fig. 2-16 and 2-17. The two temperature measurements made under the same conditions in input-output experiment No. III(d) are plotted for comparison. Temperatures measured in the detailed experiment were somewhat lower (30 degrees at 80 mm and 70 degrees at 6.05 mm). The complete NO mole fraction profile is plotted in Fig. 2-18. Little NO is present in the luminous zone. The maximum NO mole fraction of about 50 ppm is not reached until beyond 30 mm above the burner where the temperature has dropped more than 100 degrees from its maximum value of 1992 K. This suggests that the rate of formation of thermal NO in a fuel-rich flame may not be as temperature dependent as in a lean flame.

T2-6
F2-16
F2-17
F2-16
F2-17
F2-18

Also plotted in Fig. 2-18 are the calculated equilibrium NO values for these conditions. Fenimore (Ref. 21) had obtained a correlation in ethylene flames that indicated that the amount of prompt NO formed in very rich flames was approximately equal to the amount of NO that would form at chemical equilibrium. Since our NO profile does not have the shape obtained by Fenimore, it is not possible to separate out prompt NO but the total NO is greater than the equilibrium NO. The calculated equilibrium NO is fairly temperature sensitive under these

F2-18
R21 BR

---

26. Yamagishi, K. et al., " A Study of NO_x Emission Characteristics in Two-Stage Combustion", Fifteenth Symposium (International) on Combustion, p. 1157, 1974.

127 6022-D

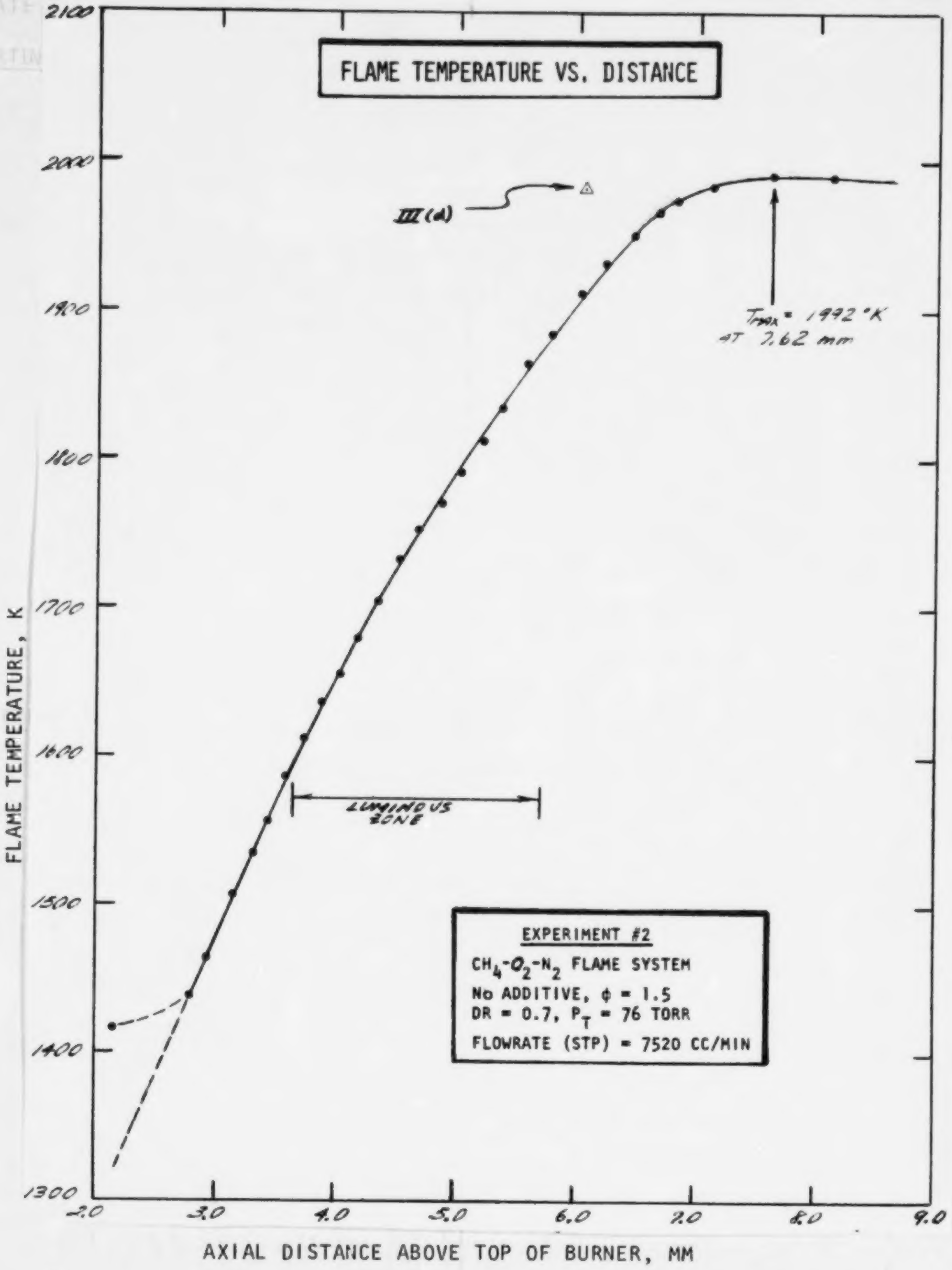

Figure 2-16. Experiment 2 - Temperature Profile

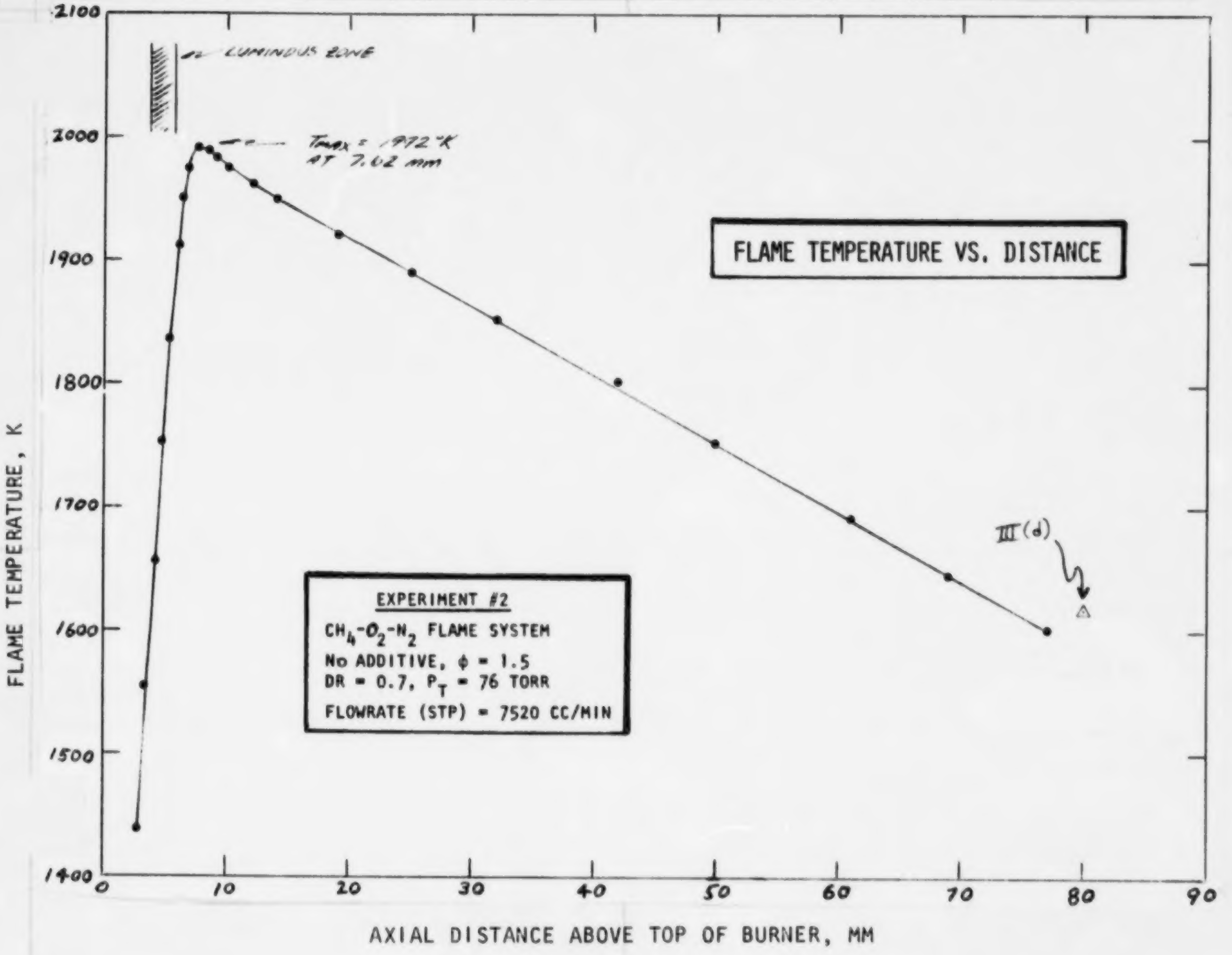

Figure 2-17. Experiment 2 - Temperature Profile

USE SPECIAL DROPOUT BLUE PENCIL
ONLY TO INDICATE CORRECTIONS
STARTING LINE
CLASSIFICATION
PAGE

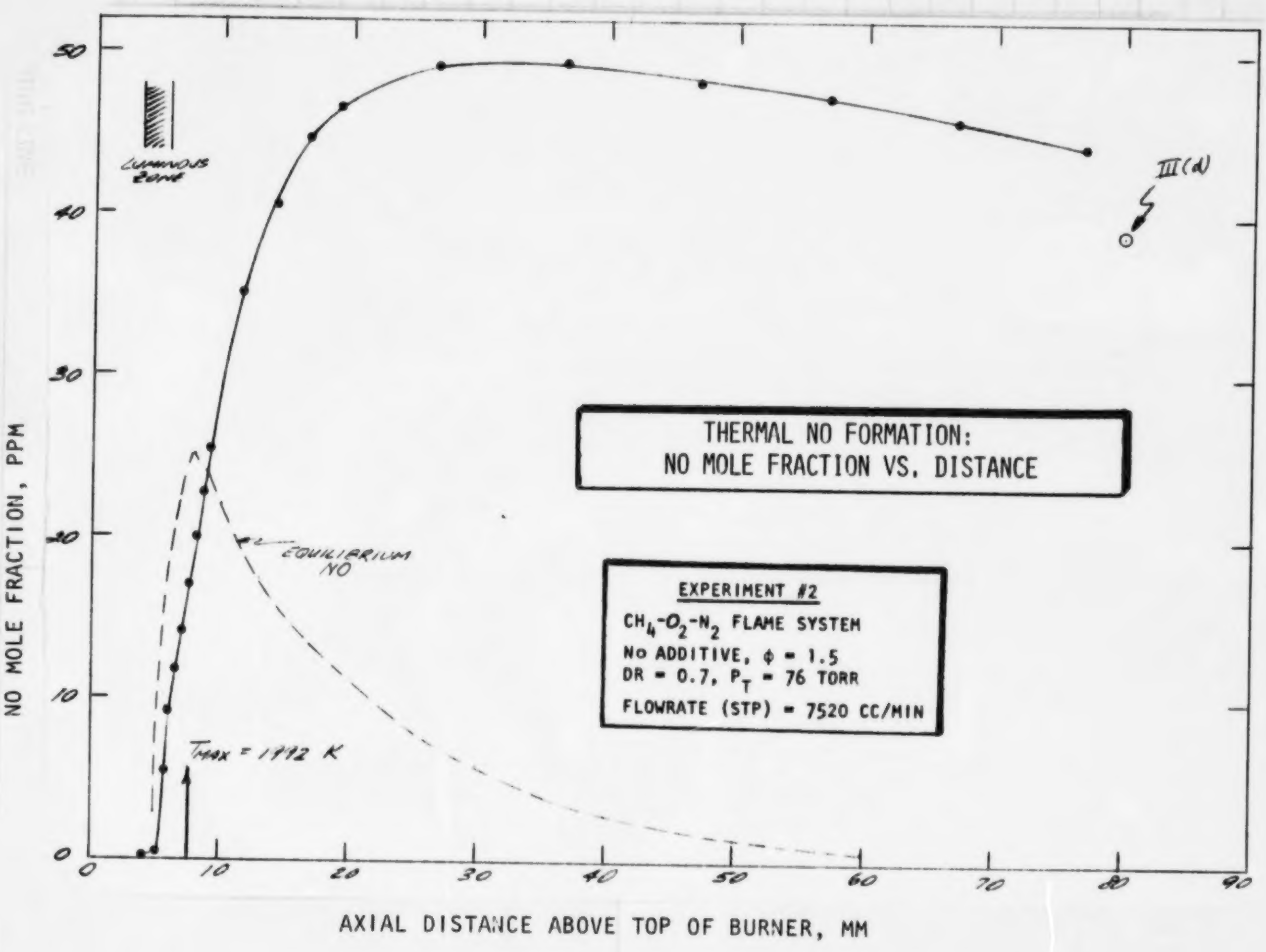

Figure 2-18. Experiment 2 - NO Mole Fraction Profile

DOCUMENT NUMBER
PAGE NUMBER
CLASSIFICATION
TYPIST 130

conditions, doubling every 68 degrees. Thus, if the measured temperatures were low by 70 degrees for some reason, the measured NO would not exceed the equilibrium values. Even if the measured temperatures were in error by this amount (which is unlikely), the fact that the NO profile continues to increase in the region where the temperature is decreasing establishes that our NO yield is not limited by chemical equilibrium.

Plotted in Fig. 2-19 on an expanded distance scale are the measured mole fractions of HCN, NO and NO_2. The NO concentrations measured earlier in input-output experiment No. III(d) are plotted in Fig. 2-18 and 2-19 and agree quite well. The HCN reaches its maximum mole fraction of 35 ppm just above the top of the luminous zone.

The species flux profiles calculated for experiment No. 2 are plotted in Fig. 2-20 and 2-21. It can be seen that most of the NO forms well above the luminous zone where the HCN is disappearing. Only 20% of the NO has formed at the point of maximum temperature where the HCN flux reaches its maximum. It is possible that nearly all of the NO forms from HCN under these conditions since the amount of HCN disappearing between 7 and 19 mm is about 90% of the amount of NO formed in that region and some HCN probably forms there also. The rate of NO formation at 12.5 mm is 83% of the rate of HCN decay. However, for all of the NO to form from HCN would apparently require the NO yield from HCN to be substantially higher than the 60% yield that would be expected under these conditions (e.g., Fig. 2-8).

The maximum net rate of HCN formation (slope of the flux curve on a distance plot) occurs below the top of the luminous zone but almost 40% of the maximum HCN "forms" above the luminous zone (Fig. 2-21). This discussion refers only to net yields of HCN since HCN is probably being both formed and consumed at various points in the flame. The maximum HCN flux is 75% of the maximum NO flux.

The NO flux curve in Fig. 2-20 does not have the typical "prompt" NO shape. This is because the temperature drops rapidly beyond the point of maximum temperature and the purge gas apparently begins to mix in beyond 30 mm above the burner,

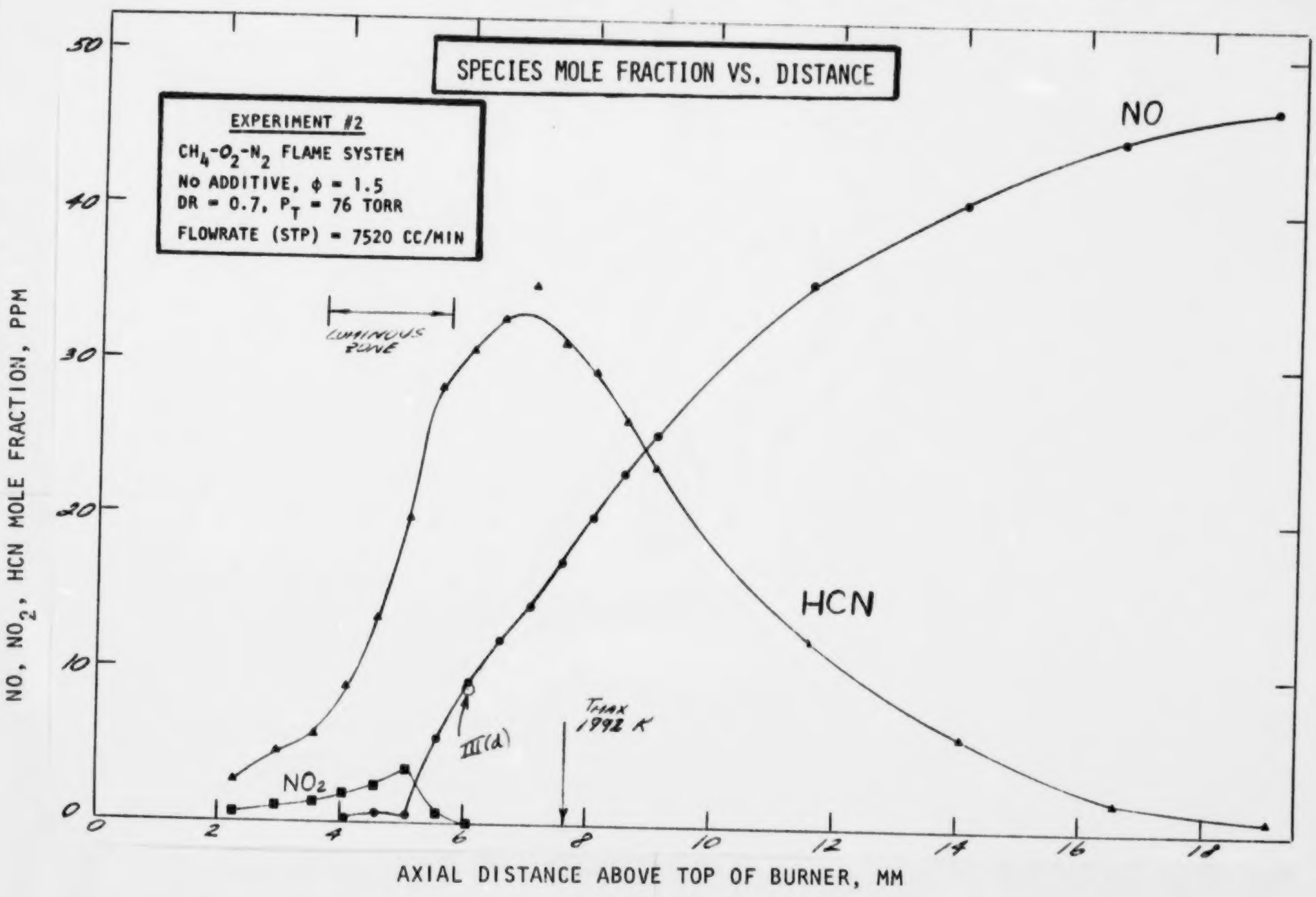

Figure 2-19. Experiment 2 - NO, NO_2 and HCN Mole Fraction Profiles

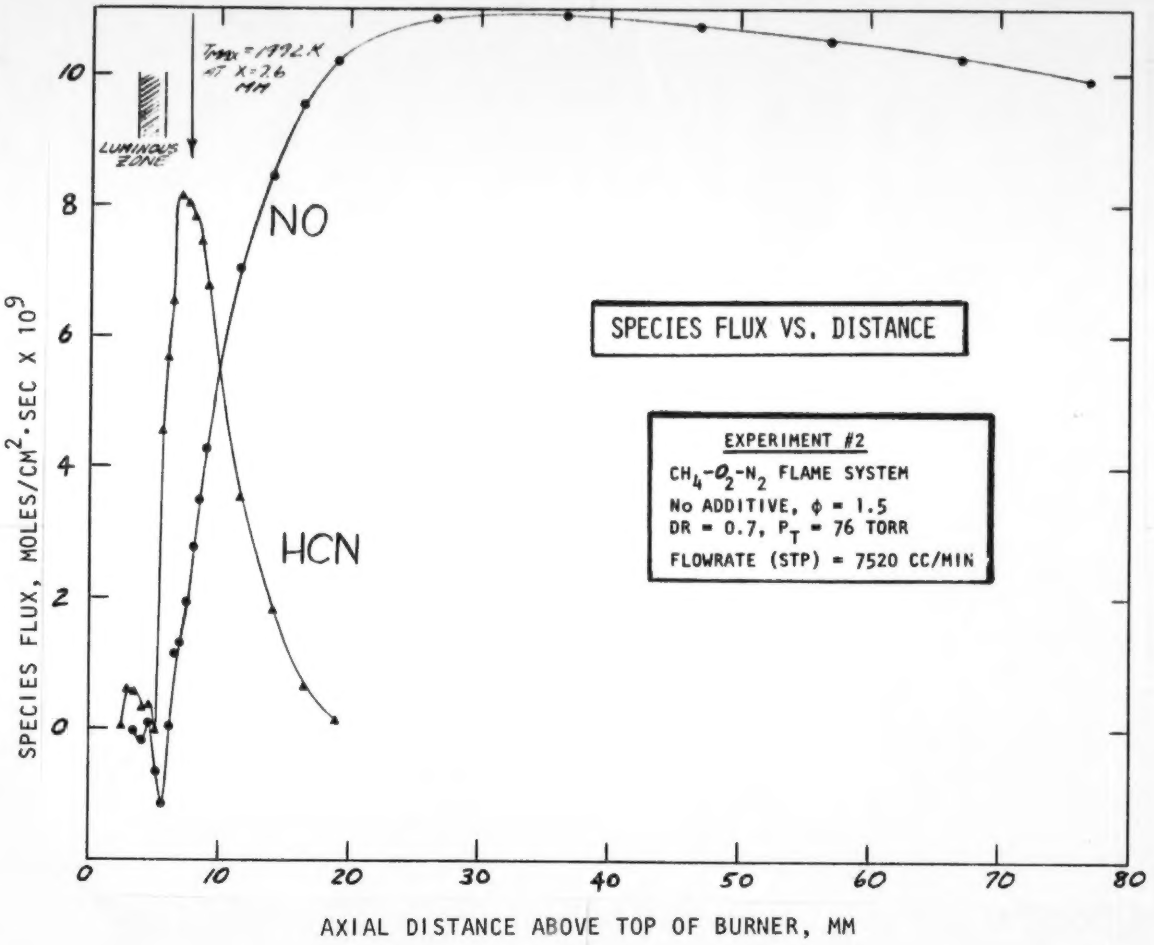

Figure 2-20. Experiment 2 - Species Flux Profiles

USE SPECIAL DROPOUT BLUE PENCIL ONLY TO INDICATE CORRECTIONS
CLASSIFICATION

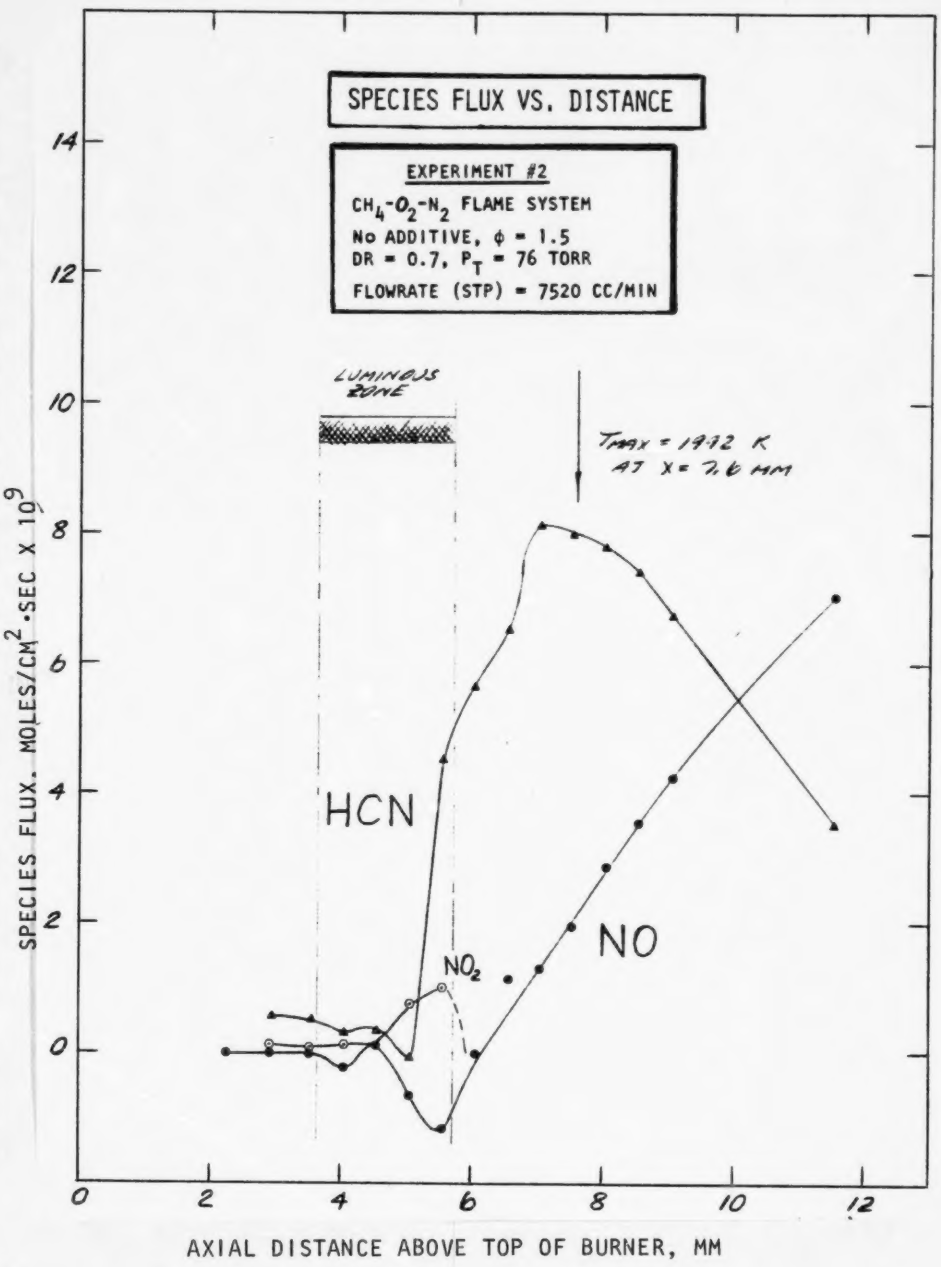

Figure 2-21. Experiment 2 - Species Flux Profiles

causing the NO flux to decay. However, calculations presented below show that this is undoubtedly "prompt" NO since its maximum rate of formation is more than 10^4 times the Zeldovich rate (assuming equilibrium O atom). Also, the formation of HCN as a principal intermediate indicates that the dominant mechanism is not the Zeldovich mechanism. It is remotely possible, of course, that prompt NO forms via the Zeldovich mechanism and then the NO reacts with the fuel to form HCN.

The maximum rate of NO formation in the fuel-rich experiment No. 2 can be compared with that predicted by the Zeldovich mechanism as follows. Ignoring the slight surge of NO at the top of luminous zone (Fig. 2-21), the maximum rate of NO formation occurs between 6 and 9 mm on the assigned distance scale and has a value of 1.5×10^{-8} m/cc-sec. The temperature is about 1990 K in this region and the mole fraction of N_2 is 0.54. The calculated equilibrium oxygen atom mole fraction is 4.0×10^{-6} (using the Rocketdyne thermochemical code).

Using Baulch's rate expression of

$$k = 7.6 \times 10^{13} \exp(-38{,}000/T), \text{ cc/mole-sec}$$

for the reaction $O + N_2 = NO + N$

$$k = 3.9 \times 10^{5}$$

$$(N_2) = 3.3 \times 10^{-7}$$

$$(O) = 2.4 \times 10^{-12}$$

$$d(NO)/dt = 2k(O)(N_2) = 6.2 \times 10^{-13} \text{ moles/cc-sec}$$

Thus, the measured rate exceeds the predicted Zeldovich rate by a factor of 2.4×10^4 and nearly all of the NO formed in experiment No. 2 is apparently "prompt" NO. It seems very unlikely that an oxygen atom overshoot at this magnitude could occur.

USE SPECIAL DROPOUT BLUE PENCIL ONLY TO INDICATE CORRECTIONS
CLASSIFICATION
PAGE
STARTING LINE

Detailed Flame Experiment No. 3 (50 ppm NH_3 Added)

In this experiment, 50 ppm NH_3 was added to the feed gas to the fuel-rich (ϕ=1.5) CH_4-O_2-N_2 flame studied in experiment No. 2. The conditions were otherwise the same (Table 2-6). The results obtained in experiment No. 3 are plotted in Fig. 2-22 through 2-26. Some results from the baseline rich flame, experiment No. 2, are included in these figures for comparison.

The temperature curves for experiments 2 and 3 are compared in Fig. 2-22. The differences at the lower temperatures are attributed to a distance error rather than a temperature error. Some sagging of the thermocouple was encountered.

The mole fraction curves are shown in Fig. 2-23 and 2-24. The NO mole fraction curve from experiment No. 2 is plotted in Fig. 2-23 for comparison. The addition of 50 ppm NH_3 increased the maximum NO mole fraction from 49 ppm to 90 ppm indicating an apparent 83% yield of NO from the added NH_3 (based on mole fractions and assuming that the yields of thermal NO and fuel NO are purely additive). The maximum HCN mole fraction (Fig. 2-24) increased from 35 ppm to 73 ppm indiciating an apparent HCN yield from NH_3 of 76% gain based on maximum mole fractions (assuming that no HCN reacts before the maximum is reached which does not seem likely).

A better estimation of the NO and HCN yields from the added NH_3 can be made from the calculated flux curves (Fig. 2-25 and 2-26) because these correct for diffusion of species upstream and downstream. The NO flux profiles with and without added NH_3 are compared in Fig. 2-27. The maximum NO flux increases from 11.0 x 10^{-9} to 20.0 x 10^{-9} for an added NH_3 flux of 10.0 x 10^{-9}. The conversion of NH_3 to NO is, therefore, 90% based on maximum fluxes.

It can be seen from the HCN flux curves compared in Fig. 2-28 that the addition of NH_3 at a flux of 10.0 x 10^{-9} increases the maximum HCN flux by 11 x 10^{-9} indicating that all of the NH_3 forms HCN in this fuel-rich flame.

The results obtained in experiment No. 3 have a number of interesting features. First of all, the conversion of the added NH_3 to HCN was apparently complete and the conversion of the HCN to NO was on the order of 90%. At higher fuel-N

DOCUMENT NUMBER
PAGE NUMBER
CLASSIFICATION
TYPIST

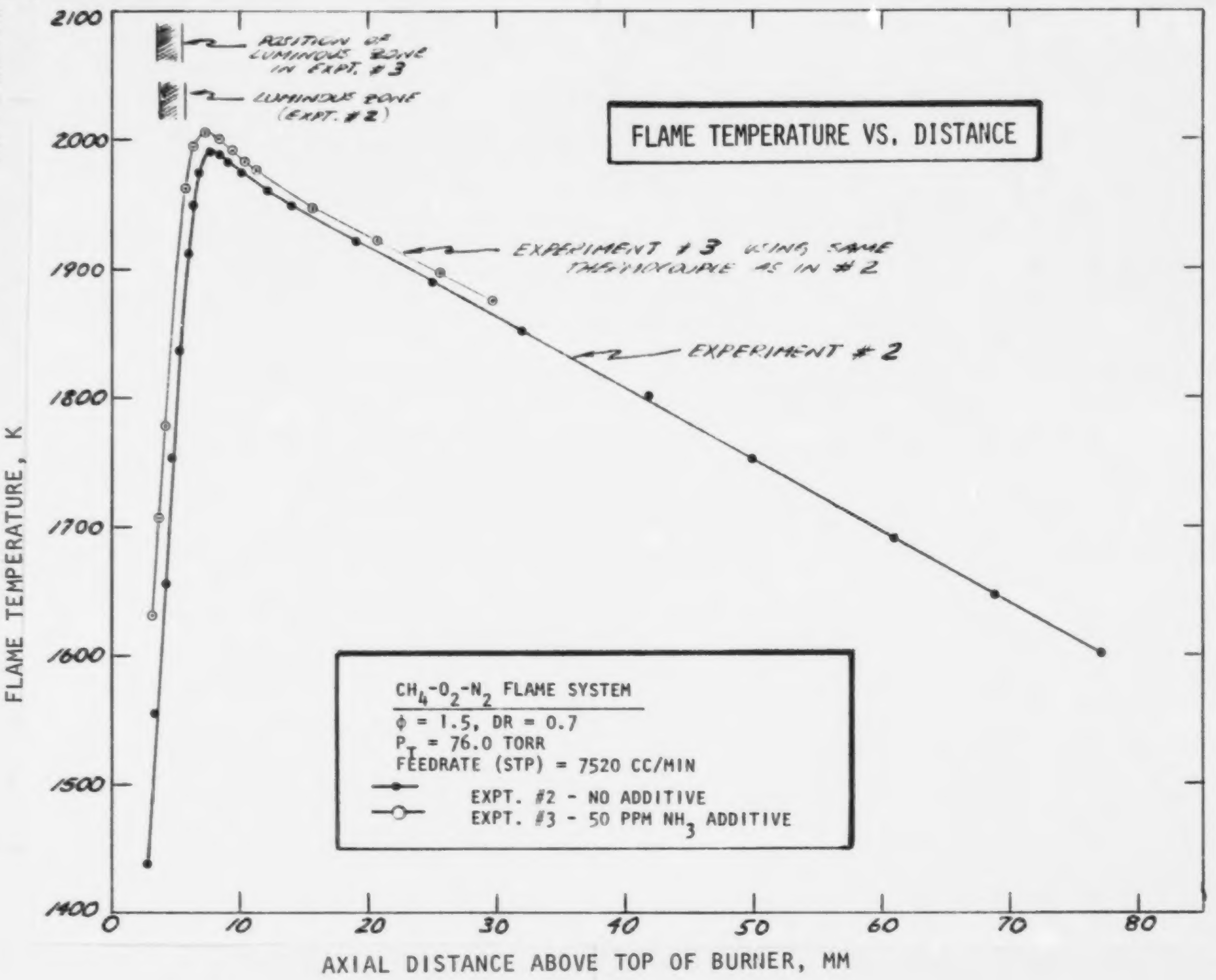

Figure 2-22. Comparison of Flame Temperature Profiles from Experiments 2 and 3

137

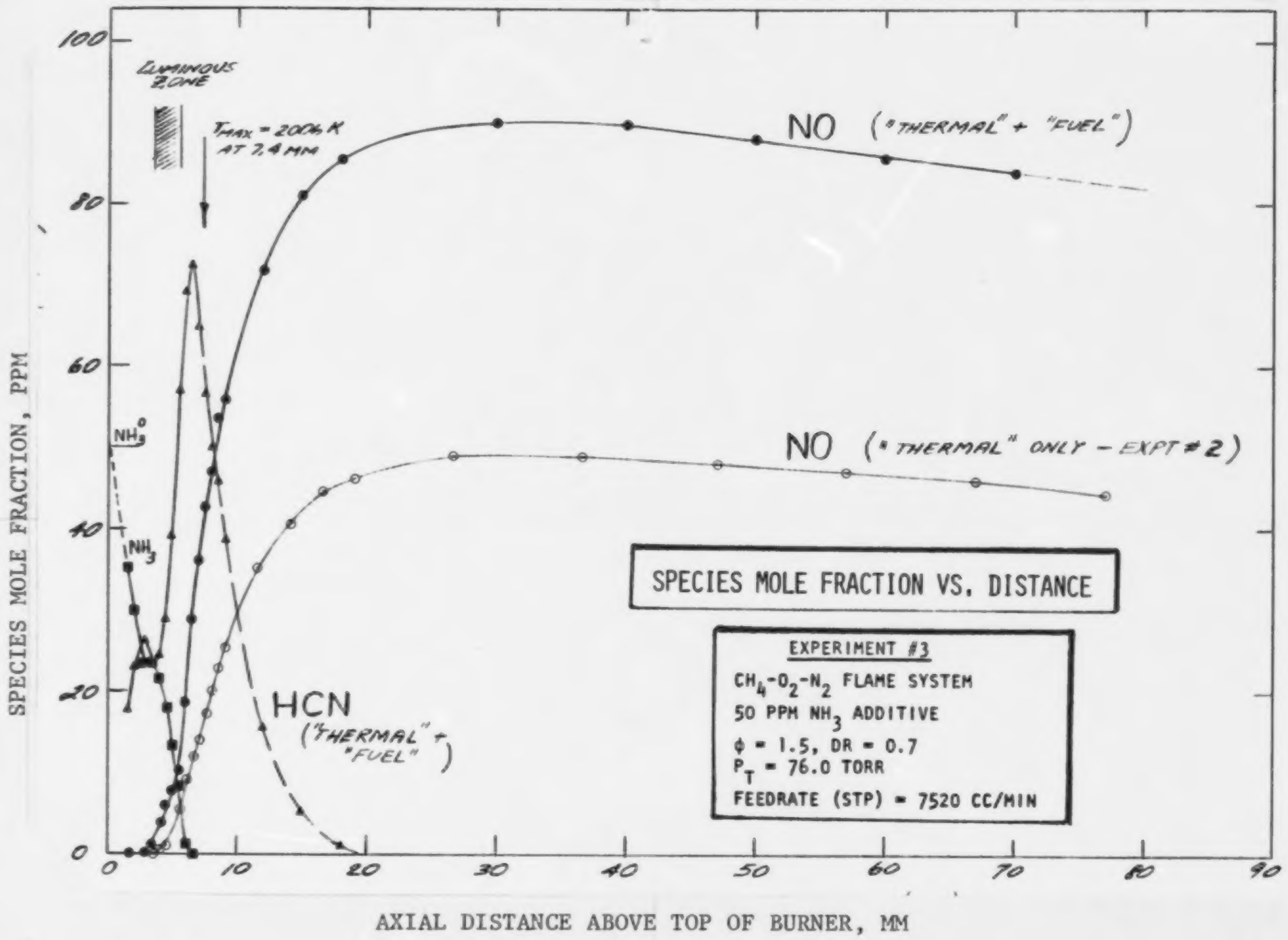

Figure 2-23. Experiment 3 - NH_3, HCN and NO Mole Fraction Profiles

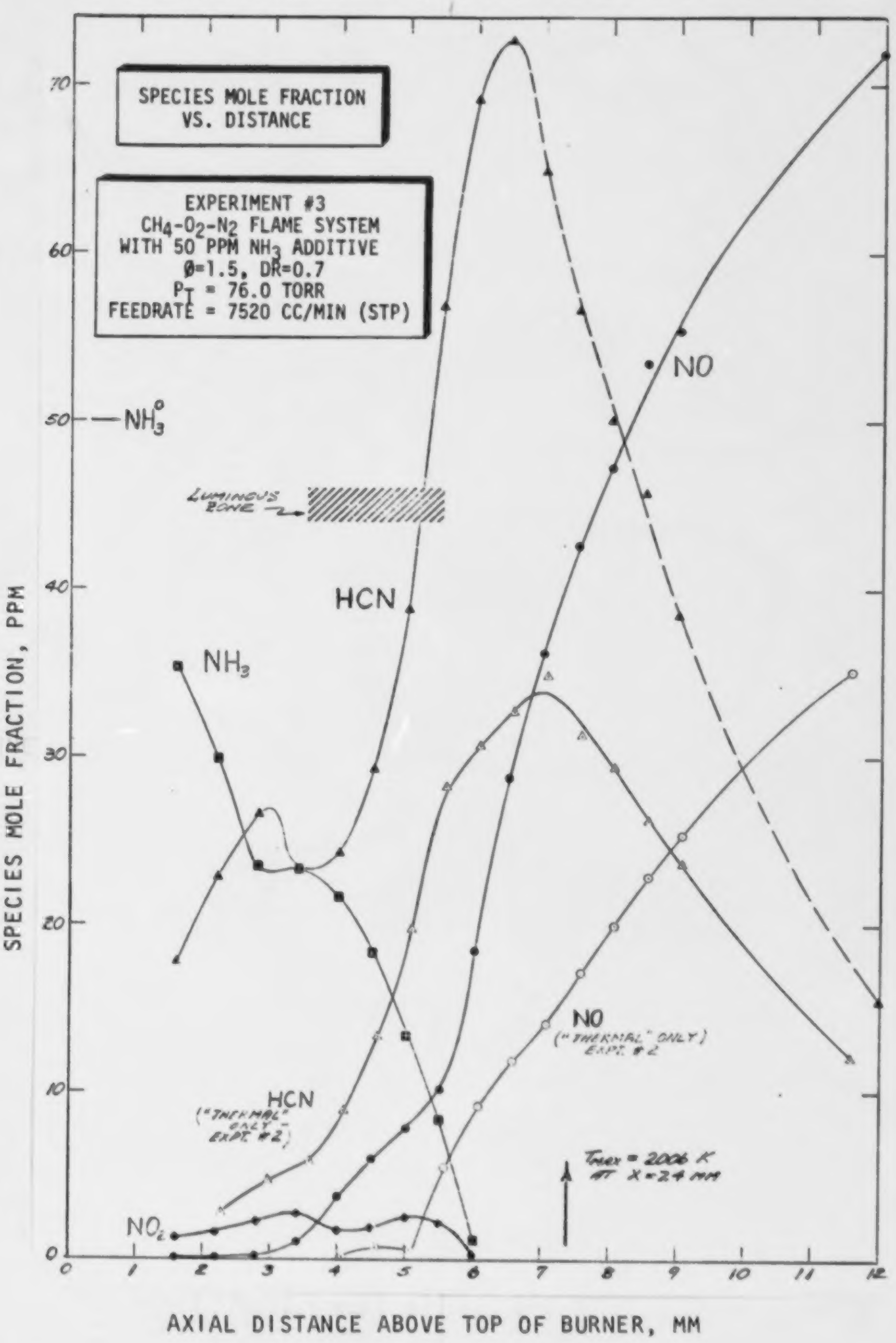

Figure 2-24. Experiment 3 - NH_3, HCN and NO Mole Fraction Profiles

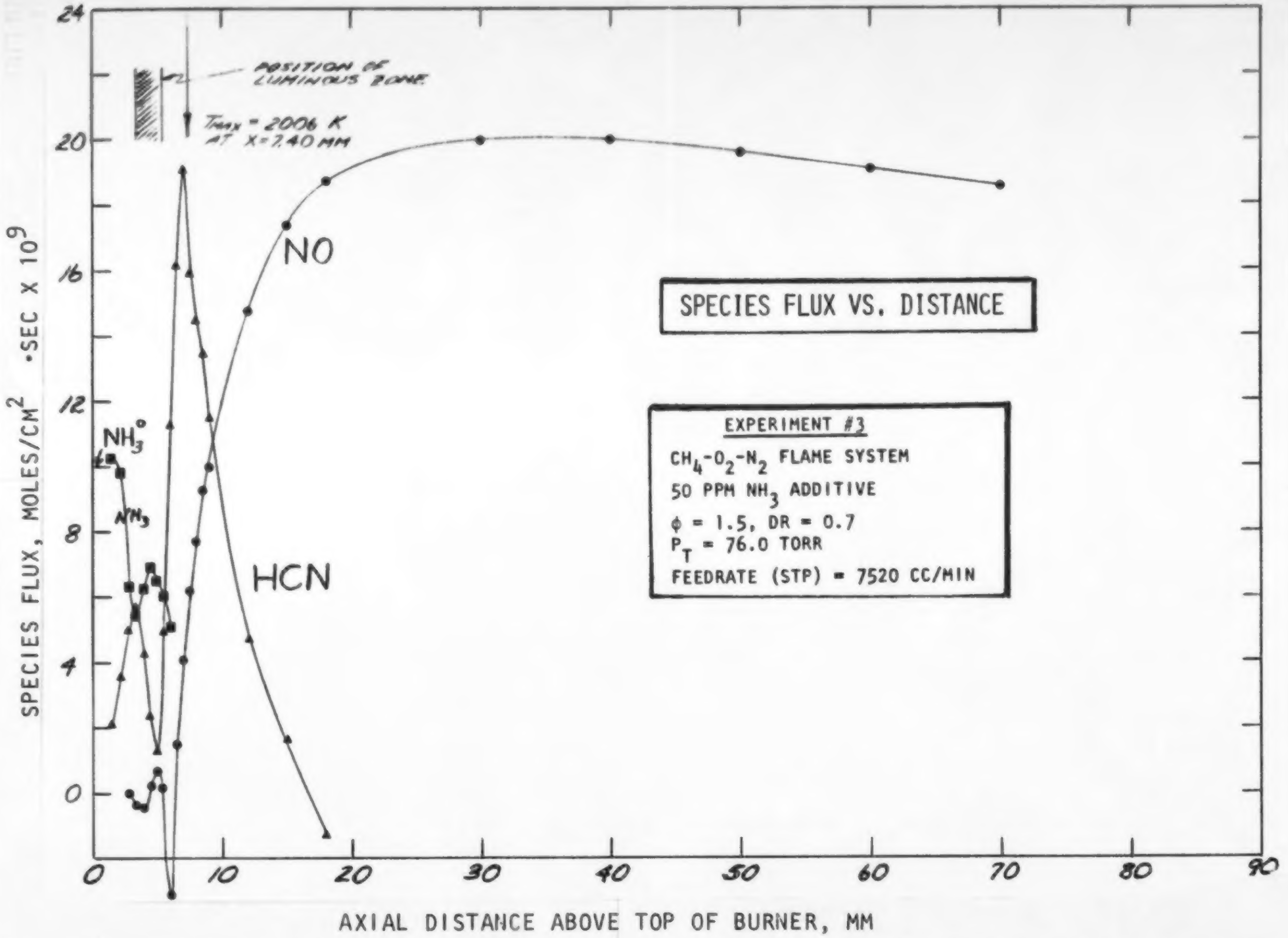

Figure 2-25. Experiment 3 - Species Flux Profiles

USE SPECIAL DROPOUT BLUE PENCIL ONLY TO INDICATE CTIONS
CLASSIFICATION

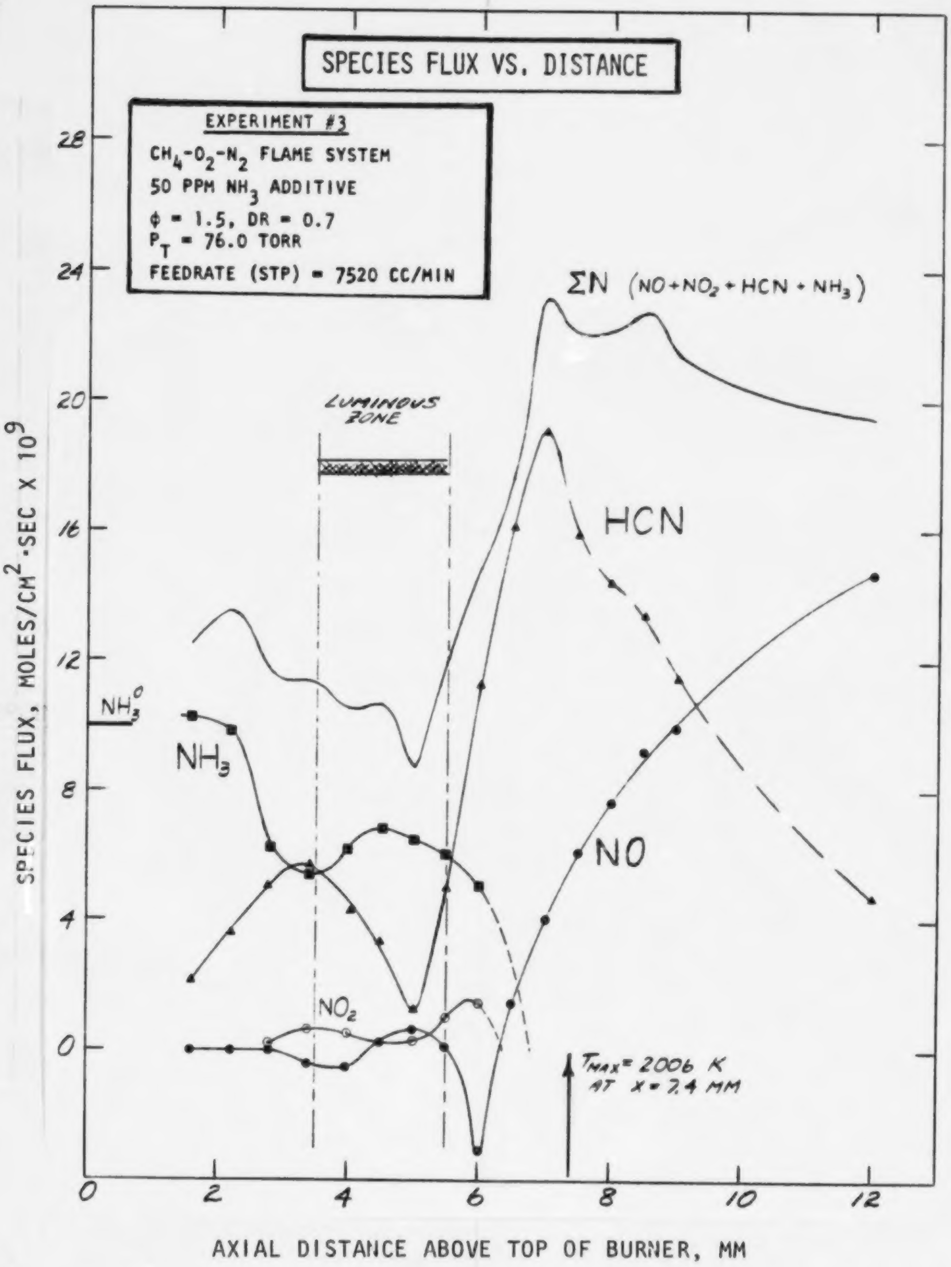

Figure 2-26. Experiment 3 - Species Flux Profiles

DOCUMENT NUMBER
PAGE NUMBER

CLASSIFICATION
TYPIST 191

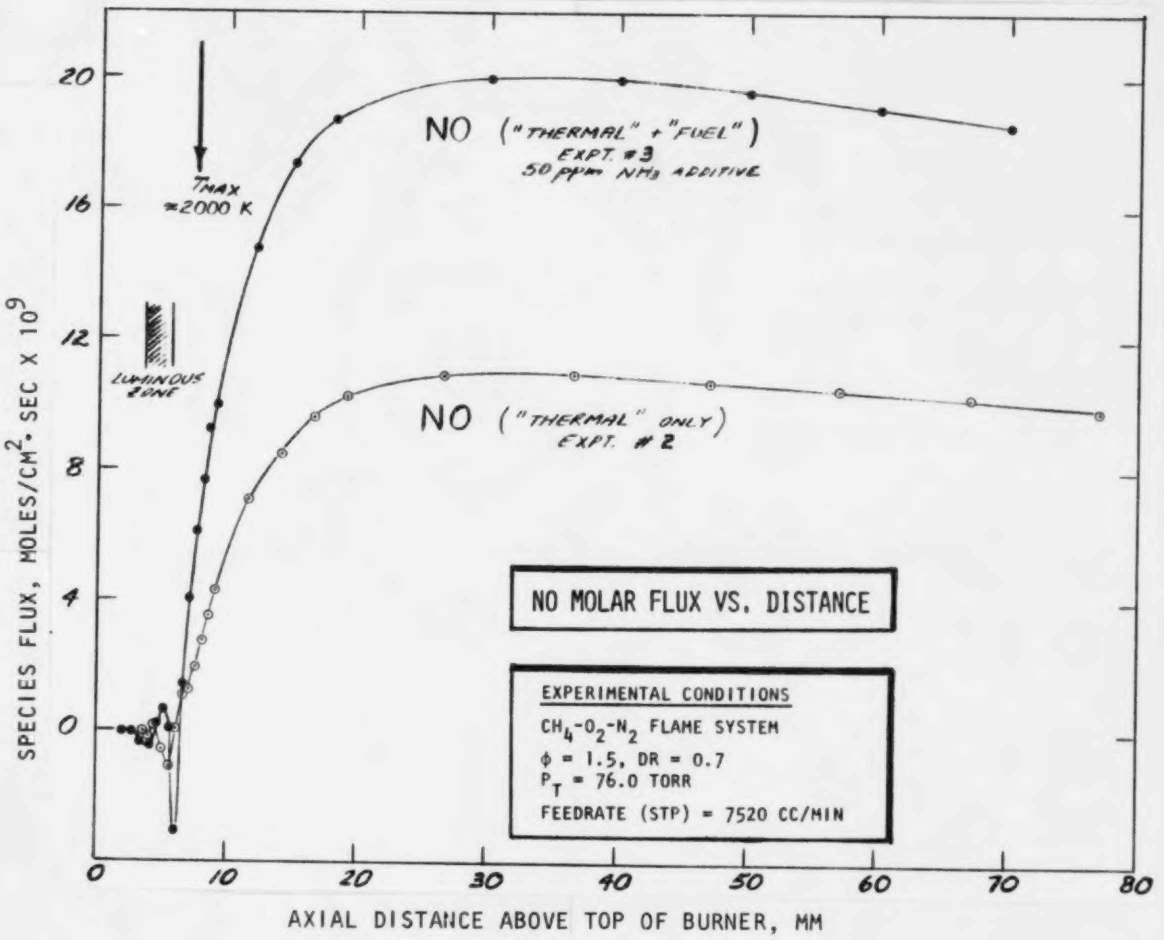

Figure 2-27. Comparison of NO Molar Flux Profiles from Experiments 2 and 3

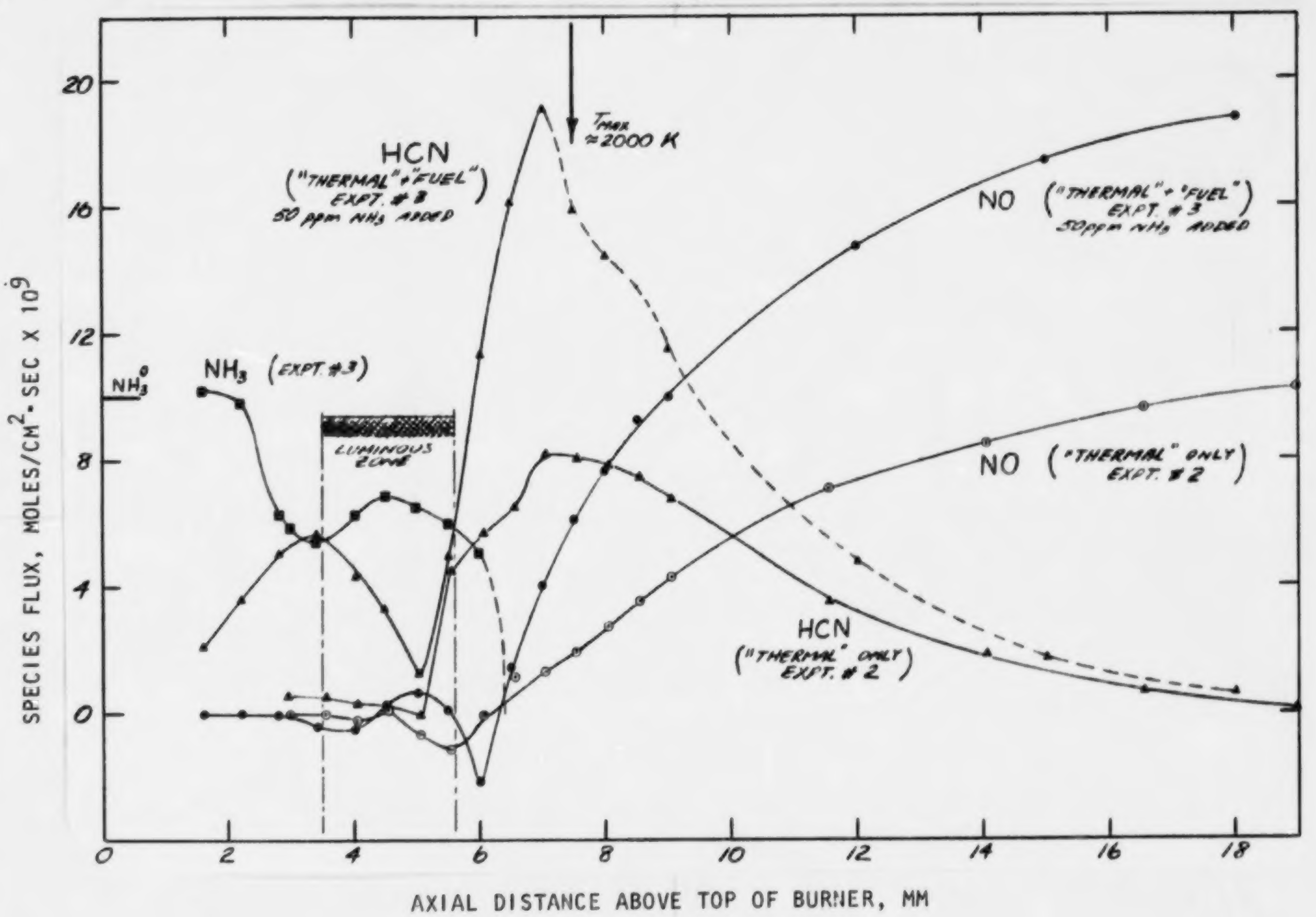

Figure 2-28. Comparison of Molar Flux Profiles for HCN and NO from Experiments 2 and 3

concentrations, the yield of NO is much lower in a fuel-rich flame (e.g., Fig. 2-15). It is well known, however, that in general the fractional conversion of fuel-N to NO decreases with increasing fuel-N concentration. At the low NH_3 concentrations employed in experiment No. 2, the fuel NO yield is high even at $\phi=1.5$ and, as will be shown, the thermal (prompt) NO yield is higher under fuel-rich conditions then with an excess of oxygen. *This situation may place an ultimate limit on the reduction in NO that can be achieved in staged combustion.* The increase in NO yield at lower fuel-N concentrations is in agreement with Fenimore's hypothesis that there is a competition between the oxidation of fuel-N to NO and the reduction of NO to N_2 by reaction with fuel-N intermediates (Ref. 27).

The HCN and NO fluxes from experiments 2 and 3 are compared in Fig. 2-28. The HCN flux peaks at the same distance above the burner in each case and the HCN forms rapidly just below the top of the luminous zone in each. Likewise, the thermal and fuel NO both have their maximum rates of formation above the luminous zone in the region of maximum temperature. This comparison reveals for the first time the striking commonality between the chemical mechanisms involved in the formation of thermal (prompt) and fuel NO in a rich methane flame.

Profiles of Major Species in Rich Flame. Mass spectrometric analysis was used to measure the mole fractions of the major species in the fuel-rich CH_4-O_2-N_2 flame of experiment No. 3. Thirteen gas samples were obtained as described in the experimental section. Each was sealed in a 1-liter flask at a total pressure of approximately 1 torr. One sample was obtained directly from a standard calibration gas cylinder, the contents of which had been analyzed previously and found to contain 2.76% CH_4, 4.03% O_2, 5.75% CO_2 and 88.42% CO + N_2. A second sample contained the initial feed gas mixture passing through the burner in a cold-flow mode. Based upon volumetric flowrates, this sample should consist of 60.1% N_2, 22.8% O_2, and 17.1% CH_4. The remaining 11 combustion gas samples

---

27. Fenimore, C.P. "Reactions of Fuel-Nitrogen in Rich Flames," Comb. and Flame, 26, 249 (1976).

were obtained during hot-fire conditions beginning just above the burner screen at 1.75 mm on the assigned distance scale to well above the top of the luminous zone at 8.00 mm downstream. At each point where a gas sample was obtained, a corresponding NO concentration reading was recorded. The thirteen gas samples were sent to West Coast Technical Services of Cerritos, California for analysis on their mass spectrometer.

In these CH_4-O_2-N_2 flame products, the mass spectrometric analysis determines the concentrations of the species CH_4, O_2, H_2 and CO_2 relative to the sum of $CO+N_2$. The CO and N_2 cannot be measured separately in a low-resolution mass spectrometer because they have the same molecular weight and masses of the lower molecular weight fragments formed are not unique to these two species. The water vapor partial pressure also cannot be measured accurately because of water's affinity for surfaces. An iterative computer program was written that calculates the amount of CO required to balance the C/N ratio of each sample to the C/N ratio in the reactants. Then, as was done in the previous program (Ref. 1), the concentration of water in each sample was adjusted to balance the H/N ratio to that of the reactants.

The mole fractions of the major species in experiment No. 3, as corrected by this computational procedure, are plotted in Fig. 2-29. The calculated H_2O mole fraction (not shown) begins to increase just above 3 mm and levels off at 19 mol % at about 5.5 mm. The theoretical final mole fraction of H_2O is 20.5%, indicating that the hydrogen balance in the reported results is excellent.

The predicted equilibrium mole fractions of CO and CO_2 at this temperature are 10.5 and 4.9%, respectively. This is in fair agreement with the measured values at 8 mm of 8.5 and 5.7% (Fig. 2-29).

The mole fractions of O_2 and CH_4 measured in an unburned sample of reactants are plotted at the left side of Fig. 2-29 (X=0). These are in good agreement with the metered values shown as dotted lines at X=0.

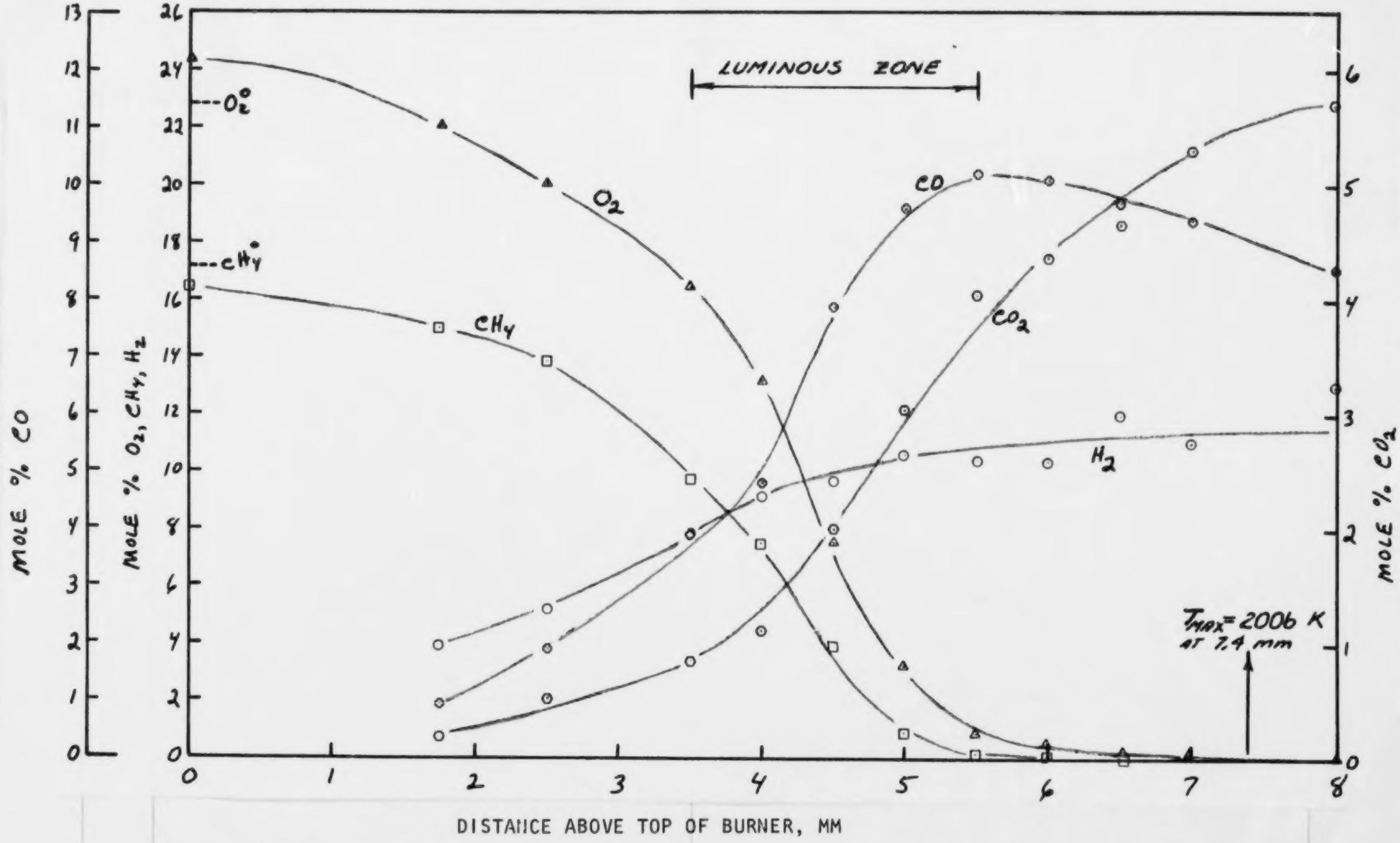

Figure 2-29. Mole Fraction Profiles of Major Species from Experiment 3 (ϕ= 1.5)

Because H_2 diffuses so rapidly, its mole fraction profile is quite flat. It can be seen that H_2 formed in the flame front diffuses upstream toward and possibly through the screen flame holder. The H_2 mole fraction is nearly 4% at the first data point which is only 0.6 mm above the top of the screen (the screen extends from 0 to 1.1 mm of the assigned distance scale). This is in agreement with the predictions of some preliminary kinetic-diffusion model calculations that were carried out on this flame.

To facilitate the calculation of molar fluxes for each of the major species from the mole fraction data, a generalized computer program was written and verified using the data from experiment No. 3. Required input data to the program include:

1. Gas temperature profile (T vs X)
2. Gas properties vs temperature
3. Mole fraction profile for each named species (f_i vs X)
4. Slopes measured at selected points on the mole fraction plots (i.e., df_i/dx)
5. Overall experimental conditions, including equivalence ratio, diluent ratio, gas feed rate, and total system pressure

The program also has an option for plotting the molar flux profile for each species.

The molar flux profiles calculated for the major species in experiment No. 3 are plotted (by hand) in Fig. 2-30. F2-30

It can be seen from Fig. 2-30 that the O_2 and CH_4 react rapidly in the upper half F2-30 of the luminous zone forming H_2 and CO. Part of the H_2 diffuses below the luminous zone where it is consumed. The CO_2 forms slowly in and above the luminous zone.

Detailed Flame Experiment No. 4 (50 ppm HCN Added)

In this experiment, 50 ppm HCN was added to the fuel-rich (ϕ=1.5) CH_4-O_2-N_2 flame studied in experiment No. 2. The conditions were otherwise the same (Table 2-6). T2-6

USE SPECIAL DROPOUT BLUE PENCIL
ONLY TO INDICATE CORRECTIONS
CLASSIFICATION
PAGE
STARTING LINE

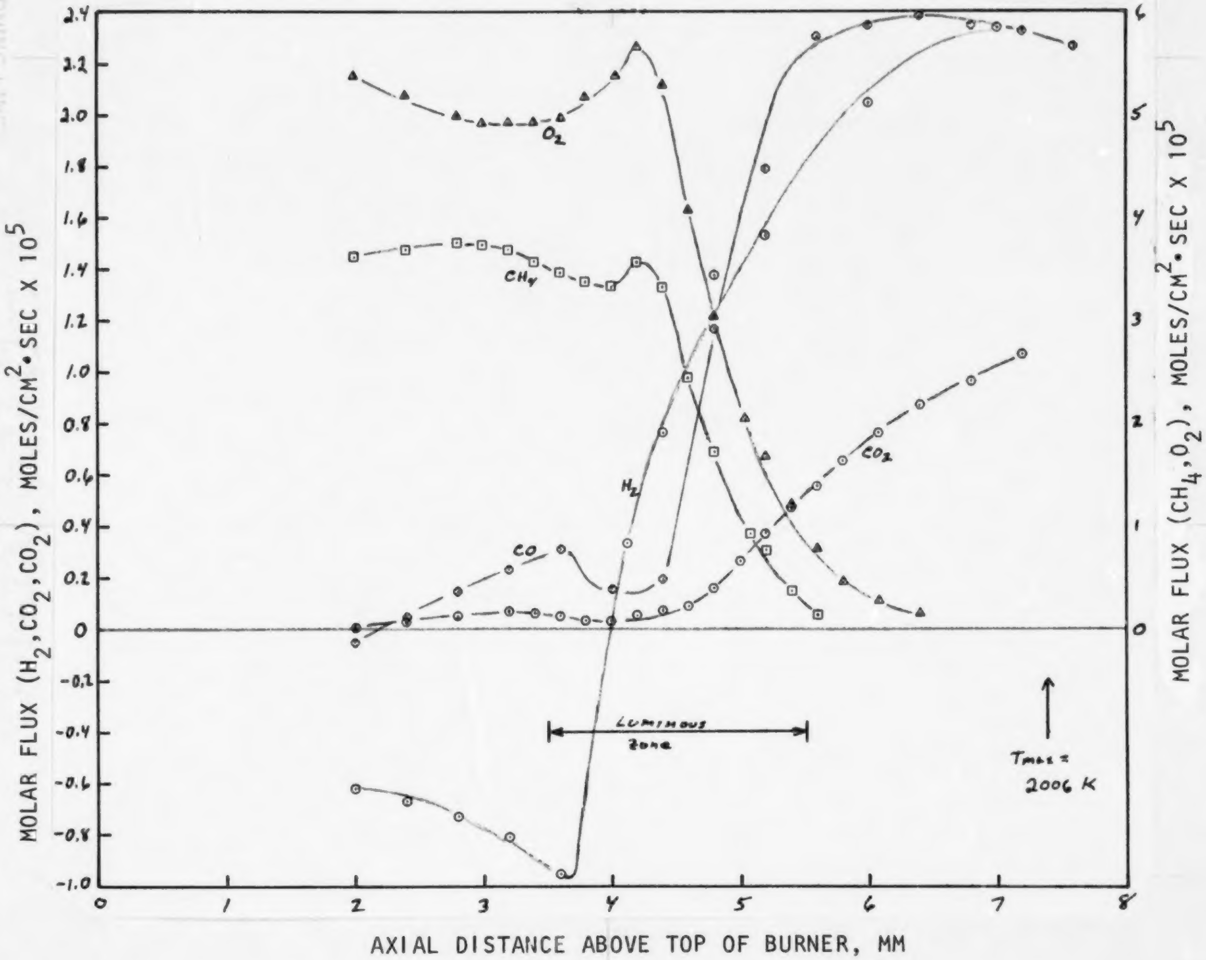

Figure 2-30. Molar Flux Profiles of Major Species from Experiment 3 (ϕ = 1.5)

WARNING LINE
STOP
DOCUMENT NUMBER
PAGE NUMBER
CLASSIFICATION
TYPIST

148

The purpose of this experiment was to investigate the rate and extent of the conversion of added HCN to NO in a fuel-rich CH_4-O_2-N_2 flame.

Immediately prior to commencing each detailed probing experiment, several system calibration checks were routinely performed. These include calibrating the cheiluminescent analyzer and determining the initial area of the orifice of the quartz microprobe, as well as conducting a cold-flow experiment with premixed unburned combustion gases to check the initial N-additive mole fraction. The cold-flow test before experiment No. 4 indicated that additional HCN flowmeter calibrations should be performed in the region of the low additive flowrate required in this experiment (9.17 cc/min of a 4.0% HCN in N_2 mixture). The results of these calibrations are plotted in Fig. 2-31.

Using this calibration curve, a calibration check of the stainless-steel converter used for the conversion of HCN to NO (1073 K with O_2 leak) was carried out at low HCN additive concentrations (20 to 80 ppm). These tests were carried out by cold-flowing mixtures of pure N_2 and a 4.0% HCN in N_2 calibration gas into the burner chamber and sampling at 76 torr using the quartz microprobe. As usual, a "leak" upstream of the stainless-steel converter introduced oxygen into the sampled gas. Tests at five HCN additive mole fractions between 26 and 80 ppm all yielded, within experimental error, 100% conversion of the HCN to NO. Earlier initial stainless-steel converter calibrations for HCN gave 91% conversion of the HCN to NO at the 80 ppm additive level.

Using the revised stainless steel converter calibration for HCN and the HCN flowmeter calibration curve shown in Fig. 2-31, a cold-flow experiment with premixed unburned combustible gases produced excellent agreement between the calculated (49.8 ppm) and experimentally determined (49.4 ppm) HCN inlet mole fraction. The average of the two values corresponded to an inlet HCN additive flux of 9.90 x 10^{-9} moles/cm^2·sec.

F2-25

The results observed in experiment No. 4 are plotted in Fig. 2-32 through 2-37. Some results from the baseline rich flame, experiment No. 2, are included in these figures for comparison.

F2-32 & F2-37

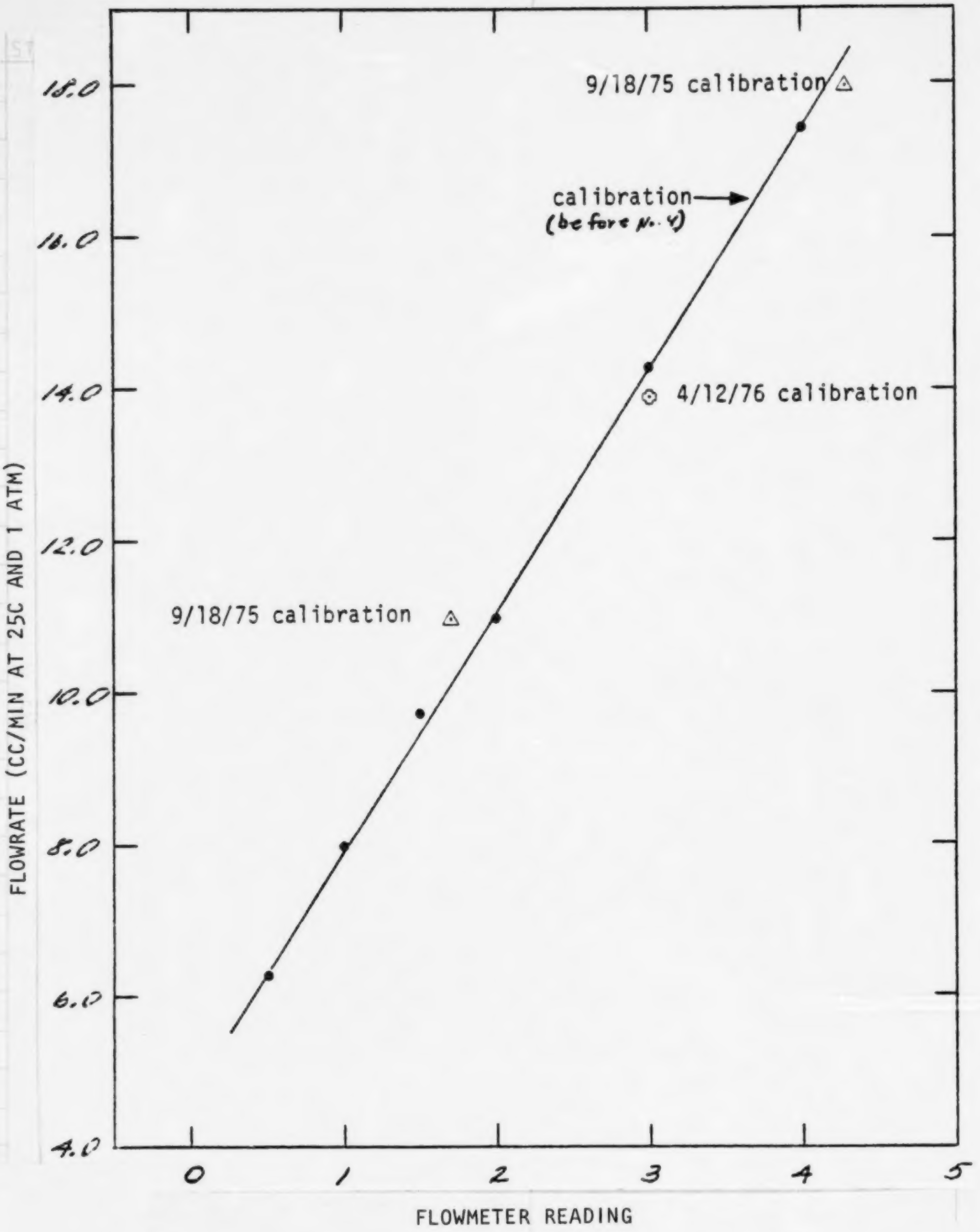

Figure 2-31. Flowmeter Calibration Curve for 4.0% HCN in N_2 Gas Mixture (Regulator Pressure = + 3.0 psig)

The temperature profile along the centerline of the burner (corrected for radiation) is shown on two different scales in Fig. 2-32 and 2-33. The temperature profile obtained in experiment No. 2 is included in Fig. 2-32 for comparison. The agreement between these two profiles is fairly good, with the position of the luminous zone and the maximum temperature point occurring at virtually the same location. The maximum temperature measured in experiment No. 4 was 2040 K compared to 1992 K in experiment No. 2. The two profiles differ by approximately 40 to 50 K over the entire range of the measurement (2.0 to 77.0 mm).

The mole fraction profiles for the fuel-nitrogen species are plotted in Fig. 2-34 and 2-35, together with the thermal NO and thermal HCN profile (Fig. 2-35 only) obtained in experiment No. 2. The addition of 49.8 ppm HCN increased the maximum NO mole fraction from 49.2 to 82.9 ppm, indicating a 68% yield of NO from the added HCN based on mole fractions. This assumes that the yields of thermal and fuel NO are purely additive. The NO formed well above the luminous zone where the HCN is disappearing.

Note that the measured HCN mole fraction in experiment No. 6 initially decreases and reaches a minimum of 42.5 ppm at a point (2.6 mm) where the thermal HCN is also very low, and then increases to nearly 60 ppm indicating the formation of "fuel" HCN. Both the fuel and thermal HCN mole fraction profiles have maximum points above the top of the luminous zone and just below the point where the maximum flame temperature is reached. Using the Cosorb solid trapping agent in conjunction with the stainless-steel converter, NH_3 levels of 0.6 to 1.8 ppm were measured below and in the flame front between 1.8 and 5.0 mm. However, it should be pointed out that these values were obtained by subtracting two numbers that differ by less than 0.8 ppm and therefore must be considered only as approximate.

The maximum HCN mole fraction above the luminous zone in Fig. 2-35 increased from 35 to 60 ppm when 50 ppm of HCN was added indicating that 50% of the added HCN survived the flamefront (assuming that the added HCN does not suppress the formation of thermal HCN).

USE SPECIAL DROPOUT BLUE PENCIL
ONLY TO INDICATE CORRECTIONS
CLASSIFICATION
PAGE
STARTING LINE
WARNING LINE
STOP

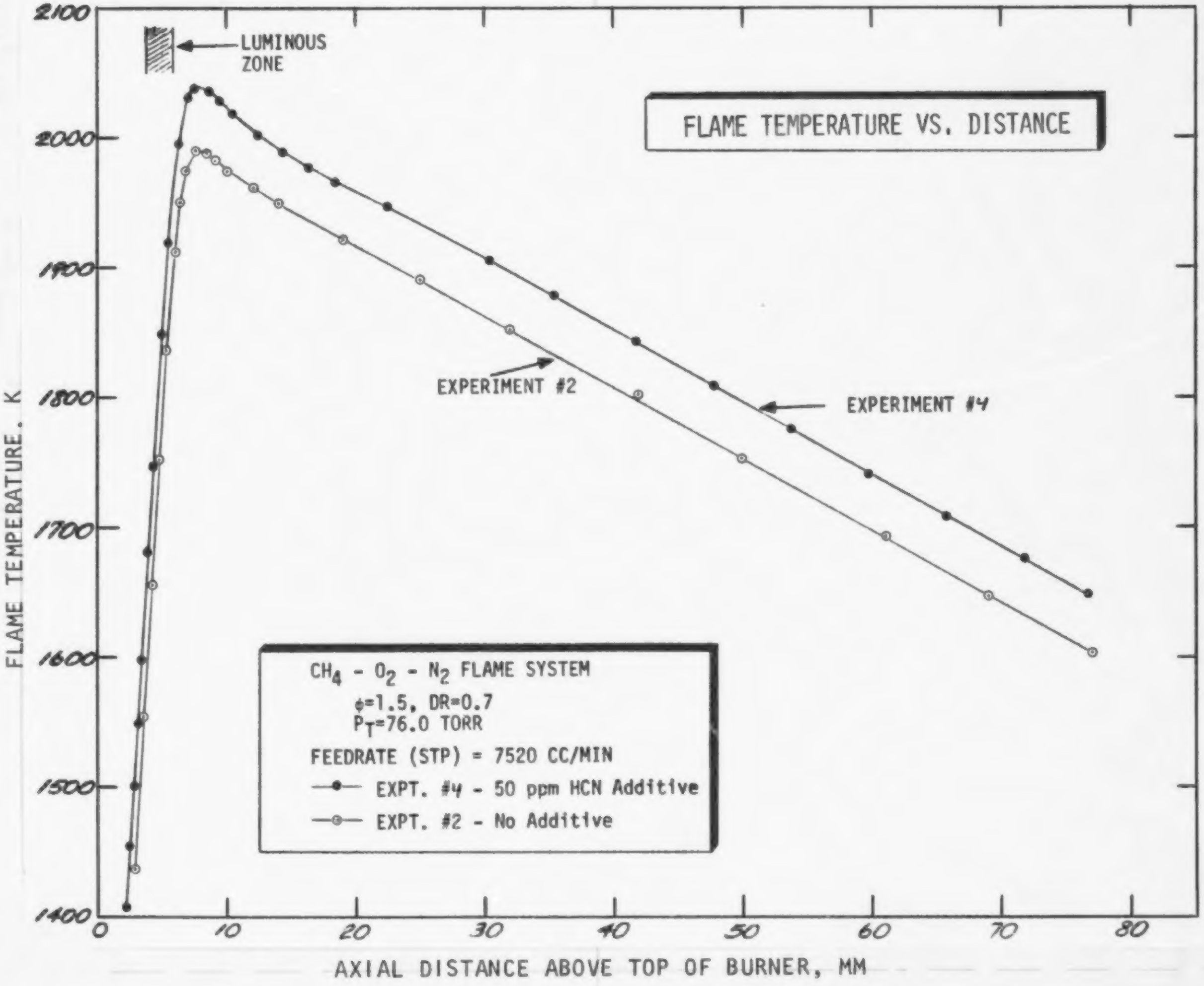

Figure 2-32. Comparison of Flame Temperature Profiles from Experiments 2 and 4

DOCUMENT NUMBER
PAGE NUMBER
CLASSIFICATION
TYPIST 152

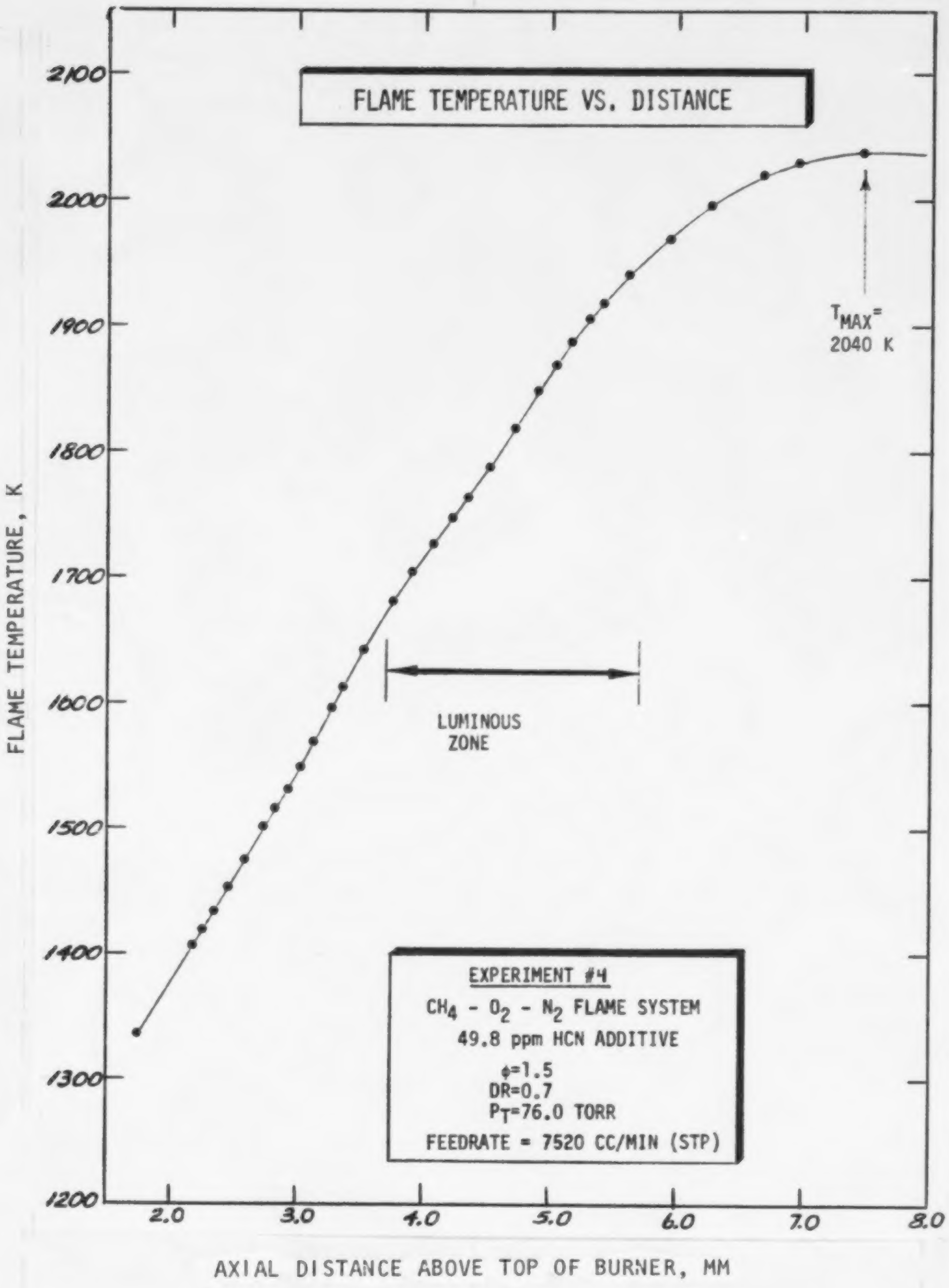

Figure 2-33. Experiment 4 - Temperature Profile

USE SPECIAL DROPOUT BLUE PENCIL
ONLY TO INDICATE CORRECTIONS
CLASSIFICATION
PAGE

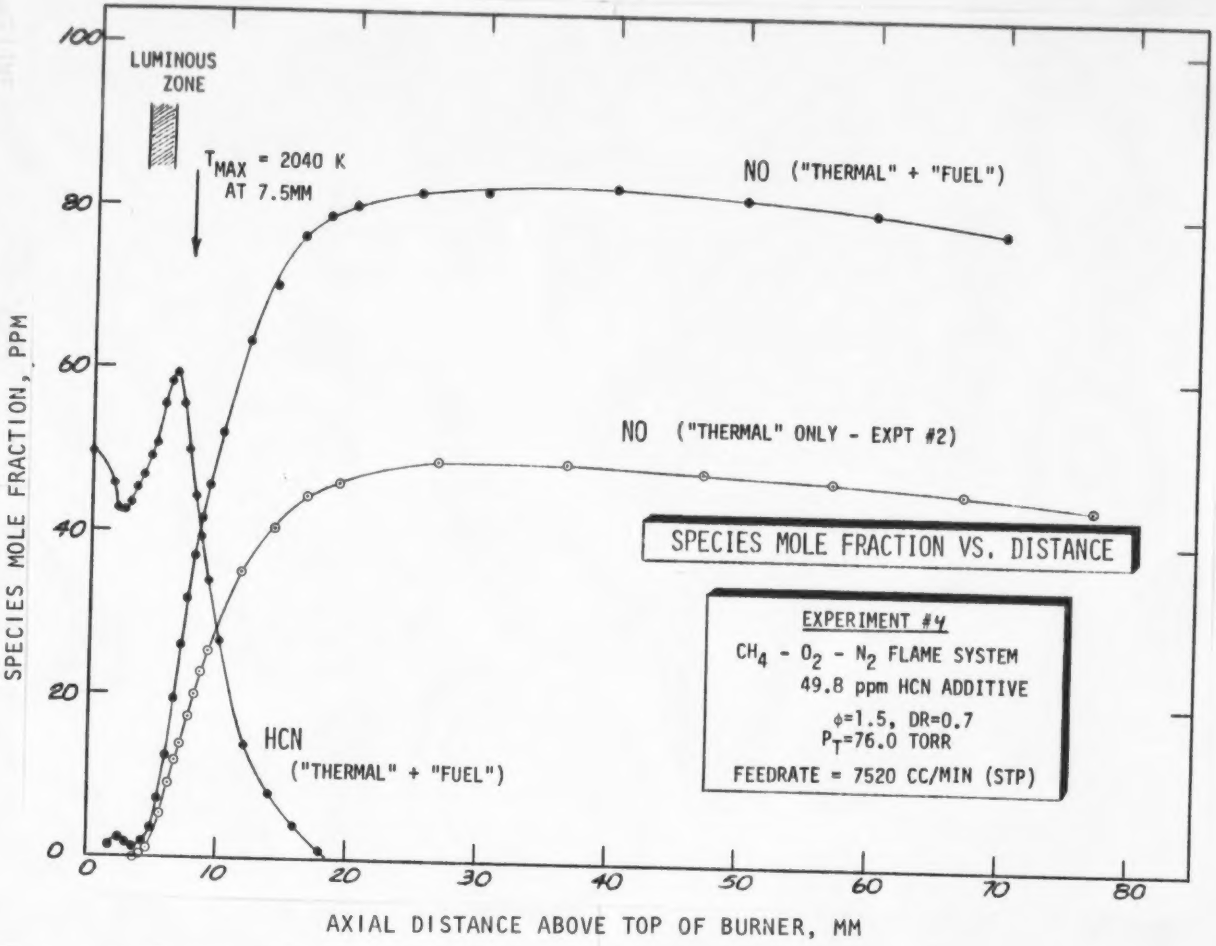

Figure 2-34. Experiment 4 - Species Mole Fraction Profile

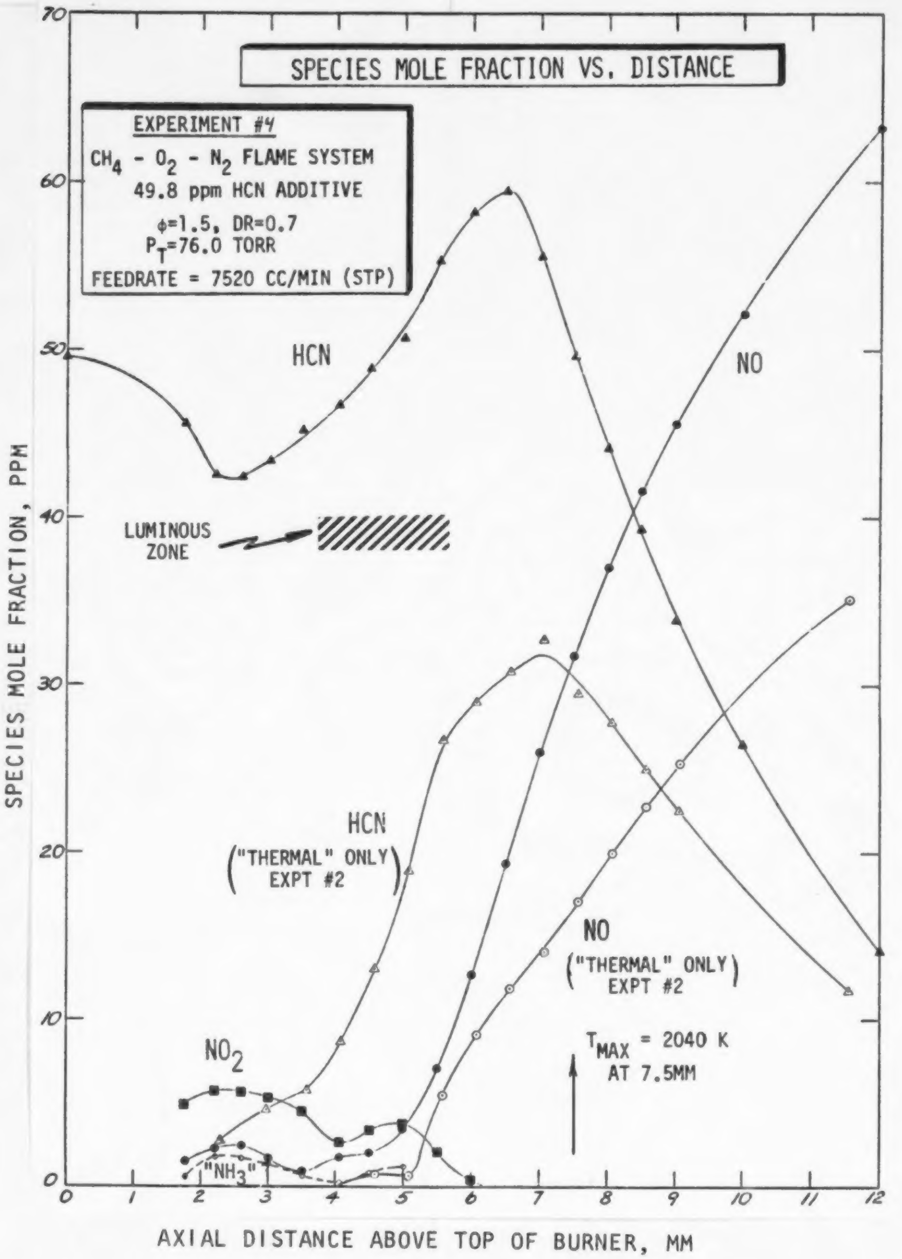

Figure 2-35. Experiment 4 - Species Mole Fraction Profiles

The species flux curves calculated for experiment No. 4 are plotted in Fig. 2-36 and 2-37. The species flux curves from the fuel-rich experiments No. 2 (no additive), No. 3 (added NH_3) and No. 4 (added HCN) are compared in Fig. 2-38 and 2-39. The yield of NO from the added HCN was only 74% compared with 90% from NH_3. Based on the flux curves, 78% of the HCN survives the flame front.

It can be seen from Fig. 2-38 and 2-39 that there is a marked similarity between: (1) the point of maximum HCN flux, (2) the region of maximum NO formation, and (3) the region in which the HCN reacts whether the nitrogen species in the feed gas is NH_3, HCN, or N_2.

It can be seen from Fig. 2-39 that the maximum rate of HCN oxidation occurs at approximately the same point as the maximum NO formation rate. In experiment No. 4 at 7.0 mm, $[d(NO)/dt]_{max}$ was found to be 3.1×10^{-8} moles/cm^3·sec, while $[-d(HCN)/dt]_{max}$ was determined to be 2.7×10^{-8} moles/cm^3·sec.

Morley (Ref. 28) described a novel method for the direct sampling of natural flame ions into a mass spectrometer for the measurement of HCN, NH_3, and NO in fuel-rich atmospheric pressure flames with and without fuel-nitrogen addition. He subsequently studied HCN oxidation within flames between 2300 and 2560 K, and found the rate to be consistent with the following reaction being the rate-limiting steps:

$$CN + OH \xrightarrow{k} NCO + H$$

Morley derived a rate expression for this reaction:

$$d\ln(HCN)/dt = k\,[(H_2O)/(H_2)]\cdot 6\times 10^{25}\lambda^2 \exp(-135{,}000/RT)$$

---

28. Morley, C., "The Formation and Destruction of HCN From Atmospheric and Fuel Nitrogen in Rich Atmospheric-Pressure Flames," Comb. and Flame, 27, 189 (1976).

USE SPECIAL DROPOUT BLUE PENCIL ONLY TO INDICATE CORRECTIONS
CLASSIFICATION
PAGE
STARTING LINE

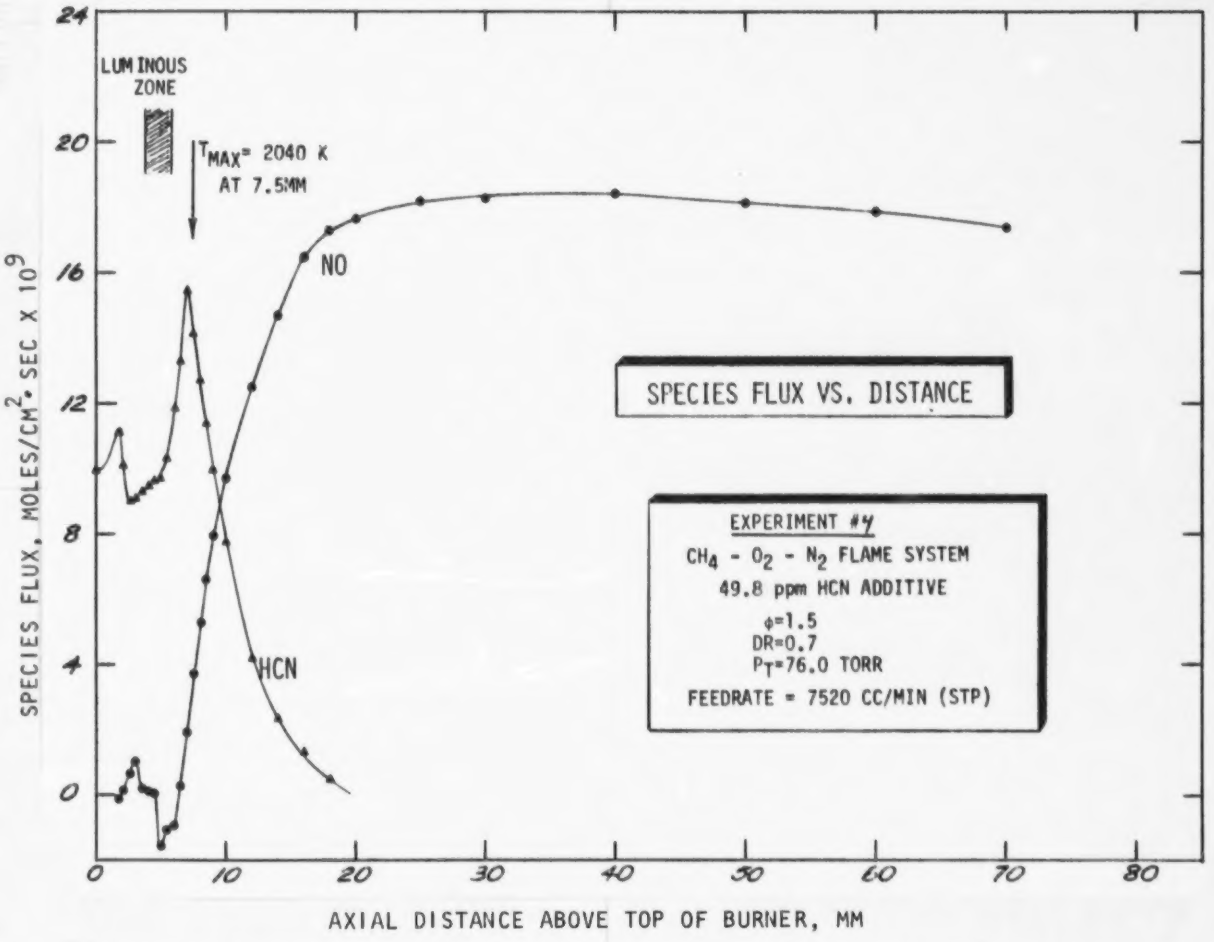

Figure 2-36. Experiment 4 - Species Flux Profiles

DOCUMENT NUMBER
PAGE NUMBER
CLASSIFICATION
TYPIST 157

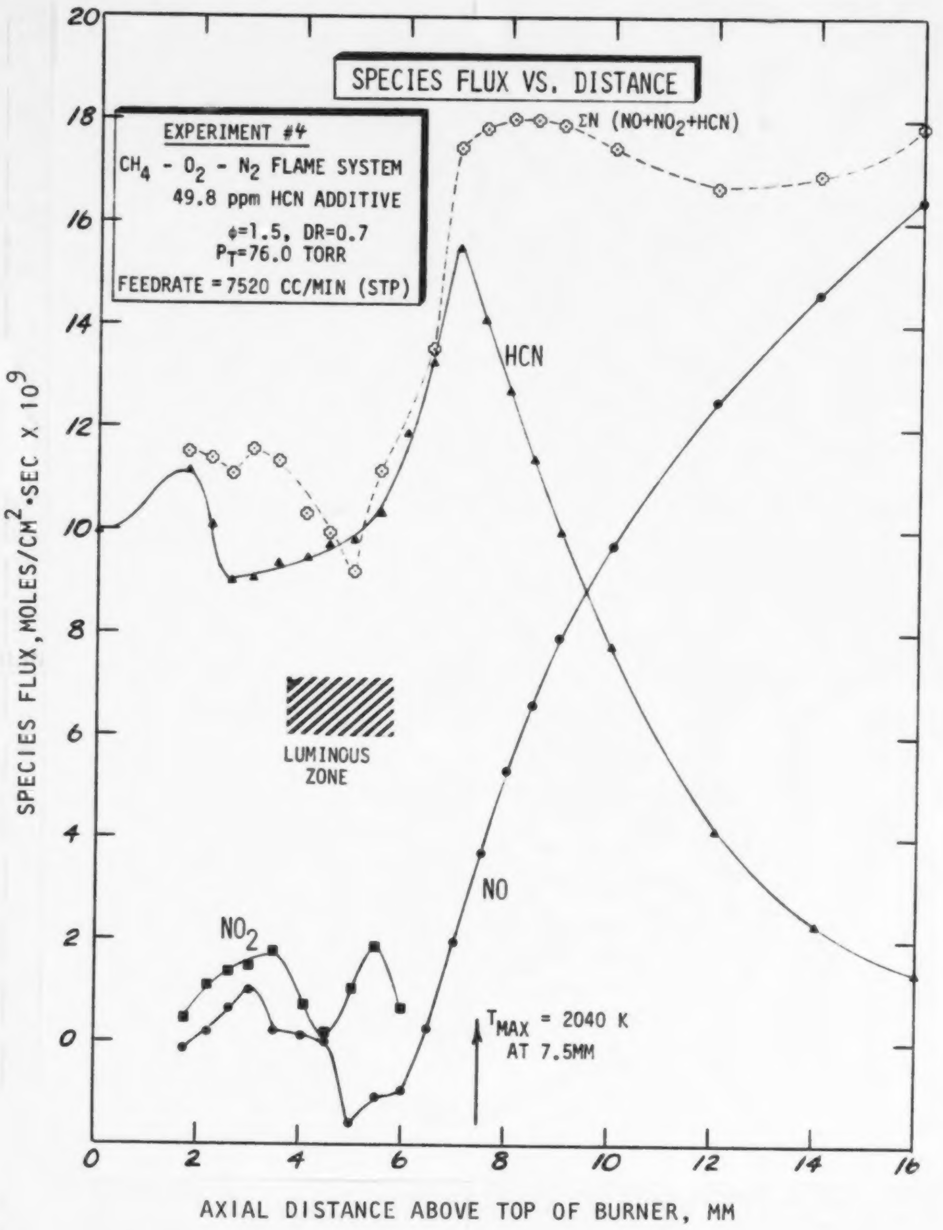

Figure 2-37. Experiment 4 - Species Flux Profiles

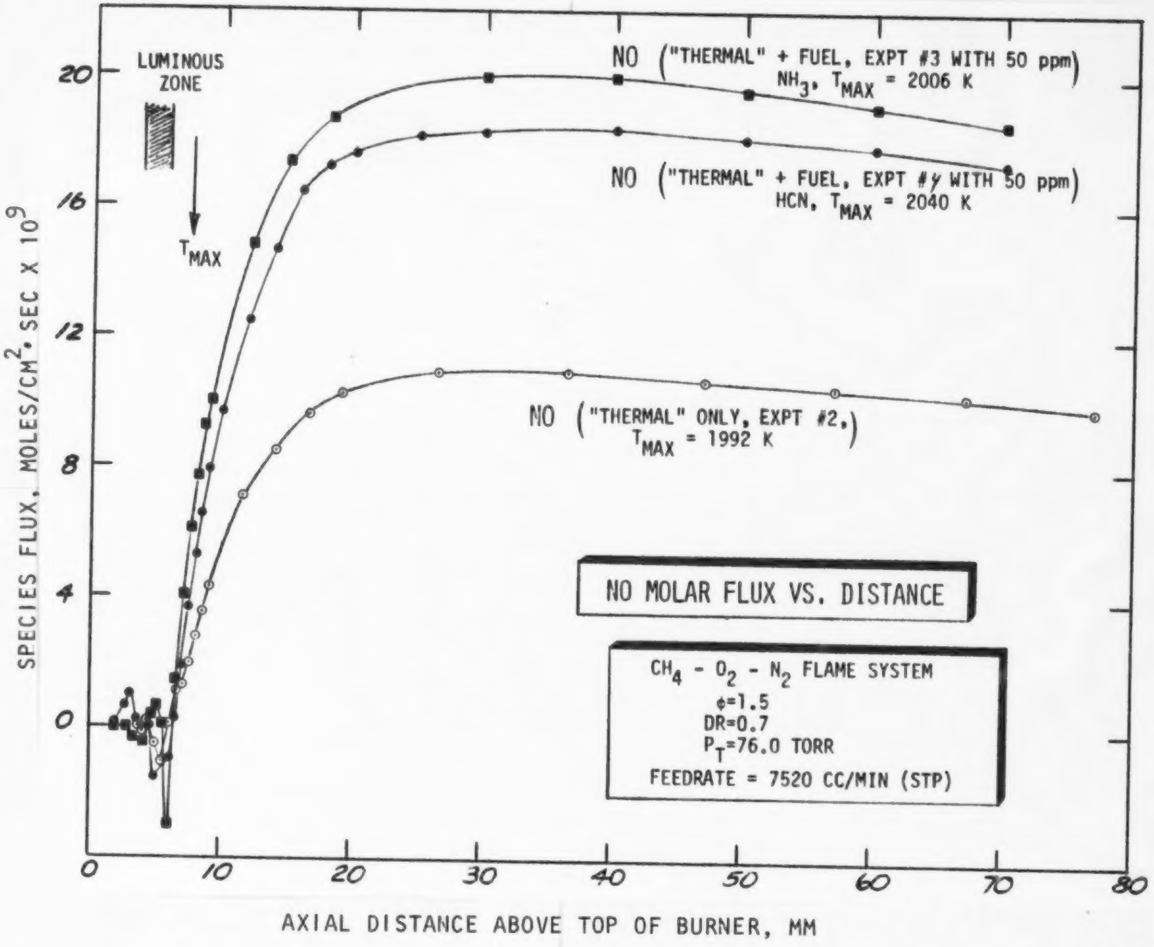

Figure 2-38. Comparison of NO Flux Profiles from Experiments 2, 3 and 4

USE SPECIAL DROPOUT BLUE PENCIL
ONLY TO INDICATE CORRECTIONS
CLASSIFICATION
PAGE
STARTING LINE

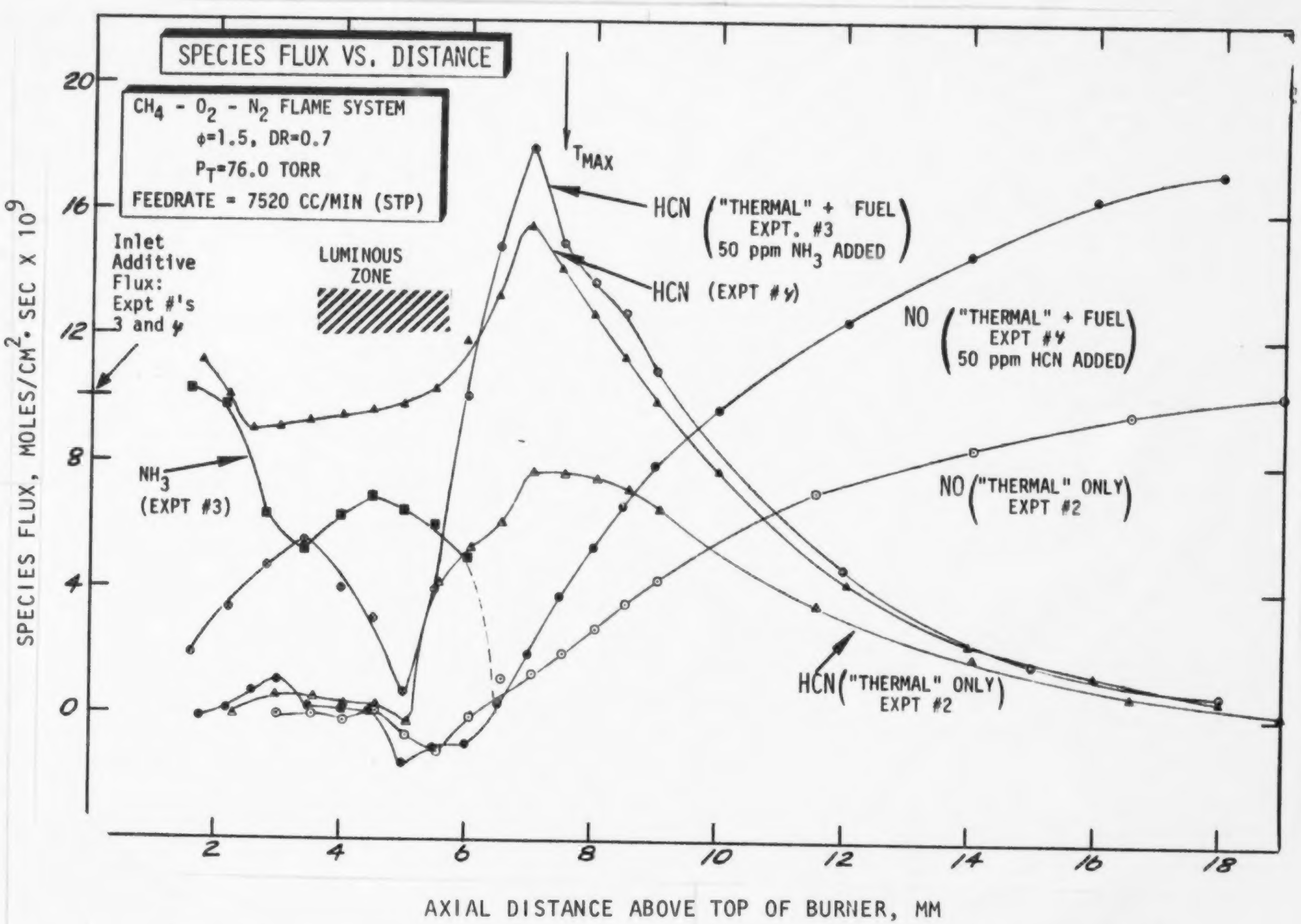

Figure 2-39. Comparison of HCN and NO Flux Profiles from Experiments 2, 3 and 4

DOCUMENT NUMBER
PAGE NUMBER
CLASSIFICATION
TYPIST 160

where λ is a factor which takes into account any disequilibrium in the radical concentrations in the flame, and $k = 1 \times 10^{-10}$ cm^3/molecule·sec. The rate data are plotted in the Arrhenius form for equivalence ratios of 2.05, 1.8, and 1.56.

Using the rate data obtained in our experiment No. 4 at 7.4 mm downstream (T=2040 K), letting λ=1 and

$$(H_2O)/(H_2) = [(H_2O)/H_2)]_{eq.\ at\ 2040\ K} = 2.11,$$

$$[d\ln(HCN)/dt](H_2)/(H_2O) = 425$$

at $1/T = 4.90 \times 10^{-4}$ K^{-1}. If Morley's data points in his Fig. 10 (Ref. 28) for ϕ=1.56 are connected by a straight line, the data point obtained above for experiment No. 4 of this work would lie very close to this line. Morley's plot is reproduced below for comparison.

#10
R28

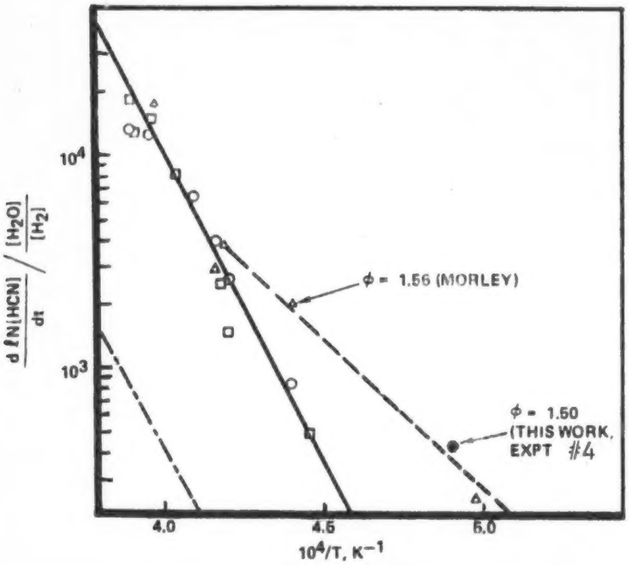

Arrhenius Plot for HCN Oxidation Given by Morley (Ref. 28). Solid Line Corresponds to Mechanism A (136 kcal/mole) for Equivalence Ratios: ○, 2.05; □, 1.8; △, 1.56. Broken Line (—— – ——) Corresponds to the Predicted Rate for Morley's Mechanism B.

USE SPECIAL DROPOUT BLUE PENCIL
ONLY TO INDICATE CORRECTIONS
CLASSIFICATION
PAGE
STARTING LINE

Conclusions From Fuel-Rich CH_4-O_2-N_2 Flame

The results of this study of the fuel-rich methane flame demonstrate quite clearly a very marked similarity between the mechanisms involved in the formation of thermal (prompt) and fuel NO when the fuel-N is at a relatively low concentration. This commonality in mechanisms appears to result from the fact that HCN is the major intermediate even when the NO is formed from N_2.

FUEL-LEAN CH_4-O_2-N_2 FLAME

The purpose of this series of experiments No. 5 and No. 6 in Table 2-6, with a lean CH_4-O_2-N_2 flame was to investigate the mechanism and rate of thermal NO_x formation under fuel-lean conditions and to compare directly thermal and fuel NO_x formation. These two detailed probing experiments were carried out at an equivalence ratio of 0.8, a diluent ratio of 0.7, a total pressure of 76 torr, and an inlet gas feed rate of 7520 cm^3/min (STP). These conditions were established in input-output experiment III.

CENTERLINE

The reactants in experiment No. 5 contained no additive so that all of the NO formed from N_2. In experiment No. 6, 50 ppm of NH_3 was added to compare fuel NO formation with thermal NO formation in the presence of excess oxygen.

Detailed Flame Experiment No. 5 (Thermal NO)

The results obtained with the additive-free, fuel-lean CH_4-O_2-N_2 flame (experiment No. 5 in Table 2-6) are plotted in Fig. 2-40 through 2-45. The conditions of experiment No. 5 are the same as those employed in input/output experiment III(c). The temperature data points measured in III(c) are plotted in Fig. 2-40 for comparison. The maximum flame temperature measured in experiment No. 5 was 1953 K at 5.15 mm compared to 1988 K measured at 5.0 mm in III(c). At 80 mm downstream, the temperatures measured in III(c) were 1554 and 1634 K, respectively.

WARNING LINE
STOP

USE SPECIAL DROPOUT BLUE PENCIL
ONLY TO INDICATE CORRECTIONS
CLASSIFICATION
PAGE
STARTING LINE
RUNNING LINE
STOP
DOCUMENT NUMBER
CLASSIFICATION
TYPIST

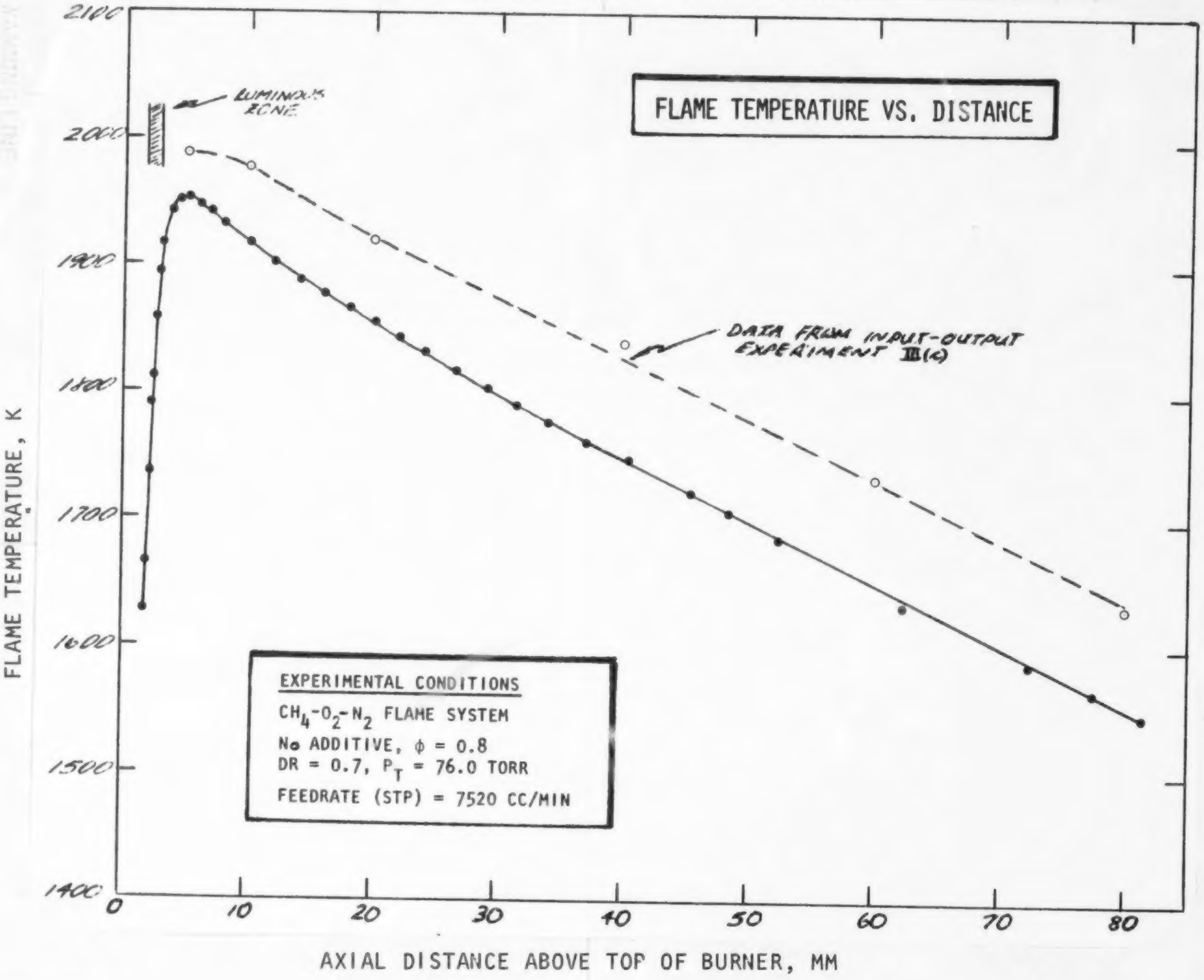

Figure 2-40. Experiment 5 - Temperature Profile

163

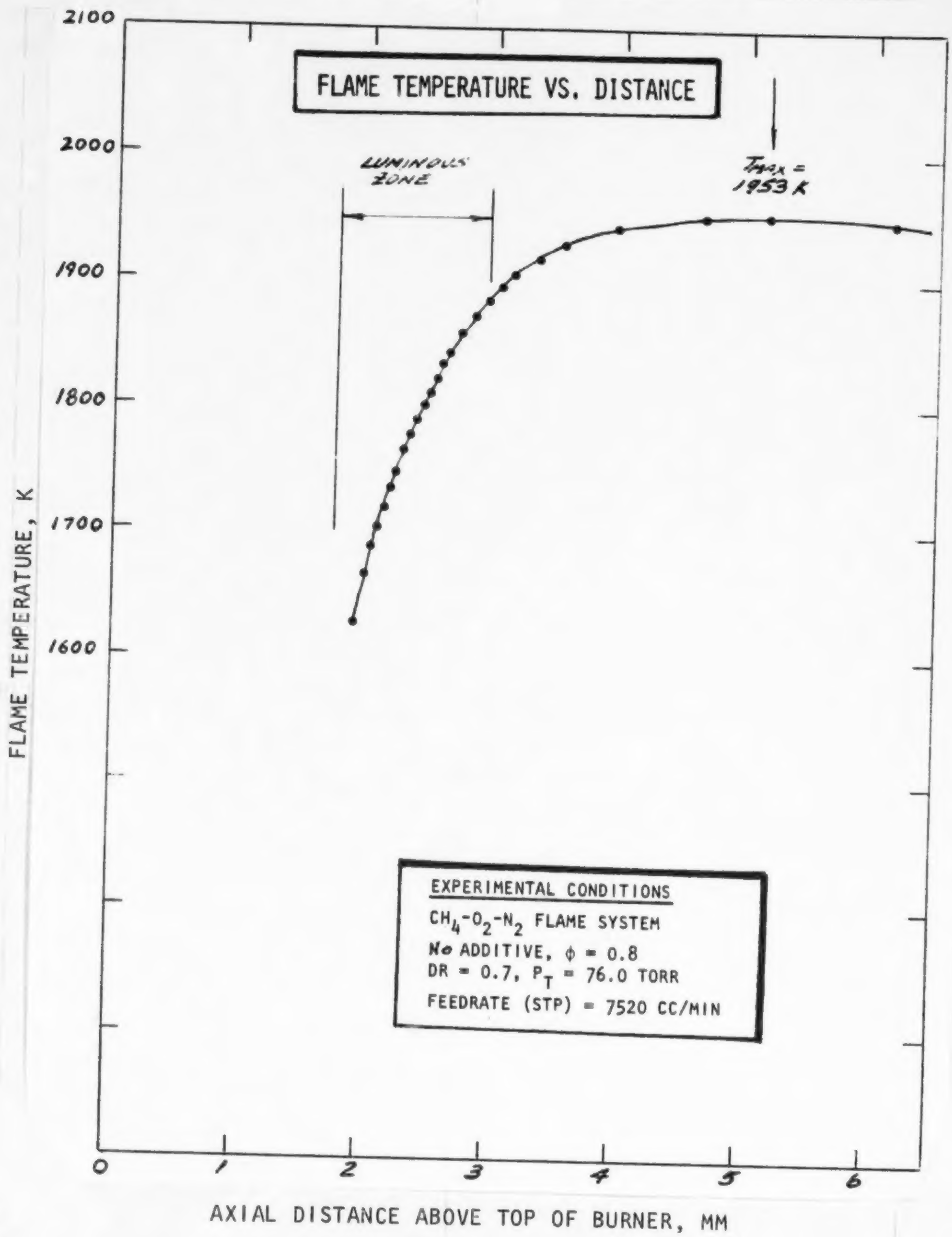

Figure 2-41. Experiment 5 - Temperature Profile

The NO mole fraction curves for experiment No. 5 and input/output experiment III(c) are compared in Fig. 2-42. The maximum NO mole fractions are 9.3 and 10.2 ppm, respectively, and occur at approximately the same downstream location (47 mm). The agreement of the NO profiles is excellent just above the top of the luminous zone, while they differ by less than 1 ppm at 80 mm downstream. The mole fractions of NO and NO_2 in experiment No. 5 are shown on an expanded scale in Fig. 2-43. No attempt was made to measure HCN or NH_3 under these conditions.

F2-42
F2-43

The molar flux profiles for NO are given in Fig. 2-44 and 2-45. It is clear from Fig. 2-45 that the maximum rate of NO formation occurs just above the top of the luminous zone. The rate becomes nearly constant just beyond the location of the maximum gas temperature and eventually becomes zero at about 40 to 50 mm downstream (Fig. 2-44). NO_2 appears to be forming in the luminous zone (Fig. 2-45) and the maximum rate of NO_2 disappearance coincides with the maximum NO production rate at a point just above the top of the luminous zone.

F2-44
F2-45
F2-44
F2-45

Discussion of Thermal NO Formation Rate. Table 2-7 compares the rate of NO formation (slope of the NO flux profile) measured at three points along the NO flux curve of Fig. 2-45 with that predicted by the Zeldovich mechanism assuming equilibrium oxygen atom concentration. The latter is calculated as follows using the data point at $\Delta X = 3.0$ to 3.2 mm as an example. The average gas temperature is 1900 K in this region and the mole fraction of N_2 is 0.65. From the mass spectrometric data of experiment No. 6 (presented in the next section), the O_2 mole fraction at this location is 0.106. Using the equilibrium constant for O_2 dissociation, the equilibrium oxygen atom mole fraction is calculated to be 3.04×10^{-4}. Baulch's rate expression of $K = 7.6 \times 10^{13} \exp(-76{,}000/RT)$, cm^3/mole-sec is used for the reaction $O + N_2 \rightarrow NO + N$. At 0.1 atm, $[N_2] = 4.18 \times 10^{-7}$ mole/cm^3 and $[O]_e = 1.95 \times 10^{-10}$ mole/cm^3. Then

T2-7
F2-45

$$d[NO]/dt = 2\ k\ [O]_e\ [N_2] = 2.55 \times 10^{-11} \text{ moles/cm}^3\text{-sec}$$

Thus the measured rate exceeds the predicted Zeldovich rate (assuming equilibrium oxygen atom concentration) by a factor of 4.6×10^3 at the top of the luminous zone, but decreases to only a factor of 10 at 8.00 mm downstream (i.e., 5 mm above top of luminous zone).

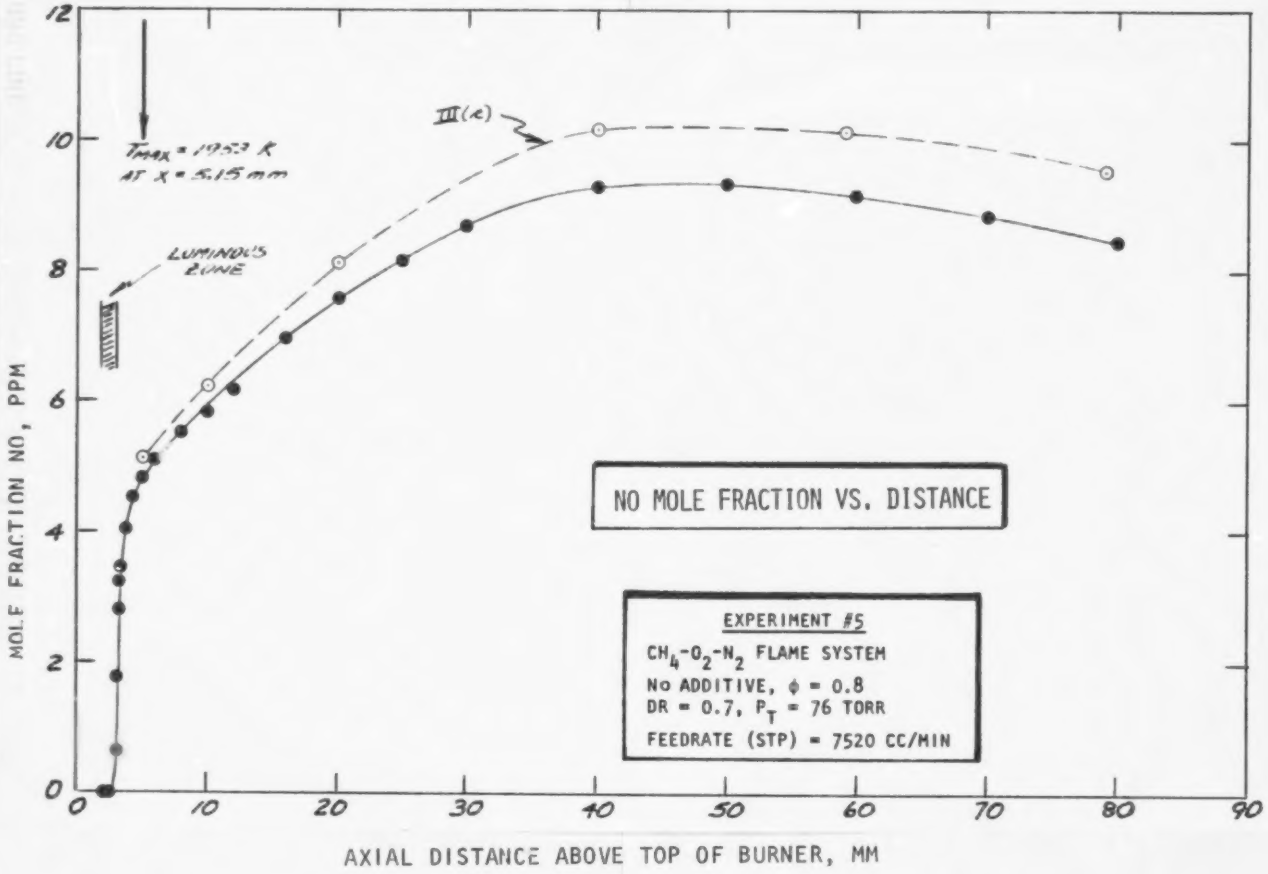

Figure 2-42. Experiment 5 - NO Mole Fraction Profile

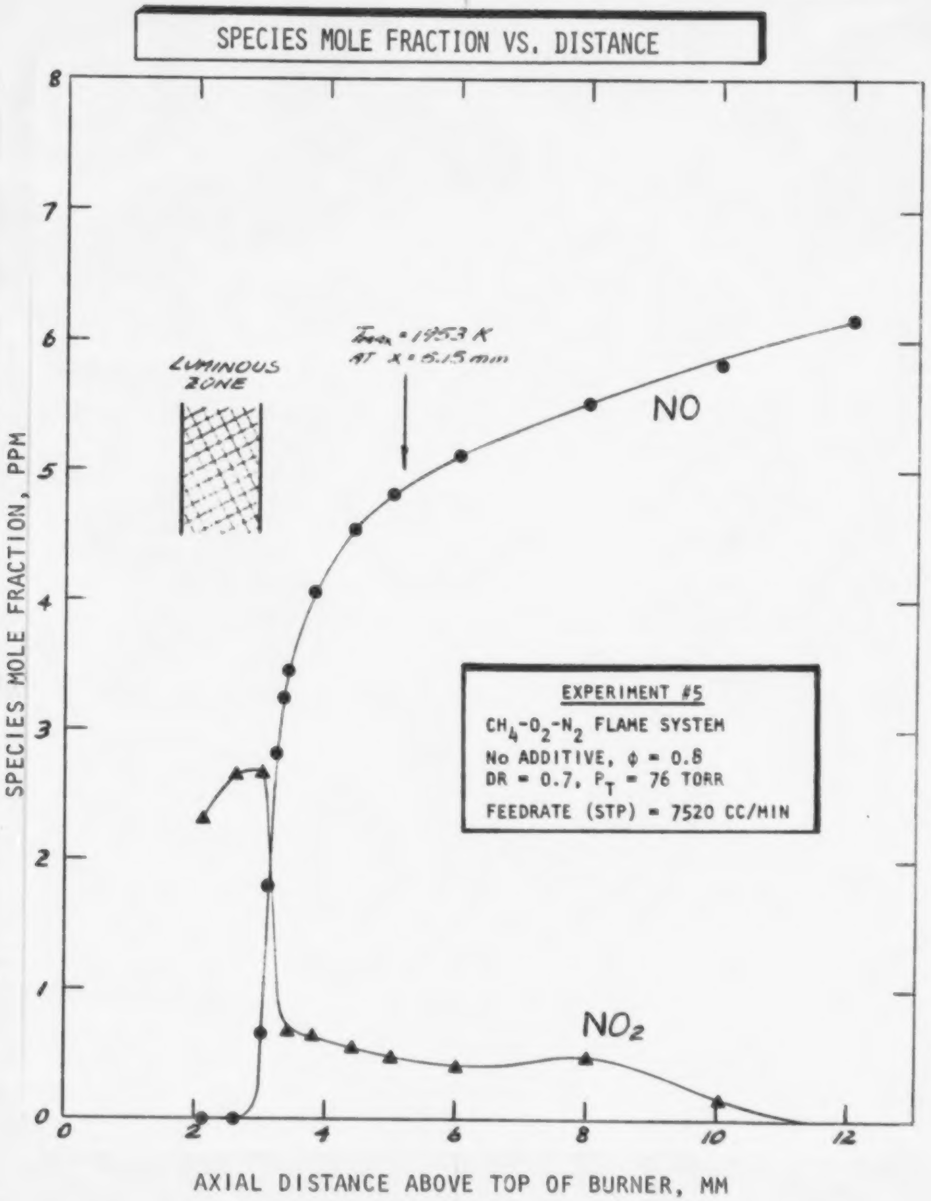

Figure 2-43. Experiment 5 - NO and NO_2 Mole Fraction Profiles

USE SPECIAL DROPOUT BLUE PENCIL ONLY TO INDICATE CORRECTIONS
CLASSIFICATION
PAGE
STARTING LINE

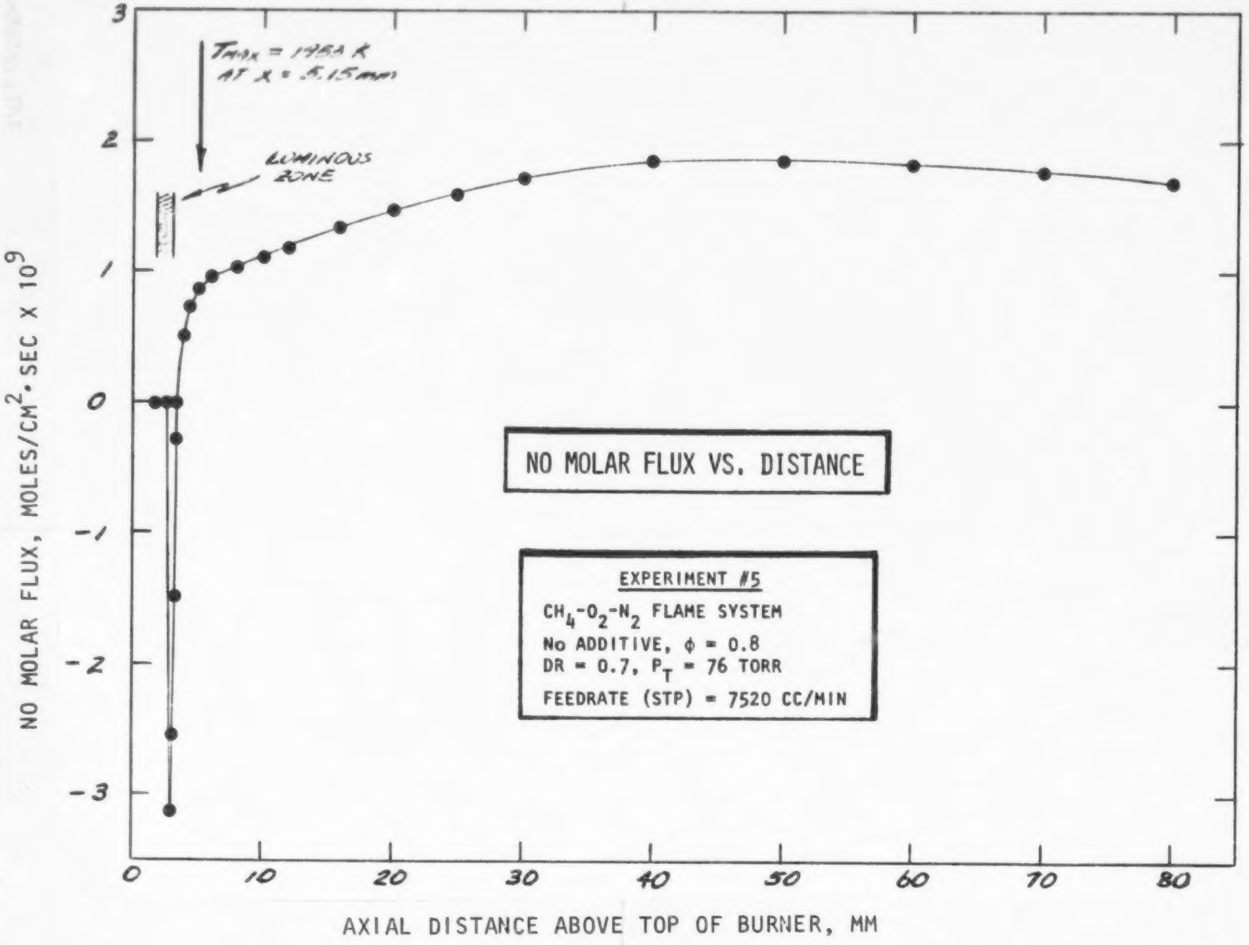

Figure 2-44. Experiment 5 - NO Flux Profile

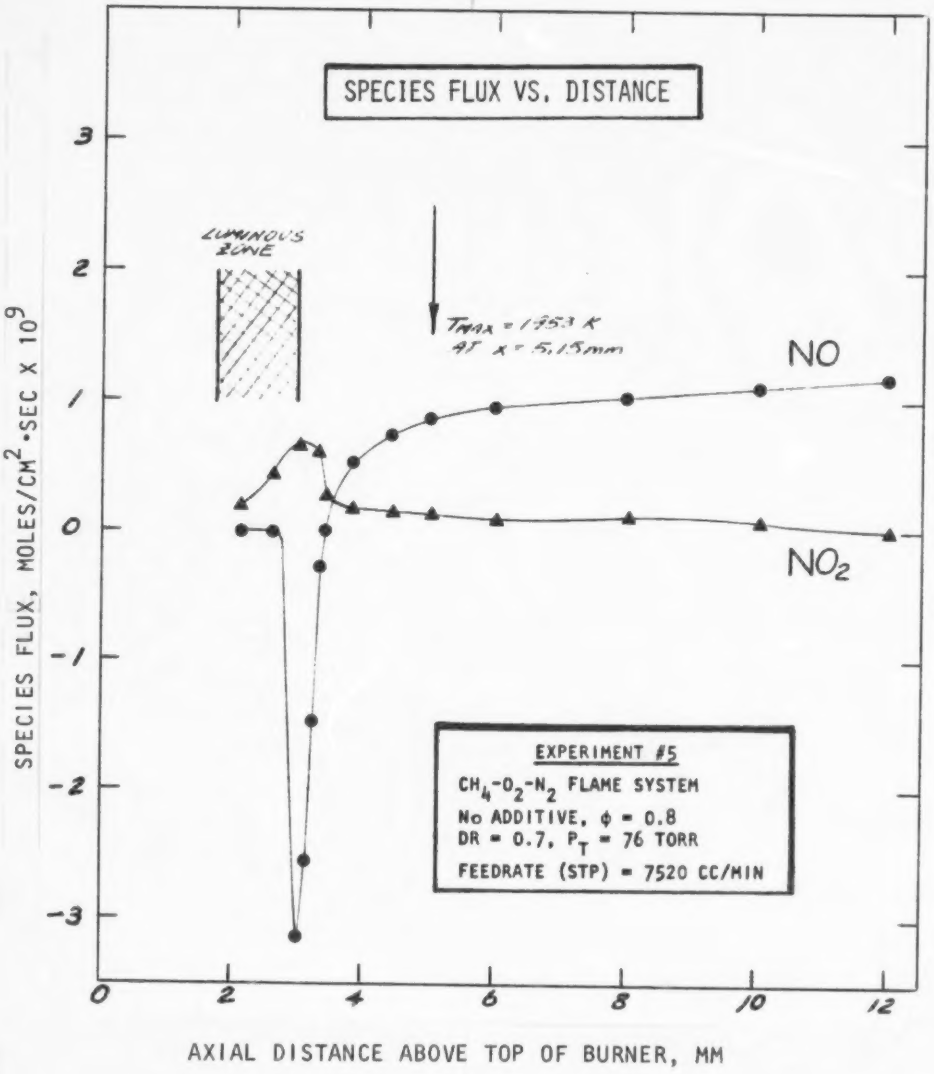

Figure 2-45. Experiment 5 - NO and NO_2 Flux Profiles

TABLE 2-7. COMPARISON OF EXPERIMENTALLY MEASURED NO FORMATION RATES WITH THOSE PREDICTED BY EQUILIBRIUM ZELDOVICH KINETICS

Axial Location Above Top of Burner	Measured Gas Temperature[(a)], K	Measured NO Rate[(b)], moles/cm^3-sec	Calculated NO Rate[(c)], moles/cm^3-sec	$\frac{R_{meas}}{R_{calc}}$
ΔX = 3.0 to 3.2 mm At Top of Luminous Zone	1900	1.16×10^{-7}	2.55×10^{-11}	4550
ΔX = 5.15 mm Location of Maximum Gas Temperature	1953	1.59×10^{-9}	5.84×10^{-11}	27
ΔX = 8.0 mm Constant NO Formation Rate	1953	3.70×10^{-10}	3.66×10^{-11}	10

[(a)] Corrected for thermocouple radiation loss

[(b)] See Fig. 2-45

[(c)] Assumes equilibrium concentration of [O] and Zeldovich reactions only

Sarofim and Pohl (Ref. 22) have studied NO formation in premixed methane-air flames (1 atm) at equivalence ratios, ϕ, of 0.89, 1.05, and 1.15. At ϕ = 0.89 (T_{max} = 2000 K), their NO mole fraction peaked at approximately 10.5 ppm, which is in good agreement with the maximum NO mole fraction of 9.3 ppm obtained in this study at ϕ=0.8 (DR=0.7, T_{max} = 1953 K). They found that the peak rates of NO formation in the "flame zone" were 1 to 3 orders of magnitude greater than in the "post-flame" zone, and determined that the peak rates of NO formation which they observed are in agreement with Zeldovich kinetics when the free radicals are calculated from the concentration of stable species using the partial-equilibrium assumptions for the fast-flame reactions. Thus, the experimental data and partial equilibrium calculations of Sarofim and Pohl provide a plausible explanation for the differences in measured versus calculated NO formation rates shown in Table 2-7, i.e., the presence of a very large excess of oxygen atoms in the lean flame.

Detailed Flame Experiment No. 6 (55 ppm NH_3 Added)

Shown in Fig. 2-46 through 2-51 are the temperature, mole fraction and molar flux profiles for experiment No. 6 (54.5 ppm NH_3 added to the conditions of experiment No. 5). The temperature profile is shown on two different scales in Fig. 2-46 and 2-47. The agreement between this profile and those presented in Fig. 2-40 and 2-41 is very good. The maximum temperature measured in experiment No. 6 was 1940 K compared to 1953 K found in experiment No. 5. The temperature profiles are strikingly similar in the vicinity of the luminous zone and differ by only about 30 K at 80 mm downstream.

72-46
to
72-51
72-46
72-40
72-41

The mole fraction profiles are plotted in Fig. 2-48 and 2-49 together with the thermal NO profile obtained in experiment No. 5 for comparison. The addition of 55 ppm NH_3 increased the maximum NO mole fraction from 9.3 ppm to 61 ppm, indicating a 95% yield of NO from the added NH_3. This assumes that the yields of thermal and fuel NO are purely additive. From Fig. 2-50, it can be seen that the maximum NO flux increased from 1.9 x 10^{-9} moles/cm^2-sec to 12.1 x 10^{-9} moles/cm^2-sec for an added NH_3 flux of 10.9 x 10^{-9} moles/cm^2-sec. The conversion of NH_3 to NO is thus also 95% based on maxiumum flux. The yield of NO from NH_3 in experiment No. 6 compares very favorably with the data obtained in input/output experiment V(a) shown at the top of Fig. 2-8.

Figure 2-51 reveals that the maximum rate of NO formation in both experiments No. 5 and No. 6 occur at exactly the same location, namely, 3.2 mm above the top of the burner and just above the top of the luminous zone (3.0 mm). This is in the region where both the NH_3 and NO_2 flux profiles are decreasing rapidly. The NH_3 flux begins to decrease abruptly at the bottom of the luminous zone and finally disappears just beyond the point where the NO flux has reached its maximum value (3.5 to 4.0 mm).

72-51

Profiles of Major Species. In these CH_4-O_2-N_2 fuel-lean flames, the mole fractions of the major reactant and product species were also determined as a function of axial distance using mass spectrometry (as part of experiment No. 6).

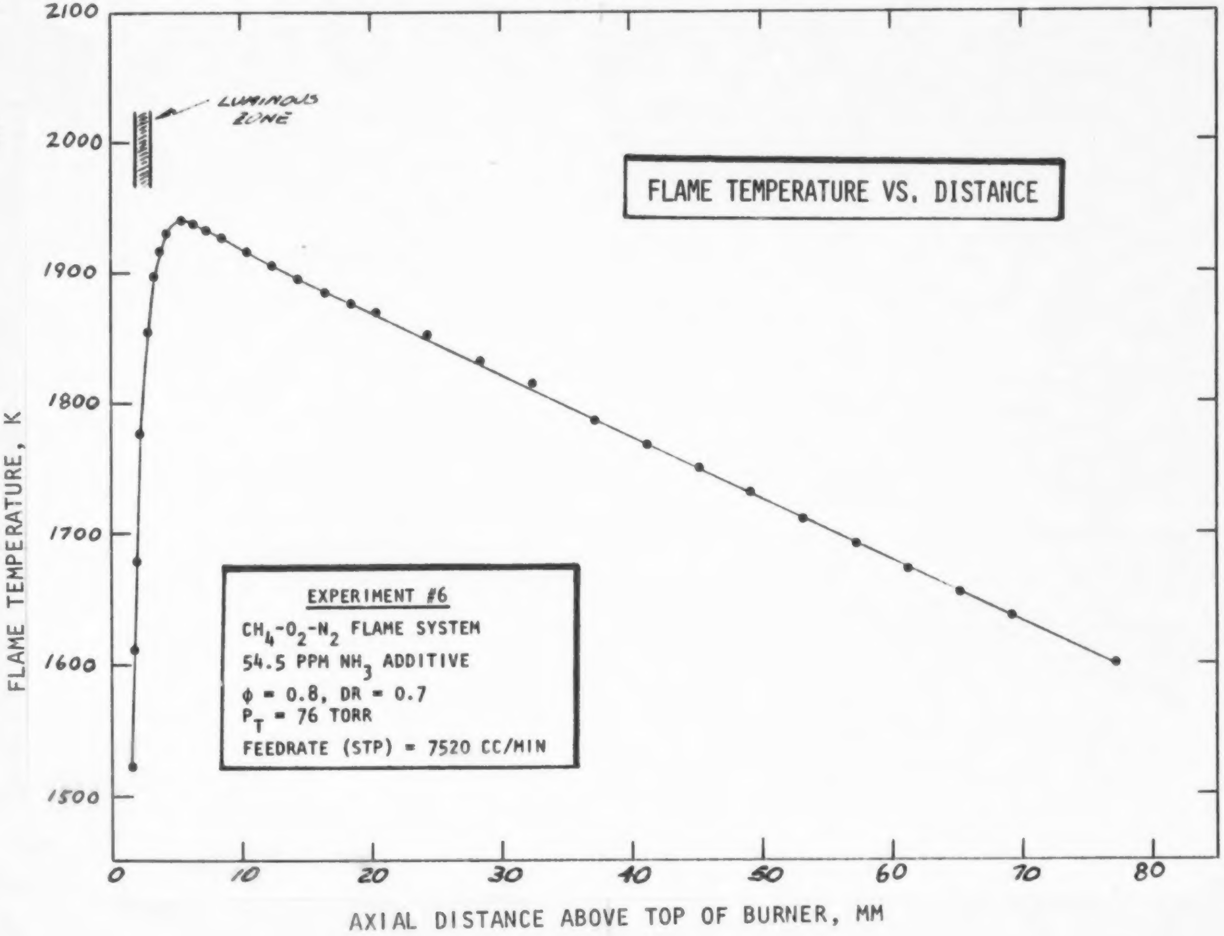

Figure 2-46. Experiment 6 - Temperature Profile

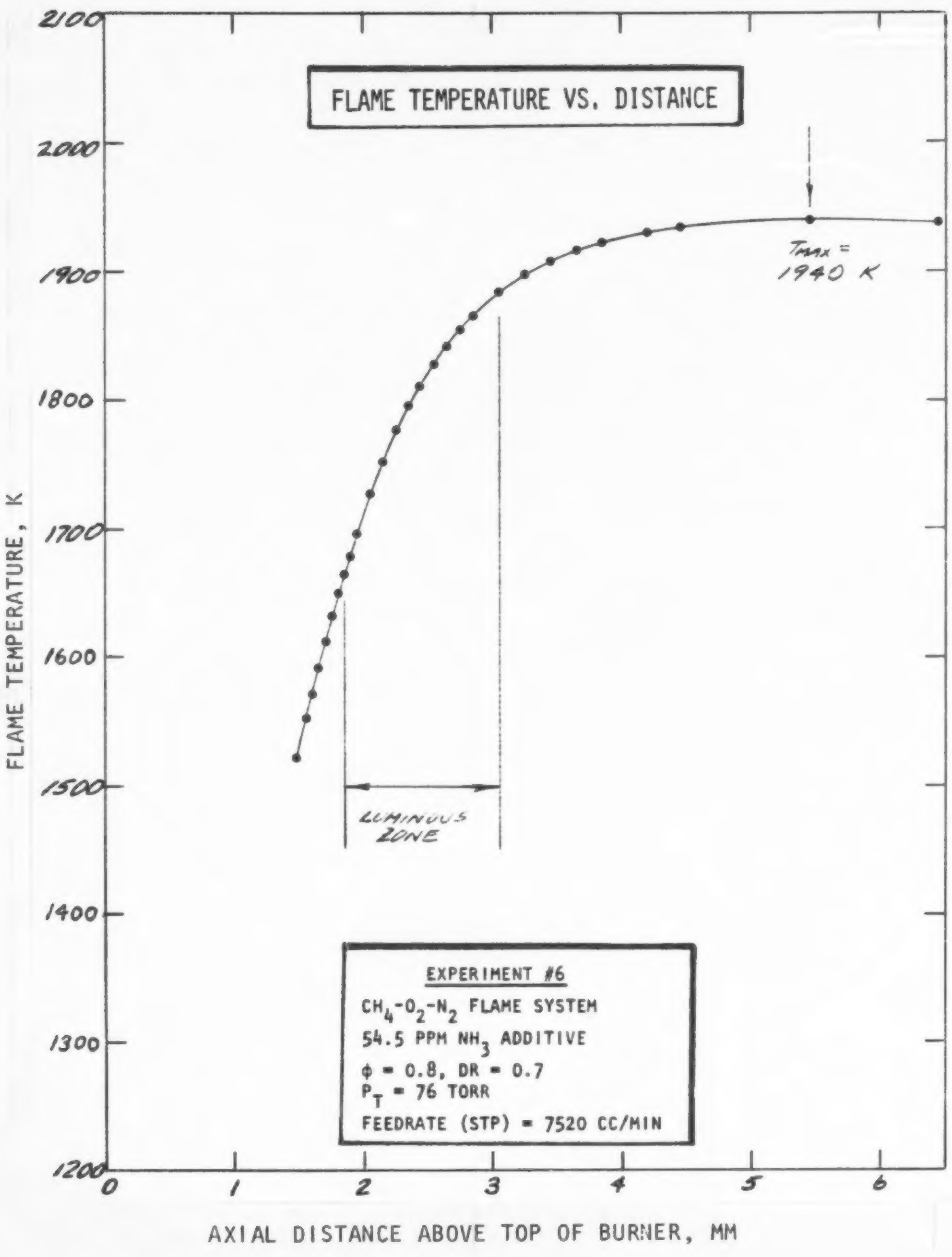

Figure 2-47. Experiment 6 - Temperature Profile

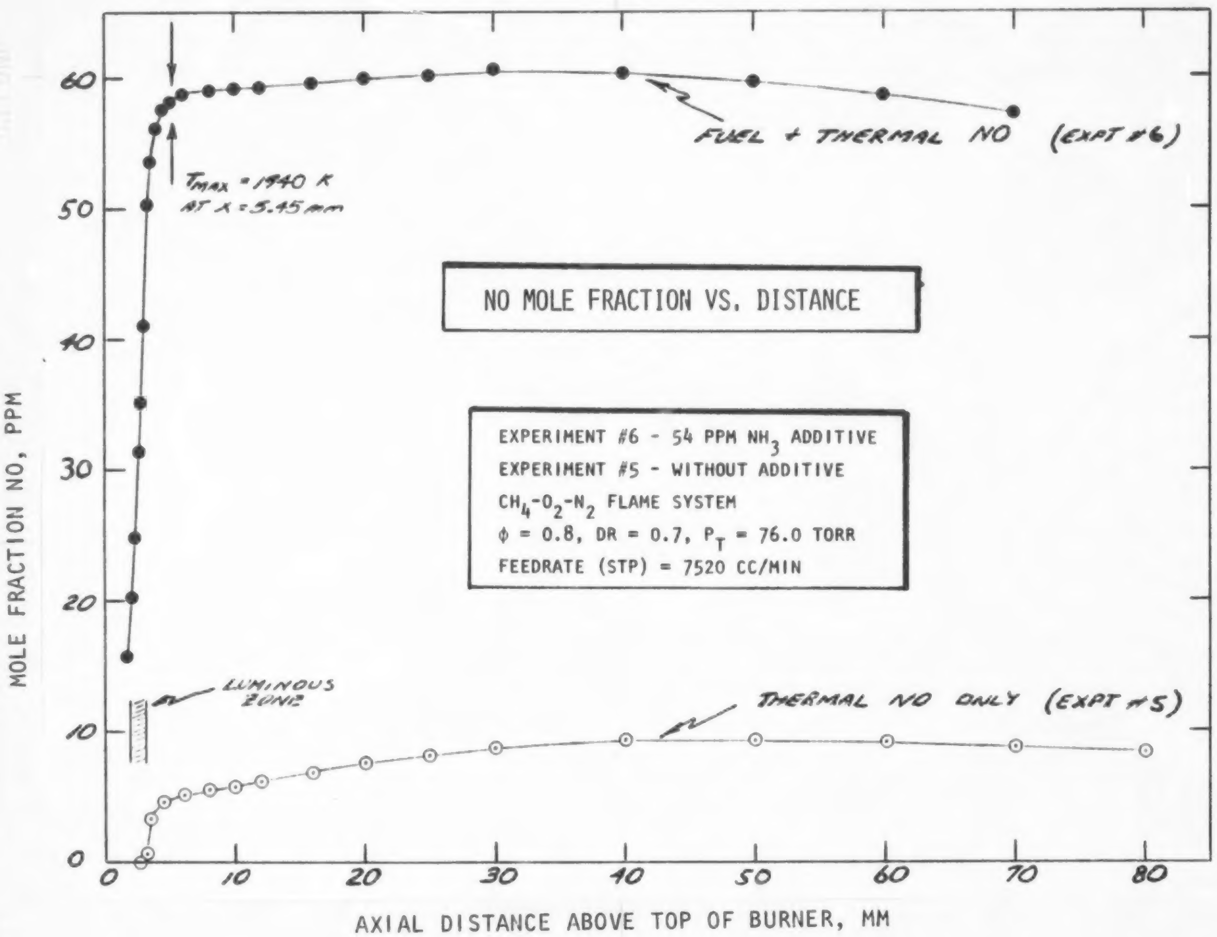

Figure 2-48. Comparison of NO Mole Fraction Profiles from Experiments 5 and 6

USE SPECIAL DROPOUT BLUE PENCIL ONLY TO INDICATE CORRECTIONS

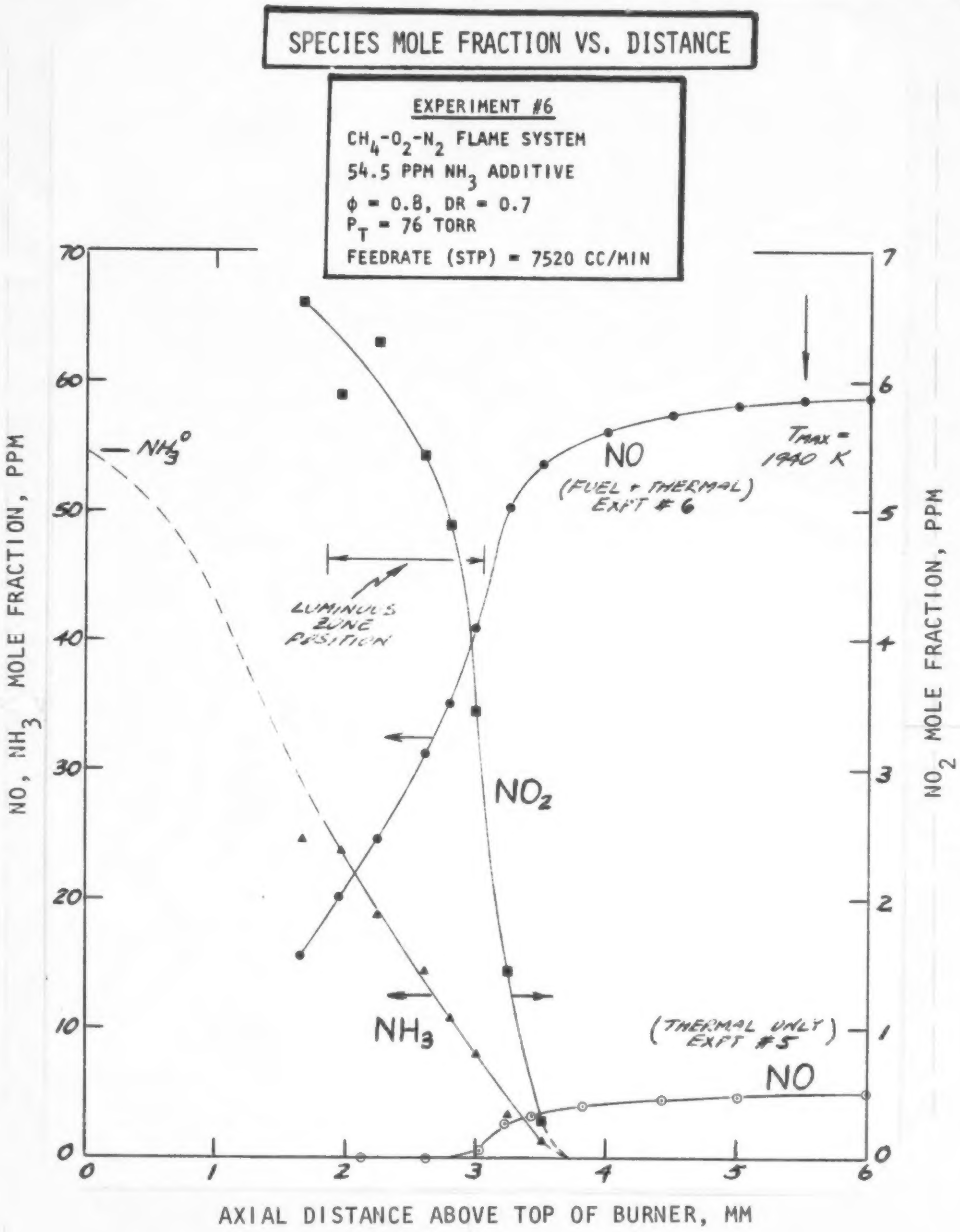

Figure 2-49. Experiment 6 - Species Mole Fraction Profiles

USE SPECIAL DROPOUT E PENCIL
ONLY TO INDICATE ONS
CLASSIFICATION
PAGE

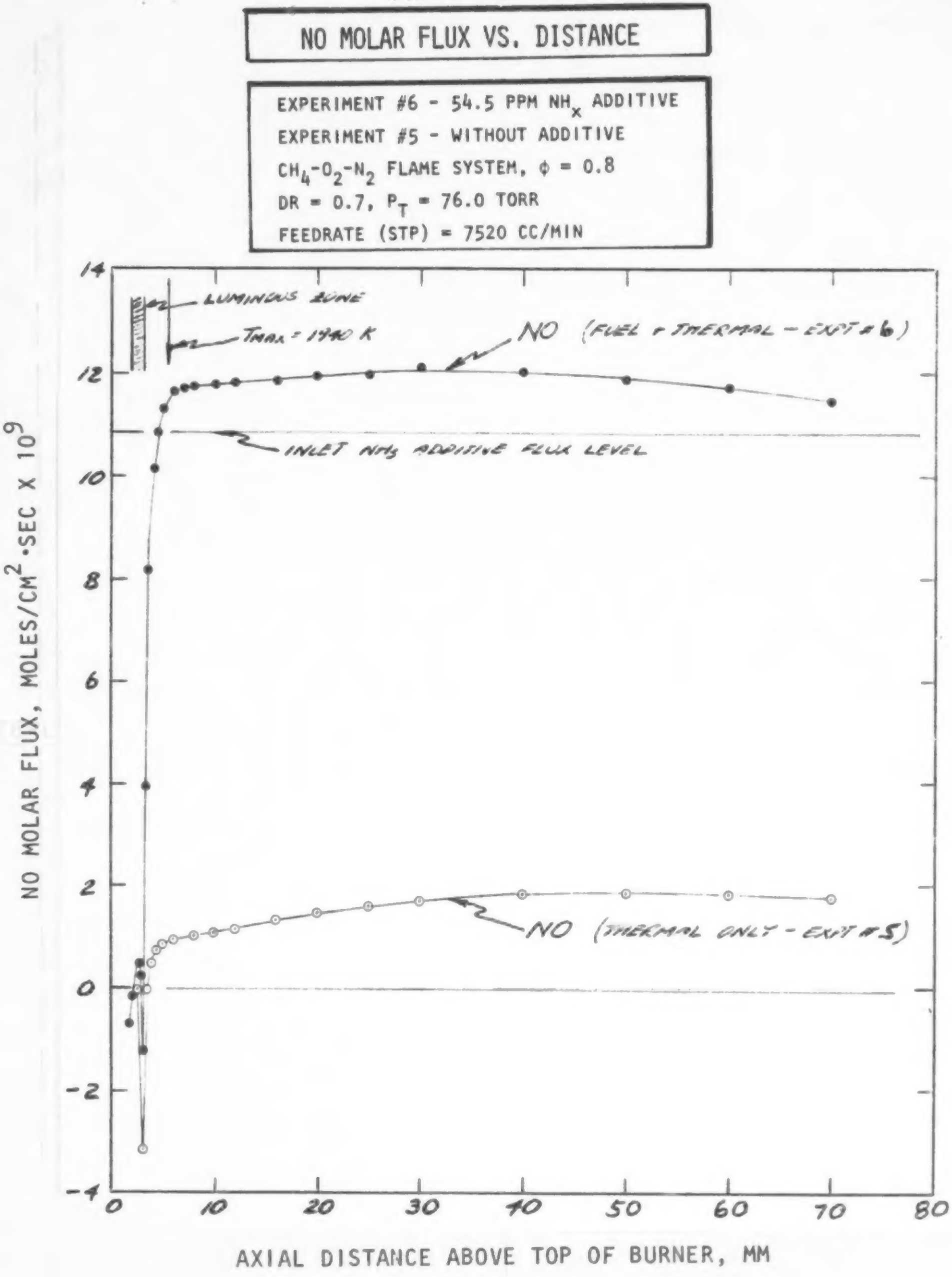

Figure 2-50. Comparison of NO Flux Profiles from Experiments 5 and 6

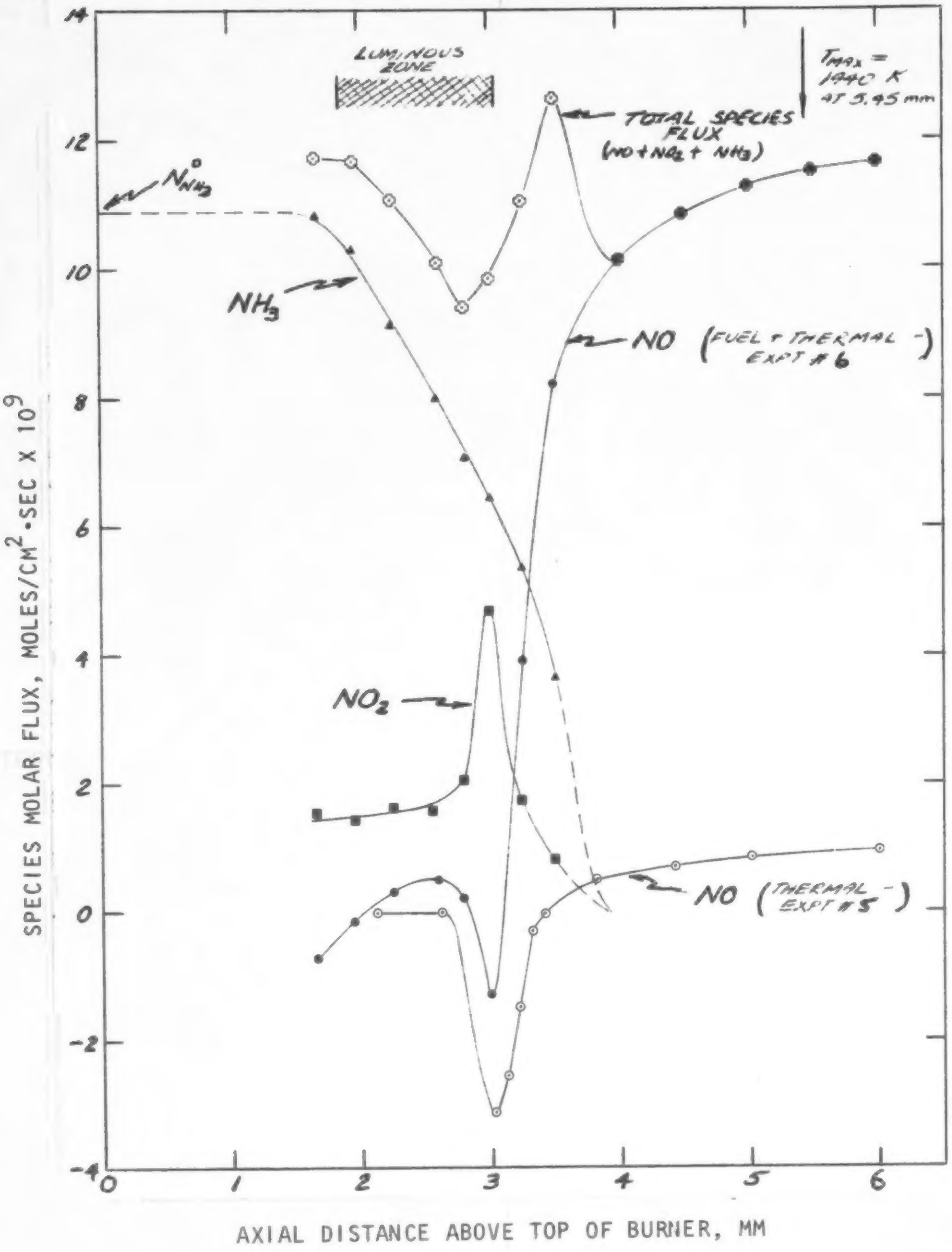

Figure 2-51. Comparison of Species Flux Profiles from Experiments 5 and 6

Following the same computational technique described previously, the mole fraction and molar flux profiles were calculated and are shown in Fig. 2-52 and 2-53 for CH_4, O_2, H_2, CO, and CO_2.

72-52
72-53

The mole fractions of O_2 and CH_4 in an unburned sample of reactants are plotted at the left side of Fig. 2-52, while the metered concentrations are indicated at X = 0 by dotted lines. The CH_4 values agree fairly well, while the measured O_2 concentration is about 8% higher than the metered value.

72-52

The predicted equilibrium concentrations of CO and CO_2 at 1953 K are 0.12 and 9.8%, respectively, which is in good agreement with the measured values at 7.0 mm of 0.25 and 9.5% (Fig. 2-52). The measured O_2 concentration at this location is 6.2% compared to the predicted value of 4.8%, but this is not unreasonable considering the measured inlet O_2 concentration. The H_2 mole fraction profile again is seen to be relatively flat, but the measured concentration of 0.70% at 7.0 mm is considerably higher than the calculated equilibrium value of 0.055%.

72-52

It can be seen from Fig. 2-53 that most of the CH_4 consumption and about one-half of the O_2 consumption occurs in the luminous zone. Considerable H_2 forms near the top of the luminous zone and then reacts just above this region where the CO is forming. The CO oxidation step again appears to be the slowest reaction involving the major species.

72-53

Conclusions From Fuel-Lean CH_4-O_2-N_2 Flames

It was found that less thermal (prompt) NO forms in fuel-lean combustion than in fuel-rich combustion. The fuel fragments oxidize more rapidly and are not as available to react with N_2 to form the CN species that are apparently precursors to prompt NO. As expected, added NH_3 is converted almost completely to NO under these conditions.

72-51

Comparing the results in Fig. 2-51 with those in Fig. 58 of Ref. 1, it can be seen that when small amounts of NH_3 are added to this flame there is not a point in the luminous zone where most of the fuel nitrogen is "missing" (as was the case with 2500 ppm NH_3 addition).

USE SPECIAL DROPOUT BLUE PENCIL
ONLY TO INDICATE CORRECTIONS
CLASSIFICATION
PAGE
STARTING LINE

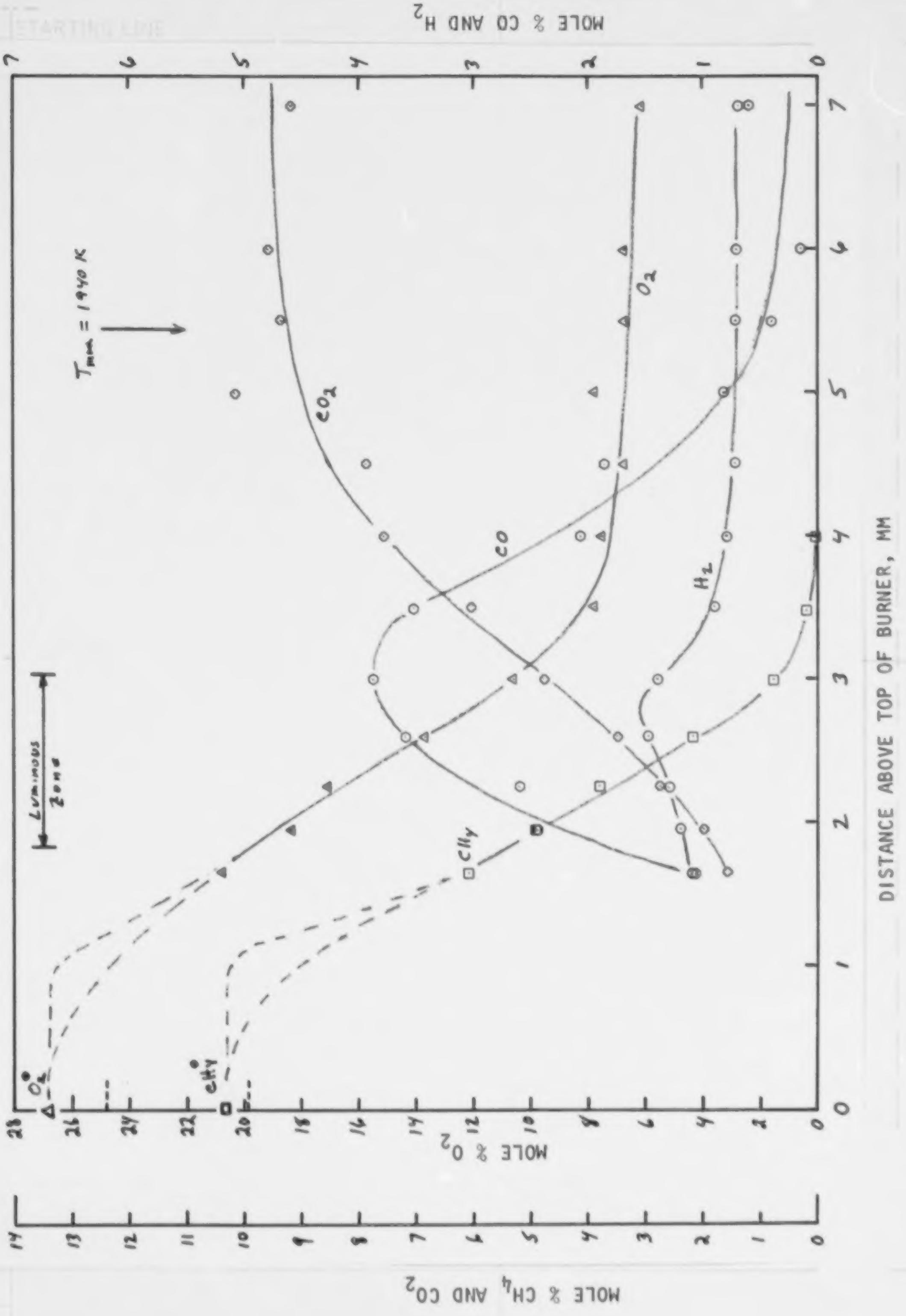

Figure 2-52. Mole Fraction Profiles of Major Species from Experiment 6 (φ= 0.8)

TYPIST 179

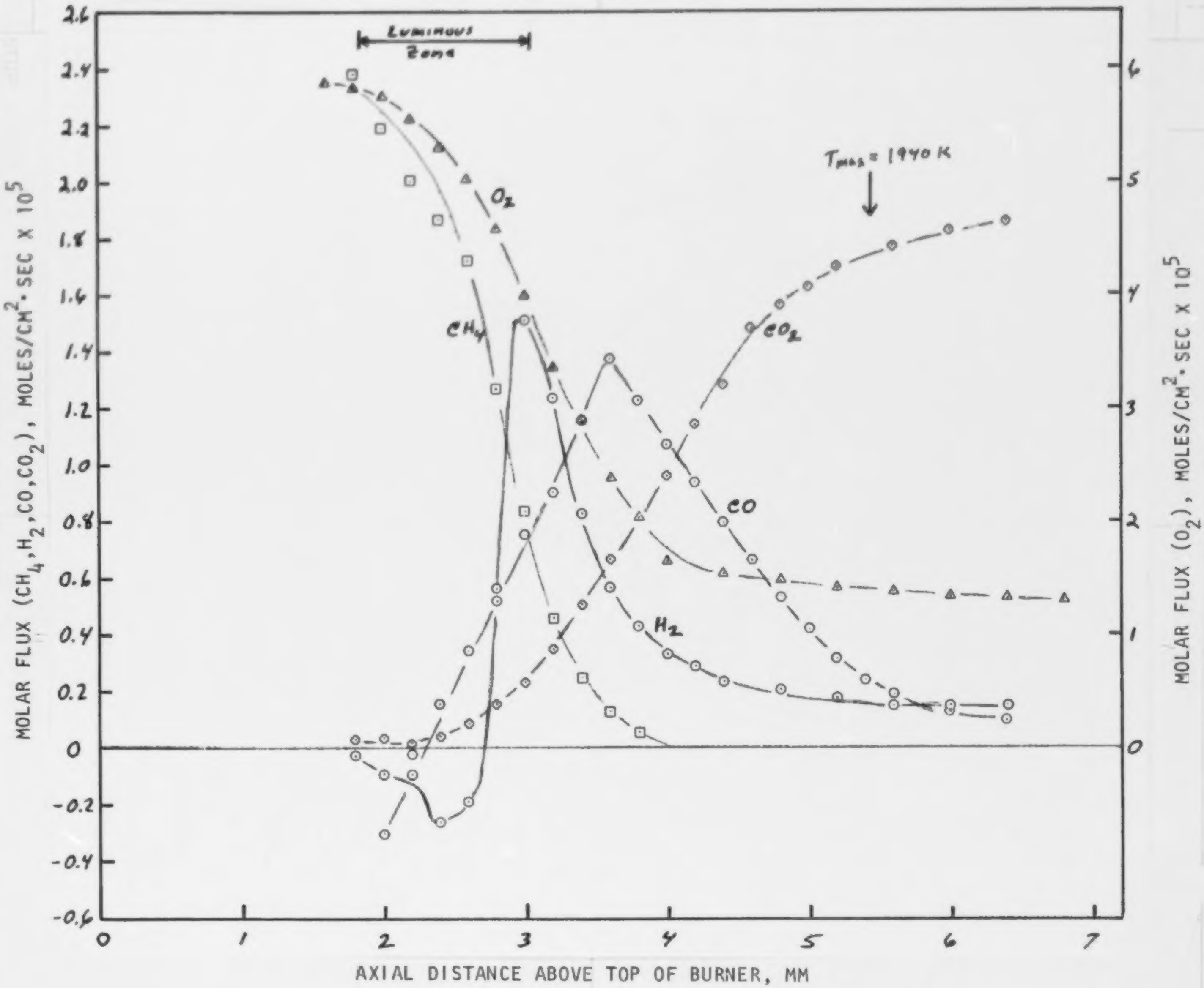

Figure 2-53. Molar Flux Plots of Major Species from Experiment 6

SIMULATED LOW BTU FUEL COMBUSTION (H_2-CO-O_2-Ar)

There is considerable interest in burning low Btu gas, which can be obtained from coal gasification processes, in commercial powerplants. However, these synthetic gases may contain trace quantities of fuel nitrogen species, such as NH_3, which can be converted to NO_x during combustion. Preliminary calculations reported in the literature (Ref. 29 through 31) have shown that proper combustion design can contribute significantly to reduction of NO_x emissions from low Btu gas systems and that staging of the combustion process has the potential for reducing NO_x emissions by a factor of 3 or 4. Fundamental kinetic data on the conversion of fuel-nitrogen species in a low Btu gas system, particularly under fuel-rich conditions, would be very useful in developing combustion models for determining optimum conditions for reducing NO_x emissions from low Btu gas power generation systems. To employ a low-pressure, flat-flame burner system to collect such information, the data should be obtained at flame temperatures which correspond approximately to those measured in real combustor configurations when using low Btu gas derived from a typical coal conversion process.

The basis for the experimental burner conditions subsequently chosen for the present study came from the work by Tyson (Ref. 30), who developed a kinetic model for NO_x emissions in a low Btu gas combustor, validated the model by comparison with experimental data, and applied this information to idealized combustor configurations for two representative combined cycle systems. In one

---

29. Martin, G.B., "NO_x Considerations in Alternate Fuel Combustion," presented at EPA Symposium; Environmental Aspects of Fuel Conversion Processes, Hollywood, Florida, 14-18 December 1975.
30. Tyson, T. J., "Chemical and Physical Limitations on Low BTU Gas Combustor NO_x Emissions," presented at EPA Combustion Research Branch Contractors Meeting, MIT, Cambridge, Mass., August 1976.
31. Heap, M. P., T. J. Tyson, J. E. Cichanowicz, R. Gershman, E. J. Kau, G. B. Martin, and W. S. Lanier, "Environmental Aspects of Low BTU Gas Combustion," presented at the 16th Symposium (International) on Combustion, MIT, Cambridge, Mass., August 1976.

case, for an advanced technology, high-temperature gas turbine with a waste-heat boiler, the optimum design for an adiabatic gas generator was found to be a rich ($1.33 < \phi < 1.45$) primary reactor section (200 msec residence time) followed by a gradual mixing of the primary products into the dilution air stream. Using the staged system as opposed to an unstaged system resulted in calculated NO_x emissions reduced by a factor of 4.

The fuel composition employed by Tyson in his gas turbine combustor calculations was that of a typical air-blown Lurgi gas and contained 10.1% H_2O, 19.6% H_2, 13.3% CO, 13.3 CO_2, 5.5% CH_4, 37.6% N_2, and 0.4% NH_3. This value for the NH_3 mole fraction was arrived at by assuming a hot-gas removal process for H_2S (1088 K), and was based on the high-temperature cleanup data reported by Robson (Ref. 32). The fuel gas inlet temperature and the air inlet temperature were 1090 and 810 K, respectively, while the total pressure was maintained at 10 atm.

The H_2/CO ratio chosen in the present work was set at 1.4 to simulate the H_2/CO ratio found in the low Btu gas derived from the typical air-blown Lurgi process. Argon was selected as the diluent to preclude the possibility of thermal NO_x formation and to permit the CO to be measured mass spectrometrically. From Tyson's conclusions, a fuel-rich condition appeared to be the most interesting for these studies, and an equivalence ratio (ϕ) of 1.4 was chosen.

A number of adiabatic flame temperature calculations were carried out to aid in selecting the diluent ratio to be used in these experiments (i.e., the amount of argon to be added to the H_2-CO-O_2 mixture). These calculated temperatures are plotted in Fig. 2-54. Most of the calculations were made for a H_2-CO-O_2-NH_3 flame at 0.1 atmosphere with $H_2/CO = 1.43$ and 4000 ppm NH_3 in the simulated fuel. Adiabatic flame temperature curves for CH_4-O_2-Ar and CH_4-air at 0.1 atm are shown for comparison.

---

32. Robsen, F. L., and A. J. Giramonti, "The Environmental Impact of Coal-Based Advanced Power Systems," Symposium Proceedings; Environmental Aspects of Fuel Conversion Technology, EPA-650/2-74-118, October 1974, pp. 237-257.

USE SPECIAL DROPOUT BLUE PENCIL ONLY TO INDICATE CORRECTIONS
CLASSIFICATION
PAGE
STARTING LINE

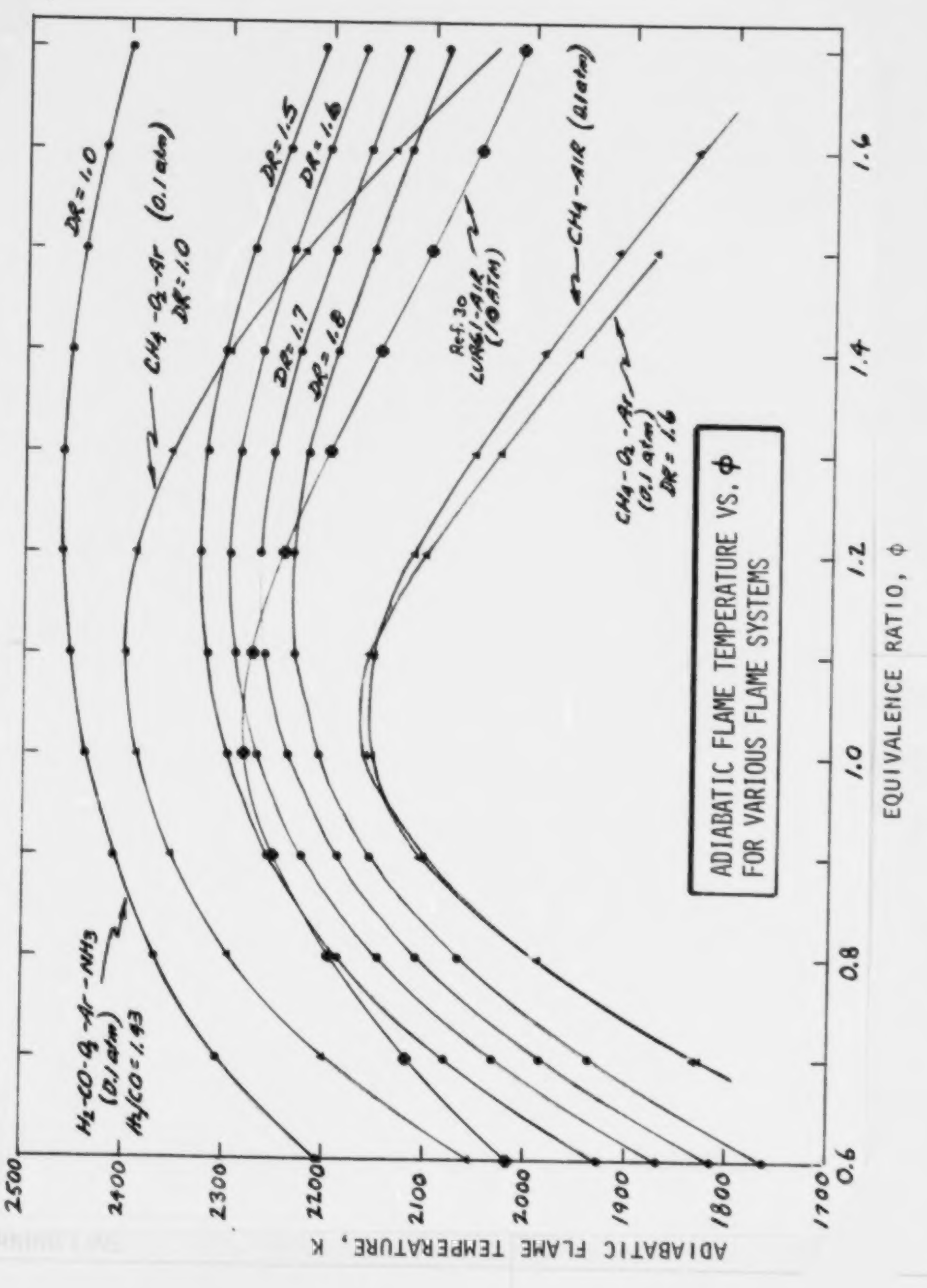

Figure 2-54. Adiabatic Flame Temperatures vs φ

FINISH LINE
STOP
DOCUMENT NUMBER
PAGE NUMBER
CLASSIFICATION
TYPIST

One of the objectives of the current experimental series is to provide fundamental kinetic data on the conversion of fuel-nitrogen species in a low Btu gas system, particularly under fuel-rich conditions. The data collected in the low pressure flat-flame burner system should be obtained at flame temperatures which correspond approximately to those measured in real combustor configurations using low Btu gas derived from a typical coal conversion process. The Lurgi-air adiabatic flame temperature calculated as a function of ϕ by Tyson (Ref. 30) under the conditions mentioned above were replotted in Fig. 2-54.

Based on Tyson's calculations, it would appear reasonable to select the fuel-rich condition to be used in the present study (experiments No. 8 through 13) as $\phi=1.4$. It can be seen from Fig. 2-54 that at $\phi=1.4$ the adiabatic flame temperature of the H_2-CO-O_2-Ar-NH_3 system (0.1 atm) and that of the Lurgi-air system (10 atm) would be nearly the same (2150 K) at DR $\cong$ 1.9. Assuming that the H_2O, CO_2, and N_2 present in the Lurgi gas act as a diluent, the effective diluent ratio for the Lurgi-air system at $\phi=1.4$ was calculated to be 1.8. The flame temperature for the CO/H_2 mixture is higher than for CH_4 (Fig. 2-54). This large amount of argon must be added to replace both the nitrogen in air and the inerts in a real low Btu fuel.

It was decided that the diluent ratio would initially be set at 1.8 to match approximately the adiabatic flame temperature that would be obtained from a Lurgi-air combustion system at $\phi=1.4$. However, it should be pointed out the maximum temperatures obtained will be lower than those indicated in Fig. 2-54 due to heat transfer losses from the flat-flame burner system. The maximum flame temperature of 2100 K has been an upper temperature limit on all work carried out in this apparatus and no attempt was made to go above that temperature in these experiments.

Preliminary Observations

Preliminary screening experiments with the H_2-CO-O_2-Ar flame system, outlined in Table 2-8, revealed that this fuel burns much differently in a low-pressure burner than does methane. It was found that to position the luminous zone above the

TABLE 2-8. PRELIMINARY OBSERVATIONS OF H_2-CO-O_2-Ar FLAME (H_2/CO=1.43)

- Fuel-Lean Flame, ϕ=0.8

  DR=1.8 and 1.9, $\overline{F}$=7500 cc/min, P=76 torr:

  Luminous zone (LZ) is a faint thin blue band just above top of burner screen, and less intense than for a comparable CH_4-O_2-Ar flame. Entire visible flame region is diffuse (milky blue color) extending almost 100 mm downstream of burner. At DR=1.9, maximum thermocouple wire temperature, T_{max}, is about 1700 K (T_a=2025 K).* Conditions acceptable for detailed probing.

  DR=1.9, $\overline{F}$=8750 cc/min, P=76 torr:

  LZ moves slightly further from top of burner and T_{max} increases by about 40 K.

  DR=1.9, $\overline{F}$=7500 cc/min, P=50 torr:

  LZ thickens and moves relatively far above the burner (10.6 to 17.0 mm) and begins to flutter. Condition not acceptable for probing.

- Fuel-Rich Flame, ϕ=1.4

  DR=1.8 and 1.9, $\overline{F}$=7500 and 8750 cc/min, P=76 torr:

  Bottom of LZ impinges top of burner screen causing it to glow with faint reddish hue. At 1.9 and 7500, $T_{max} \simeq 1630$ K (T_a=2155 K). Increasing flowrate has little effect on LZ position or T_{max}. Condition not acceptable for probing.

  DR=1.9, $\overline{F}$=8750 cc/min, P=50 torr:

  LZ becomes more distinct and moves away from burner to a position 3.4 to 7.6 mm above burner top. $T_{max} \simeq 1730$ K. 3-mil thermocouple wire breaks due to melting. Condition appears acceptable for detailed probing. Adding 150 cc/min CH_4 causes flame to dim considerably and LZ moves very close to top of burner screen.

  DR=1.5, $\overline{F}$=7500 cc/min, P=50 torr:

  LZ moves very close to burner screen causing it to glow faint red. Not acceptable for detailed probing.

---

*T_a is calculated adiabatic flame temperature.

burner so that suitable detailed probing measurements could be made at $\phi=1.4$, the total system pressure had to be reduced to 50 torr, while the total inlet gas feed rate was increased 17% over that employed in the previous CH_4 flame studies to 8750 cc/mm (STP).

In these preliminary observations, a very unexpected phenomenon was discovered to occur with rich H_2-CO-O_2-Ar flames. The 3-mil coated Pt-Pt/Rh thermocouples used in all of the methane flames were found to burn out quite rapidly. Surprisingly, the Pt/Rh half of the thermocouple always glowed much brighter than the Pt half before burnout. There is no obvious explanation for this effect since the theoretical products from a rich CO-H_2 flame are essentially the same as from a rich CH_4 flame.

This temperature measurement problem and the methods that were tried to solve it are described in Appendix C for the interested reader. Although considerable effort was expended on this problem, no simple solution was found.

Since all four of the detailed probing experiments were conducted under the same nominal conditions, except for additive type or concentration, one temperature profile was measured (experiment No. 8) and used for experiments No. 8 through No. 11. This temperature profile was measured as rapidly as possible to avoid burnout of the Pt/Pt-Rh thermocouple.

Preliminary Probing Experiment No. 7 (H_2-CO-O_2-Ar-NH_3)

The preliminary experiments described above provided the basis for choosing the conditions ultimately used in experiment No. 7: 4000 ppm NH_3 (Lurgi fuel basis) added to a H_2-CO-O_2-Ar flame at a total feedrate of 8750 cc/min (STP) and a total system pressure of 50.0 torr (Table 2-6). As ϕ was varied from 0.8 to 1.8 at a diluent ratio of 1.9, the maximum flame temperature was to be measured and the conversion of NH_3 to NO (and temperature) determined at a downstream location of 60 mm. At $\phi=1.4$, the diluent ratio was to be reduced from 1.9 to find the optimum DR for subsequent detailed probings.

USE SPECIAL DROPOUT BLUE PENCIL ONLY TO INDICATE CORRECTIONS

It was planned that experiment No. 7 be carried out in two separate parts, temperature probing measurements (T_{max} and T at $\Delta X=60$ mm) and NO concentration measurements ($\Delta X=60$ mm). The results obtained during the temperature measurements are outlined on Table 2-9. It can be seen from the table that the first indication of a thermocouple measurement problem was apparent at $\phi=1.0$. By $\phi=1.4$, the Pt/Rh side of the 3-mil Al_2O_3-coated wire was glowing considerably brighter than the pure Pt side, and eventually the 3-mil Pt/Rh side of the thermocouple melted. Three thermocouples failed during the initial low Btu gas experiments and each failed in the manner just described.

Detailed Probing Experiment No. 8 (H_2-CO-O_2-Ar-NH_3)

The nominal conditions for this first detailed probing of a simulated low Btu fuel flame were the same as in experiment No. 7 (Table 2-6). NH_3 was added to the flame in experiment No. 8 at 2740 ppm on a total feed basis, which is equivalent to 4200 ppm on a Lurgi fuel basis.

Prior to commencing the detailed probing for the N-species, a cold-flow experiment with premixed unburned combustibles was run to check the inlet NH_3 concentration. The calculated inlet NH_3 mole fraction based on flow calibrations was 2720 ppm. This compares favorably with the experimental value of 2740 ppm measured using the chemiluminescent analyzer (stainless-steel converter at 1070 K with the O_2 leak). The latter value corresponds to an inlet NH_3 additive flux of 6.36×10^{-7} moles/cm^2·sec.

The temperature profile along the centerline of the burner (corrected for radiation) is shown on two different distance scales in Fig. 2-55 and 2-56. The luminous zone extended between 3.3 and 8.2 mm above the top of the burner. The maximum flame temperature of 1857 K ($T_{adiabatic}=2144$ K) was at 12.9 mm. The detailed probing was performed with a 3-mil Al_2O_3-coated Pt-Pt/10% Rh thermocouple. It was pointed out that this type of thermocouple could not withstand the high-temperature reducing conditions encountered in experiment No. 8 without considerable deterioration of the Al_2O_3 coating and subsequent melting of the Pt-Rh alloy. In experiment No. 7 at fuel-rich conditions, the deterioration occurred rapidly in the region of the luminous zone and the time required for melting the

TABLE 2-9. RESULTS OF TEMPERATURE MEASUREMENTS IN EXPERIMENT NO. 7 WITH H_2-CO-O_2-Ar FLAME (DR=1.9, P=50 torr, $\overline{F}$=8750 cc/min, 4000 ppm NH_3 - Fuel Basis and H_2/CO=1.43)

Equivalence Ratio, ϕ	Luminous Zone Position Above Top of Burner, mm	Elapsed Time of Thermocouple Exposure to Hot Combustion Gases, minutes	Maximum Thermocouple Wire Temperature, K	Experimental Observation
0.8	18.8 to 24.0	25	1743	Flame is flickering and near blowoff limit
0.9	13.9 to 18.5	60	1748	Slight decrease in flame flicker
1.0	7.35 to 12.90	85	(a) 1769 (b) 1738 (c)<1643	Flame is more stable. Triplicate thermocouple readings to determine T_{max} are inconsistent, indicating a possible thermocouple measurement problem.
1.2	4.15 to 9.50	130	(a) 1679 (b) 1669	Flame is stable and LZ flat. Pt/Rh alloy side of 3-mil thermocouple wire appears to be much hotter than Pt side. Thermocouple junction appears cooler than Pt/Rh alloy side.
1.4	3.15 to 7.30	165	-	Flame is stable. Pt/Rh side of thermocouple is glowing much hotter than Pt side. Pt/Rh 3-mil wire then melts.
1.6	2.80 to 6.85		-	
1.8	2.55 to 6.50		-	LZ is flat and steady. No indication of burner screen heating up or reddening.

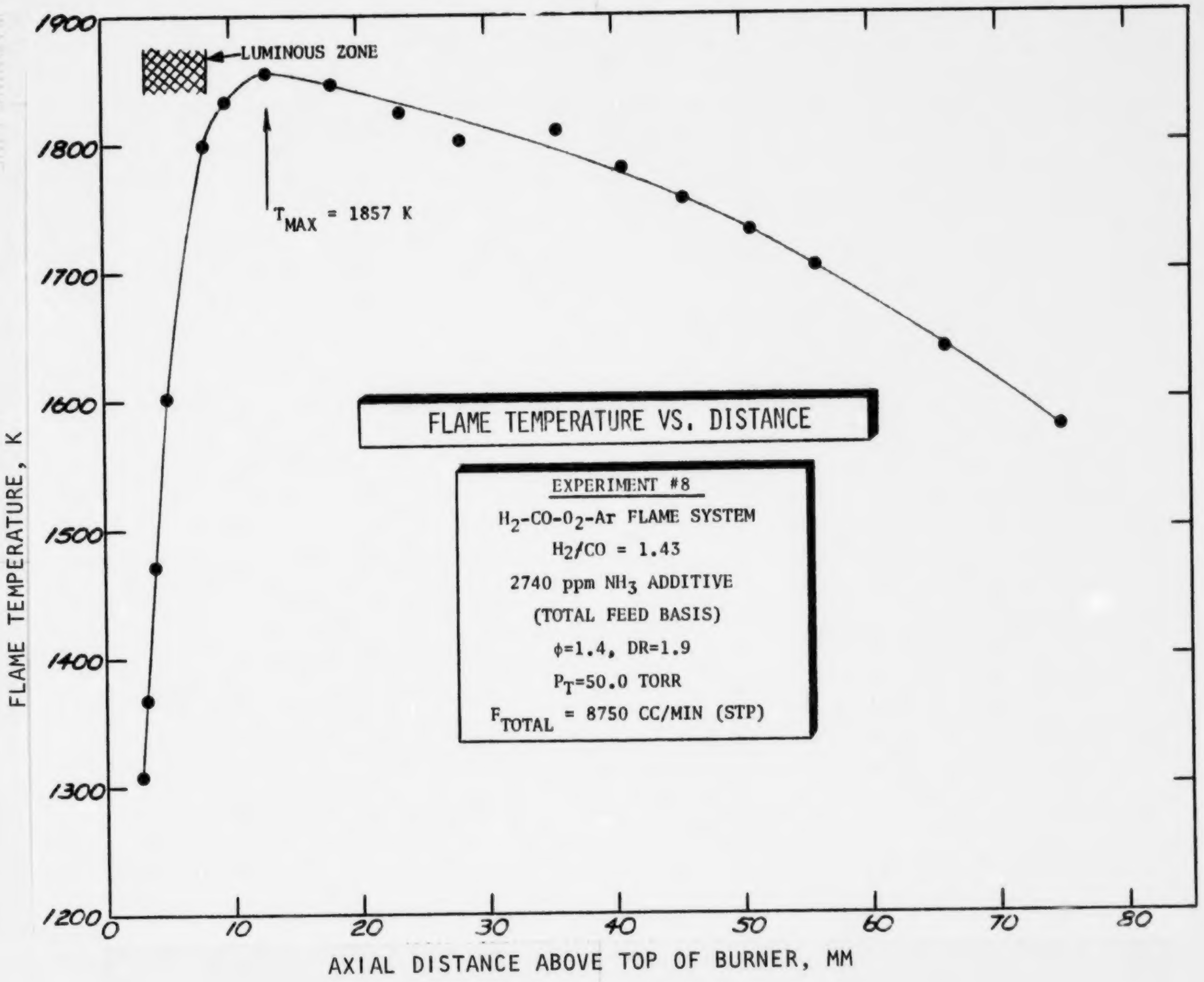

Figure 2-55. Experiment 8 - Temperature Profile

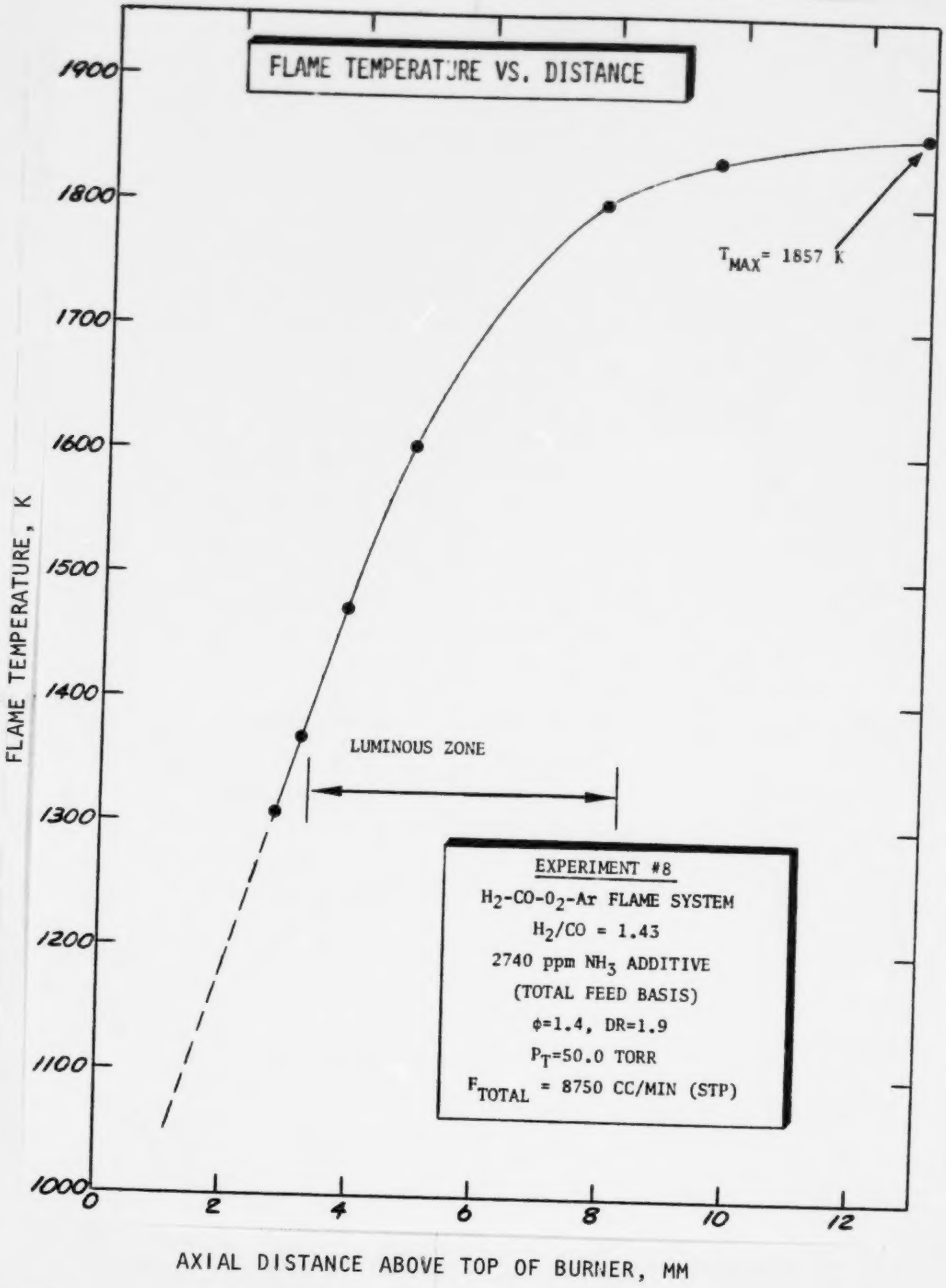

Figure 2-56. Experiment 8 - Temperature Profile

thermocouple was approximately 90 minutes. Because a suitably coated thermocouple which would be capable of withstanding the high-temperature reducing atmospheres encountered in these low Btu gases was not available, it was decided that a reasonably approximate temperature profile could be obtained with the coated Pt-Pt/10% Rh thermocouple provided that the thermocouple probe was passed fairly quickly through the luminous region.

The seven data points between 75.0 mm and 35.6 mm in Fig. 2-55 were obtained first over a period of 15 minutes. Both sides of the thermocouple junction continued to glow at the same intensity and there was no indication from the recorded output that catalytic reactions were occurring. The ten data points between 2.8 and 28.1 mm were then taken over a 5-minute period. It was observed that the Pt-Rh side of the thermocouple junction had begun to glow visibly brighter than the Pt side and the recorder output gave evidence of some catalytic reactivity of the thermocouple. At the conclusion of the detailed probing, the thermocouple probe was repositioned at 75.0 mm and the temperature recorded at this time was 19 K lower than the initial value. Although there is some scatter in the data between 20 and 40 mm, it would appear that the temperature profile obtained is a good estimate of the actual gas temperature profile. The conclusions drawn from this experiment do not appear to be critically dependent on the accuracy of the temperature measurement. If the measured profile is somewhat high, its net effect would be to place an upper limit on the N-species mole fraction and molar flux profiles.

F 2-55

The mole fraction profiles for NH_3 and NO are shown in Fig. 2-57 and 2-58. There was no measurable NO_2 or HCN within the detection limits of the analytical system. The added NH_3 (2740 ppm total basis) decreased rapidly to zero just above the bottom of the luminous zone. The NO formed below and within the luminous zone and reached a maximum of 2240 ppm (81% yield) at 6.5 mm. The NO decreased rapidly just above the luminous zone, reaching a minimum at 17.5 mm (1070 ppm), and then gradually increased to 1460 ppm at 70 mm downstream. The latter corresponds to a net yield of 53% NO based on the initial NH_3 fed to the burner.

F 2-57
2-58

186

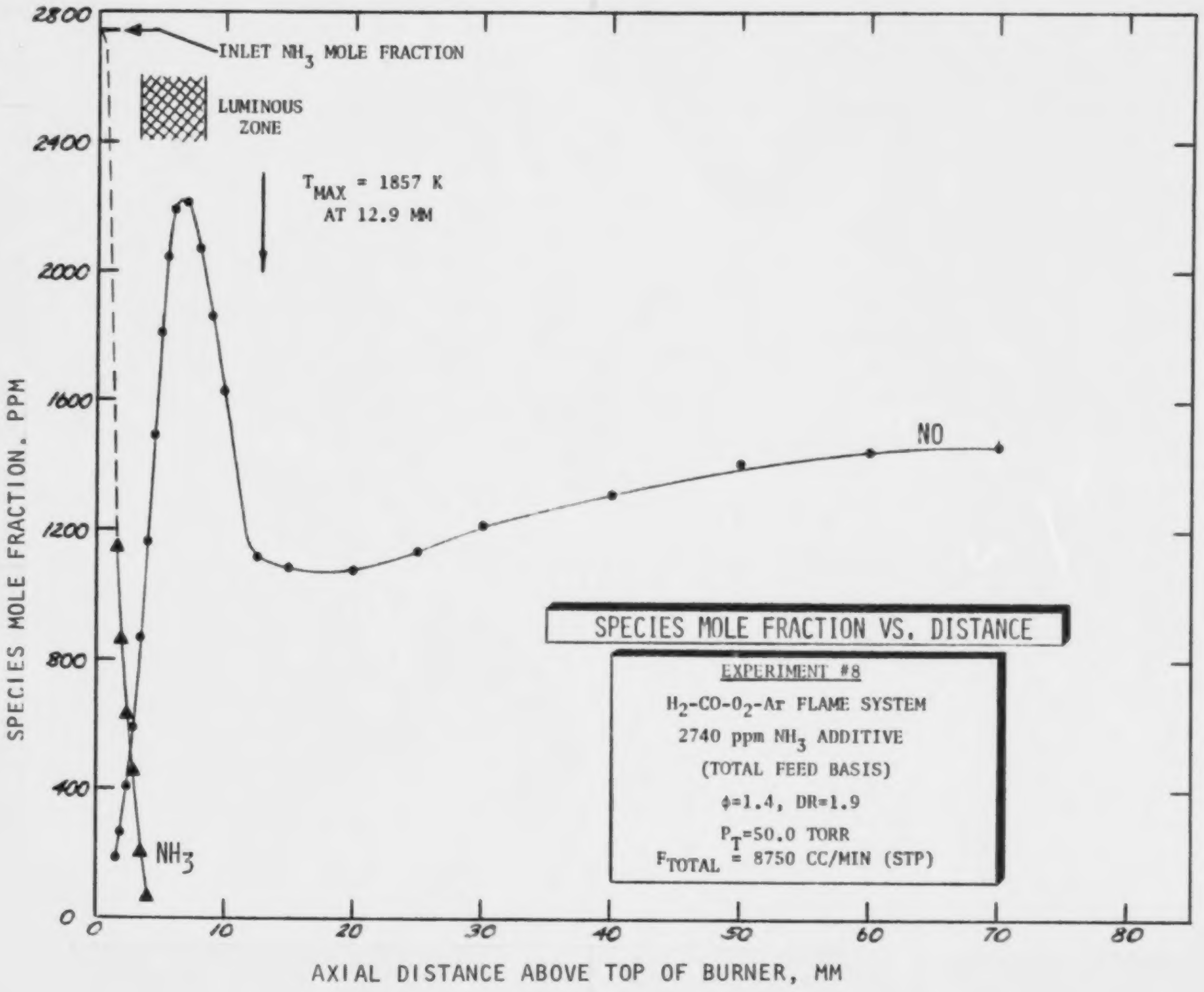

Figure 2-57. Experiment 8 - Species Mole Fraction Profiles

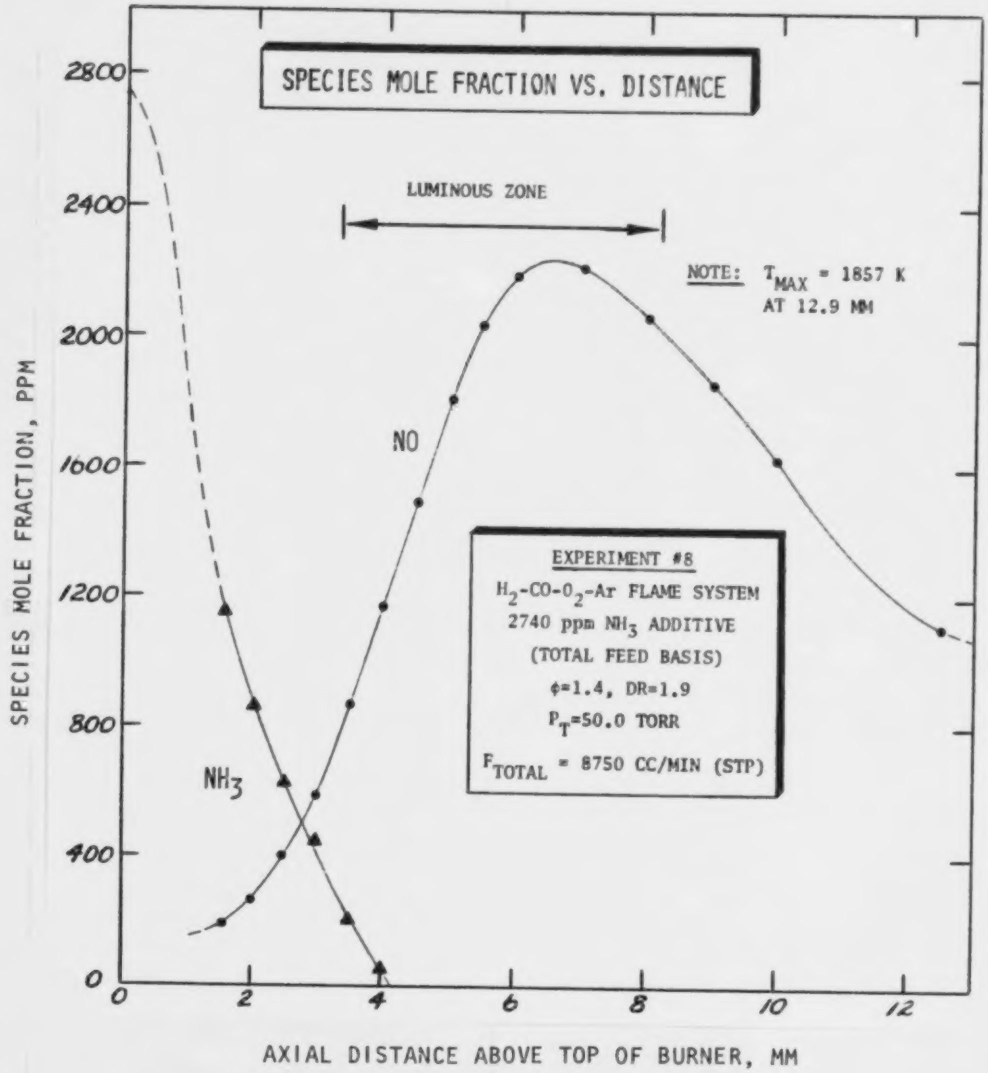

Figure 2-58. Experiment 8 - Species Mole Fraction Profiles

USE SPECIAL DROPOUT BLUE PENCIL
ONLY TO INDICATE CORRECTIONS
CLASSIFICATION
PAGE
STARTING LINE

Figure 2-59 and 2-60 depict the corresponding molar flux profiles for NH_3 and NO. The NH_3 flux curve decays in a manner very similar to the NH_3 mole fraction curve. All of the NH_3 appears to have reacted by just above the bottom of the luminous zone. The location of the maximum NH_3 decay rate corresponds approximately to the point of the initial NO formation. The maximum rate of NO formation is 1.58×10^{-6} moles/$cm^3 \cdot$sec and occurs at approximately the same point where the NH_3 flux becomes zero. The maximum NO flux of 4.84×10^{-7} moles/$cm^2 \cdot$sec (76% yield) occurs at a point roughly three-fourths of the distance into the luminous zone. Thereafter the NO is consumed, reaching a minimum near the maximum flame temperature location, and then gradually increases and levels off at 70 mm downstream. The flux at this latter location (3.10×10^{-6} moles/$cm^2 \cdot$sec) corresponds to a NO yield of 49%.

The most interesting feature of the N-species profiles can be found in Fig. 2-60 where the sum of the NH_3 and NO fluxes are plotted vs distance. Note that at 4.0 mm only 30% of the initial fuel-N is present in a form which can be measured by the chemiluminescent analyzer/converter system (NH_3, NO, NO_2 or HCN). Obviously there is an undetermined radical species (possibly NH_x) which forms in the flame as an intermediate, and subsequently can react further to yield either NO or N_2 (but forms mainly N_2 in the probe). At least one very long-lived intermediate must be involved because the NO flux continues to increase more than 40 mm above the burner and the NH_3 additive changes the visible color of the flame at even greater distances.

Profiles of major Species. A total of 14 gas samples for mass spectrometric analysis were taken during experiment No. 8 and delivered to West Coast Technical Services (WCTS). One sample contained the premixed unburned combustibles fed to the burner, while a second sample was that of a standard calibration gas mixture which has been used previously to check the WCTS analyses. In three previous analyses, the average reported composition of the standard calibration gas was: 2.78% CH_4, 4.12% O_2, 86.94% N_2 + CO, and 6.03% CO_2. For experiment No. 8, the WCTS analysis of the standard gas was 2.91% CH_4, 4.15% O_2, 86.90% N_2 + CO, and 5.98% CO_2. The agreement is very good, indicating that there had been no apparent change in the WCTS experimental or analytical procedures.

DOCUMENT NUMBER

197

PAGE NUMBER
CLASSIFICATION

194

USE SPECIAL DROPOUT BLUE PENCIL
ONLY TO INDICATE CORRECTIONS
CLASSIFICATION
PAGE
STARTING LINE

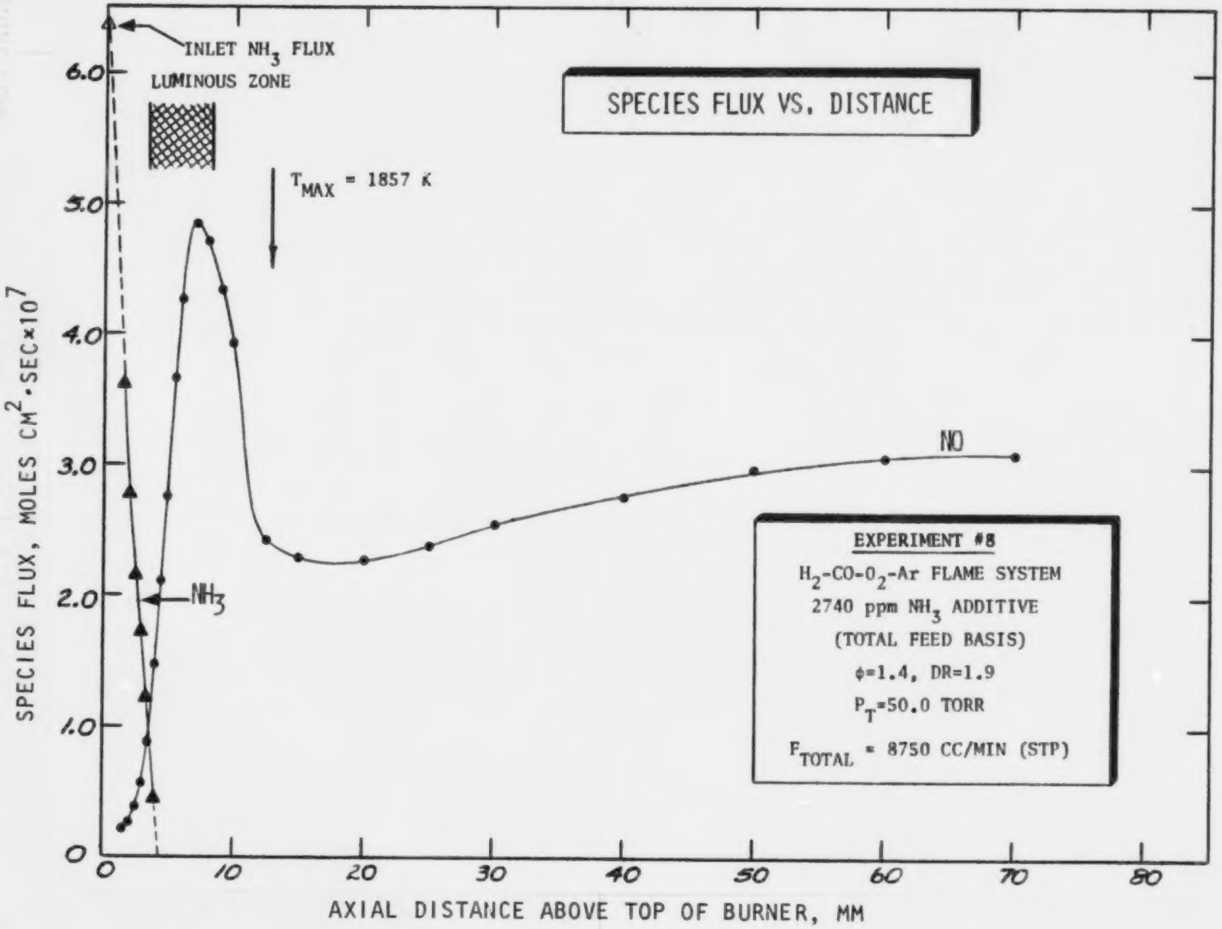

Figure 2-59. Experiment 8 - Species Flux Profiles

DOCUMENT NUMBER
PAGE NUMBER
CLASSIFICATION
TYPIST

USE SPECIAL DROPOUT BLUE PENCIL ONLY TO INDICATE CORRECTIONS

SPECIES FLUX VS. DISTANCE

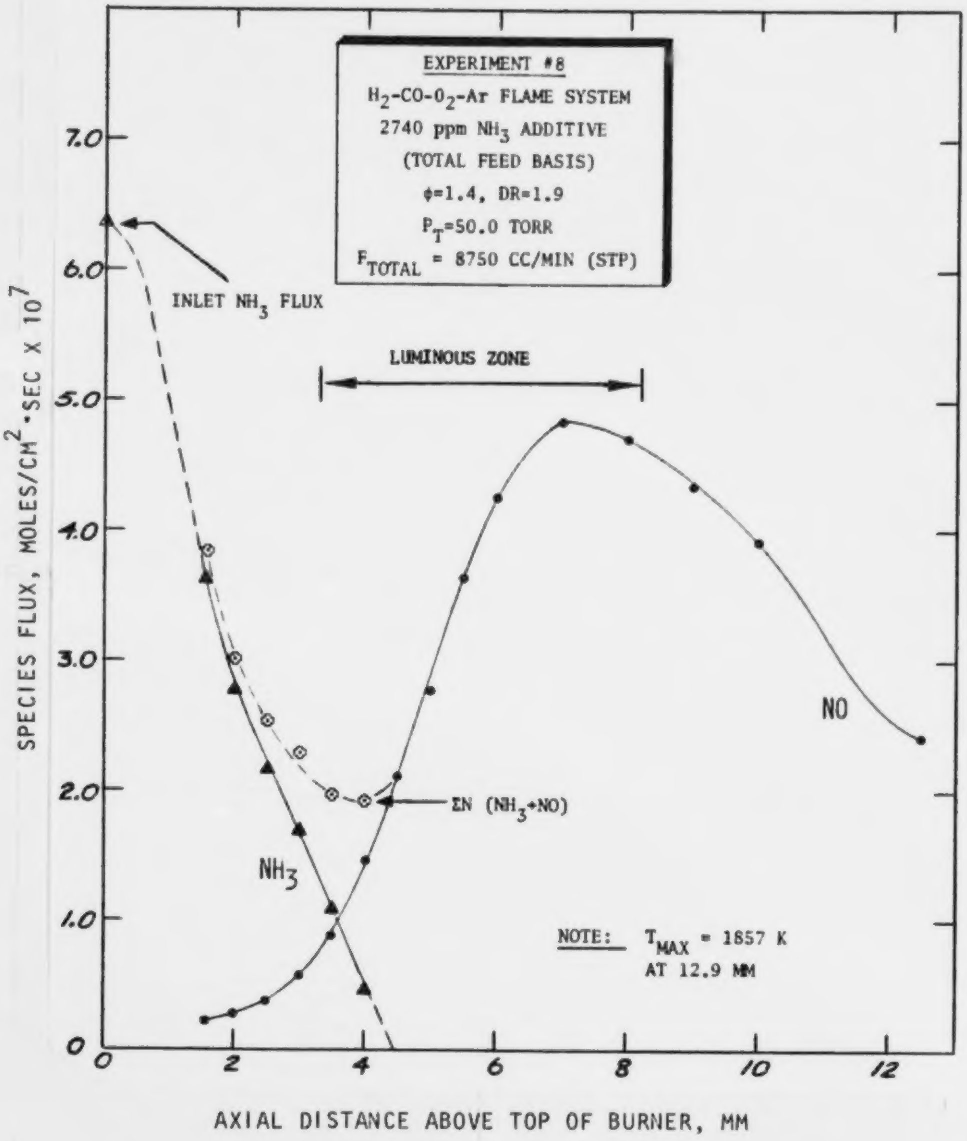

Figure 2-60. Experiment 8 - Species Flux Profiles

In this experiment, CO was measured directly in the mass spectrometer (reported as CO + N_2) since no N_2 was initially fed to the burner, and H_2O was calculated as before by balancing the H/Ar ratio to that of the burner feed. The mole fraction profiles for H_2, CO, O_2 and CO_2 are shown in Fig. 2-61. The open symbols plotted on the left axis (Δx=0), for comparison purposes, denote inlet mole fractions based on flowrate calibration data, whereas the solid symbols on this axis denote the experimentally measured cold-flow values. The theoretical H_2/CO inlet ratio should be 1.42, since these gases are obtained from a premixed standard cylinder (58.7% H_2, 41.3% CO). The experimental H_2/CO value of 1.17 was surprisingly low. This indicates that either the sensitivities of the mass spectrometer for CO and H_2 were not measured properly or air intrusion into the cold-flow sample somehow occurred. The composition of our calibration gas (selected for the CH_4 flames) was such that it gives little information on the former possibility. If the difference between the calculated and experimental inlet mol % O_2 is attributed to an air leak, then the H_2/CO ratio becomes 1.37, which is near the actual ratio. The effect of an air leak on the H_2/CO ratio results from the fact that any nitrogen from the air would have been measured as CO.

Equilibrium calculations indicate that virtually no O_2 should remain in this fuel-rich system at complete reaction. It was not expected that any O_2 would remain unreacted above the luminous zone in the presence of excess H_2. However, kinetic-diffusion calculations reported in Task 3 predict that even at 20 mm there should be 1% O_2, 2% H_2, 3% H atom and 0.5% O atom.

From the slopes of the profiles in Fig. 2-61, the molar flux profiles for the major species were calculated and are given in Fig. 2-62. As expected, H_2 reacts at a much faster initial rate than does CO. Above the top of the luminous zone, however, some H_2 appears to reform. If this small increase in H_2 concentration is real and results from the recombination of H-atoms, the H-atoms present at 9 mm must have reacted with O_2 in the probe rather than recombining to H_2. It is apparent that the probing of flames containing high concentrations of radicals has an inherent uncertainty associated with the potential reaction paths of the radicals during the quenching process.

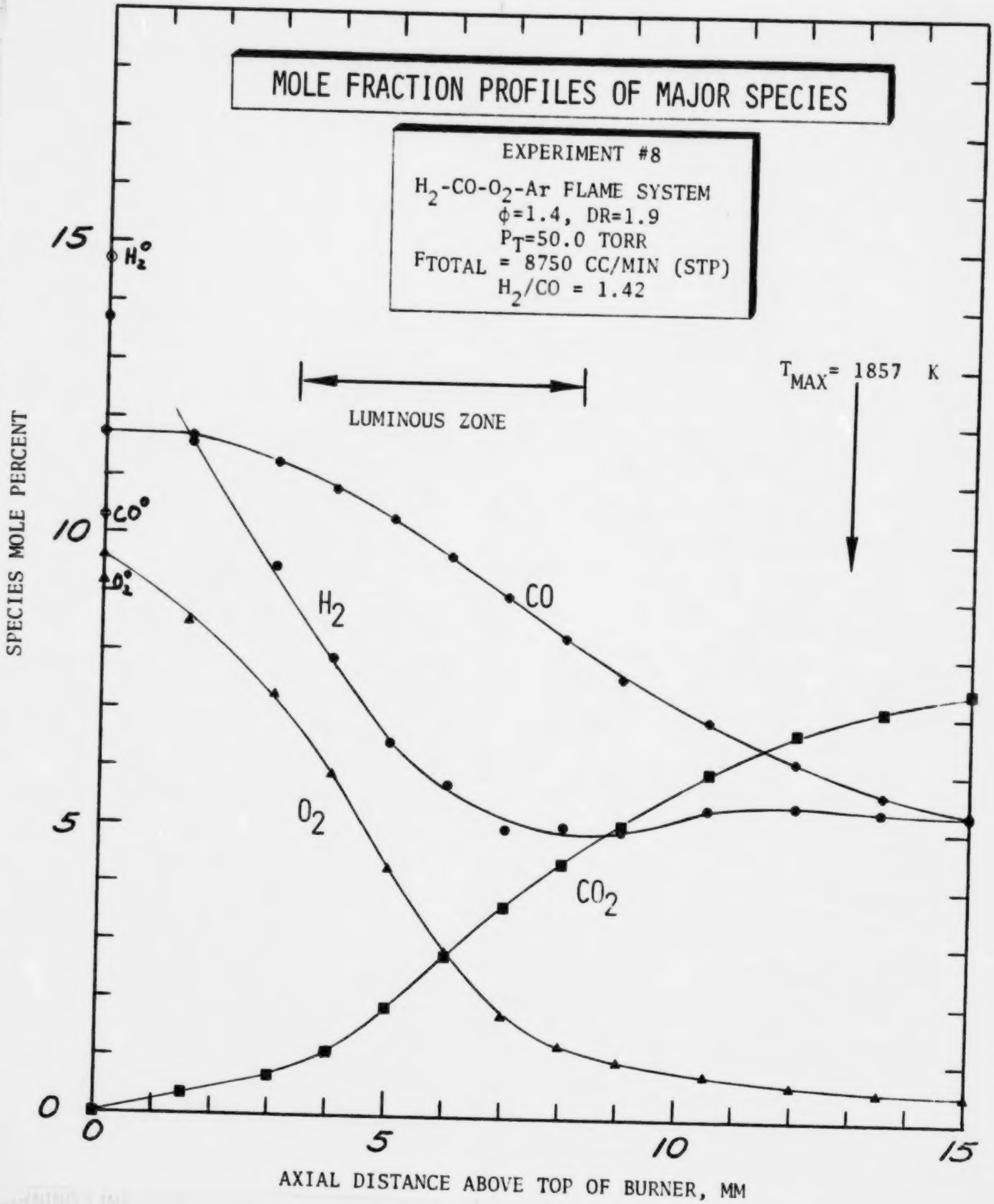

Figure 2-61. Mole Fraction Profiles of Major Species from Experiment 8

USE SPECIAL DROPOUT BLUE PENCIL ONLY TO INDICATE
CLASSIFICATION

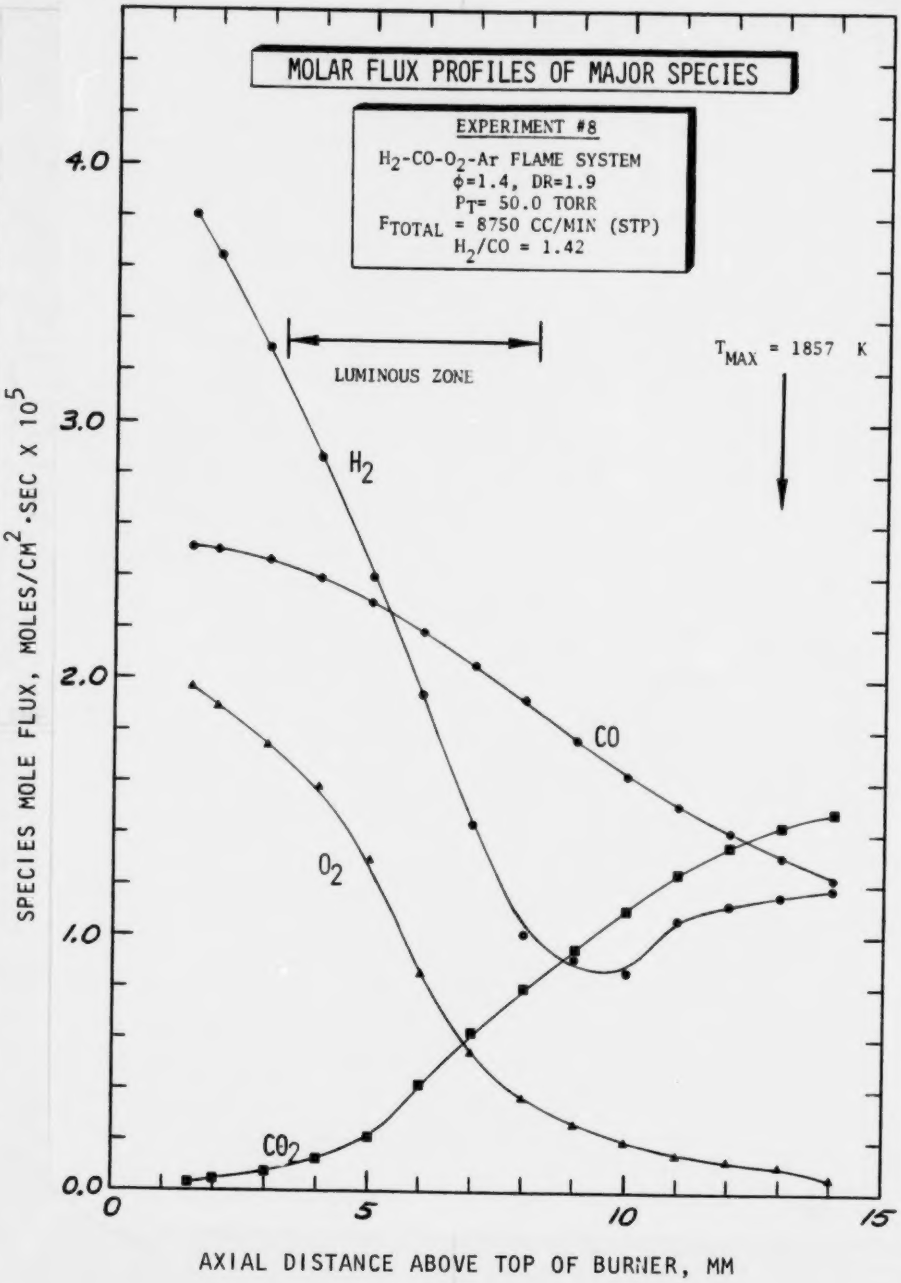

Figure 2-62. Molar Flux Profiles of Major Species from Experiment 8

Detailed Probing Experiment No. 9 (H_2-CO-O_2-Ar-NO)

Because much of the NO that forms from the added NH_3 is unexpectedly consumed above the luminous zone and then partially reforms (experiment No. 8), NO was added in the absence of NH_3 in this experiment (No. 9 in Table 2-6) to see how much, if any, is consumed above the luminous zone. The conditions utilized in this experiment were identical to those employed in experiment No. 8 ($\phi = 1.4$, DR = 1.9, 50 torr, and 8750 cc/min), with the exception that 2230 ppm NO was added as the fuel-N species instead of NH_3. This amount of NO additive was determined directly by a cold-flow experiment with premixed unburned combustible gases just prior to burner ignition.

The mole fraction profile for NO is shown in Fig. 2-63 and 2-64. There was no measurable NO_2, NH_3 or HCN within the detection limits of the analytical system. The amount of NO at the burner inlet (~ 2500 ppm) extrapolated from the experimental data is somewhat higher than that determined directly from the cold-flow measurement. This is probably due to the temperature profile being higher than the actual gas temperature profile. The mole fraction of the added NO begins to decrease near the bottom of the luminous zone, reaching a minimum of 2020 ppm at 17 mm. The NO mole fraction then gradually increases to a maximum of 2120 ppm at 45 mm downstream and, thereafter, decreases to 2060 ppm at 70 mm.

Figures 2-65 and 2-66 present the NO molar flux profiles. These figures are very similar to the NO mole fraction curves. The maximum rate of NO disappearance occurs just at the top of the luminous zone. The molar flux at 70 mm downstream corresponds to a NO yield of 84%.

The N-species molar flux profiles in experiments No. 8 and NO. 9 are compared directly in Fig. 2-67 and 2-68. The NO flux in experiment No. 9 remains relatively constant at its initial value up to about 4.5 mm. The initial decrease in NO flux in experiment No. 9 corresponds to the point in the luminous zone where the NO formation rate in experiment No. 8 begins to decrease from its maximum value. In

USE SPECIAL DROPOUT BLUE PENCIL
ONLY TO INDICATE CORRECTIONS

CLASSIFICATION

PAGE

STARTING LINE

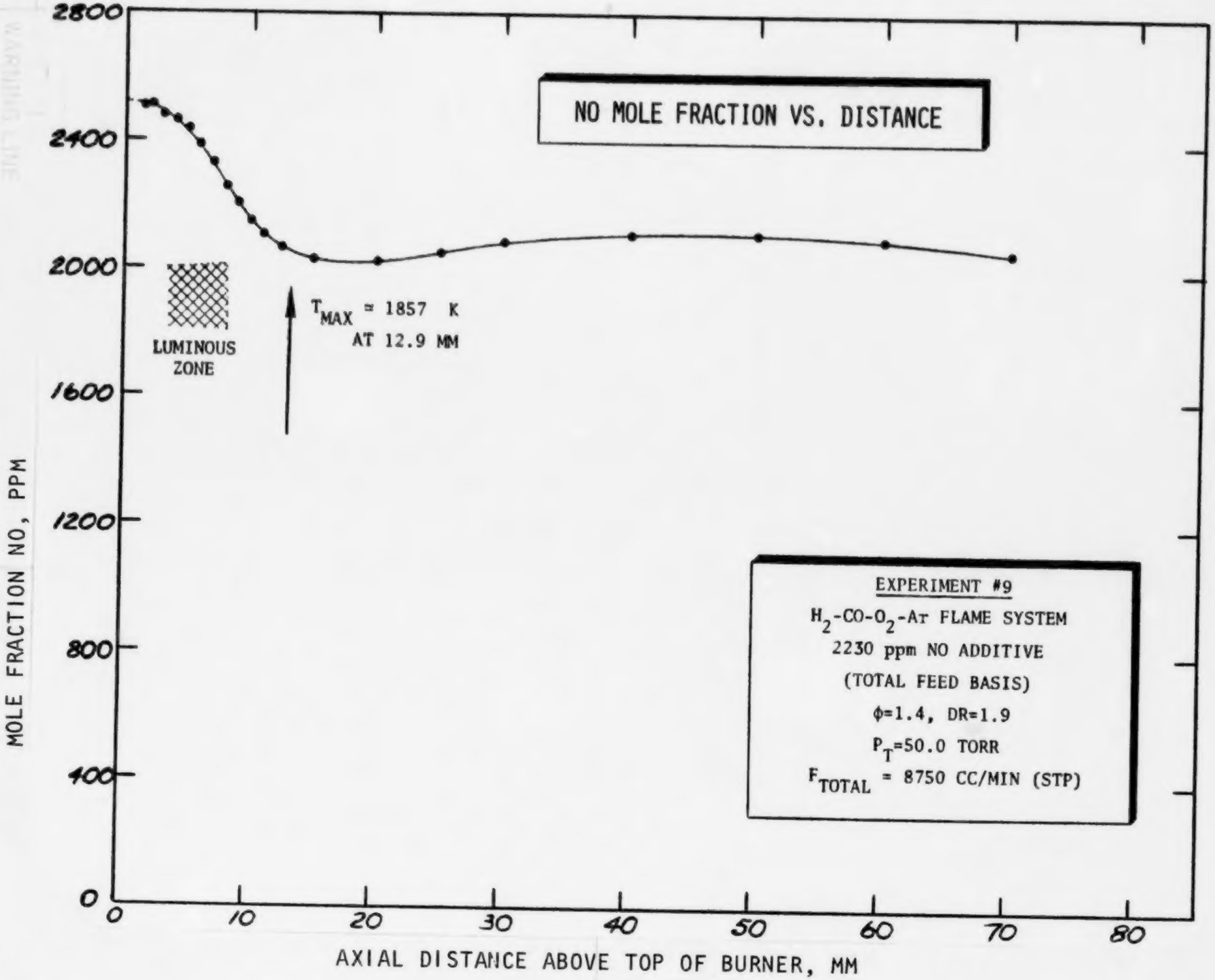

Figure 2-63. Experiment 9 - NO Mole Fraction Profile

WARNING LINE

STOP

DOCUMENT NUMBER

PAGE NUMBER

CLASSIFICATION

TYPIST

201

USE SPECIAL DROPOUT BLUE PENCIL
ONLY TO INDICATE CORRECTIONS
CLASSIFICATION
PAGE
STARTING LINE

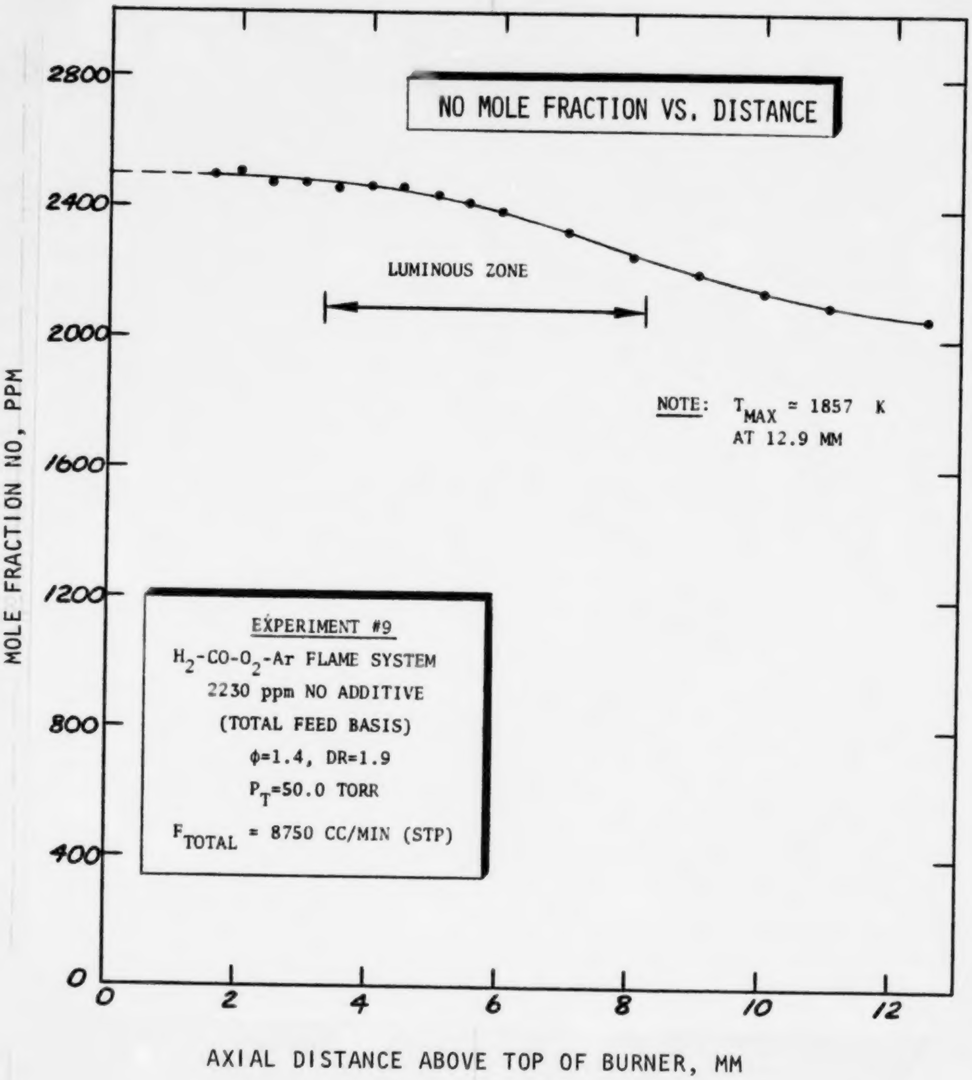

Figure 2-64. Experiment 9 - NO Mole Fraction Profile

WARNING LINE
STOP
DOCUMENT NUMBER

CLASSIFICATION
TYPIST 202

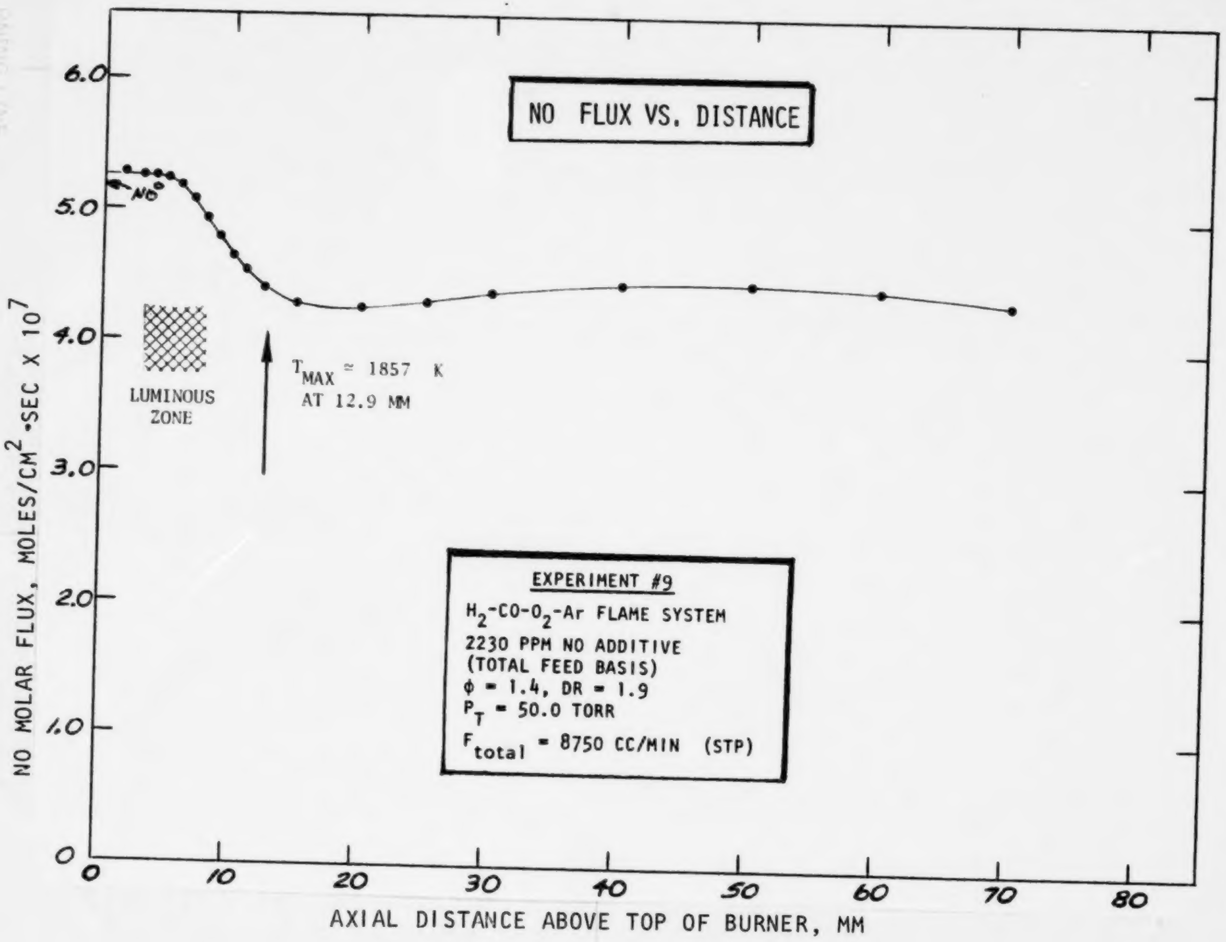

Figure 2-65. Experiment 9 - NO Flux Profile

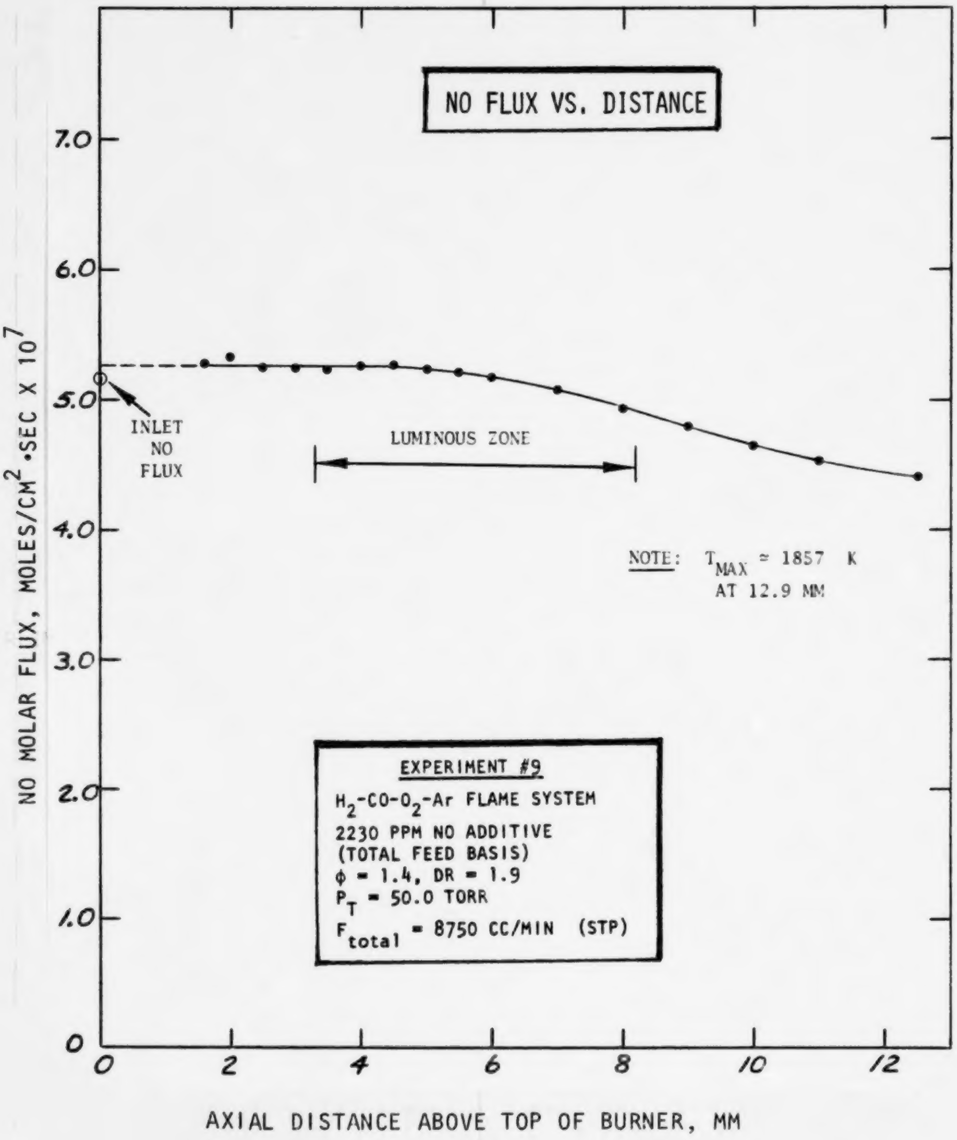

Figure 2-66. Experiment 9 - NO Flux Profile

USE SPECIAL DROPOUT BLUE PENCIL
ONLY TO INDICATE CORRECTIONS
CLASSIFICATION
PAGE
STARTING LINE

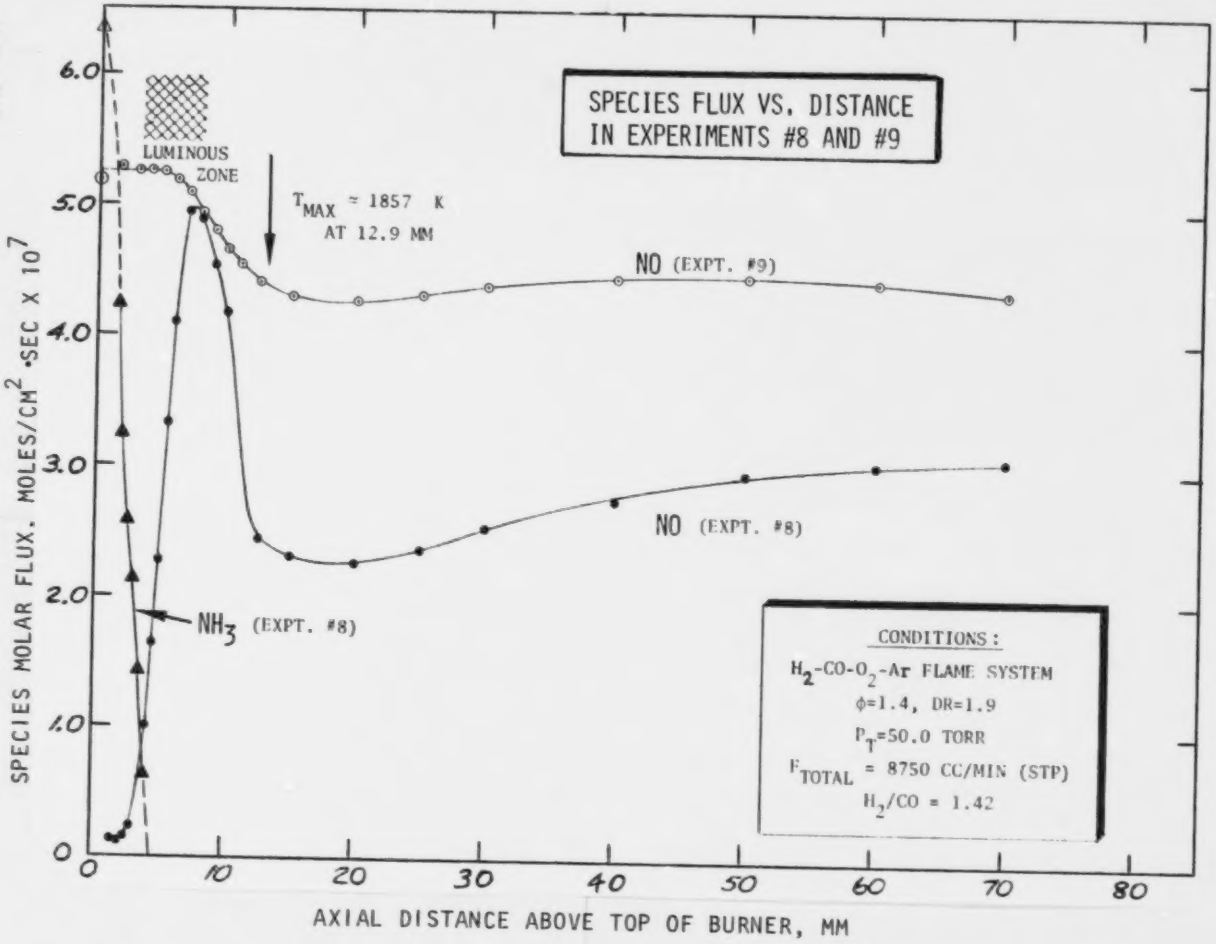

Figure 2-67. Comparison of Species Molar Flux Profiles from Experiments 8 and 9

DOCUMENT NUMBER
PAGE NUMBER
CLASSIFICATION
TYPIST

205

USE SPECIAL DROPOUT BLUE PENCIL
ONLY TO INDICATE CORRECTIONS
CLASSIFICATION
PAGE
STARTING

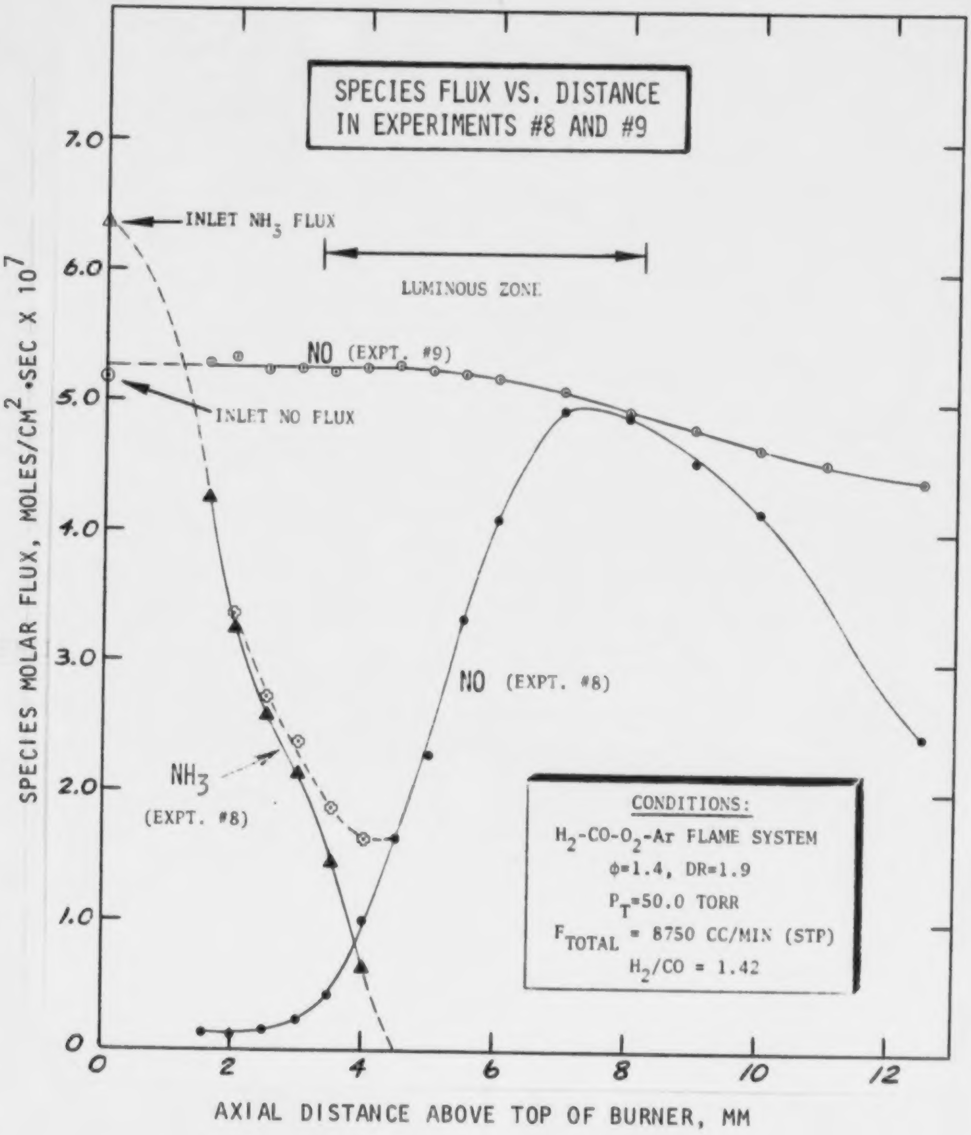

Figure 2-68. Comparison of Species Flux Profiles from Experiments 8 and 9

TYPIST

206

both experiments, the NO flux decreases rapidly near the top of the luminous zone. However, the NO flux in experiment No. 8 decreases significantly more than in No. 9. Both curves reach a minimum at the same point (approximately 18 mm) just above the maximum temperature location. It would appear that there are additional free radical species present in the experiment with NH_3 addition, which can also promote NO depletion. At least one very long-lived nitrogen intermediate must be involved in experiment No. 8 because the NO flux continues to increase more than 40 mm above the burner, whereas in experiment No. 9 the NO flux has begun to decrease.

Detailed Flame Probing Experiments No. 10 and No. 11

In experiment No. 10, both NO and NH_3 were added to a fuel-rich simulated low-Btu fuel flame (H_2-CO-H_2-Ar), while only NH_3 was added in experiment No. 11. (These experiments will be presented together for comparison.) Except for the concentrations of the additives, the flame conditions (Table 2-6) utilized in these experiments were the same as those used previously. The position of the luminous zone was observed to be approximately 3.4 to 8.5 mm above the top of the burner.

The nominal additive mole fractions (in ppm) on a total feed basis for these two experiments are compared with those of the previous two experiments in the following tabulation:

Experiment No.	Ammonia, ppm	Nitric Oxide, ppm
8	2740	None
9	None	2230
10	1370	1370
11	1370	None

The total additive concentration in experiment No. 10 was set equal to that of experiment No. 8 so that the maximum NO concentration (near the top of the flame front) would be about the same as in experiment No. 8. Since only about one-half the concentration of NH_3 decomposition products will be present at that point in experiment No. 10, any difference in the rate of NO comsumption above that point

282

6085

USE SPECIAL DROPOUT BLUE PENCIL
ONLY TO INDICATE CORRECTIONS
CLASSIFICATION
PAGE
STARTING LINE

will give important information on the reaction mechanism. In experiment No. 11, the ammonia concentration was the same as in experiment No. 10 but no nitric oxide was added to the feed gas. Comparison of the results of experiments No. 10 and No. 11 will indicate the extent to which added NO participates in the chemical process. Comparison of experiments No. 8 and No. 11 will demonstrate the effect of ammonia concentration. Thus, these results should be an interesting test for any chemical model that claims to account for the formation of NO in a low-Btu flame.

Before presenting the nitrogen species profiles from experiments No. 10 and No. 11, the major species profiles measured for experiment No. 10 will be discussed.

Major Species. A total of 16 gas samples were obtained during experiment No. 10 for analysis by mass spectrometry. Two samples were identical and contained the premixed unburned combustibles fed to the burner just prior to burner ignition. A third sample was the standard calibration gas. A fourth sample contained combustion gases obtained at a position far above the top of the burner (40 mm). The remaining 12 samples were taken at uniform distance intervals between 1.1 and 21.0 mm above the burner.

As before, the mole percent H_2O for each sample was adjusted to give an H/Ar ratio equal to that of the feed gas. The results corrected in this manner are plotted as the open symbols in Fig. 2-69 through 2-71. The results from the previous similar experiment (No. 8) are plotted as solid symbols in these figures for comparison. The arbitrary distance scale (along the centerline of the burner) reads zero at the top of the burner wall at which point the stainless steel screen flame holder is attached. The feed gas flows out of the top of the water-cooled porous plate which is about 3 mm below the bottom of the screen. The position of the assigned distance scale relative o the burner is shown in Fig. 2-69. The luminous zone extends from about 4 to 8 mm above the bottom of the screen. As can be seen in Fig. 2-69, the first samples of the combusting gas were obtained just above the top of the screen (1.1 mm on the distance scale) and then periodically up to 21 mm where the temperature, measured in experiment No. 8, was near its maximum value of 1850 K. One additional sample was obtained at 40 mm, where the temperature had dropped slightly to about 1770 K.

TYPIST
FORM 608-B-31 REV

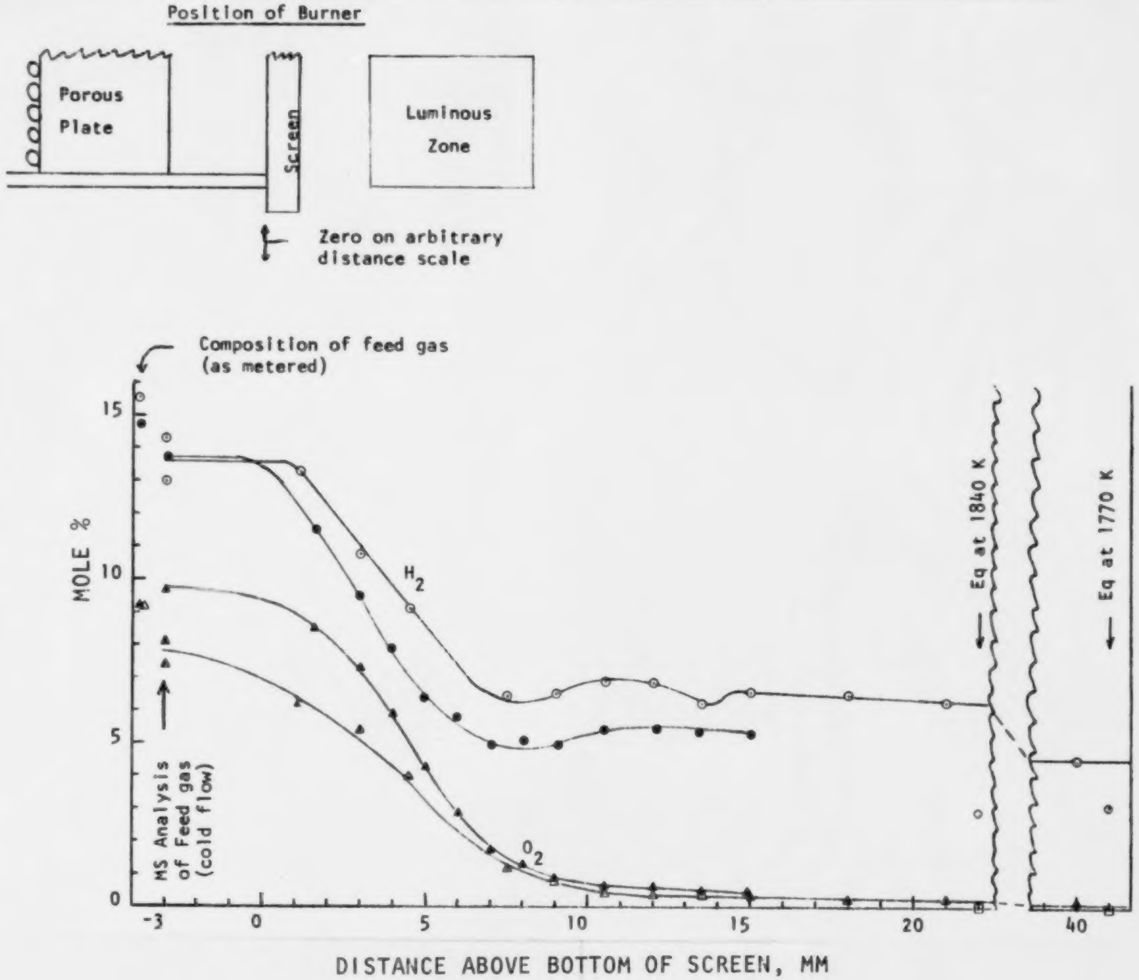

Figure 2-69. Comparison of H_2 and O_2 Mole Fraction Profiles from Experiments #8 (solid symbols) and #10 (open symbols)

209

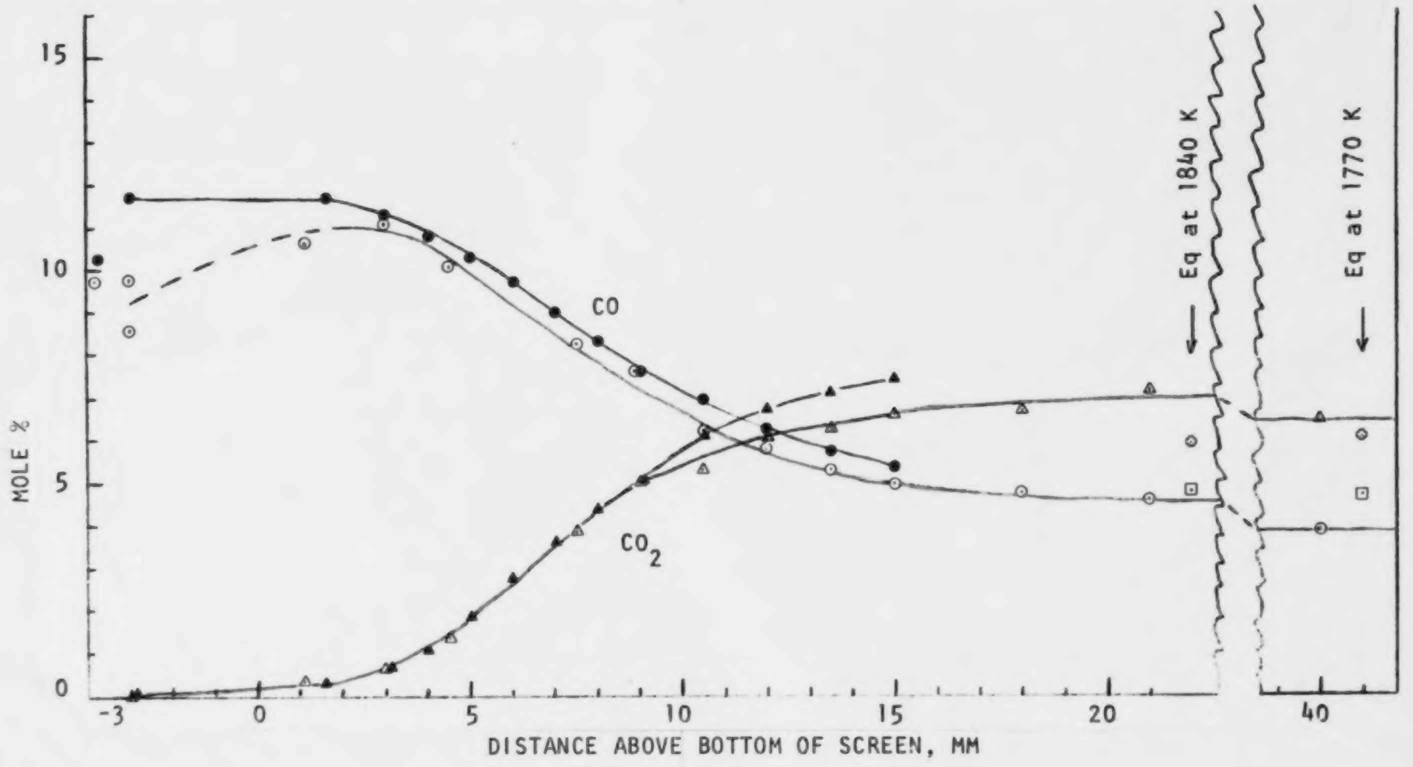

Figure 2-70. Comparison of CO and CO_2 Mole Fraction Profiles from Experiments #8 (solid) and #10 (open)

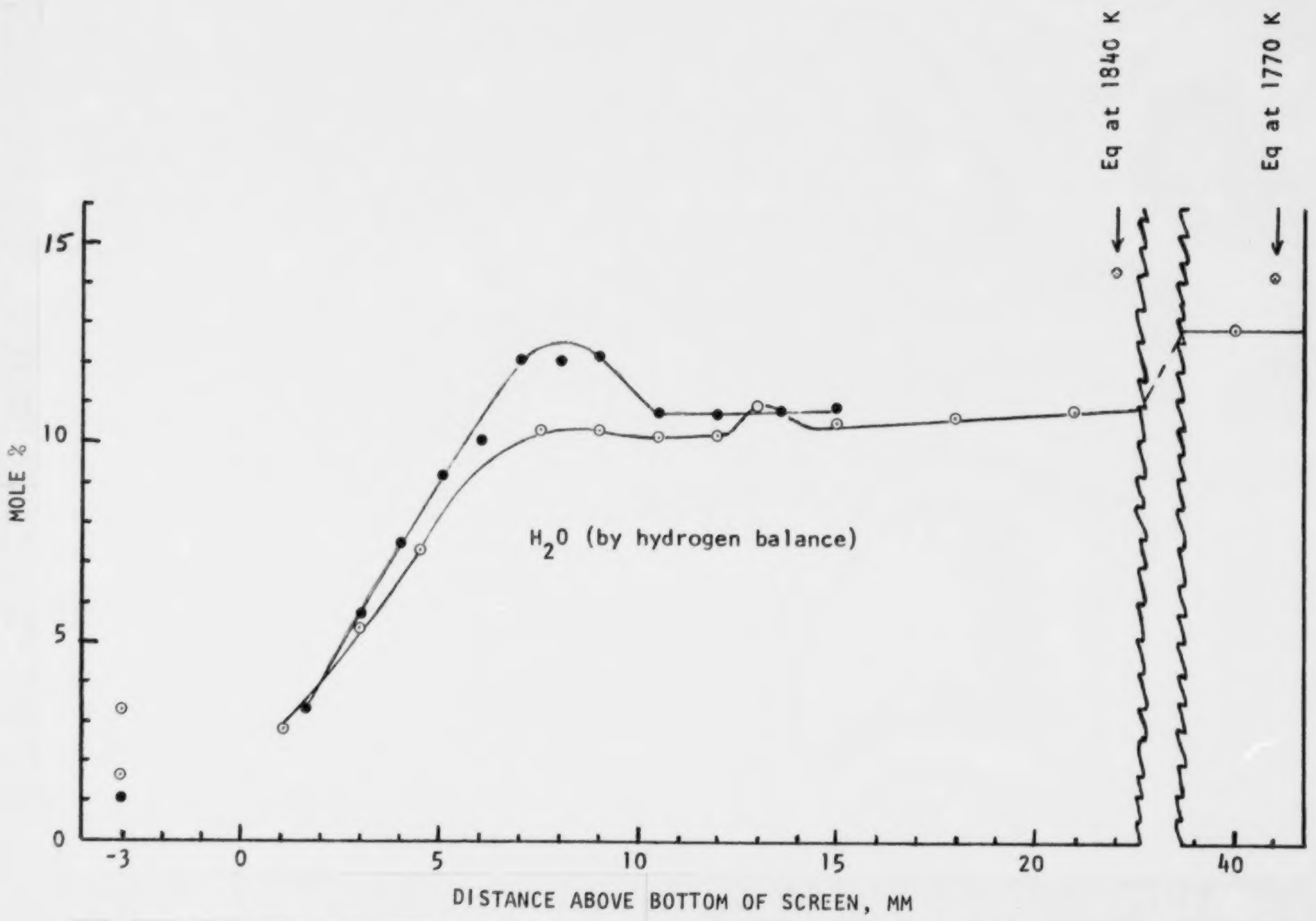

Figure 2-71. Comparison of H_2O Mole Fraction Profiles from Experiments #8 (solid) and #10 (open)

In addition to the combustion results, some other information is also plotted in these three figures. At the far left are plotted the feed gas composition for each experiment as determined from the metering of gases of known composition (H_2 + CO, O_2, Ar, and NH_3 in He). Plotted at -3 mm on the figures are compositions measured by the vendor of cold-flow samples of the feed gas. These concentrations are plotted at -3 mm because they represent the composition of the gas leaving the porous plate although the samples were actually collected with the quartz probe just above the screen (and before the burner was ignited). Plotted at 21 and 41 mm, respectively, on each figure are the calculated compositions of the post-flame gases assuming chemical equilibrium at 1840 and 1770 K.

The differences between the two O_2 profiles would appear to be attributable to a mass spectrometer calibration error. The ratio of O_2 concentrations is nearly the same in all samples including the cold-flow samples. Since the vendor calibrated his instrument more carefully in experiment No. 10 (except for the feed gas measurements in which some problems did occur), the lower O_2 curve is believed to be the more reliable. Although at chemical equilibrium almost no O_2 (<0.001%) would remain beyond 20 mm, the measured concentrations are 0.24% at 21 mm and 0.17% at 40 mm.

The two H_2 curves in Fig. 2-69 are nearly parallel suggesting an actual difference F2-69 in the amount of H_2 in the feed gas in these two experiments. The agreement of the cold-flow samples may be coincidental considering the above-mentioned problem with these. The simplest explanation for the difference between the two hydrogen curves would be an error in the CO/H_2 ratio in the fuel gas purchased for use in experiment No. 10. The fact that the CO curves are also parallel in Fig. 2-70 F2-70 (except for the feed gas samples) would tend to substantiate this.

The similarity of the shapes of the pairs of curves in Fig. 2-69 indicates that F2-69 the results from either experiment will yield the same conclusions regarding the regions in which the maximum reaction rates occur. At 41 mm the H_2 concentration is still well above its equilibrium value. This could result from the possible error in the composition of the fuel gas or from the water-gas shift reaction having

USE SPECIAL DROPOUT BLUE PENCIL
ONLY TO INDICATE CORRECTIONS
CLASSIFICATION
PAGE
STARTING LINE

not attained equilibrium. The agreement between the CO and CO_2 profiles in Fig. 2-70 is quite good considering the nature of the experiments. The CO concentration at 40 mm is considerably below its equilibrium value and the CO_2 is somewhat above. If the water-gas shift reaction, $H_2 + CO_2 \rightarrow H_2O + CO$, were to occur to the extent required to bring CO to its equilibrium value, the CO_2 would be slightly below equilibrium but the H_2 and H_2O concentrations would be brought close to their equilibrium values. Thus, these mass spectrometry results suggest that the water-gas shift reaction may not have reached equilibrium even at 40 mm above the screen.

The H_2O profiles in Fig. 2-71 are approximately mirror images of the H_2 profiles in Fig. 2-69 because the H_2O concentrations were not measured experimentally but rather were calculated to give an overall H-atom balance at each point in the flame. This procedure is only approximate, however, because it neglects the effect of diffusion on the H/Ar ratios.

Nitrogen Species. Plotted in Fig. 2-72 through 2-75 are the NO and NH_3 profiles (mole fraction and molar flux) measured in experiment No. 10. It can be seen from Fig. 2-75 that when NO and NH_3 are both added to the feed gas about 85% of the NH_3 and 60% of the NO react below the bottom of luminous zone. It will be seen from the results of experiment No. 11 that when NH_3 is added alone at this concentration, about one-half of the NH_3 reacts below the luminous zone. (At a higher NH_3 concentration, Fig. 2-60, about 75% of the NH_3 reacts below luminous zone.)

The results of experiment No. 10 indicate that the NH_3 and NO are reacting to some extent below the luminous zone. Perhaps the Lyon-Muzio reaction is occurring in which NH_3 and NO react selectively to form N_2. It should be noted, however, that more NH_3 is consumed than NO in this region.

Effect of Additive Type on NO Yield. It has been demonstrated in hydrocarbon flames that the NO yield is relatively independent of the chemical nature of the nitrogen additive (excluding, of course, N_2). Also, the NO concentration increases continually until a final concentration is reached. It can be seen

DOCUMENT NUMBER

213

USE SPECIAL DROPOUT BLUE PENCIL
ONLY TO INDICATE CORRECTIONS

CLASSIFICATION

PAGE

STARTING LINE

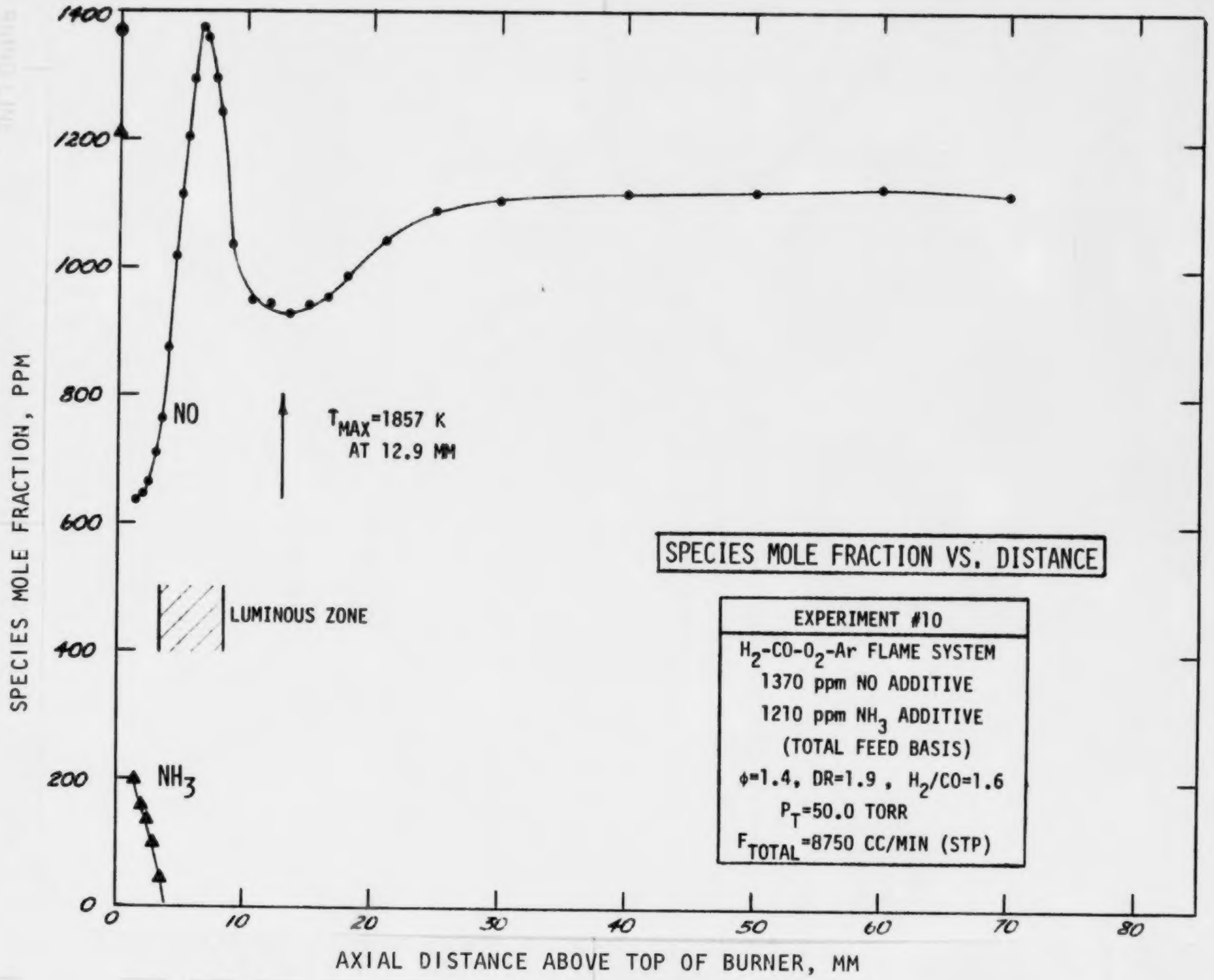

Figure 2-72. Experiment 10 - Species Mole Fraction Profiles

DOCUMENT NUMBER
PAGE NUMBER
CLASSIFICATION
TYPIST 214

USE SPECIAL DROPOUT BLUE PENCIL
ONLY TO INDICATE CORRECTIONS
CLASSIFICATION
PAGE
START

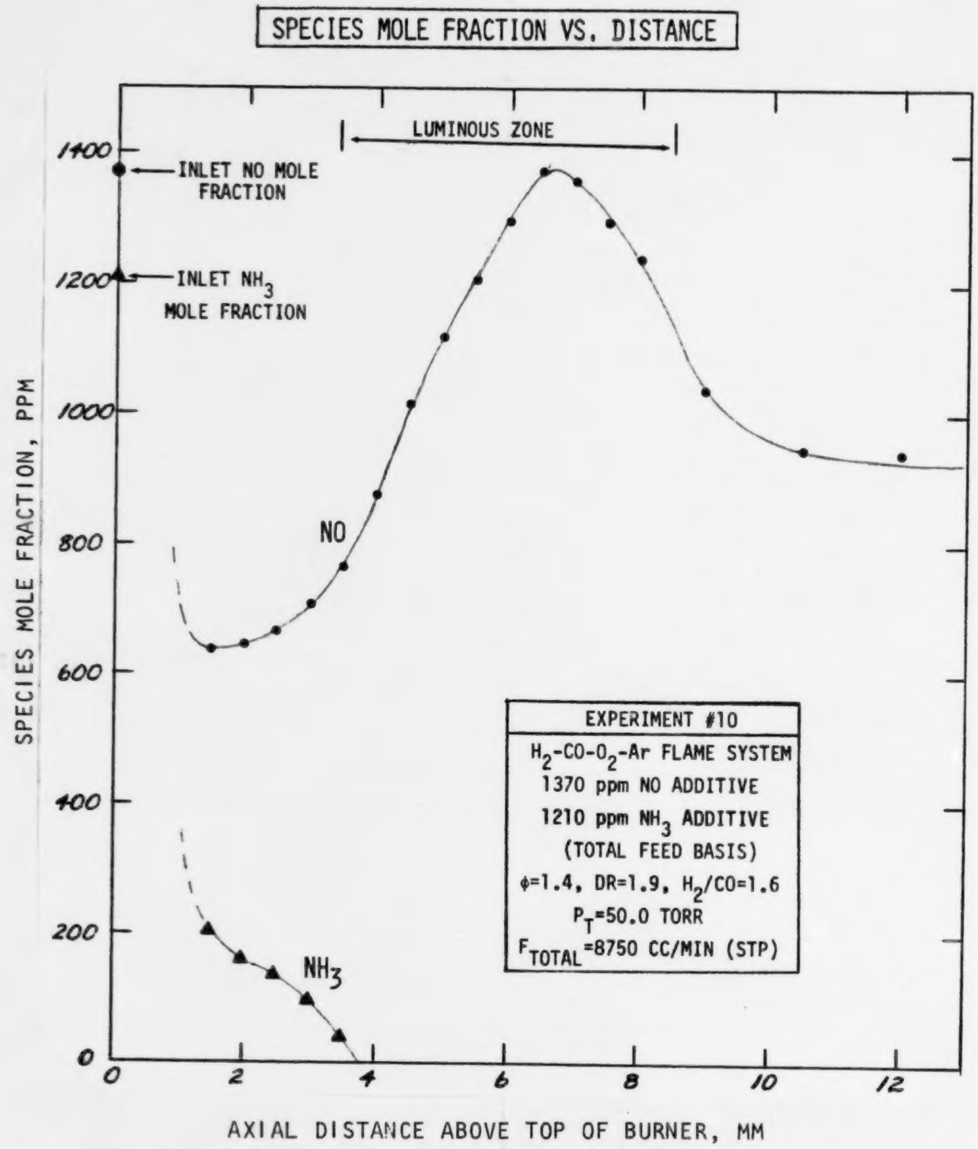

Figure 2-73. Experiment 10 - Species Mole Fraction Profiles

WARNING LINE
STOP
DOCUMENT NUMBER

PAGE NUMBER
CLASSIFICATION
TYPIST
PROOFED
CORRECTED
FORM 608-B-31 REV 7-70

USE SPECIAL DROPOUT BLUE PENCIL
ONLY TO INDICATE CORRECTIONS
CLASSIFICATION
PAGE
STARTING LINE

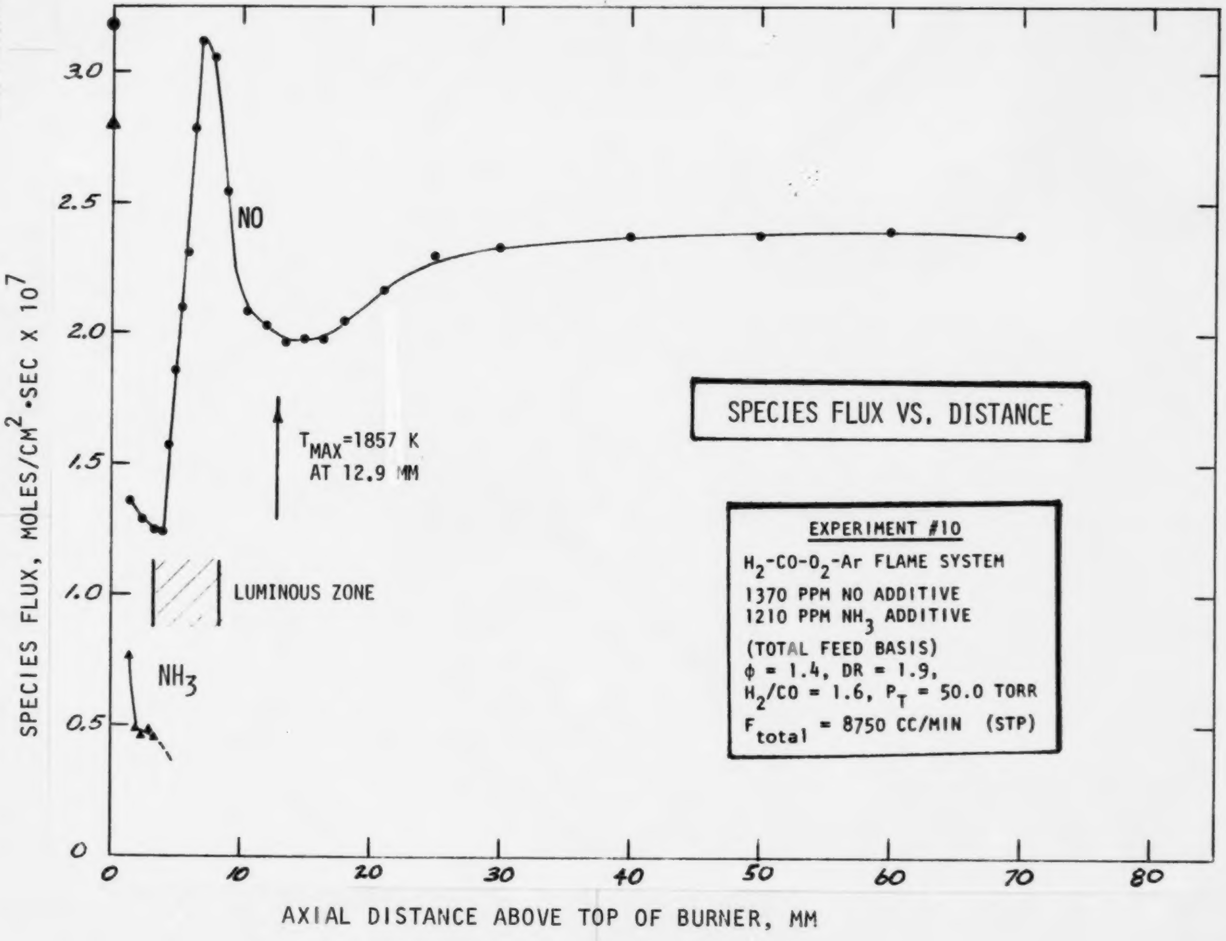

Figure 2-74. Experiment 10 - Species Flux Profiles

DOCUMENT NUMBER
PAGE NUMBER
CLASSIFICATION
TYPIST

216

USE SPECIAL DROPOUT BLUE PENCIL
ONLY TO INDICATE CORRECTIONS
CLASSIFICATION
PAGE
STARTING LINE

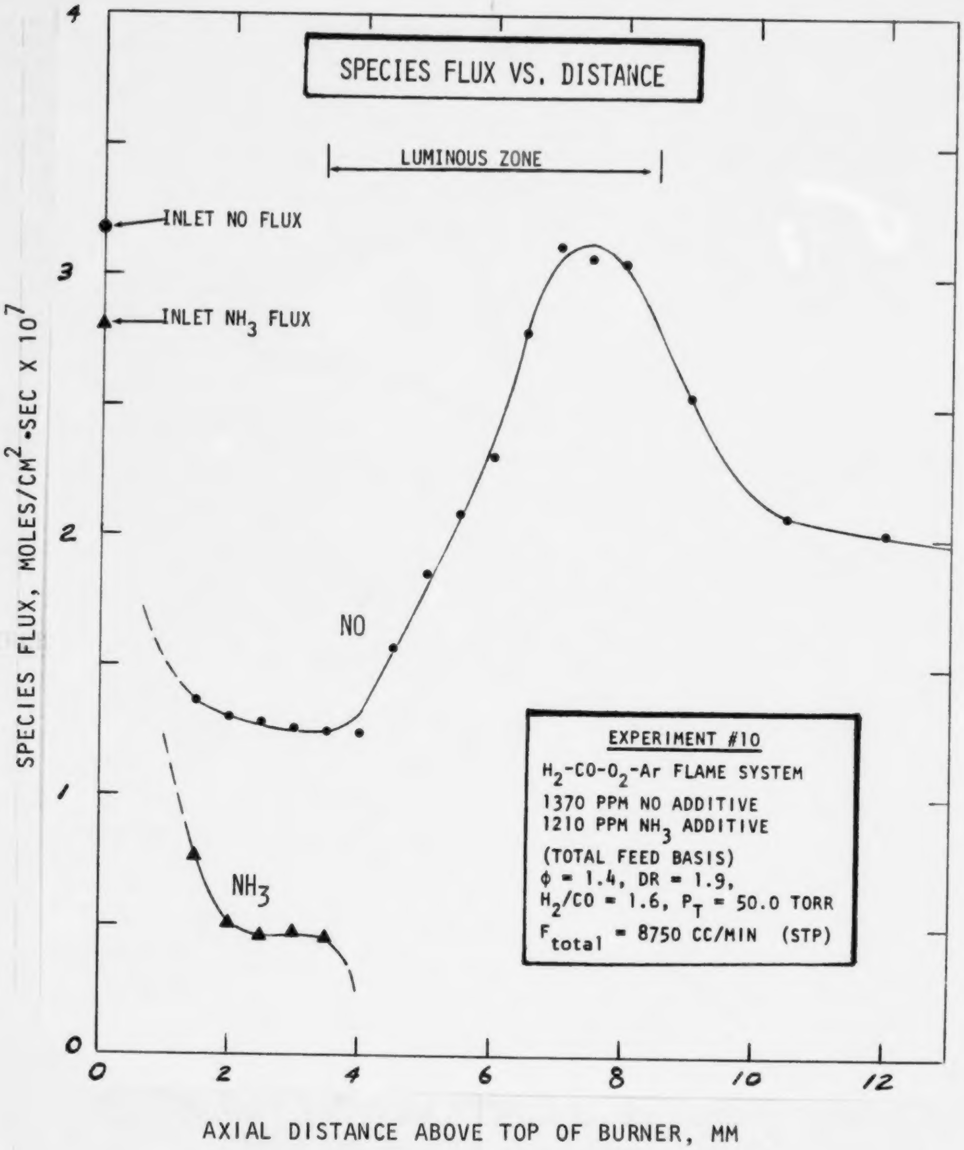

Figure 2-75. Experiment 10 - Species Flux Profiles

WARNING LINE
STOP
DOCUMENT NUMBER
PAGE NUMBER
CLASSIFICATION
TYPIST 217

USE SPECIAL DROPOUT BLUE PENCIL
ONLY TO INDICATE CORRECTIONS

CLASSIFICATION

PAGE

STARTING LINE

from Fig. 2-76 and 2-77 that the situation is quite different in a CO-H_2 flame. In experiments No. 8, 9 and 10, nominal total additive concentration was 2600 ppm but the NO yields were 40%, 49%, and 84% respectively. In addition, NO is consumed near the top of the luminous zone in each experiment and part of this NO reforms in the post-flame region.

It appears that when NH_3 is added alone, some of the initially-formed NO reacts with the NH_3 below the luminous zone to form N_2. When some NO is added with the NH_3, this process occurs to an even greater extent reducing the final yield and recovery of NO.

Effect of NH_3 Concentration on NO Yield. Plotted in Fig. 2-78 through 2-81 are the NO and NH_3 profiles for experiment No. 11 in which NH_3 alone was at one-half the concentration used in experiment No. 8. The NO yield profiles from these two experiments are compared in Fig. 2-82 and 2-83.

It was expected, based on results obtained in hydrocarbon flames, that the NO yield would increase when the additive concentration was decreased. In fact, we found the opposite effect. Both the maximum and final NO yields in experiment No. 11 were about two-thirds those obtained in experiment No. 8. This apparently results from an effect of the NH_3 concentration on the preflame reactions. If this phenomenon occurs in practical low Btu flames, the benefit that could be obtained by reducing the reactive nitrogen (NH_3) content of the fuel would be much greater than in the case of hydrocarbon fuels.

The results we have obtained on the fuel-rich H_2-CO-O_2-Ar flame indicate that the mechanism of fuel NO formation and consumption is much different than in hydrocarbon flames. It is likely that fuel NO formation will be even more sensitive to combustion modification techniques in a low Btu flame than in a hydrocarbon flame (because NO forms in high yields in the flame front and then is partially consumed in the post-flame region).

WARNING LINE

STOP

DOCUMENT NUMBER

USE SPECIAL DROPOUT BLUE PENCIL
ONLY TO INDICATE CORRECTIONS
CLASSIFICATION
PAGE
STARTING LINE

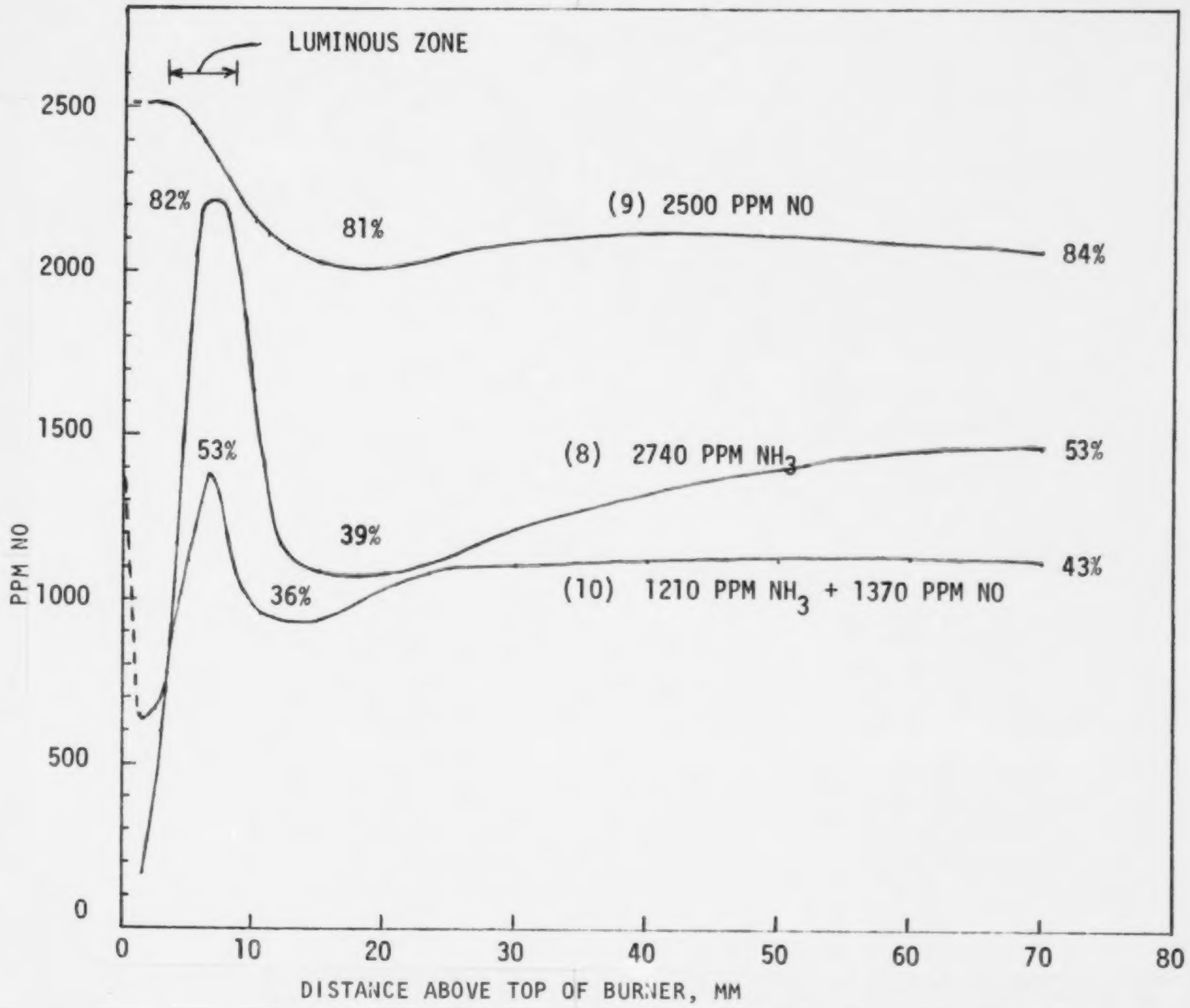

Figure 2-76. Effect of Additive Type on NO Yields in Fuel-Rich H_2-CO-O_2-Ar Low Pressure Flame (total additive concentration is about 2600 ppm in each experiment)

WARNING LINE
STOP
DOCUMENT NUMBER
PAGE NUMBER
CLASSIFICATION
TYPIST

219

USE SPECIAL DROPOUT BLUE PENCIL
ONLY TO INDICATE CORRECTIONS
CLASSIFICATION
PAGE
STARTING LINE

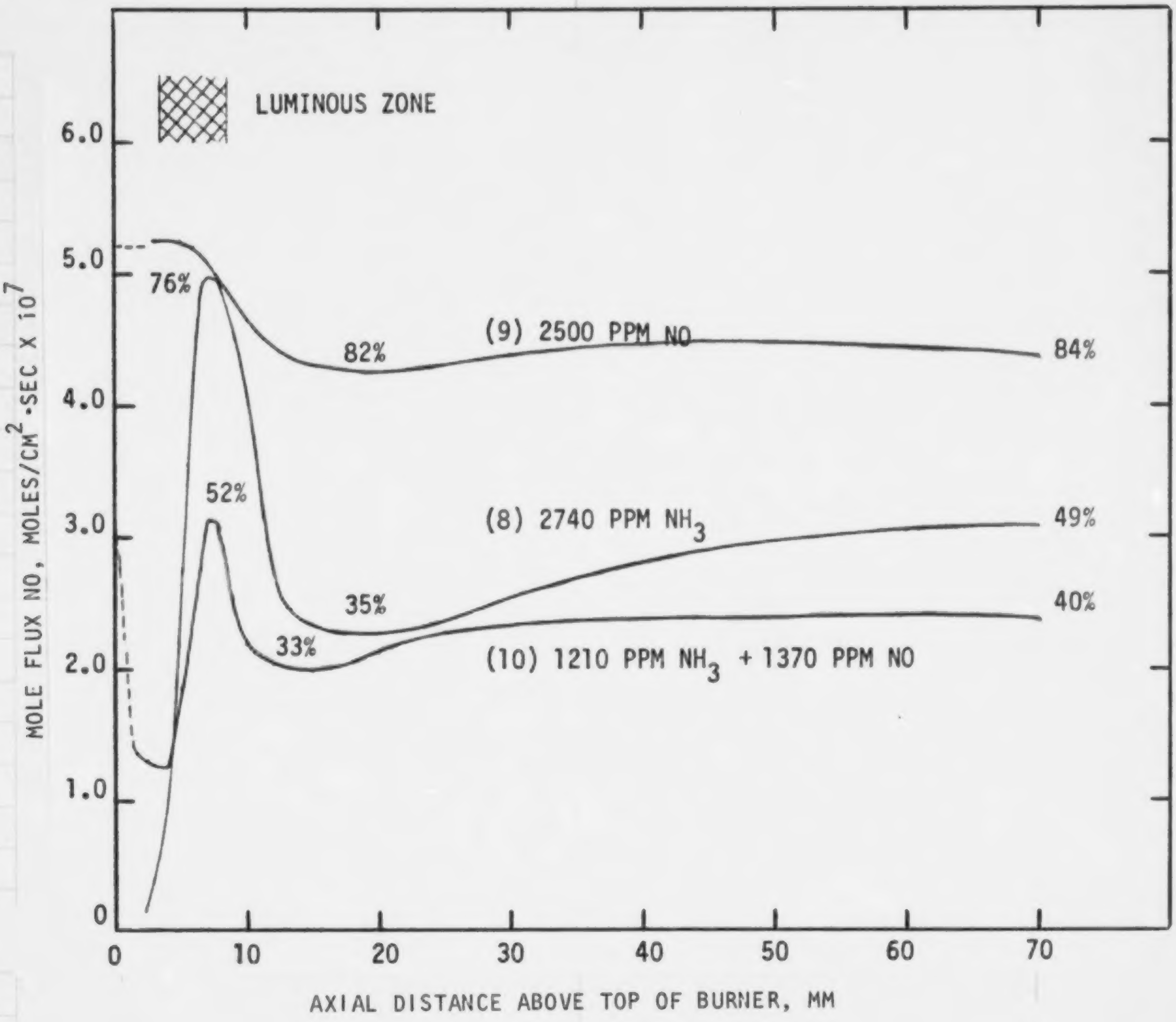

Figure 2-77. Effect of Additive Type on NO Yields in a Fuel-Rich H_2-CO-O_2-Ar Low Pressure Flame (Total Additive Concentration is about 2600 ppm in each Experiment)

WARNING LINE
STOP
DOCUMENT NUMBER

CLASSIFICATION
TYPIST

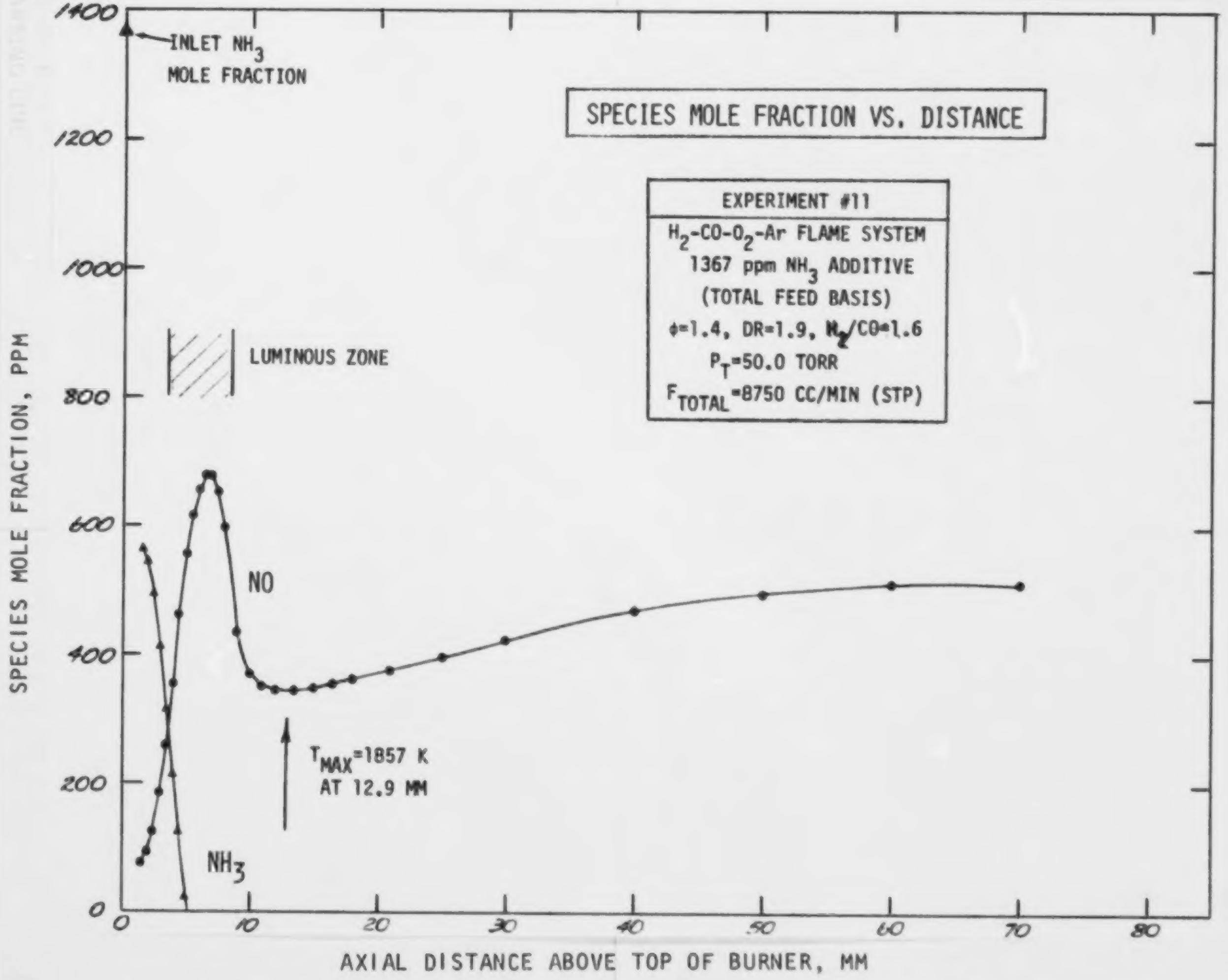

Figure 2-78. Experiment 11 - Species Mole Fraction Profiles

USE SPECIAL DROPOUT BLUE PENCIL
ONLY TO INDICATE CORRECTIONS
CLASSIFICATION
PAGE
STARTING LINE

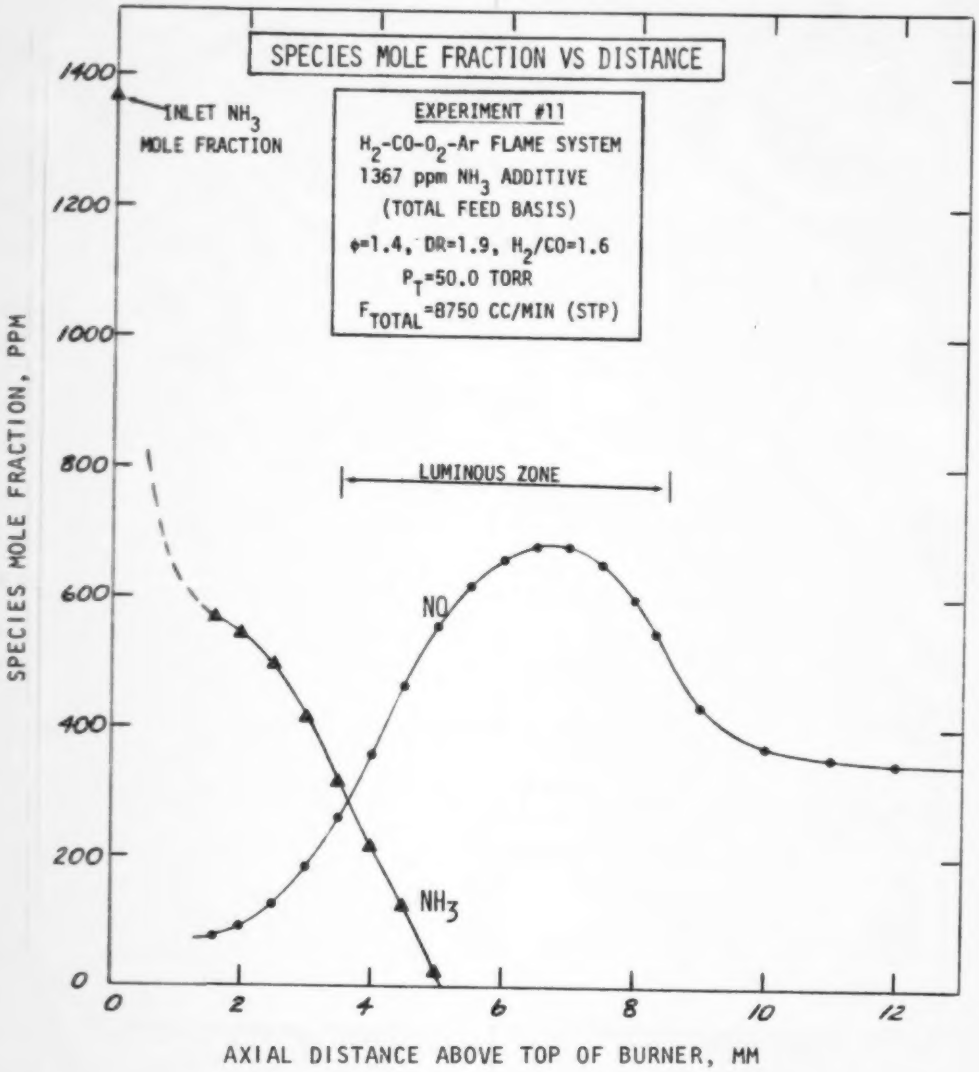

Figure 2-79. Experiment 11 - Species Mole Fraction Profiles

MARGIN LINE
STOP
DOCUMENT NUMBER
PAGE NUMBER
CLASSIFICATION
TYPIST 222

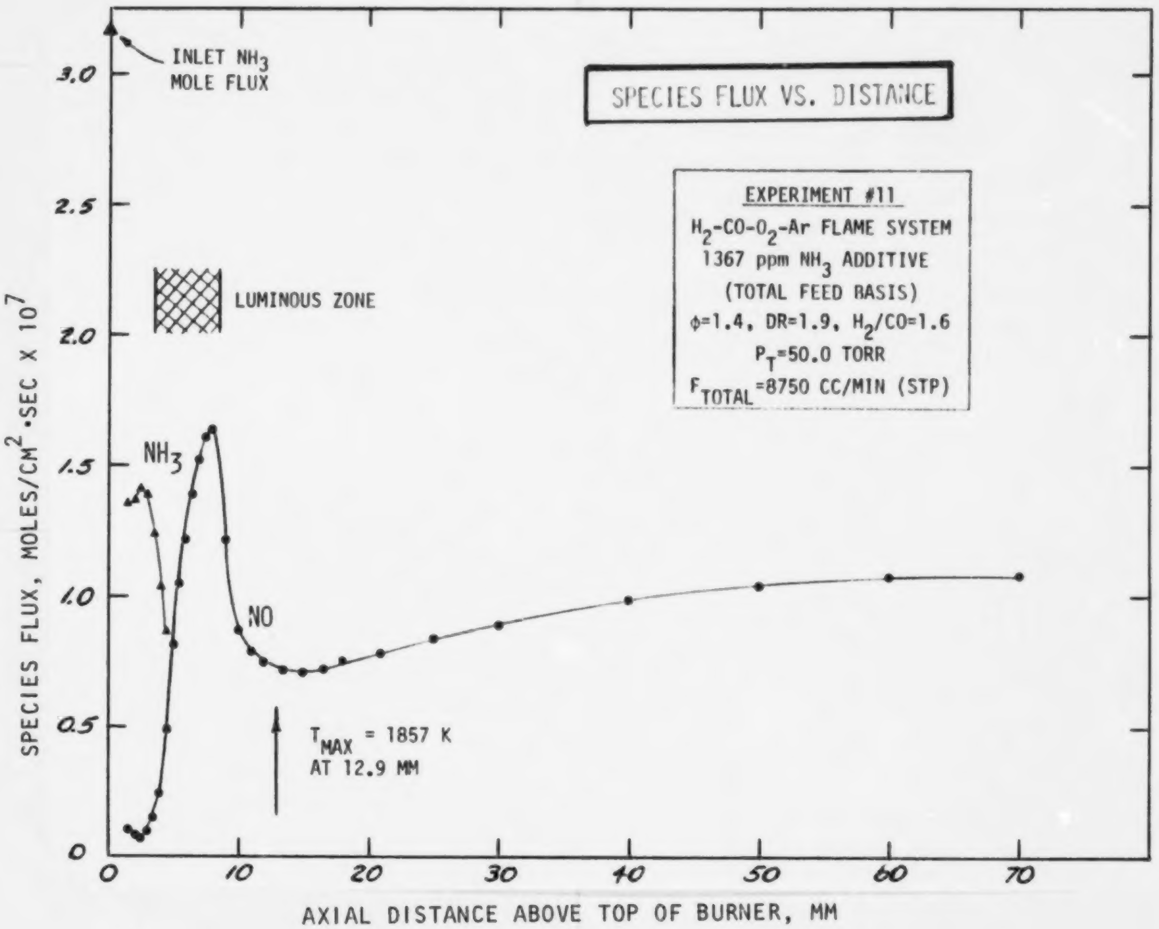

Figure 2-80. Experiment 11 - Species Flux Profiles

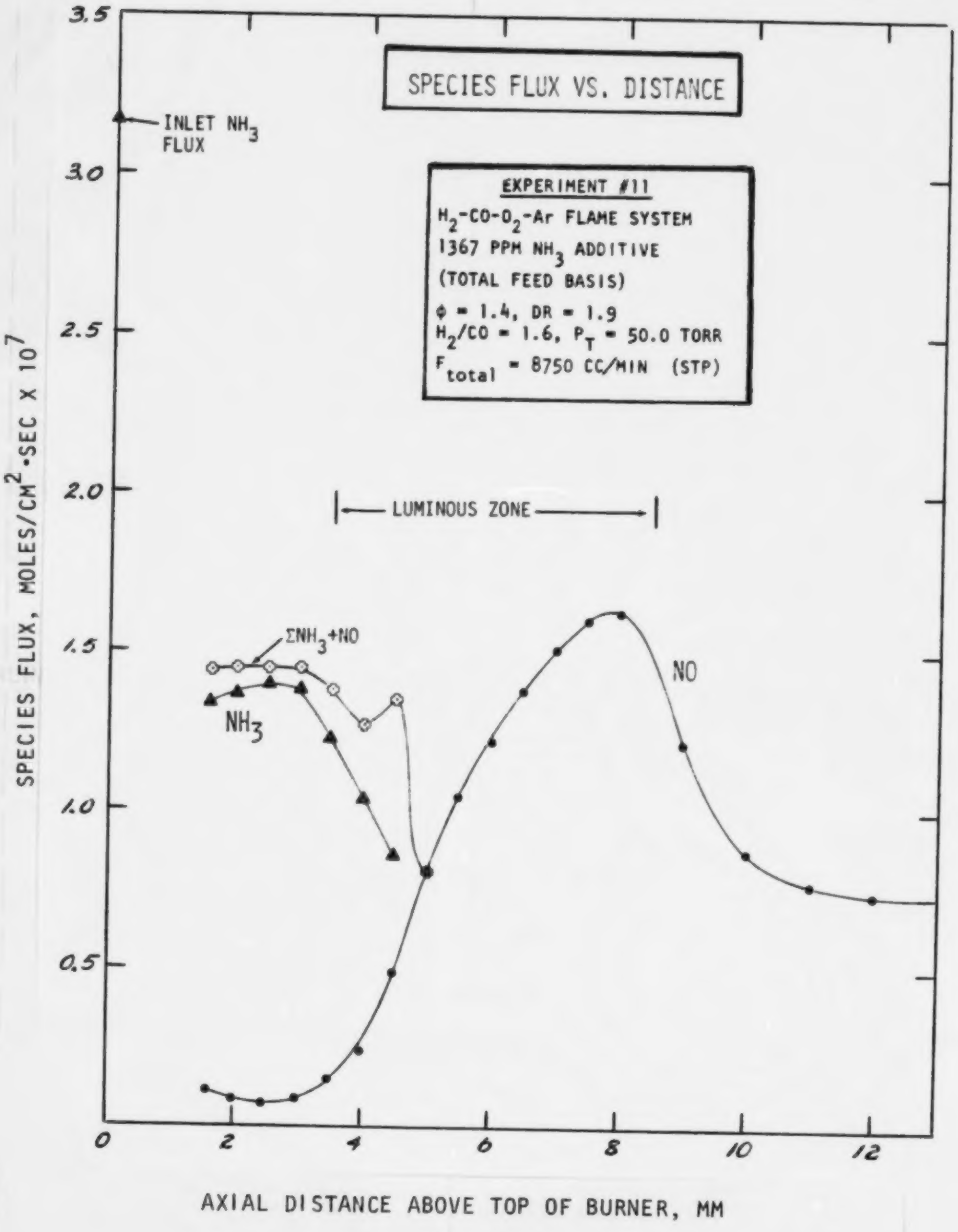

Figure 2-81. Experiment 11 - Species Flux Profiles

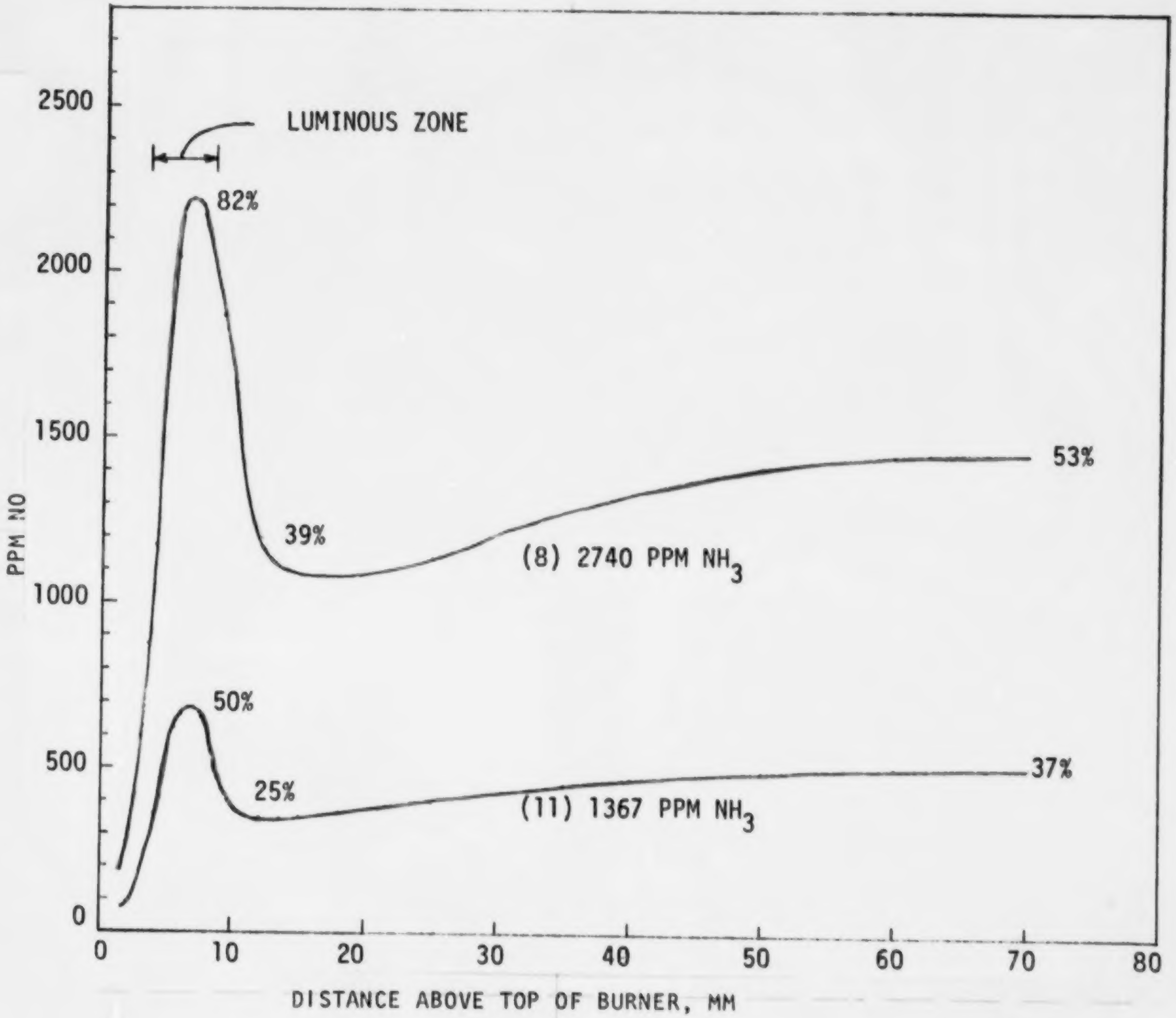

Figure 2-82. Effect of NH_3 Additive Concentration on NO Yields in Fuel Rich H_2-CO-O_2-Ar Low Pressure Flame

USE SPECIAL DROPOUT BLUE PENCIL
ONLY TO INDICATE CORRECTIONS

CLASSIFICATION

PAGE

STARTING LINE

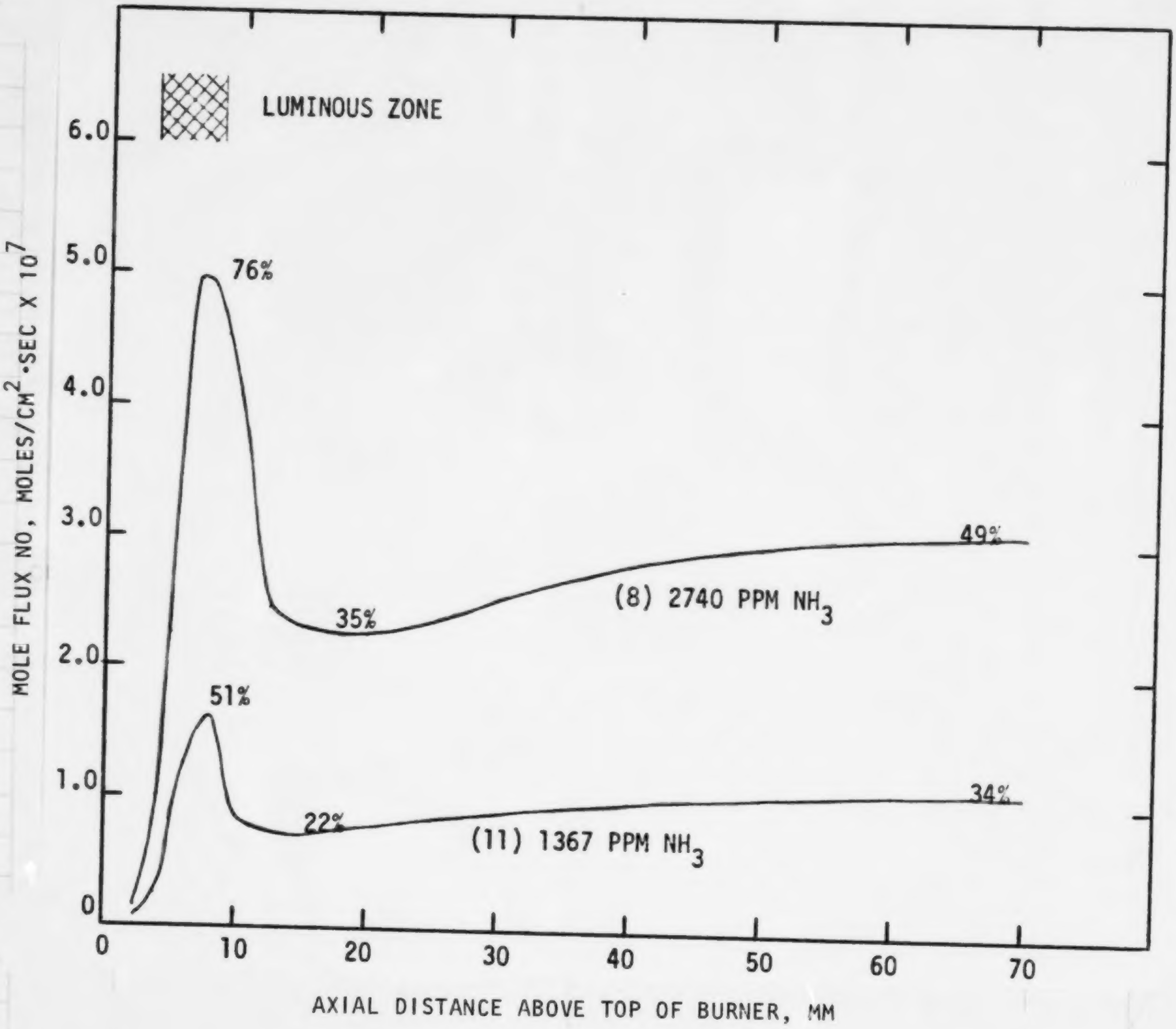

Figure 2-83. Effect of NH_3 Additive Concentration on NO Yields in a Fuel-Rich H_2-CO-O_2-Ar Low Pressure Flame

WARNING LINE

STOP

DOCUMENT NUMBER

PAGE NUMBER

CLASSIFICATION

TYPIST

USE SPECIAL DROPOUT BLUE PENCIL ONLY TO INDICATE CORRECTIONS

CLASSIFICATION

PAGE

STARTING LINE

Conclusions from Low Btu Fuel Combustion

The results obtained from the detailed probing of a fuel-rich ($\phi = 1.4$) H_2-CO-O_2-Ar flame with added NH_3 and/or NO indicate that a number of interesting and somewhat unexpected chemical processes are occurring. It should be remembered, however, that these conclusions are based on the measurement of the stable species that form when the hot combustion gases are rapidly quenched in a quartz probe.

Ammonia Addition. When NH_3 is added alone, the NH_3 is consumed below and near the bottom of the luminous zone (Fig. 2-60) forming some NO but mainly nitrogen species that are not measurable by the technique employed (i.e., they must form N_2 in the probe). These nitrogen species are then converted in high-yield to NO giving maximum NO yields in the luminous zone (based on added NH_3) of 50% to 75% (Fig. 2-83). Much of the NO that is formed initially from the NH_3 is consumed near the top of the luminous zone and then some NO reforms slowly far above the flame front giving overall yields of NO from NH_3 of 35% to 50%.

At the two initial NH_3 concentrations investigated, the higher initial concentration resulted in much higher maximum and final NO yields (Fig. 2-83). The slow formation of NO far above the luminous zone establishes that some very long-lived nitrogen species are formed (probably during the NO consumption process) that can react to form NO. This is verified by the observation that the addition of NH_3 to this flame causes a change in the color of the flame more than 40 mm above the luminous zone.

Nitric Oxide Addition. The addition of NO alone to this flame resulted in the consumption of about one-fifth of the NO in and above the luminous zone (Fig. 2-77) with a very small amount of NO reforming farther above the burner. This indicates that species are formed in the unseeded flame that can react with NO but species formed from the reaction of added NH_3 promote the consumption of NO to a much greater extent.

STOP

DOCUMENT NUMBER

CLASSIFICATION

TYPIST 227

STARTING LINE

Simultaneous Addition of Ammonia and Nitric Oxide. When both additives are included in the feed gas, 85% of the NH_3 and 60% of the NO are consumed below the luminous zone (Fig. 2-75). This indicates that a direct reaction is occurring between NH_3 and NO in the preflame region. The addition of the NO with the NH_3 decreases the apparent yield of NO from NH_3 to about zero. That is, the final NO concentration (Fig. 2-77) is about that which would have survived if this amount of NO had been added alone.

CENTERLINE

WARNING LINE

STOP

USE SPECIAL DROPOUT BLUE PENCIL ONLY TO INDICATE CORRECTIONS

TASK 3: DATA ANALYSIS

A number of calculations were carried out using a detailed kinetic-diffusion model to investigate the physical and chemical processes that occur in the low-pressure H_2-CO-O_2-Ar-NH_3 flame (experiment No. 8 in Section 2) under the conditions of this study. This modeling effort was conducted by T. Tyson and E. Kau of the Energy and Environmental Research Corporation (EER) under subcontract to Rocketdyne. Their final series of computations is reported here. An H_2-CO-O_2 flame was modeled rather than a CH_4-O_2 flame because the rate constants involved in the reactions of the fuel species in the former appear to be better established (i.e., the hydrocarbon chemistry is less certain).

It will be seen that it was not possible (at least at the time these calculations were made) to obtain even an approximate agreement between the predicted and measured mole fractions of the stable chemical species. A number of factors prevented the development of a satisfactory detailed model. Certain physical parameters were either unknown or were very uncertain. These included (1) temperature of the porous plate, (2) temperature of the screen (flame holder), (3) heat flux to the porous plate, and (4) gas temperature profile between the porous plate and the bottom of the luminous zone. In addition, many of the rate constants involved in the analysis were essentially unknown especially at the lower temperatures that exist below the flame front, and the carbon balance was not good in the experimentally measured products. Finally, there is a strong possibility that the metal screen can promote oxidation or recombination reactions.

The 59 reactions included in the computer model are listed in Table 3-1 along with their assigned rate constants and heat of reacton. All of the rate parameters were believed to represent the "best values" in 1978 except for reaction 14* in which the best value A-factor was multiplied by a factor of 100. This was necessary to cause the model to "hold" the flame to the burner. It was assumed in the calculations presented here that the flame holder screen is an efficient catalyst for the recombination of radicals. This assumption resulted in the closest agreement with the experimental results even though the agreement was poor.

---

*$CO + O + M = CO_2 + M$

USE SPECIAL DROPOUT BLUE PENCIL
ONLY TO INDICATE CORRECTIONS
CLASSIFICATION
PAGE
STARTING LINE

TABLE 3-1. REACTIONS INCLUDED IN KINETIC DIFFUSION MODEL

NO.	Reaction	Type[b]	Kinetic Parameter[a]			
			$\text{Log}_{10}A$	N	β	ΔH[c]
1	$H + O_2 = HO_2$	T	15.48	0	1.0	
2	$H + O = OH$	T	15.90	0	0	
3	$H_2O = OH + H$	T	24.36	2	122.6	119.4
4	$O + O = O_2$	T	18.00	1	0	-119.2
5	$H + H = H_2$	T	18.00	1	0	-104.2
6	$H + OH = H_2 + O$	B	17.43	0.94	14.69	-2.0
7	$O + OH = H + O_2$	B	11.80	-0.5	0	-17.0
8	$OH + H_2 = H + H_2O$	B	13.38	0	5.2	-15.2
9	$OH + OH = H_2O + O$	B	12.78	0	1.0	-17.2
10	$HO_2 + O = OH + O_2$	B	13.70	0	1.0	-55.1
11	$HO_2 + H = OH + OH$	B	14.38	0	1.9	-38.1
12	$HO_2 + H = O_2 + H_2$	B	13.38	0	0.7	-57.1
13	$HO_2 + OH = H_2O + O_2$	B	13.70	0	1.0	-72.3
14	$CO + O = CO_2$	T	18.56	1	2.5	-127.2
15	$CO + OH = CO_2 + H$	B	7.19	-1.3	-0.8	-25.0
16	$CHO = CO + H$	T	20.38	1.5	16.8	+16.7
17	$CHO + O_2 = CO + HO_2$	B	13.48	0	0	-30.4
18	$CHO + O = CO_2 + H$	B	11.5	0	0	-110.5
19	$CHO + O = CO + OH$	B	11.73	-0.5	0	-85.4
20	$CHO + OH = CO + H_2O$	B	14.00	0	0	-102.7
21	$CHO + H = CO + H_2$	B	10.48	-1	0	-87.5
22	$NH_2 + O_2 = NH_2 + HO_2$	B	11.70	-0.5	56.0	+56.0
23	$NH_2 + O = NH_2 + OH$	B	12.18	0	6.0	+1.0
24	$NH_3 + H = NH_2 + H_2$	B	7.28	-0.67	3.4	-1.1
25	$NH_3 + OH = NH_2 + H_2O$	B	17.51	0	19.0	-16.2
26	$NH_2 + O_2 = NH + HO_2$	B	13.00	0	50.5	+54.9
27	$NH_2 + O = NH + OH$	B	11.96	-0.5	0	-0.1
28	$NH_2 + H = NH + H_2$	B	11.15	-0.67	4.3	-2.2
29	$NH_2 + OH = NH + H_2O$	B	10.48	-0.68	1.3	-17.4
30	$NH_2 + NH_2 = NH_3 + NH$	B	11.23	-0.63	3.6	-1.1

DOCUMENT NUMBER
PAGE NUMBER
CLASSIFICATION

USE SPECIAL DROPOUT BLUE PENCIL
ONLY TO INDICATE CORRECTIONS

CLASSIFICATION

PAGE

STARTING LINE

TABLE 3-1. (Continued)

			Kinetic Parameter[(a)]			
NO.	Reaction	Type[(b)]	$\log_{10}A$	N	β	ΔH[(c)]
31	$NH_2 + NO = N_2 + H_2O$	B	12.74	0	0	-119.4
32	$NH + H = N + H_2$	B	11.80	-0.5	8.0	-29.1
33	$NH + O = NO + H$	B	11.80	-0.5	0	-75.9
34	$NH + OH = H_2O + N$	B	11.70	-0.5	2.0	-44.3
35	$NH + OH = NO + H_2$	B	11.70	-0.5	2.0	-77.9
36	$N + NO = N_2 + O$	B	13.49	0	0.3	-75.0
37	$N + O_2 = NO + O$	B	9.78	-1	6.3	-31.9
38	$N + OH = H + NO$	B	11.80	-0.5	0	-48.8
39	$NO + O = NO_2$	T	21.11	1.82	0	-73.2
40	$NO + H = HNO$	T	16.30	0	0	-49.2
41	$NO + HO_2 = NO_2 + HO$	B	11.70	-0.5	3.5	-9.2
42	$NCO + H = NH + CO$	B	11.70	-0.5	6.9	-26.5
43	$HNO + O = OH + NO$	B	11.70	-0.5	0	-53.0
44	$HNO + O = NH + O_2$	B	11.00	-0.5	7.0	+5.9
45	$HNO + OH = H_2O + NO$	B	12.00	0	1.0	-70.2
46	$HNO + H = H_2 + NO$	B	13.00	0	2.5	-55.0
47	$HNO + CO = CO_2 + NH$	B	11.00	-0.5	7.0	-2.1
48	$N_2O = N_2 + O$	T	14.60	0	51.4	+39.9
49	$N_2O + O = NO + NO$	B	14.00	0	28.0	-36.0
50	$N_2O + O = N_2 + O_2$	B	14.00	0	28.0	-79.2
51	$NO_2 + H = NO + OH$	B	14.50	0	1.5	-28.9
52	$N_2O + H = N_2 + OH$	B	13.90	0	15.0	-62.2
53	$N_2O + H = NH + NO$	B	11.00	-0.5	30.0	+39.9
54	$N_2O + OH = HO_2 + N_2$	B	13.50	0	15.0	-24.1
55	$HCN + OH = CN + H_2O$	B	11.30	-0.6	5.0	+4.4
56	$CN + O = CO + N$	B	11.80	-0.5	0	-77.0
57	$CN + H_2 - HCN + H$	B	12.79	0	5.3	-19.6
58	$CN + OH = NCO + H$	B	13.79	0	0	-23.4
59	$CN + CO_2 = NCO + CO$	B	12.57	0	0	+1.6

CENTERLINE

WARNING LINE

STOP

DOCUMENT NUMBER

USE SPECIAL DROPOUT BLUE PENCIL
ONLY TO INDICATE CORRECTIONS
CLASSIFICATION
PAGE

TABLE 3-1. (Concluded)

NOTES:

(a) The rate constant is defined as $k = A\cdot T^{-N} \exp(-1000\cdot\beta/RT)$ with units cm^3/mole-sec for bimolecular and "three-body" dissociation reactions, and $cm^6/mole^2$-sec for three-body recombination reactions.

(b) T denotes three-body reactions in which the rate is proportional to the total pressure and B denotes bimolecular (second-order) reactions.

(c) Heat of reaction at 298 K in kcal/mole.

DOCUMENT NUMBER

225

CLASSIFICATION
TYPIST

232

Shown in Fig. 3-1 is a comparison of the mole fractions of the major species measured in experiment No. 8 with the profiles calculated from the kinetic-diffusion model. It can be seen that the model predicts a lower flame temperature and that the main combustion reactions occur much nearer to the burner top than is observed.

Plotted in Fig. 3-2 are the predicted mole fractions of the radicals H, O, and OH. A very large concentration of H atoms (~4 mole %) is predicted even far above the flame front. These H atoms would probably recombine in the quartz probe. This would account for part of the difference between the two H_2 curves in Fig. 3-1.

The experimental and predicted profiles for the nitrogen species are compared in Fig. 3-3. In agreement with the trend in Fig. 3-1, the NH_3 is predicted to react much earlier than is observed experimentally. The predicted NO profile shows no indication of the consumption of NO above the flamefront that is observed. Therefore, some fuel nitrogen chemistry not included in the 59 reaction set must be occurring in the flame (or in the probe).

It was unexpected that the kinetic-diffusion calculations would predict that large concentrations of H, H_2, and O_2 exist well above the flame front without undergoing rapid reaction to form water. Our analysis of the EER calculations has led us to the conclusion that in their model H_2 is converted to H_2O in the low-temperature region of the flame via the fast metathesis reaction:

$$H_2 + OH \longrightarrow H_2O + H$$

but, at higher temperatures, this reaction reaches equilibrium and can no longer produce a rapid net production of H_2O even though the reaction is extremely rapid. H_2O must then form via slow three-body reactions.

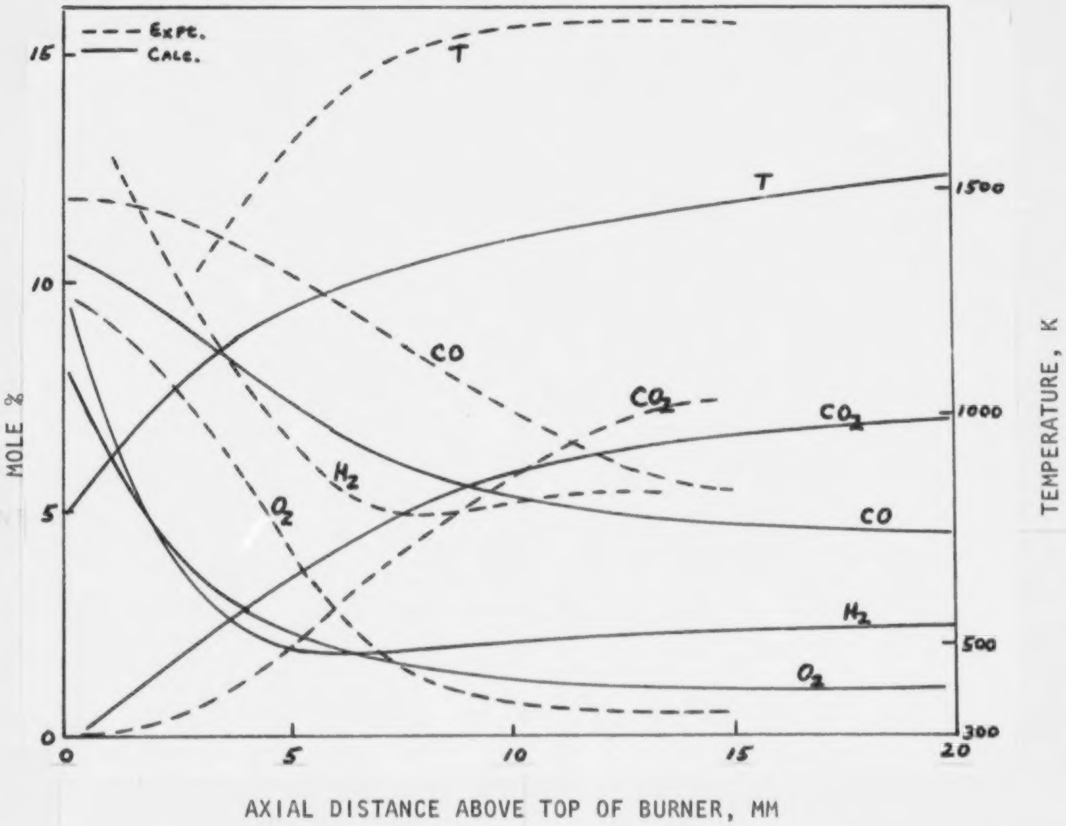

Figure 3-1. Comparison of Measured and Calculated Mole Fraction Profiles for Major Species (experiment No. 8, Tw = 800 K and Catalytic screen)

USE SPECIAL DROPOUT BLUE PENCIL
ONLY TO INDICATE CORRECTIONS
CLASSIFICATION
PAGE
STARTING LINE

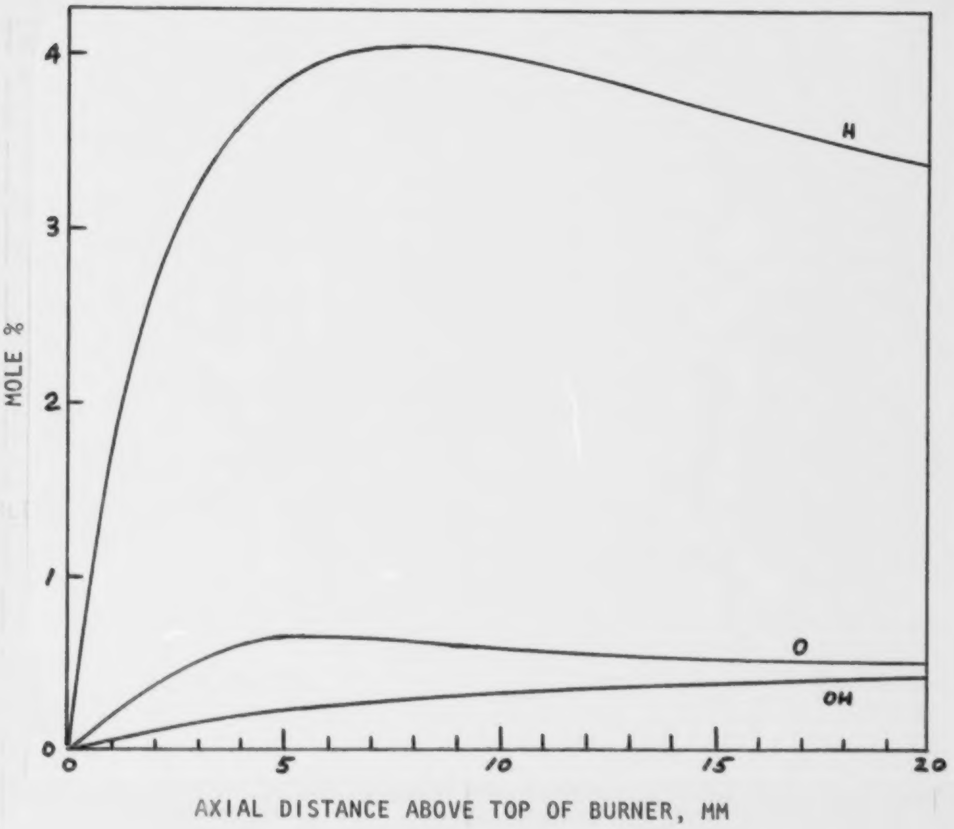

Figure 3-2. Free Radical Concentrations Predicted by Model

CENTERLINE
BARRING LINE
STOP
DOCUMENT NUMBER
PAGE NUMBER

CLASSIFICATION
TYPIST

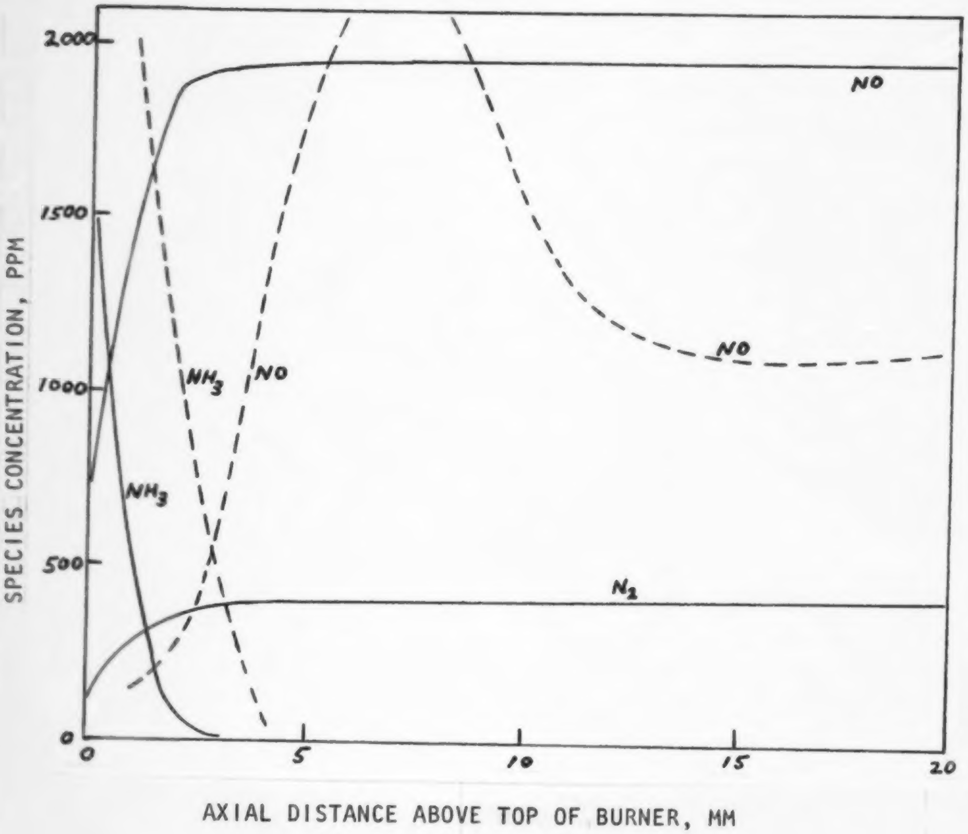

Figure 3-3. Comparison of the Measured and Calculated Mole Fraction Profiles of the Nitrogen Species

3-3

USE SPECIAL DROPOUT BLUE PENCIL
ONLY TO INDICATE CORRECTIONS
CLASSIFICATION
PAGE
STARTING LINE

It appears that a kinetic paradox is involved in this result because the rate of H_2O formation decreases rapidly solely from an increase in the temperature. It is difficult to believe that H_2 would burn faster if a heat sink were present to moderate the temperature rise, but that is what these kindetic calculations seem to indicate.

This kinetic trapping of the H atoms should be independent of the presence of CO and CO_2 and should also occur in an H_2-O_2 flame. The presence of CO_2 could catalyze the water gas shift reaction via:

$$H + CO_2 \longrightarrow OH + CO$$

and

$$H_2 + OH \longrightarrow H_2O + H.$$

CONCLUSIONS FROM KINETIC-DIFFUSION CALCULATIONS

CENTERLINE

The conclusions that can be drawn from the results of these calculations on a fuel-rich H_2-CO-O_2-Ar flame are limited to the following because of the pon fit between the predicted and experimental results: (1) deficiencies exist in the model and/or the experimental data, (2) the chemical reaction scheme employed predicts that about one mole percent O_2 will be present far above the luminous zone even under fuel-rich conditions and large concentrations of H atoms (4%) will be present in the pst-flame gases, and (3) the nitrogen-species model predicts that about 70% of the added NH_3 will be converted to NO below the luminous zone and the NO concentration remains constant thereafter. It appears that in addition to the deficiencies in the physical model and data, the chemical model for the nitrogen species does not contain all of the chemical reactions that are important in this system.

WARNING LINE
STOP
DOCUMENT NUMBER

CLASSIFICATION
TYPIST

USE SPECIAL DROPOUT BLUE PENCIL ONLY TO INDICATE CORRECTIONS
CLASSIFICATION
PAGE
STARTING LINE

APPENDIX A

DESCRIPTION OF FUEL SAMPLES

FUEL H

Fuel H is a No. 6 fuel oil supplied by Ultrasystems near the start of this program, 13 February 1976. According to their analysis, it contains 0.71% N. This fuel was used as the "baseline oil" throughout this study.

FUEL I

Fuel I is a liquefied coal prepared by the SYNTHOIL process. It was received from the ERDA-PERC on 17 December 1975. This oil was produced using a nominally 1/2-ton/day unit with a 14.5 foot long catalytic reactor. Conditions were 4000 psig, 450 C, liquid feed at 25 lb/hr. The catalyst was 1/8 inch pellets of cobalt moly on alumina. The analysis supplied is listed in Table A-1 and the analysis of the West Virginia Feed Coal (Pittsburgh Seam from Ireland Mine) is listed in Table A-2.

FUEL J AND K

A number of synthetic fuel samples were supplied to use in April 1976 by J. E. Haebig of Gulf Research and Development Co. The supplied analyses are listed in Table A-3. Fuel J was a full-boiling-range treated shale oil (Sample No. 12 in the table) and Fuel K was the treated middle distilled (Sample No. 17 in the table).

FUEL III

Fuel No. III is a Pittsburgh No. 8 seam coal supplied by Aerotherm/Acurex in January 1976. We had duplicate samples analyzed by Commercial Testing and Engineering in May 1976 (Table A-4). The results agreed except for the nitrogen values. The higher values agreed with the analyses obtained by Aerotherm (Table A-4).

Preceding page blank

USE SPECIAL DROPOUT BLUE PENCIL
ONLY TO INDICATE CORRECTIONS
CLASSIFICATION
PAGE
STARTING LINE

TABLE A-1. ANALYSIS OF SYNTHOIL

S in Product, wt %	0.60
Ash in Product, wt %	1.60
Viscosity of Product, SSF and 180 F	104
Specific Gravity of Product	1.14
N in Product, wt %	1.3
Solvent Analysis (wt %) (Ash Free)	
Organic Benzene Insolubles	7.2
Asphaltenes (Pentane Insolubles from Benzene Solubles)	28.1
Oil (Pentane Solubles from Benzene Solubles)	64.7

CENTER LINE

TABLE A-2. ANALYSIS OF SYNTHOIL FEED COAL

Proximate Analysis, wt % (as received)	
Moisture	1.6
Volatile Matter	41.6
Fixed Carbon	48.6
Ash	8.1
Ultimate Analysis, wt %	
Hydrogen	5.3
Carbon	73.8
Nitrogen	1.4
Oxygen	7.6
Sulfur	3.8
Ash	8.1
Forms of Sulfur, wt %	
Sulfate	0.09
Pyritic	1.79
Organic	1.92
Caloric Value, Btu/lb	13,400

WARNING LINE
STOP

USE SPECIAL DROPOUT BLUE PENCIL
ONLY TO INDICATE CORRECTIONS
CLASSIFICATION
PAGE
STARTING LINE

TABLE A-3. SAMPLES OF SYNTHETIC FUELS FOR USE IN ROCKETDYNE PROJECT FOR EPA ON COMBUSTION NO_x

Sample No.	Identity	Distillation, F (%)[a]	Elemental Composition, %			
			C	H	N	S
7	Anthracene Oil[c] (Reilly Tar & Chem Co.)	500 (10%) 900 (90%)	91.32	5.70	0.88	0.67
8	Raw Shale Oil	> 960°	85.80	10.05	2.68	0.62
9	Raw Shale Oil	680-960°[b]	85.43	11.24	2.02	0.35
10	Raw Shale Oil	375-680°[b]	84.84	12.16	1.55	0.61
11	Raw Shale Oil,[c] full boiling range	392 (10%) 960 (73%)	87.01	11.42	2.05	0.57
12	Treated Shale Oil full boiling range		86.84	13.11	0.27	0.04
13	Aromatic Heavy Distillate Petroleum Oil[c]	661 (10%) 978 (90%)	87.47	12.12	0.07	0.49
14	Hydrogenative Noncatalytic Coal Liquid, Middle Distillate	412 (10%) 606 (90%)	88.11	7.48	0.5	0.35
15	Hydrogenative Catalytic Coal Liquid Middle Distillate	374 (10%) 595 (90%)	79.99	7.34	0.52	0.17
16	Raw Shale Oil[c] Middle Distillate	270-670[b]	86.00	12.15	1.60	0.57
17	Treated Shale Oil, Middle Distillate	270-670[b]	86.31	3.64	0.18	0.04
18	Hydrogenative Catalytic Coal Liquid, not distilled	420 (10%)	83.18	8.96	0.40	0.04

---

a) ASTM D86, temp. at which given % vaporized.

b) Initial and final boiling points.

c) Larger amounts available, e.g., 1 gal.-1 bbl.

References:

J.E. Haebig, B.E. Davis, E.R. Dzuna, "Preliminary Small Scale Combustion Tests of Coal Liquids", Envir. Sci. Tech.

E.R. Dzuna, "Combustion Tests on Shale Oils", Meeting of the Central States Section of the Combustion Institute, Columbus, April 5-7, 1976.

LINE
STOP
DOCUMENT NUMBER

233

PAGE NUMBER
CLASSIFICATION
TYPIST

~~240~~ 241

TABLE A-4. COMPARISON OF ANALYSES ON AEROTHERM PULVERIZED COAL SAMPLES

	Pittsburgh #8 Seam				Montana Powder River		
	Com. Test. for Aerotherm	Pitts. Test. for Aerotherm	Com. Test. for Rocketdyne	Com. Test. for Rocketdyne	Com. Test. for Aerotherm	Com. Test. for Rocketdyne	Com. Test. for Rocketdyne
Ultimate Analysis, % dry							
Carbon		77.2	76.97	76.65	67.2	66.89	66.67
Hydrogen		5.2	5.25	5.24	4.4	3.89	4.44
Nitrogen	1.19	1.23	0.82	1.21	1.10	1.09	1.06
Sulfur		2.6	2.58	2.58	0.9	0.88	0.90
Oxygen		5.9	6.53	6.43	14.0	15.17	13.91
Ash		7.9	7.72	7.78	11.7		
BTU, wet		13,700	13,742	13,677	8,900	8,868	8,974
Proximate Analysis, % wet							
Volatiles		37.0	38.04	37.96	30.48	30.60	30.77
Fixed Carbon		54.0	52.72	52.50	39.0	39.41	39.47
Moisture		1.2	1.65	1.91	21.3	20.41	20.16
Ash		7.8	7.59	7.63	9.2	9.58	9.60
% N in Volatiles Residue			1.18	1.12		0.70	0.67

USE SPECIAL DROPOUT BLUE PENCIL
ONLY TO INDICATE CORRECTIONS
CLASSIFICATION
PAGE
STARTING LINE

FUEL IV

Fuel IV is a pulverized Montana Coal supplied by Aerotherm/Acurex. The analyses obtained by Rocketdyne and by Aerotherm are listed in Table A-4.

FUEL V

Fuel V is a Montana Lignite-A coal (Savage Mine, Hva-L) supplied by MIT in January 1976. The following analysis was supplied:

- Ultimate Analysis, % dry

C	55.21
H	4.93
N	0.61
S	0.85
O (diff)	16.50

- Btu/lb (moist MM free) 8800

Proximate Analysis, % wet

H_2O	13.60
VM	36.6
Ash	8.3

FUEL VI

Fuel VI was a COED char supplied by the University of Arizona. It contains 0.98% nitrogen.

WARNING LINE
STOP
DOCUMENT NUMBER

253

TYPIST 0-5721 242 243

USE SPECIAL DROPOUT BLUE PENCIL ONLY TO INDICATE CORRECTIONS
CLASSIFICATION
PAGE
STARTING LINE

APPENDIX B

CHEMICAL ANALYSIS TECHNIQUES

The chemical analysis techniques used in or developed for the previous inert pyrolysis study were discussed in Appendix A of Ref. 1. Some of these techniques were not suitable for use in oxidative pyrolysis experiments, because of the presence of large amounts of oxygen in the carrier gas, and had to be modified. These modified techniques are described herein.

HYDROGEN CYANIDE MEASUREMENT

For the inert pyrolysis experiments, the Modified ASTM method D2036-72, described in Appendix A and C of Ref. 1 is quite satisfactory and gives good sensitivity (~0.2 mg). The HCN is scrubbed from the carrier gas in Na_2CO_3 solution. After neutralization of the solution, chloramine-T is added to oxidize the cyanide and then barbituric acid in pyridine is added to develop a color that is measured spectrophotometrically. When fuels containing sulfur are pyrolyzed, $CdCO_3$ is suspended in the Na_2CO_3 collecting solution to react with the sulfide ions before they can react with the cyanide ions. The $CdCO_3$ is centrifuged from solution immediately after the sample flow through the bubbler has stopped.

This colorimetric method for measuring HCN was also found to be satisfactory for use in the experiments on the oxidative pyrolysis of the model compounds pyridine and benzonitrile because these samples contain no sulfur. In the experiments involving the oxidative pyrolysis of fossil fuels, however, much or most of the fuel sulfur is likely to form SO_2 that will be trapped in the alkaline scrubber solution used for collecting HCN and form sulfite ions.

It was found in the previous program that, under inert pyrolysis conditions, any sulfide ion collected in the aqueous scrubber solution interferes with the colorimetric method for HCN determination but this interference could be eliminated by using dispersed $CdCO_3$ in the scrubber solution. However, it was discovered that $CdCO_3$ did not eliminate the interference caused by "aged" sulfide ion.

CENTERLINE
WARNING LINE
STOP
Preceding page blank
DOCUMENT NUMBER

CLASSIFICATION
TYPIST

1049 243 245

STARTING LINE

Further investigation revealed that sulfite ion also interfered in the color development. Sulfite at 20 to 40 times the CN^- level, on a weight basis, caused a 50 to 80% reduction in color development.

Most No. 6 fuel oil samples have sulfur-to-nitrogen weight ratios between 1 and 6 with the average being about 3. In most coal samples, this ratio is lower by about a factor of 2 because of the higher nitrogen contents of the coals. Therefore, the worst case likely to be encountered with respect to SO_2 interference is with a fuel that has a sulfur to nitrogen ratio of 5, and a conversion of nitrogen to HCN in a yield of about 15%. In this case, the maximum weight ratio of SO_2/HCN would be about 35 (the molecular weight ratios SO_2/HCN and S/N are nearly identical) and significant interference would be expected.

Three methods of eliminating the sulfite interference in the colorimetric determination of HCN were investigated: (1) use of lead carbonate to remove $SO_3^=$; (2) initial addition of Chloramine T to the bubbler solution to prevent interaction between $SO_3^=$ and CN^-; and (3) low-temperature scrubbing or trapping of the effluent to prevent interaction between $SO_3^=$ and CN^-.

CENTERLINE

Use of $PbCO_3$ to Remove $SO_3^=$

Lead and cadmium carbonates have been recommended for removal of sulfide from aqueous solutions prior to colorimetric determination for cyanide. It appeared from the relative solubilities of the various salts of lead that lead carbonate might also effect the removal of sulfite from aqueous solutions. The following tabulation shows the relative solubilities of lead and cadmium compounds:

Element	Solubilities in Water			
	Carbonate	Cyanide	Sulfite	Sulfide
Lead	0.00011 g/100 g	v.sl.s.	i	0.00009 g/100 g
Cadmium	i	0.00247 g/100 g	sl,.s	0.000001 g/100 g

STOP

103 [illegible] 246

USE SPECIAL DROPOUT BLUE PENCIL
ONLY TO INDICATE CORRECTIONS
CLASSIFICATION
PAGE

Experiments to prove the utility of lead carbonate failed however. In the presence or absence of dispersed lead carbonate, the addition of 16 micrograms of $SO_3^=$ to a solution containing 2.7 micrograms of HCN resulted in only about 25% recovery of the CN^- value by the colorimetric method.

Initial Addition of Chloramine T to Bubbler Solution

The first step in the colorimetric method after collecting the sample is the addition of Chloramine T to the solution at pH 6-7 to convert CN^- to cyanogen chloride, CNCl. If Chloramine T were added to the aqueous scrubber solution before collection of the sample, the sulfite interference might be eliminated since conversion of CN^- to CNCl would occur before interference by $SO_3^=$. In a static system, this approach was successful. However, when applied to a flowing system (with either He or O_2 bubbling through the aqueous scrubber solution), recovery of CN^- was low (85%) presumably because some of the CNCl evaporated into the carrier gas before the barbituric acid reagent was added. When it was found that prior addition of both reagents, to the scrubber solution resulted in no color formation at all, this approach was abandoned.

Low-Temperature Sample Collection

A series of experiment was carried out with a flowing system of either He, He and O_2, or O_2 to study the effect of low temperature trapping of HCN and SO_2 in an aqueous scrubber and to determine if the interaction of $SO_3^=$ and CN^- could be prevented by lowering the temperature significantly. Table B-1 summarizes the results obtained. The reduced temperature experiments were carried out in the following manner: a known amount of CN^- was pipetted into 25 ml of scrubber solution (125 mg Na_2CO_3/25 ml). The solution was cooled in an ice bath and then attached to the exit of the fuel pyrolysis apparatus, so that the carrier gas bubbled through at a rate of 40 cc/min. SO_2 was immediately injected into the flowing gas at the apparatus inlet and flow continued for 3 minutes with the scrubber solution maintained at low temperature. The scrubber was then removed and immediately analyzed for CN^- by the colorimetric method. It can be seen that

USE SPECIAL DROPOUT BLUE PENCIL
ONLY TO INDICATE CORRECTIONS
CLASSIFICATION
PAGE
STARTING LINE

TABLE B-1. EFFECT OF TEMPERATURE ON HCN RECOVERY

ug HCN Added	ug SO_2	SO_2/HCN (wt ratio)	Scrubber Temperature, °C	Gas Flow	HCN Recovery, percent
2.7	--	--	25	He*	98.0
2.7	258	96	25	He*	62.2
2.7	258	96	0	He*	83.1
2.7	258	96	-10 (20% MeOH)	He*	79.8
2.7	129	48	0	He*	93.0
2.7	129	48	0	He*	97.9
2.7	129	48	0	He (20% O_2)*	94.7
2.7	129	48	0	O_2*	96.2
6.75	129	19	25	O_2*	73.4
6.75	129	19	0	O_2*	98.8

*3 minutes--Time between SO_2 introduction and removal of scrubber from flow system

at a SO_2/HCN ratio of 48, the recovery of HCN averages better than 95% at 0^{o}C. At higher SO_2/HCN ratios, recovery is incomplete down to -10 C. At an SO_2/HCN ratio of 19, only 73% of the HCN is received at 25 C. These experiments indicate that at the SO_2 levels encountered in the oxidative pyrolysis of fuel oils and coal, the interference in the colorimetric HCN method can be negated by simply maintaining the scrubber solution at ice bath temperature. This modified procedure was used, therefore, in the study of the oxidative pyrolysis of fossil fuels.

NITRIC OXIDE AND NITROGEN DIOXIDE MEASUREMENT

A TECO Chemiluminescent Analyzer was used to measure the NO_x formed in the model compound oxidative pyrolysis experiments and a trapping technique was used in conjunction with the Saltzman reagent to measure NO_x from the oxidation of fossil fuels.

WARNING LINE
STOP
DOCUMENT NUMBER

CLASSIFICATION
TYPIST 1052 24 248

Model Compound Oxidative Pyrolysis

The model compound oxidative pyrolysis experiments were continuous steady-state experiments so that it was possible to flow the carrier gas stream from the reactor through the TECO Chemiluminescent Analyzer (CA) to measure NO and NO_2. A moly converter in the CA, operating at 450 C, converted NO_2 to NO so that the NO_2 could be measured by difference (with or without the converter in line).

The product stream from the model compound reactor flowed continuously through a gas-sampling valve (Fig. 1-5) and was vented to a hood when the CA was not being used. For the NO measurements, the reactor effluent flowed through a needle valve and then into the CA. The needle valve was adjusted to maintain atmospheric pressure in the model compound reactor. The CA was calibrated by flowing the same amount (40 cm^3/min) of NO-He and NO-N_2 standards into it. At the O_3/O_2 flowrate employed and a chamber pressure of 9 torr, the NO reading was nearly proportional to the sample flowrate and independent of the molecular weight of the sample gas.

Calibration experiments were conducted in which NO and NO_2 standards were flowed through the reactor under various conditions. Quantitative recovery of NO_2 was never achieved. A standard containing 107 ppm NO_2 in N_2 usually read only 60 to 95 ppm NO_x on the CA whether it was flowed directly from the bottle or through the reactor and part of the NO_2 was measured as NO. It is possible that a part of the NO_2 in this standard had decomposed to NO in the bottle. The following results show, however, that the NO_2 standard did not change in composition when passed through the reactor (without oxygen) at temperatures below 800 C:

Reactor Temperature, C	Measured, ppm		
	NO_2	NO	NO + NO_2
206	75	19	94
587	72	23	95
701	69	25	94
736	68	26	94
898	23	72	95

A mixture of NO in helium was prepared so that NO could be flowed through the model compound system at a concentration of 0.8%. With helium as the carrier gas, all of the NO reached the CA at all reactor temperatures. With 75% O_2 in the carrier gas, however, only about one-third of the NO reached the CA (as either NO or NO_2) at all reactor temperatures. In the presence of O_2 only about 10% of the NO is recovered as N_2. The remainder must have been converted to NO_2 and then somehow formed a solid salt on the wall of the flow system. Calculations indicate that the homogeneous reaction of NO with O_2 is too slow to account for this amount of reaction at the flowrates involved. A heterogeneous oxidation of NO must be occurring at some point in the system. These results indicate that a probe would have to be installed at the exit of the reactor if reliable NO and NO_2 measurements were to be made.

It can be seen from the above calibration experiments that the actual yields of NO and NO_2 may be greater than the values measured by this technique.

Fossil Fuel Oxidative Pyrolysis

In the fuel oxidative pyrolysis experiments, the products are formed and swept out of the reactor in a very short period of time (probably less than 1 second). It might be possible to measure the NO formed under such conditions with the TECO CA by recording and integrating the CA output curve. However, this approach did not appear promising so a modification of the Saltzman technique used previously (Appendix A and E of Ref. 1) was selected.

To measure NO by the Saltzman procedure it must be mixed with oxygen at a sufficiently high NO concentration that it will be oxidized to NO_2 in a reasonable length of time. For that reason, a method was developed in which the NO present in the product stream is trapped in one loop of Beckmann gas sampling valve. In this way the collection of the sample did not have to be timed with the initiation of the pyrolysis process and the sample could be introduced into an evacuated flask containing the Saltzman reagent at 0 C by simply turning the sampling valve. The flask was then filled with O_2 at atmospheric pressure and the next day the color of the reagent was measured.

USE SPECIAL DROPOUT BLUE PENCIL
ONLY TO INDICATE CORRECTIONS
CLASSIFICATION
PAGE
STARTING LINE

Since the NO is well below its vapor pressure at -196 C, a method of trapping the NO out of the product gas stream had to be developed. The method developed was fairly satisfactory at the 2 μgm level of NO.

It was found that small amounts of NO could be readily trapped on molecular sieve 13X at -80 C. However, when the NO was released into a Saltzman reactor by heating the trap rapidly to room temperature little of the absorbed NO was recovered. Increasing the release temperature to as high as 300 C did not increase the NO recovery above 50%. Thus, a molecular sieve 13X trap is not satisfactory for this purpose.

It was found that NO can be trapped on stainless steel at -196 C and released near quantitatively at room temperature. A calibration gas containing 2.4 micrograms of NO (10 cc of the 202 ppm NO-N_2 standard) was injected into a helium carrier gas upstream of the fuel reactor, which was at room temperature. The reactor effluent was passed through an empty stainless-steel trap cooled with LN_2 and then vented. The gas sampling valve attached to the cooled trap was turned to an evacuated flask containing 20 ml of Saltzman reagent. The trap was then warmed and O_2 was passed through the trap to fill the Saltzman flask. The average recovery of NO under these conditions was 87% (after allowing 16 to 20 hours for the NO to oxidize). When the carrier gas was 20% O_2 in helium and a 10-minute purge was allowed before switching the loop out of the carrier gas stream, the average recovery of NO was 84%. The latter condition represents the situation that is encountered in the slowest of the single-stage fuel oxidation experiments. The mechanism by which the NO was trapped must be due to adsorption on the metal surface since the vapor pressure of NO is such that it would not remain condensed under these conditions.

When the above procedure was calibrated later in the program (2.5 μgm NO and helium carrier gas), recoveries on the order of only 30% were obtained with this same trap. Use of a new stainless-steel trap increased the average recovery to about 75%. It is likely that an activation procedure could be developed that would increase the effectiveness of these traps and their reproducibility. When the 2:1 O_2/He carrier gas was used in these calibration experiments (with the new trap), however, the NO recovery was decreased dramatically. In the previous single-stage and calibration experiments, the carrier gas contained only 20% oxygen and 85% recoveries of NO were obtained.

Since the vapor pressure of O_2 is about 180 torr at the boiling point of nitrogen and the 2:1 carrier stream contained nearly 500 torr O_2, it was hypothesized that O_2 was condensing on the wall of the trap covering the active absorption sites. With 20% oxygen, the partial pressure was 150 torr and the O_2 did not condense. The vapor pressure of O_2 is about 500 torr at the boiling point of argon (-189 C) and, therefore, O_2 should not condense from the carrier gas with this coolant. Calibration experiments confirmed this to be the case. With argon as the coolant, ~70% recoveries of NO were obtained with helium or the 2:1 O_2/He mixture as the carrier gas. The argon-cooled empty stainless trap was used in conjunction with the Saltzman procedure to measure the NO formed in the oxidative pyrolysis of fossil fuels. Since this trapping technique is only about 70% effective, the NO values obtained were corrected by dividing by 0.7.

Just at the end of this program, it was established under an Air Force-sponsored program at Rocketdyne (Contract F08635-77-C-0064) that the packing of the stainless-steel trap with powdered stainless-steel (36% nickel) greatly increased the low-temperature NO trapping efficiency without increasing the retention of NO at elevated temperatures.

NITROUS OXIDE, CARBON DIOXIDE AND ETHANE

In the inert pyrolysis experiments, the N_2O and CO_2 were measured simultaneously by isothermal gas chromatography using a molecular sieve 5A column at 160 C. The smaller N_2O peak just reaches the baseline before the CO_2 peak is eluted.

In the oxidative pyrolysis of the model compounds, the gas sample in the Caryle gas sampling valve is simply introduced into the helium carrier gas stream to this GC. The oxygen peak was eluted well ahead of the N_2O peak which was followed by the CO_2 peak.

The carrier gas from the fuel oxidative pyrolysis experiments could not be flowed directly into the GC because it contained one-third oxygen. It was found that the N_2O and CO_2 could be effectively trapped in a Beckmann gas sampling valve on molecular sieve 13X at room temperature. The H_2O and CO_2 were then introduced into the GC carrier gas stream by turning the valve and then heating the trap rapidly to 150 C. This transfer technique had another advantage in that it allowed the reactor to be operated at atmospheric pressure.

Some other product peaks also appeared besides N_2O and CO_2 but none of these interferred with the N_2O peak as long as the trap was kept packed with fresh material. Because one of the other product peaks tended to overlap the CO_2 peak on the 5A GC column, it was necessary to replace the GC column with Poropak Q at 40 C to separate the CO_2 from the other peak that was identified as ethane based on its retention characteristics on the two GC column materials and on the molecular sieve 13X in the trap. The ethane could also be measured using the 13X trap and the Poropak Q GC column.

NITROGEN AND CARBON MONOXIDE

In the inert pyrolysis experiments, the molecular sieve GC column was operated at room to separate and measure the N_2 and CO. This GC column was also used to measure the N_2 and CO in the model compound oxidative pyrolysis experiments by use of the Caryle gas sampling valve. Since no method was developed for effectively trapping N_2 and CO from the oxygen-containing carrier gas, these species were not measured in the oxidative pyrolysis of fossil fuels. Preliminary trapping tests indicated that N_2 can be trapped on molecular sieve 13X at -80 C and released at room temperature.

AMMONIA

The phenate method described in Appendix A of Ref. 1 was used in this study without modification.

APPENDIX C

TEMPERATURE MEASUREMENT IN FLAMES

At the end of the 68-02-0635 program (Ref. 1) both the thermocouple and the quartz probe used in the flat flame burner experiments were in a damaged condition. A new quartz probe and 17 Al_2O_3-coated thermocouples were fabricated at the Rockwell Science Center for use on this program. These thermocouples were quite satisfactory but failed in the low Btu fuel flames as described in the text.

THERMOCOUPLE FAILURE IN PRELIMINARY LOW BTU EXPERIMENT

Following the preliminary low Btu gas trials, the failed 3-mil Al_2O_3-coated Pt-Pt/10%Rh thermocouple was inspected under a binocular microscope. It revealed that a thin film of a reddish-brown substance had become deposited on the Al_2O_3 coating. No deposit was observed on the bare 10-mil Pt or Pt/Rh support wires.

Gaydon (Ref. 33) reports that carbon monoxide which has been stored in steel cylinders is often contaminated with iron carbonyl, and that CO flame spectra then show strong bands of iron oxide. A telephone conversation with a technical representative from Matheson Gas Products confirmed the existence of iron carbonyl in cylinders containing CO. Apparently the high surface roughness of the iron cylinder wall and the high CO partial pressure is sufficient to result in iron carbonyl formation in trace quantities.

It appeared likely that iron carbonyl from the H_2/CO cylinder passed through the inlet flow lines of the flat-flame burner system, reacted in the flame to produce iron oxide and subsequently vapor deposited onto the thermocouple wire. The fact that the thermocouple wire melted was surprising, since the adiabatic flame temperatures for the H_2-CO-O_2-Ar flames tested were below those for corresponding CH_4-O_2-Ar flames and the combustion products are similar. It should be noted that the emissivity of an Al_2O_3-coated Pt wire is about 0.2 at these flame conditions, whereas that for an iron oxide surface is roughly 0.9.

---

33. A. G. Gaydon, "The Spectroscopy of Flames," 2nd ed., New York, John Wiley & Sons, 1974.

Preceding page blank

Y2-0317 255

Both sources of information suggested that iron carbonyl can be removed by passing the gas through a bed of activated charcoal. Therefore, prior to experiment No. 7, a packed bed of activated charcoal pellets (American Norit Co., type RBW-1) was installed immediately downstream of the H_2/CO cylinder regulator. Gas samples obtained before and after passing through the charcoal trap were analyzed via GC for CO and H_2 and indicated no difference in the H_2/CO ratio due to the charcoal bed. The charcoal trap was used in all subsequent burner experiments involving CO as a fuel. However, this did not resolve the thermocouple failure problem.

THERMOCOUPLE FAILURE IN EXPERIMENT NO. 7

The thermocouple probe employed in experiment NO. 7 was initially inspected under a binocular microscope. The Pt-Rh alloy side of the 3-mil wire had melted approximately midway between the thermocouple junction and the 10-mil Pt-Rh support wire (forming a bead at each side of the break). In the region of the thermocouple junction,the Al_2O_3 coating had the usual crazed or fine cracked structure, but there wre no visible bare metal patches exposed. Where the 3-mil Pt and Pt/Rh wires were attached to the 10-mil leads, the coating had become considerably damaged and patches of Al_2O_3 had deposited onto the 10-mil support wires. The Al_2O_3 coating on the 3-mil wires wrapped around the 10-mil support wires had completely disappeared.

Both segments of the 3-mil thermocouple employed in experiment No. 7 were subjected to electron microprobe and X-ray dispersive analysis. An identical but unused 3-mil Al_2O_3-coated Pt-Pt/10%Rh thermocouple was similarly tested for comparison. The X-ray dispersive analysis gave no indication of any impurity in either the used or unused wires. Specifically, no traces of Fe, Si, or Cu were detected beyond the background noise of the instrument. This indicates that the charcoal trap is working satisfactorily and the failure of the first thermocouple was not caused by the deposition of the iron oxide.

The electron microprobe photographs, however, revealed several intersting features. First, the coating on both the Pt and Pt/Rh portions of the used wire were considerably damaged, with large areas of the bare metal surface exposed. The coating at the junction appeared to be less disintegrated than for adjacent regions along each wire. The attack of the coating on the Pt/Rh side appeared to be more severe than on the Pt side. Surprisingly, the Al_2O_3 coating on the unused thermocouple was not completely uniform. Large patches of bare metal were exposed at the thermocouple junction and along both the Pt and Pt/Rh wires. Apparently the sputtering procedure used to apply this coating was not completely satisfactory.

ASSESSMENT OF THERMOCOUPLE PROBLEM

It would appear that there are three possible explanations for the failure of the Pt-Rh thermocouple wire:

1. Due to the imperfect Al_2O_3 coating, catalytic oxidation and recombination reactions occurring at the bare metal surface cause sufficient local heating to melt the Pt-Rh wire.

2. An impurity in the alumina coating is reduced at high temperature in the presence of H_2 to form a compound which then is transported to the metal surface, causing embrittlement and/or formation of a low-melting point eutectic with the Pt/Rh alloy.

3. The high-temperature H_2-rich atmosphere reacts with the alumina, reducing it to Al which then diffuses in the bulk noble metal to form a low melting eutectic with the Pt/Rh alloy.

Explanation (1) is not acceptable since both Pt/Rh and Pt are good oxidation catalysts. As revealed by the scanning electron microphotographs, large patches of bare metal existed on both sides of the thermocouple junction. Since Pt has a lower melting point than Pt-10%Rh (by about 60 C), it would be more reasonable to find the Pt side melting first.

Explanation (2) is reasonable since there are a number of literature references (Ref. 34 through 36) that describe the instability of Pt/Rh alloys sheathed in refractory oxides. Impurities such as iron oxide and silicon oxide are known to be reduced at high temperatures to form Fe or Si. These can be readily transported to the wire surface, diffuse into the bulk noble metal, and result in the formation of a low melting point eutectic which causes premature mechanical failure. The problem with this reasoning is that the X-ray dispersive analysis of the Pt-Rh melt revealed no detectable impurity other than Al. In addition, the alumina used in the vacuum RF sputtering of the 3-mil thermocouple wires was of 99.98% purity (MARZ grade Al_2O_3, Materials Research Corp.). It would appear that any impurity arising from the alumina would be too low in concentration to cause any serious degradation of the Pt-Rh wire.

The third explanation is the most likely, but no literature data has been found to confirm this hypothesis.

APPROACH TO SOLUTION OF THERMOCOUPLE PROBLEM

Since one of the main objectives of the current experimental series is to provide fundamental kinetic data on the conversion of fuel-nitrogen species in a low Btu gas system under fuel-rich conditions, it is essential to utilize a coated thermocouple which will not rapidly deteriorate under high-temperature reducing atmospheres. It would appear from the previous discussion that the present Al_2O_3 coating on the Pt-Pt/10%Rh thermocouple plays some role in the degradation of the Pt-Rh alloy. Thus, the solution to the thermocouple problem is one of finding a better coating material.

---

34. B. E. Walker, C. T. Ewing, and T. T. Miller, Rev. Sci. Instr., 33, 10 (1962).
35. A. S. Darling and G. L. Selman, "Some Effects of Environment on the Performance of Noble Metal Thermocouples," Temperature, Its Measurement and Control in Science and Industry, vol. 4, pt, 3, Instrument Society of America, 1972.
36. P. A. Kinzie, "Thermocouple Temperature Measurement," New York, John Wiley & Sons, 1973.

Kent (Ref. 37) has described a mixed oxides coating for Pt-Pt/Rh thermocouples which prevents catalytic action in flames and is capable of withstanding high temperature H_2 environments. The coating is composed of yttrium oxide containing 10 to 15% beryllium oxide. It has a fusing temperature below the melting point of platinum and can be used for protection up to a wire temperature of 1875 K. Kent reports no reactivity between the coating and the thermocouple. There was no drift of the thermocouple within 1.0% experimental error after 20 hours in a Meker burner flame at 1775 K (wire temperature) or 0.5% error after 15 hours in a turbulent H_2 diffusion flame at a similar temperature. The coating is prepared by dissolving both ingredients in HCl. The solution is mixed to the consistency of a thin cream and then painted onto the thermocouple. Firing of the coating is accomplished at approximately 1875 K using a Meker burner.

Several other workers involved in high-temperature flame chemistry used this yttrium oxide-beryllium oxide coating apparently with some degree of success. Arthur Levy at Battelle has coated 3-mil Pt-Pt/10%Rh thermocouples with this mixed oxide to study H_2/CO flames at fuel-lean and stoichiometric conditions. Daniel Seery at UTRC has used this same oxide coating on 3-mil Ir-Ir/40%Rh thermocouples in the study of CO flames.

From the above data, the Y_2O_3-BeO coating appears to be a promising solution to the requirement for a coating which can withstand high-temperature reducing atmospheres. Therefore, some effort was directed to the preparation of this mixed oxide coating and to its firing onto a 3-mil Pt-Pt/10%Rh thermocouple. A mixture of 12.5 wt % BeO in Y_2O_3 was dissolved in HCl to the consistency of a thin paste. For this mixed oxide composition, firing of the coating is accomplished at approximately 1875 K. Several attempts at firing the coating onto the thermocouple wire were made using a microtorch initially, and then subsequently using a Meker burner. These attempts were unsuccessful, resulting only in melting the Pt side of the 3-mil thermocouple wire (Pt M.P. = 2040 K). It became readily apparent that firing of the Y_2O_3-BeO coating onto Pt-Pt/10%Rh would not be a simple procedure.

---

37. J. H. Kent, Comb. & Flame, 14, 279 (1970).

One practical solution to this problem appeared to be to utilize a thermocouple wire pair with higher melting point properties than those of Pt and Pt/10%Rh. Dr. Seery at UTRC has used the Y_2O_3-BeO coating on 3-mil Ir-Ir/40%Rh thermocouples in the study of CO flames. The melting point of Ir is 2720 K, while that of Ir/40%Rh is 2523 K. A small quantity of 3-mil and 10-mil Ir and Ir/40%Rh wires was obtained. However, several attempts at forming the thermocouple probe failed. In each case the 3-mil Ir wire immediately adjacent to the junction bead broke after only a minimum of handling during spot-welding of the 3-mil wire to the 10-mil support wire.

Several studies have shown that Ir will fail much sooner than IR/Rh alloys (Ref. 38 and 39). It has been found that heating Ir to high temperatures (above 1300 K) can cause excessive grain growth and severe embrittlement.

R 10
38, 39

RESULTS WITH AN Ir/Ir-40%Rh THERMOCOUPLE

A thermocouple was fabricated for use on this program by the United Technologies Research Center under the supervision of Dr. Seery. The construction of the Ir/Ir-40% Rh thermocouple probe was identical to the Pt/Pt-10% Rh thermocouple probe used in all previous experiments. The 3-mil Ir and IR-40% Rh thermocouple wires were flame welded to form the junction and spot-welded to 10-mil support wires of Ir and IR-40% Rh. The latter were strung through a two-hole alumina tube and held in place with Saureisen cement. The 3-mil Ir/Ir-40% Rh thermocouple wire was coated with a mixture of approximately 12.5 wt % beryllium oxide in yttrium oxide. Firing of the coating onto the 3-mil wire was accomplished in a Meker burner flame at about 1875 K.

A series of detailed temperature measurements was subsequently performed using this thermocouple at the conditions previously used in experiment No. 8: a H_2-CO-O_2-Ar flame at an equivalence ratio of 1.40, a diluent ratio of 1.90, a total

---

38. C. E. Moeller, M. Noland and B. L. Rhodes, NASA SP-5050, 1968, Office of Technology Utilization, NASA, Washington, D.C.
39. E. O. Zysk and A. R. Robertson, "New Thermocouple Materials," Temperature, Its Measurement and Control in Science and Industry, H. H. Plumb, Editor-in-Chief, Instrument Society of America, Pittsburgh, 1972, Vol. 4, Part 3, p. 1967.

system pressure of 50 torr, and a total gas feedrate of 8750 cc/min. NH_3 was added to the flame at 2620 ppm on a total feed basis. The temperature profile of a similar flame containing some methane was also measured.

The raw emf data (Fig.C-1) obtained with the coated Ir/Ir-Rh thermocouple produced a very low noise/signal ratio in the luminous zone region of the rich low Btu flame compared to that of the Pt/Pt-Rh thermocouple. This is an indication of the relative stability of the Y_2O_3-BeO coating on the IR/Ir-Rh wire. Inspection of the thermocouple under a binocular microscope following the detailed probing measurements confirmed this hypothesis. The coating was not visibly affected by the fuel-rich conditions of the low Btu experiment which continued over a period of about 5 hours.

Analysis of the emf data indicated that the corrected gas temperature profile measured with the Ir/Ir-40% Rh thermocouple is higher than the corresponding profile measured with the Pt/Pt-10% Rh thermocouple. There are two reasons for this conclusion. First, the thermocouple wire temperatures are higher for the Ir/Ir-Rh wire than for the Pt/Pt-Rh wire at corresponding axial locations over the entire distance scale (Fig. C-1). Secondly, the radiation correction term for the coated Ir/Ir-Rh wire is reported to be much larger than for the coated Pt/Pt-Rh wire. In a private communication, Dr. Seery stated that he found the average emissivity of the 3-mil Y_2O_3-BeO Ir/Ir-40% Rh thermocouple wire to be $\varepsilon_m=0.67$ between 1300 to 1700 C. An average emissivity of $\Sigma=0.20$ had been used to calculate the radiation correction form for the Al_2O_3-coated Pt/Pt-10% Rh thermocouple wire in all of previous experiments of this study. Because the radiation correction is proportional to the wire emissivity, the radiation correction for the coated Ir/Ir-Rh wire will be substantially greater than that for the coated Pt/Pt-Rh wire.

Based on these considerations, it appears that the corrected measured temperature is unreasonably high. The only explanation appears to be that the emissivity of the coating must be much less than the value reported by Seery. Therefore, additional flame temperature calculations were carried out.

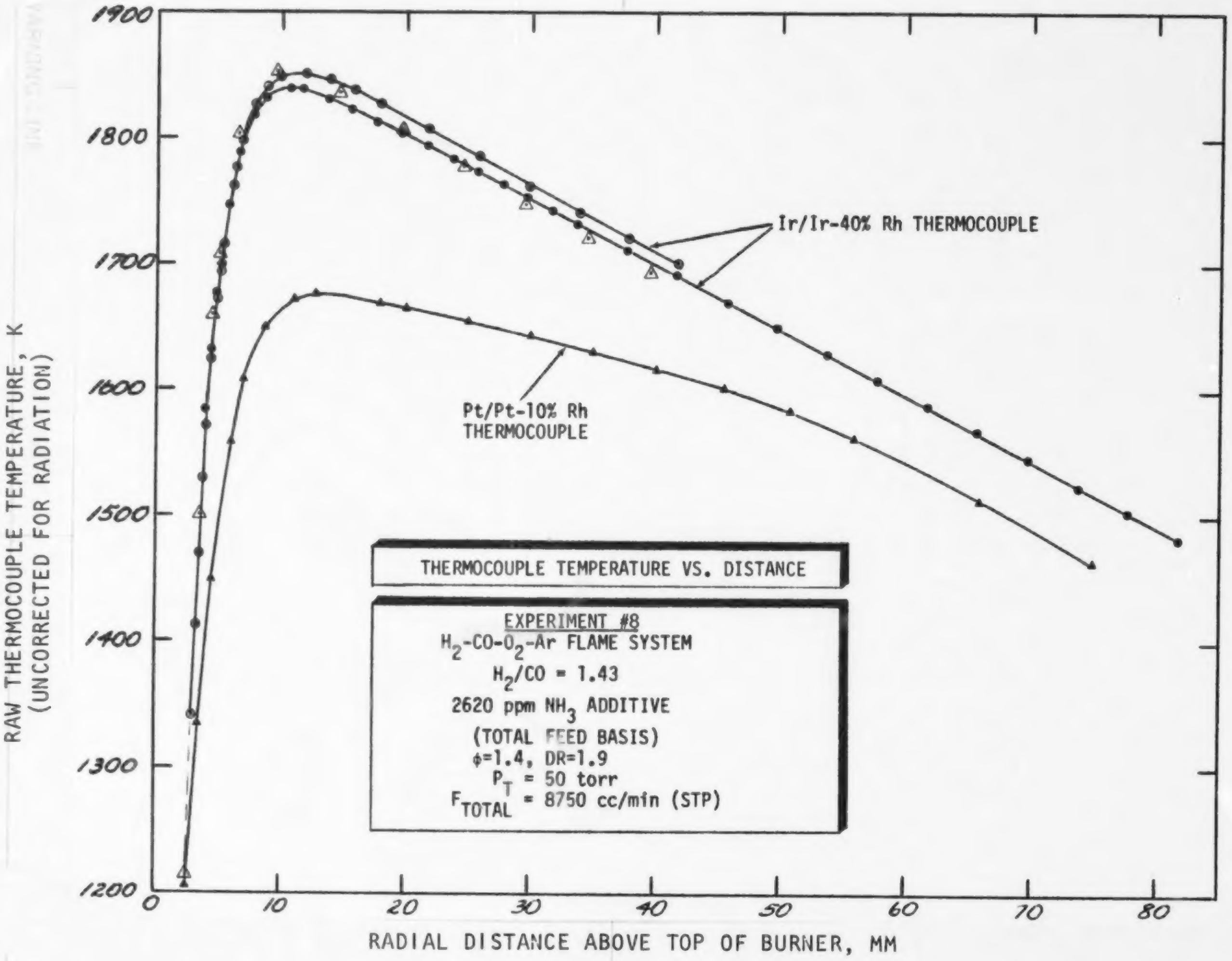

Figure C-1. Comparison of Uncorrected Temperature Readings from Two Types of Thermocouples

262

The gas temperature profile (uncorrected) along the center axis of the burner obtained previously with a 3-mil Al_2O_3-coated Pt/Pt-10%Rh thermocouple is plotted in Fig. C-1. However, it was found that this type of thermocouple could not withstand the high-temperature reducing conditions encountered in experiment No. 8 without considerable deterioration of the Al_2O_3 coating and subsequent melting of the Pt-Rh alloy. It should be pointed out that the first several data points obtained with the Pt/Pt-10%Rh thermocouple were taken far downstream of the luminous zone (75 to 50 mm above the burner top) and are therefore considered to be reasonably accurate. The raw emf data from these initial points did not reveal any evidence of thermocouple deterioration, and it is believed that catalytic heating of the thermocouple wire should be negligible in the region.

The raw temperature profile (uncorrected for radiation) obtained with the Ir/Ir-40%Rh thermocouple at the conditions of experiment No. 8 is shown in Fig. C-1. The curve drawn through the solid black dots represents the first detailed thermocouple temperature profile that was measured. The open circles are data points obtained during a subsequent rerun. The open triangles are thermocouple measurements that were taken several weeks later in conjunction with a series of optical pyrometer measurements. It can be seen that the measured thermocouple temperature profile is very reproducible, with the mean deviation being only 10 to 15 K.

It was stated that Dr. Seery had found the average emissivity (ε_m) of a similar 3-mil Y_2O_3-BeO-coated Ir/Ir-40%Rh thermocouple wire to be approximately 0.67 between 1300 and 1700 C. However, using Seery's value for ε_m, the calculated radiation correction term added to the thermocouple temperature profile shown in Fig. C-1 resulted in gas temperature values which were unreasonably high. For example, at the maximum temperature point in Fig. C-1 (11.0 to 12.0 mm), the radiation correction amounted to over 700 C, giving a corrected gas temperature of over 2500 C. The adiabatic flame temperature for this system has been calculated to be only 2150 K. Since the radiation correction is proportional to the wire emissivity, it would appear that the value of ε_m reported by Seery is too high. Furthermore, the large difference between the thermocouple temperature profiles measured with the two different types of thermocouples suggests that the raw profile measured with the Ir/Ir-40%Rh thermocouple may also be too high.

One of the quantities involved in the calculation of the radiation correction is the convective heat transfer coefficient, h_c, between the flame gas and the thermocouple. From a heat balance where catalytic effects are neglected,

$$\Delta T_{rad} = T_g - T_w = \frac{\sigma \varepsilon_m T_w^4}{h_c} \qquad (C-1)$$

where T_g = gas temperature, T_w = raw thermocouple temperature, $\sigma = 1.335 \times 10^{-12}$g cal/sec·cm^2·K^4 (Boltzmann constant), and ε_m = wire emissivity. Values of h_c are usually determined from Nusselt number (Nu) correlations for flow over uniform cylindrical wires. The expression used in this work

$$Nu = 0.8\ Re^{0.25} \qquad (C-2)$$

is the same one given by Kaskan (Ref. 40) and by Fristrom and Westenberg (Ref. 41). Another more general correlation which has been employed by Bradley and Matthews (Ref. 42) in flame work is:

$$Nu = 0.42\ Pr^{0.2} + 0.57\ Pr^{0.33}\ re^{0.5} \qquad (C-3)$$

The dimensionless groups in Eq. C-2 and C-3 are the Nusselt number, $Nu = h_3 D_w/k$, Reynolds number, $Re = D_w U\rho/\mu$, and Prandtl number, $Pr = C_p \mu/k$.

Table C-1 summarizes a series of calculations to determine h_c as a function of temperature in experiment No. 8. The values of C_p, μ, k and ρ were calculated from the properties of the burnt gas. An average wire diameter of 0.0080 cm was assumed in each case. Note that the value of h_c obtained from the Bradley and Matthews correlation is on average about 21% higher than that obtained from the Kaskan equation. Hayhurst and Kittelson (Ref. 43) have performed similar

---

40. Kaskan, W. E., Sixth Symposium (International) on Combustion, Reinhold, New York, 1957, p. 134.
41. Fristrom, R. M. and A. A. Westenberg, Flame Structure, McGraw-Hill, New York, 1965.
42. Bradley, D. and K. S. Matthews, J. Mech. Eng. Sci., 10, 299 (1968).
43. Hayhurst, A. N. and D. B. Kittelson, Combustion and Flame, 28, 301 (1977).

TABLE C-1.

THERMOCOUPLE HEAT TRANSFER COEFFICIENTS
CALCULATED AT CONDITIONS OF EXPERIMENT # 8

TEMPERATURE (°K)	Re $\left(\frac{DU\rho}{\mu}\right)$	Pr $\left(\frac{C_p\mu}{k}\right)$	Equation (2) (Kaskan)		Equation (3) (Bradley & Matthews)		% Diff. $\left(\frac{h_{c(3)} - h_{c(2)}}{h_{c(2)}}\right)$
			Nu	h_c (cal/cm^2·sec°K)	Nu	h_c (cal/cm^2·sec°K)	
1400	0.0973	0.618	0.447	0.01039	0.533	0.01239	20.4
1500	0.0928	0.623	0.442	0.01077	0.531	0.01294	20.2
1600	0.0888	0.626	0.437	0.01114	0.528	0.01346	20.8
1700	0.0852	0.624	0.432	0.01156	0.525	0.01404	21.5
1800	0.0821	0.625	0.428	0.01193	0.522	0.01455	22.0

calculations for wires of various diameters and found that the use of Eq. C-3 results in values of h_c which are approximately 8 to 10% higher than those computed from Eq. C-2. Furthermore, they report that their measured values of h_c agree to within 10% with those predicted by Eq. C-2 and by $\pm 13\%$ when using the simpler expression of Eq. C-2. Since the actual radiation correction is inversely proportional to h_c, it is reasonable to conclude from the above data that the large error involved in the ΔT_{rad} correction term in the present work must be associated with ε_m and/or T_w and not in the determination of h_c.

One method of calculating an approximate point value of ε_m is to use the gas temperature measured far downstream of the burner with the Pt/Pt-10%Rh thermocouple and the corresponding thermocouple wire temperature measured with the Ir/Ir-40%Rh thermocouple. Then,

$$\varepsilon_m = \frac{\Delta T_{rad}\, h_c}{\sigma T_w^4} \tag{C-4}$$

neglecting catalytic effects. Thus at $\Delta X = 75.0$ mm, $T_{gas} = 1579$ K, while $T_w = 1518$ K. The value of h_c is determined from Table C-1 at a mean film temperature of $T_f = 1/2\ (T_g + T_w) = 1548$ K, and is found to be 0.01095 $\text{cal/cm}^2\cdot\text{sec K}$. Substituting these values into Eq. C-4 gives $\varepsilon_m = 0.093$. Hayhurst and Kittelson (Ref. 43) report a geometric mean emissivity for a bare Ir/Ir-40%Rh thermocouple wire of

$$\varepsilon_m = 0.8767 \times 10^{-4}\ T_w + 0.0135 \pm 10\% \tag{C-5}$$

Thus at $T_w = 1518$ K, $\varepsilon_m = 0.147 \pm 0.015$. Since this latter value represents a lower limit for the emissivity of the coated wire, it would also appear that ΔT_{rad} is too low or that the measured wire temperature is too high.

Figure C-2 is a plot of some tabular data for thermocouples of iridium-rhodium alloys vs iridium given by Blackburn and Caldwell (Ref. 44), in which at several constant temperatures the variation in thermal emf is shown as a function of

---

44. Blackburn, G. F. and F. R. Caldwell, J. Res. Nat'l Bureau of Standards, 68C, 41 (1964).

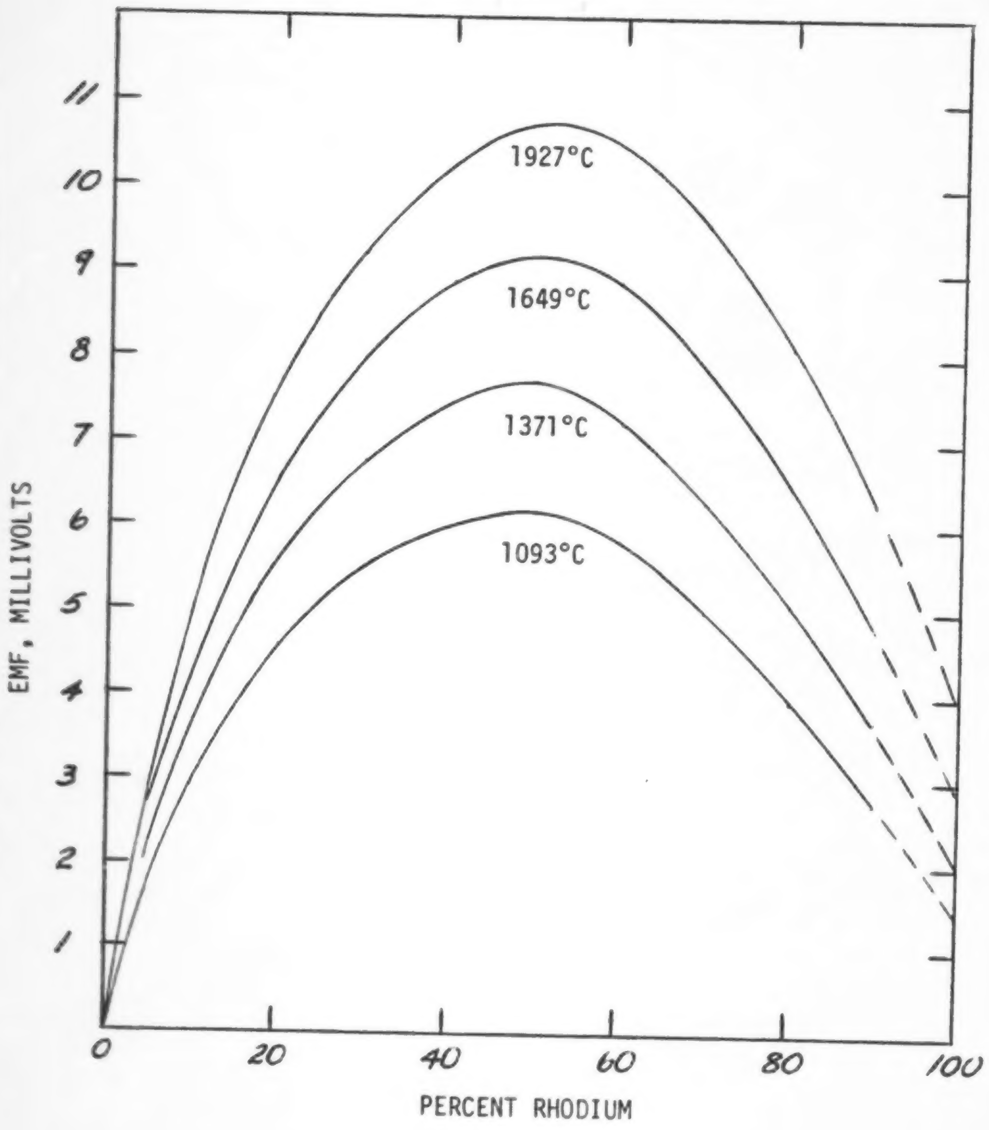

Figure C-2. Variation at Constant Temperature of Thermal EMF with Percent Rhodium in the Alloy Legs of Ir-Rh vs Ir Thermocouples (Ref. 44) percent rhodium in the alloy leg of the thermocouple. Note that the curves are approximately symmetrical about the 50%Ir-50% Rh value. Even if the Rh content of the alloy leg was actually 50% rather than the stated value of 40%, the measured temperature would be highly less than 100°.

In conclusion, it would appear that the average emissivity value reported by Seery for the 3-mil Y_2O_3-BeO-coated Ir/Ir-40%Rh thermocouple ($\varepsilon_m = 0.67$, T = 1300 to 1700 C) is much too high to give radiation correction terms which yield reasonable values of gas temperature. The equation for the mean emissivity of a bare Ir/Ir-40%Rh thermocouple reported by Hayhurst and Kittleson (Ref. 43) gives a much more reasonable estimate of the correction term.

APPENDIX D

MEASUREMENT OF NITROGEN SPECIES IN PRODUCTS OF LOW-PRESSURE HYDROCARBON FLAMES

INTRODUCTION

A chemiluminescent analyzer (CA) was used in the previous program (Ref. 1) to measure NO directly and NO_2, HCN, and NH_3 after conversion of these species to NO. This permitted the extreme sensitivity of the CA for NO measurement to be utilized for other species as well. A molybdenum catalyst converter was used at 400°C to convert NO_2 and at 800°C to convert HCN and NH_3 to NO. Calibration plots of % conversion of HCN and NH_3 to NO as a function of concentration were developed for this purpose (e.g., Fig. 46 of Ref. 1). Although the differences in conversion efficiencies for HCN and NH_3 on the molybdenum catalyst surface did permit tentative conclusions to be drawn from the experimental species flux curves (p. 236 of Ref. 1), the converter-CA system could not distinguish directly between HCN and NH_3. It appeared that much of the added NH_3 was converted to HCN in the fuel-rich flame but this conclusion was tentative because of the limitations of the analytical procedure employed.

Other techniques have been employed for the measurement of nitrogen species in flames but these do not appear to be suitable at present for low-pressure flames. De Soete (Ref. 45) and Haynes et al (Ref. 25) measured HCN in atmospheric pressure flames by drawing the gas through a cooled probe and a bubbler containing basic solution. De Soete measured the HCN in the trapping solution by a wet chemical method employing silver nitrate and KI, and Haynes et al used a cyanide specific ion electrode. De Soete found that NH_3 and other amines are partially converted to HCN in rich ethylene flames. Haynes et al detected HCN in the post-flame gases of all sufficiently fuel-rich unseeded hydrocarbon air flames. The amounts detected depended on the fuel and the

---

45. De Soete, G., "The Mechanism of Formation of NO from Ammonia and Amines in Hydrocarbon Flames." Ref. Inst. Fr. Petr. Ann. Combust. Liquide, 28, 96-108 (1973).

stoichiometry of the flame. Acetylene flames gave the highest concentrations of HCN (250 ppm at $\phi = 1.95$) with lesser amounts in ethylene (90 ppm, $\phi = 1.68$) and propane (70 ppm, $\phi = 1.45$) flames. Only small amounts of HCN (<3 ppm) were observed in CH_4-air flames which were difficult to stabilize at $\phi > 1.20$. They also reported the formation of HCN in rich pyridine-seeded propane-air flames but did not state if the addition of the pyridine increased the amount of HCN that formed. Matthews et al also developed methods for the measurement of nitrogen species in flames (Ref. 46). Their general approach encompasses the type of method we used in that they employ chemical separation and, for some species, conversions to NO which is measured with a chemiluminescent analyzer. Most of their work was with atmospheric pressure samples. Matthews et al used acidic $Cr_2O_7^{-2}$ on firebrick to remove NH_3 from the combustion product sample but did not report if this gave a quantitative separation of HCN and NH_3.

A major objective of the present program, under EPA contract 68-02-1886, was to develop and utilize a chemical analysis technique which would clearly differentiate between HCN and NH_3 in the combustion zone. The new analytical method that was developed is described here and data from a typical combustion experiment will be presented to illustrate the utility of the method for uniquely determining NO, NO_2, NH_3 and HCN in the products of a low-pressure methane flame.

DESCRIPTION OF THE EXPERIMENTAL APPARATUS

A schematic of the flat-flame burner and analysis system is shown in Figure 2-2. HCN and NH_3 were added to premixed CH_4-O_2-Ar and CH_4-O_2-N_2 flames to investigate the combustion kinetics involved in the formation of NO from these combustion intermediates.

---

46. Matthews, R. D., et al, "Measurement of Low Molecular Weight Nitrogen Compounds in Flame Systems", Fall 1975 Meeting of the WSS/CI, paper 75-16.

Methane, oxygen, and argon (or nitrogen) were metered with critical flow orifices consisting of accurately sized sapphire orifice jewels (Aurele Gatti, Inc.). As long as the pressure ratio is greater than the critical ratio, namely $\left(\frac{2}{1+\gamma}\right)^{\gamma/(\gamma-1)}$, the orifice flowrate will be independent of the downstream pressure. The inlet flow system is similar to that reported by Anderson and Friedman (Ref. 47).

The design of the water-cooled burner is shown in Fig. 2-1. The burner was enclosed in a glass envelope so that a pressure of 0.1 atm could be maintained to spread the flame and permit more detailed probing. An uncooled quartz microprobe was used to measure species concentrations at various distances through the flat flame along the centerline of the burner. The reacting gases were quenched aerodynamically by expanding them from the reaction chamber pressure (usually 76 torr) to about 1 torr. The probe was constructed from 9 mm quartz tubing which was pulled to taper down to a very small-diameter tip containing the sonic sampling orifice. The diameter of the sonic orifice was maintained between 75 and 100 microns, while a taper of approximately 30° was used to minimize the flow disturbance occurring upstream of the probe as a result of gas sampling (Ref. 41). Temperature measurements, also along the centerline of the flame, were performed with a 3-mil, Al_2O_3-coated Pt-Pt/10% Rh thermocouple. Coating the Pt wire prevents the catalysis of reactions on its surface which would otherwise heat the wire and result in erroneous temperature measurements.

The mole fractions of the major stable species were measured by mass spectrometry. A chemiluminescent analyzer (CA) was used to measure NO directly and NO_2, HCN, and NH_3 by conversion of these species to NO. The CA employed was a Model 10A self-contained NO-NO_x Gas Analyzer manufactured by the Thermo Electron Corporation (TECO). This instrument utilizes the chemiluminescent reaction between NO and O_3 as a means of monitoring NO concentration, i.e.,

$$NO + O_3 \longrightarrow NO_2^* + O_2$$

$$NO_2^* \longrightarrow NO_2 + h\nu$$

---

47. Andersen, J. W. and R. Friedman, "An Accurate Gas Metering System for Laminar Flow Studies," Rev. Sci. Instr., 20, 61 (1949).

USE SPECIAL DROPOUT BLUE PENCIL
ONLY TO INDICATE CORRECTIONS
CLASSIFICATION
PAGE
STARTING LINE

The ozone is produced from an O_2 supply by an ozonator in the instrument and mixed with the sample gas in a flow reactor. A photomultiplier and optical filter mounted at one end of the reactor monitors photons emitted by the electronically excited NO_2. The number of photons detected per unit time is primarily a function of both NO concentration and the sample flowrate through the reactor. The residence time of gas in the CA reactor is quite large compared to the reaction time so that the photon emission rate is directly proportional to the feed rate. The pressure in the reaction chamber was adjusted by turning a control valve installed in the ozone feed line until the reactor pressure was 0.8 torr with no sample feed. With sample feed, the reactor pressure was maintained between 0.8 and 1.1 torr depending upon the diluent chosen and other flow conditions.

Since the excited NO_2 can also lose energy via collisions with other species, the rate of photon emission could be a function of pressure and gas composition and alter the direct relationship between the sample flowrate and the photon emission rate. This had to be checked under the conditions of our experiments. It was found that, because the gas in our CA was mainly O_2, the composition of the sample had little effect on the CA reading.

The CA was calibrated with a NO in N_2 standard gas contained in a treated aluminum cylinder (supplied by Airco). Contained within the CA is a temperature-regulated stainless steel catalytic converter for converting NO_2, NH_3 and HCN to NO. In the absence of sufficient oxygen in the gas sample, the percent conversion of NH_3 and HCN in the stainless steel converter drops appreciably. Thus, a controlled air leak, fabricated as a small hole in a piece of quartz tubing, was installed in the gas sample line just prior to entering the Model 10A analyzer. The leak was used in all experiments in which fuel-rich conditions were employed but oxygen was supplied to the leak in the later experiments (see text). A modular molybdenum catalytic NO-NO_x converter unit (and a temperature regulator) also manufactured by TECO was available for converting only NO_2 to NO (Fig. 2-1).

WARNING LINE
STOP
DOCUMENT NUMBER

CLASSIFICATION
TYPIST

DEVELOPMENT OF AN ANALYTICAL TECHNIQUE TO DISTINGUISH BETWEEN HCN AND NH_3

As mentioned earlier, the possible interconversion of NH_3 to HCN (and vice versa) in and above the flame front is a very important point that relates to all the mechanisms that have been proposed for the formation of fuel NO. Unless selective catalytic conversions to NO or chemical seaparations can be carried out upstream of the CA, only the sum of NO_2, HCN and NH_3 can be determined. Measurements of the conversion of NO_2 to NO on the molybdenum catalyst demonstrated that nearly 100% conversion of NO_2 to NO could be achieved at a catalyst temperature of 350°C, while at these same conditions less than 1% conversion of NH_3 or HCN to NO was obtained. The problem was therefore reduced to one of finding a selective technique for distinguishing between NH_3 and HCN at a sampling pressure of approximately 1 torr.

The first objective was to investigate the conversion of HCN and NH_3 to NO on the stainless steel catalyst as a function of temperature and reactant concentration. At a concentration level of 100 ppm in argon containing 5.8% 0_2, the conversion of NH_3 to NO increased from 4% at 400°C to 90% at 840°C, while that of HCN increased from 2% to 75% over this same temperature range. These typical results and others indicated that the stainless steel converter alone could not be used as a selective conversion technique to distinguish between HCN and NH_3. A search of the recent chemical literature did not reveal any metal or carbon-metal composite catalyst which had been proven to separate successfully the $HCN \rightarrow NO$ conversion from the $NH_3 \rightarrow NO$ conversion.

An effort was therefore made to find a chemical trapping agent which, when installed in the gas sampling line upstream of the catalytic converters, would remove HCN without affecting the other nitrogen species. An Ascarite trap had been employed successfully in the fuel pyrolysis experiments of the previous program for selectively removing HCN from a stream containing NH_3 (Ref. 1). A specially fabricated manifold was constructed and installed between the quartz sampling probe and the modular molybdenum catalyst unit upstream of the inlet line to the CA. The manifold contained a series of removable cartridges and extensive valving to permit rapid evaluation of candidate solid absorbents. A description of the four solid absorbents which were tested is given in Table D-1. It was felt that the basic nature of these solids would cause preferential removal of HCN while allowing the NH_3 to pass unretarded through the absorbent bed.

Table D-2 summarizes the response of each of the absorbents to the passage of gas mixtures containing HCN, NH_3, NO and NO_2, respectively. The significant quantity to note in Table D-2 is the difference in measured NO concentration between conditions (a) and (b) for each gas mixture. It was readily apparent from experiment I that the Ascarite, Caroxite and Cosorb were highly successful in removing practically all the added HCN, whereas the 5% polyethylene imine on Chromosorb W would not be an acceptable HCN absorbent. Experiment II revealed that the Ascarite and Cosorb allowed essentially complete passage of the NH_3, while a small percentage of NH_3 was held up on the Caroxite. Each of the three potential HCN solid absorbents did remove a small fraction of NO, as evidenced in experiment III. However, following experiment IV, it was clear that the Cosorb solid absorbent satisfied the experimental requirements of the present program: (1) it quantitatively removed HCN and NO_2, (2) it allowed complete passage of NH_3, and (3) it removed only a small percentage of NO. A Cosorb trap was installed in the system (Fig. 2-1). The Cosorb solid absorbent was only tested over a narrow fuel-N additive concentration range to satisfy the particular requirements of the present program. When used under other conditions, calibration experiments should be carried out and the amount of Cosorb adjusted to give complete removal of HCN without appreciable loss of NO.

Based on these results, a generalized scheme for uniquely determining NO, NO_2, HCN and NH_3 is depicted in Figure 2-3 in the text. NO is first measured without the use of either catalytic converter or chemical traps (1). NO_2 is determined by passage through the molybdenum catalyst at 350°C (2) and measuring the incremental NO over the previous reading. After using (1) and

USE SPECIAL DROPOUT BLUE PENCIL
ONLY TO INDICATE CORRECTIONS
CLASSIFICATION
PAGE
STARTING LINE

TABLE D-1. CANDIDATE SOLID ABSORBENTS TESTED FOR SELECTIVE REMOVAL OF HCN

REAGENT NAME (AND MANUFACTURER)	PARTICLE SIZE ANALYSIS	TYPICAL USE
Ascarite® (Arthur H. Thomas Company)	20-30 mesh	An indicating CO_2 absorbent used in combustion and GC analyzers.
Caroxite® (Fisher Scientific Company)	20-30 mesh	An indicating CO_2 absorbent used in gas purification trains.
Cosorb® (Mallinckrodt)	33-140 mesh	An indicating CO_2 absorbent used in Coleman combustion analyzers.
5% Polyethylene Imine deposited on Chromosorb W-HP (In-house preparation)	80-100 mesh	A specially prepared solid having the potential for absorbing acidic components. Chromosorb W is a widely used support material in GC columns.

STOP
DOCUMENT NUMBER
PAGE NUMBER

CLASSIFICATION
TYPIST

TABLE D-2. SUMMARY OF SOLID ABSORBENT PERFORMANCE IN REMOVING HCN, NH_3, NO AND NO_2, RESPECTIVELY, FROM GAS MIXTURES

Gas Mixture	Experimental Flow Condition	Chemiluminescent Analyzer (CA) NO Concentration (PPM)			
		Ascarite	Caroxite	Cosorb	5% Polyethylene Imine on Chromosorb W
I. HCN: 6.7% O_2 in N_2 with 134 ppm HCN Additive	a) Through S.S. Converter (720°C), only.	122	120	122	122
	b) Through absorbent + S.S. Converter (720°C) After 10 min.	<1	<1	<1	108
II. NH_3: 6.7% O_2 in N_2 with 137 ppm NH_3 Additive	a) Through S.S. Converter (720°C), only.	107	110	115	115
	b) Through absorbent + S.S. Converter (720°C) After 30 min.	107	105	115	94
IIIA. NO: 470 ppm (nominal) NO in N_2	a) Through NO Mode of CA, only	479	479	479	---
	b) Through absorbent + NO Mode of CA After 10 min.	475	472	469	---
IIIB. NO: 135 ppm (nominal) NO in N_2	a) Through NO Mode of CA, only	---	---	135	---
	b) Through absorbent + NO Mode of CA After 10 min.	---	---	130	---
IV. NO_2: 110 ppm (nominal) NO in N_2	a) Through S.S. Converter (800°C), only	111	110	110	---
	b) Through absorbent + S.S. Converter (800°C) After 20 min.	>40	>15	<1	---

(2), the inlet gas mixture is allowed to flow through the chemical trap (3) to remove HCN prior to passage through the stainless steel converter at approximately 800°C. Subsequent use of the stainless steel converter without the trapping agent (4) gives the HCN present in the mixture by difference.

SAMPLE CASE ILLUSTRATING THE ANALYTICAL METHOD

To illustrate the use of this method of measuring the HCN, NH_3, NO_2 and NO concentrations in a mixture of these gases, data from the fuel-rich Input-Output Experiment IB (described in the text) will be presented. The experimental procedure and the concentration data obtained from the chemiluminescent analyzer are illustrated diagramatically in Figure D-1 at the 5.50 mm downstream position.

At these conditions, x, y and z were determined in calibration experiments to be 0.90, 0.75, and 0.048 respectively. The data in Figure D-1 are solved as four equations in the four unknown species concentrations to yield the final computed results presented in Table D-3. The calculations at 5.50 mm downstream revealed that 78% of the initial NH_3 additive was recovered as HCN, demonstrating that NH_3 reacts in the fuel-rich flame to form high yields of HCN most of which survives the flame front.

COMMENTS

It is apparent that this method will only meas-ure stable species that are present in the combustion products after quenching in the probe. CN radicals present in the flame will probably form HCN in the probe and NH and NH_2 should form NH_3 (although $NH + NH \rightarrow N_2 + 2H$ could occur). The fate in the probe of N, H, and O atoms and NCO radicals is less certain.

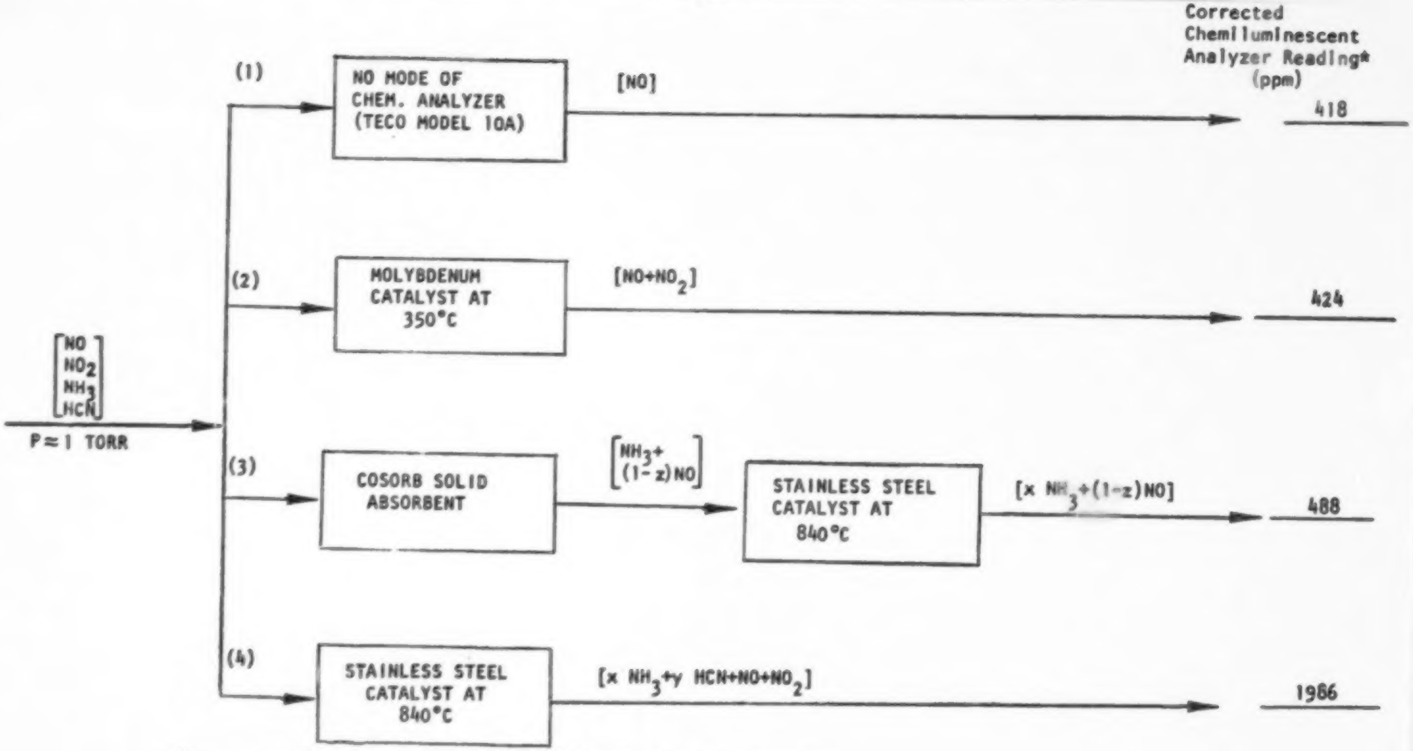
Corrected Chemiluminescent Analyzer Reading* (ppm)
[NO NO2 NH3 HCN]
P ≈ 1 TORR
(1)
NO MODE OF CHEM. ANALYZER (TECO MODEL 10A)
[NO]
418
(2)
MOLYBDENUM CATALYST AT 350°C
[NO+NO2]
424
(3)
COSORB SOLID ABSORBENT
[NH3+ (1-z)NO]
STAINLESS STEEL CATALYST AT 840°C
[x NH3+(1-z)NO]
488
(4)
STAINLESS STEEL CATALYST AT 840°C
[x NH3+y HCN+NO+NO2]
1986

Where: x = Fractional conversion of NH_3 in the S.S. converter
y = Fractional conversion of HCN in the S.S. converter
z = Fractional absorption of NO in Cosorb

*NOTE: CA readings corrected for air leak at fuel rich flame condition and for corrections due to sample temperature and composition.

Figure D-1. Sample Case Data and Calculation Procedure

TABLE D-3. SAMPLE CASE DATA SUMMARY

Experimental Conditions	Axial Distance From Top of Burner (mm)	Axial Temperature (°K)	Combustion Product Composition Data		
			Species	Concentration (ppm)	Percent of Initial NH_3 Additive
• CH_4-O_2-Ar Flame • P_{total} = 76 torr • Ø = 1.5 • D.R. = 1.0 • Additive = 2529 ppm NH_3 (total basis) • 6247 cm^3/min feed rate at 298°K and 1 atm	5.50	1987	NO NO_2 HCN NH_3	418 6 1963 100	16.5 0.2 77.6 4.0
	80.00	1565	NO NO_2 HCN NH_3	794 --- 107 ---	31.4 --- 4.2 ---

REFERENCES

1. Axworthy, A. E., G. R. Schneider, M. D. Schuman, and V. H. Dayan, "Chemistry of Fuel Nitrogen Conversion to Nitrogen Oxides in Combustion," EPA-600/2-76-039 (NTIS No. PB 250373/AS), February, 1976.

2. Pershing, D. W., G. B. Martin, and E. E. Berkau, "Influence of Design Variables on the Production of Thermal and Fuel NO from Residual Oil and Coal Combustion," AIChE Symposium Series No. 148, 1975, 71, 19 (presented at the 66th Annual AIChE Meeting, 1973).

3. Turner, D. W., R. L. Andrews, and C. W. Siegmund, "Influence of Combustion Modification and Fuel Nitrogen Contents on Nitrogen Oxides Emissions from Fuel Oil Combustion" (presented at the 64th Annual AIChE Meeting, 1971), AIChE Symposium Series No. 126, 1972, 68, 55.

4. Muzio, L. J., R. P. Wilson, Jr., and C. McComis, "Package Boiler Flame Modifications for Reducing Nitric Oxide Emissions - Phase II of III," EPA-R2-73-292b (NTIS No. PB 236752/AS), June 1975.

5. Flagan, R. C., "The Formation of NO from Organic Nitrogen Contained in Fossil Fuels," Ph.D. Thesis, Massachusetts Institute of Technology, 1973.

6. Martin, G. B. and E. E. Berkau, "An Investigation of the Conversion of Various Fuel Nitrogen Compounds to Nitrogen Oxides in Oil Combustion" (presented at the 64th Annual AIChE Meeting, 1971) AIChE Symposium Series No. 126, 1972, 68, 45.

7. Dykema, O. W. and R. E. Hall, "Analysis of Gas-, Oil-, and Coal-Fired Utility Boiler Test Data," pp IV-115 to -162, Proc. Stationary Source Combustion Symposium, Vol. III. Field Testing and Surveys, EPA-600/2-76-152c (NTIS No. PB 257146/AS), June 1976.

8. Martin, G. B. and E. E. Berkau, "Evaluation of Various Combustion Modification Techniques for Control of Thermal- and Fuel-Related Nitrogen Oxide Emissions" (presented at the 14th Symposium (Int.) on Combustion), 1972.

9. Heap, M. P., T. M. Lowes, R. Walmsley, and H. Bartelds, "Burner Design Principles for Minimum NO_x Emissions," pp 141-171, Proc. Coal Combustion Seminar, 19-20 June 1973, EPA-650/2-73-021 (NTIS No. PB 224210/AS), September 1973.

Preceding page blank

10. Axworthy, A. E., V. H. Dayan, and G. B. Martin, "Reactions of Fuel Nitrogen Compounds under Conditions of Inert Pyrolysis," FUEL, 57, 29 (1978).

11. Axworthy, A. E., G. R. Schneider, and V. H. Dayan, "Chemical Reactions in the Conversion of Fuel Nitrogen to NO_x," Proceedings of the (First) Stationary Source Combustion Symposium, September 1975, Vol. I, Fundamental Research, EPA-600/2-76-152a, Rockwell International, Rocketdyne Division, Canoga Park, CA, June 1976.

12. Pohl, J. H., and A. F. Sarofim, "Kinetics of Devolatilization and Oxidation of Coal Nitrogen," 16th Symposium (International) on Combustion, 491, 1976.

13. Sugiyama, S. et al., "Reducing Fuel NO_x Emission: N_2 Formation from Fuel N," Env. Sci & Tech, 12, 175 (1978).

14. Sobolev, G. F., "High Temperature Oxidation and Burning of Carbon Monoxide," Seventh Symposium (International) on Combustion, p. 386, 1958.

15. Dryer, F., D. Naegeli, and I. Glassman, "Temperature Dependence of the reaction $CO + OH = CO_2 + H$," Combustion and Flame, 17, 270 (1971).

16. MacLean, D. I. and H. G. Wagner, "The Structure of the Reaction Zones of Ammonia-Oxygen and Hydrazine Decomposition Flames," Eleventh Symposium (International) on Combustion, 871, 1966.

17. Sternling, C. V. and J. O. Wendt, "Kinetic Mechanisms Governing the Fate of Chemically Bound Sulfur and Nitrogen in Combustion," EPA-650/2-74-017 (NTIS-PB 230 895/AS), 1974.

18. Parks, D. J., and E. A. Fletcher, "Formation and Emission of Nitric Oxide in Fluidized Bed Combustion," Environ. Sci. Technol., 9 (8), 749-756 (1975).

19. Petersen, E. E., J. Landau, and E. Saucedo, "Micro and Macro Changes in a Stainless-Steel Catalyst During Reduction of NO," The Catalytic Chemistry of Nitrogen Oxides, Plenum Press, New York, 1965, pp. 119-131.

20. De Soete, G. G., "La Formation des Oxydes D'Azote dans la Zone O'Oxydation des Flammes D'Hydroearbures (in French)", Institut Franeais der Petrole, Report 23309, June 1975, (Compte-Rendu Final des Travaux, Contrat No. 73-56, Avdc le ministere de la Prutation de la Nature et de L'Envirinnement, 1. 4. 1973 Aer 31. 3. 1975).

21. Fenimore, C. P. "Formation of NO in Premixed Hydrocarbon Flames," *Thirteenth Symposium (International) on Combustion*, p. 373, 1970.

22. Sarofim, A. F. and J. H. Pohl, "Kinetics of NO Formation in Premixed Laminer Flames," *Fourteenth Symposium (International) on Combustion*, p. 739, 1972.

23. Iverach, D., K. S. Basden, and N. Y. Kirov, "Formation of NO in Fuel-Lean and Fuel-Rich Flames," *Fourteenth Symposium (International on Combustion*, p. 767, 1972.

24. Bachmaier, F, K. H. Eberius and T. Just, "HCN in Premixed Hydrocarbon-Air Flames at One Atmosphere," *Comb. Sci. and Tech*, *7*, (1973).

25. Haynes, B. S., D. Iverach, and N. Y. Kirov, "The Behavior of Nitrogen Species in Fuel-Rich Hydrocarbon Flames," *Fifteenth Symposium (International) on Combustion*, p. 1103, 1974.

26. Yamagishi, K. et al., "A Study of NO_x Emission Characteristics in Two-Stage Combustion," *Fifteenth Symposium (International) on Combustion*, p. 1157, 1974.

27. Fenimore, C. P. "Reactions of Fuel-Nitrogen in Rich Flames," *Comb. and Flame*, *26*, 249 (1976).

28. Morley, C., "The Formation and Destruction of HCN From Atmospheric and Fuel Nitrogen in Rich Atmospheric-Pressure Flames," *Comb. and Flame*, *27*, 189 (1976).

29. Martin, G. B., "NO_x Considerations in Alternate Fuel Combustion," presented at EPA Symposium; *Environmental Aspects of Fuel Conversion Processes*, Hollywood, Florida, 14-18 December 1975.

30. Tyson, T. J., "Chemical and Physical Limitations on Low BTU Gas Combustor NO_x Emissions," *presented at EPA Combustion Research Branch Contractors Meeting*, MIT, Cambridge, Mass., August 1976.

31. Heap, M. P., T. J. Tyson, J. E. Cichanowicz, R. Gershman, E. J. Kau, G. B. Martin, and W. S. Lanier, "Environmental Aspects of Low BTU Gas Combustion," presented at the *16th Symposium (International) on Combustion*, MIT, Cambridge, Mass., August 1976.

32. Robsen, F. L., and A. J. Giramonti, "The Environmental Impact of Coal-Based Advanced Power Systems," Symposium Proceedings; *Environmental Aspects of Fuel Conversion Technology*, EPA-650/2-74-118, October 1974, pp. 237-257.

USE SPECIAL DROPOUT BLUE PENCIL
ONLY TO INDICATE CORRECTIONS
CLASSIFICATION
PAGE

33. A. G. Gaydon, The Spectroscopy of Flames, 2nd ed., New York, John Wiley & Sons, 1974.

34. B. E. Walker, C. T. Ewing, and T. T. Miller, Rev. Sci. Instr., 33, 10 1962).

35. A. S. Darling and G. L. Selman, "Some Effects of Environment on the Performance of Noble Metal Thermocouples," Temperature, Its Measurement and Control in Science and Industry, vol. 4, pt, 3, Instrument Society of America, 1972.

36. P. A. Kinzie, Thermocouple Temperature Measurement, New York, John Wiley & Sons, 1973.

37. J. H. Kent, Comb. & Flame, 14, 279 (1970).

38. C. E. Moeller, M. Noland and B. L. Rhodes, NASA SP-5050, 1968, Office of Technology Utilization, NASA, Washington, D.C.

39. E. O. Zysk and A. R. Robertson, "New Thermocouple Materials," Temperature, Its Measurement and Control in Science and Industry, H. H. Plumb, Editor-in-Chief, Instrument Society of America, Pittsburgh, 1972, Vol. 4, Part 3, p. 1967.

40. Kaskan, W. E., Sixth Symposium (International) on Combustion, Reinhold, New York, 1957, p. 134.

41. Fristrom, R. M. and A. A. Westenberg, Flame Structure, McGraw-Hill, New York, 1965.

42. Bradley, D. and K. S. Matthews, J. Mech. Eng. Sci., 10, 299 (1968).

43. Hayhurst, A. N. and D. B. Kittelson, Combustion and Flame, 28, 301 (1977).

44. Blackburn, G. F. and F. R. Caldwell, J. Res. Nat'l Bureau of Standards, 68C, 41 (1964).

45. De Soete, G., "The Mechanism of Formation of NO from Ammonia and Amines in Hydrocarbon Flames." Ref. Inst. Fr. Petr. Ann. Combust. Liquide, 28, 96-108 (1973).

46. Matthews, R. D., et al, "Measurement of Low Molecular Weight Nitrogen Compounds in Flame Systems", Fall 1975 Meeting of the WSS/CI, paper 75-16.

47. Andersen, J. W. and R. Friedman, "An Accurate Gas Metering System for Laminar Flow Studies," Rev. Sci. Instr., 20, 61 (1949).

262